

Preface

The 2nd ISAMP workshop continued the review of ice scour effects relevant to the safe design and operation of marine pipelines offshore, and addressed the issues of damage control and oil spill cleanup. The 1st Ice Scour & Arctic Marine Pipelines workshop was held in February 1998. The proceedings of that workshop are available from C-CORE. The general aims of the workshop were to exchange information through the review of progress in understanding the ice scouring process and the related issues of pipeline burial, protection and damage control.

The Minerals Management Service, C-CORE, OSCORA and the Sakhalin Oil & Gas Institute (SOGI) jointly organized this second workshop. The workshop was held jointly with the 15th International Symposium on Okhotsk & Sea Ice (organized by The Okhotsk Sea & Cold Ocean Research Association (OSCORA) and International Association for the Physical Sciences of the Ocean (IAPSO)) in Mombetsu Hokkaido, Japan from February 7 to 9, 2000.

The workshop executive committee included Dr. Aota, OSCORA; Dr. Astafiev, SOGI; Dr. A. Palmer, Cambridge University; Dr. R. Phillips, C-CORE, Dr. Saeki, Hokkaido University and Dr. C. Smith of Minerals Management Service.

The workshop attendance was open to all symposium attendees and involved about 40 participants. Twenty invited presentations were given by representatives from oil & gas industries, regulatory authorities, research institutes and consultants from both the Russian Federation, NATO and Asian countries.

DISCUSSION - DEFINITION FUTURE NEEDS

The workshop was sponsored by:

- BP Amoco
- Chevron Petroleum Technology Company
- Geological Survey of Canada
- Minerals Management Service, and
- US Office of Naval Research

To receive further information on the Ice Scour and Arctic Marine Pipelines Workshop, please contact:

Dr. Ryan Phillips, C-CORE, Memorial University, St. John's, Newfoundland, Canada, A1B 3X5
Phone: +1 709 737 8354, Fax: +1 709 737 4706, E-mail: ryanp@morgan.ucs.mun.ca

**PROCEEDINGS OF
2nd ICE SCOUR & ARCTIC MARINE PIPELINES WORKSHOP**

held at

**15th INTERNATIONAL SYMPOSIUM ON OKHOTSK SEA & SEA ICE
Mombetsu, Japan, February 7-9, 2000**

Organised by:

C-CORE, Memorial University
St John's, Newfoundland, Canada, A1B 3X5
Phone: +1-709-737-8354 Fax: +1 709 737 4706

Minerals Management Service
US Department of Interior, 381 Elden St., Mail Stop 4700, Herndon,
Virginia 22070-4817

Okhotsk Sea and Cold Ocean Research Association
Okhotsk Sea Ice Science Research Co., 25-2
Motomombetsu, Mombetsu 094, Japan,

and

Sakhalin Oil & Gas Institute
18 Karl Marx St., Sakhalin, Okha 694460, Russia

Sponsorship for this workshop was provided by BP Amoco Corporation, Chevron Petroleum Technology Company, Geological Survey of Canada (through the program of Energy Research and Development), Minerals Management Service (US Department of Interior) and US Office of Naval Research International Field Office.

Proceedings Published By C-CORE, May, 2000

TABLE OF CONTENTS

Preface.	i
Technical Program	v
Registered Participants List	vii
Presentation Abstracts.	x
Ahmaogak, G	
Offshore Oil Development in the Alaskan Arctic: Who Bears the Risk	1
Palmer, AC	
Gouging in the Context of Critical Issues for Arctic Offshore Pipeline Development	5
Smith, CE	
Integrity of Offshore Pipelines: Two Recent Workshops	11
McHale, J, Dickins, D, and Glover, NW	
Oil Spill Response in Ice Infested Waters	15
Jensen, H and McHale, J	
Mechanical Oil Recovery In Ice Infested Waters (MORICE)	53
Surkov GA, Polomoshnov AM, Zemluk SV, Astafiev VN, Mikishin YA, Ribokov VF, Brovko PF, and Truskov PA.	
Seashore Morphology And Lithodynamic Of The North-East Sakhalin Coast	87
Stepanov, I	
Can Seabed Gouge Survey Data Be Applied to Prediction of Maximum Depths of Ice Keel Penetration?	93
Sodhi, D	
Crushing Failure During Edge-Indentation of Floating Ice Sheets	101
Croasdale, KR, McKenna, R, and Phillips, R	
Ice Aspects of Ice Scour	135
Clark, JI and Zhu, F	
Comparison of Ice Strength and Scour Resistance	141
Lau, M, Phillips, R, McKenna, R and Jones, S	
Discrete Element Simulation of Ridge Keel Resistance During Scouring: A Preliminary Study	151
Kioka, S, Yasunaga, Y, Nishimaki, H, and Saeki, H	
Behavior of Ridge Ice at a Time of Ice Scouring	163
Foriero, A and von Keviczky, A	
Numerical Simulation of Ice Scour using a Static Elastoplastic FEM Analysis and a Steady State Semi-Analytic Power Law Solution	173
Surkov G.A.	
Choosing Optimum Underwater Pipeline Burial Profile on Northeast Sakhalin Shelf	207
Kenny, S., Phillips, R., McKenna, R.F., and Clark, J.I.	
Response of Buried Arctic Marine Pipelines To Ice Gouge Events	217
Gordon , R, Hammond, J, and Swank, G	
Welding Challenges For Strain-Based Design	221
Bekker, A	
To a Problem of Construction of Sea Pipelines in the Freezing Seas.	239

Owen, L	
Northstar Pipeline Project Beaufort Sea, Alaska, Supplemental Leak Detection System	251
Discussion Session	259

2nd Ice Scour & Arctic Marine Pipeline Workshop

TECHNICAL PROGRAM

Monday 7 February		
9.00 – 17.00	Joint Sessions with Workshop on Oil Spill & Marine Environment, including: Offshore Oil Development in the Alaskan Arctic: Who Bears the Risk	George Ahmaogak, Mayor of North Slope Borough, Alaska
Tuesday 8 February		
9.00 - 12.00	ISAMP Workshop <i>ISAMP Workshop – Background</i> Gouging in the Context of Critical Issues for Arctic Offshore Pipeline Development Integrity of Offshore Pipelines: Two Recent Workshops <i>ISAMP Workshop - Oil Spill in Ice</i> Behaviour of Oil in Ice (Part 1 of 2) Mechanical Oil Recovery in Ice Infested Waters (MORICE) Oil Spill Response in Ice Infested Waters (Part 2 of 2)	Chair: Ryan Phillips Andrew Palmer, Cambridge University Charles Smith, Minerals Management Service David Dickins, DF Dickins & Associates Jim McHale, Alaska Clean Seas Jim McHale, Alaska Clean Seas
13.30 - 17.00	ISAMP Workshop <i>ISAMP Workshop - Seafloor Records</i> Ice Scour Morphology, Degradation Processes and Seabed Impact Rates, Resolute Bay, Cornwallis Island, Canadian Central Arctic Seashore Morphology and Lithodynamic of the North-East Sakhalin Coast Can Seabed Gouge Survey Data Be Applied to Prediction of Maximum Depths of Ice Keel Penetration? <i>ISAMP Workshop- Ice Limitations</i> Crushing Failure During Edge-Indentation of Floating Ice Sheets Ice Aspects of Ice Scour Comparison of Ice Strength and Scour Resistance	Chair: Chris Woodworth-Lynas Steve Blasco, Geological Survey of Canada Amolotoly Polomoshnov, Sakhalin Oil and Gas Institute Igor Stepanov, Arctic & Antarctic Research Institute Devinder Sodhi , CRREL, US Corp of Engineers Ken Croasdale, KR Croasdale & Associates Jack Clark , C-CORE

Wednesday 9 February

9.00 - 12.00	ISAMP Workshop	Chair: Ken Croasdale
	Discrete Element Simulation of Ridge Keel Resistance during Scouring	Ryan Phillips, C-CORE
	<i>ISAMP Workshop – Geotechnical Issues</i>	
	Behavior of Ridge Ice at the Time of Ice Scouring	S. Kioka, Hokkaido University
	Numerical Simulation of Ice Scour using a Static Elastoplastic FEM Analysis and a Steady State Semi-Analytic Power Law Solution	Adolfo Foriero, Université Laval
	Measuring Sub-Scour Soil Displacements in Different Soil Types Using Examples from the Geological Record	Chris Woodworth-Lynas, PETRA
	<i>ISAMP Workshop - Pipeline Considerations</i>	
	Choosing Optimum Underwater Pipeline Burial Profile on Northeast Sakhalin Shelf	Gennady Surkov, Sakhalin Oil and Gas Institute
13.30 -17.00	ISAMP Workshop	Chair: Ryan Phillips
	Response of Buried Arctic Marine Pipelines to Ice Gouge Events	Ryan Phillips, C-CORE
	Welding Challenges for Strain-Based Design	Greg Swank, Alaska State Pipeline Coordinators Office
	<i>Presentations from the floor</i>	
	To a Problem of Construction of Sea Pipelines in the Freezing Seas	Alexander Bekker, Far Eastern State Technical University
	Northstar Pipeline Integrity Assurance	Les Owen, BP Pipelines (Alaska) Inc.
	Discussion led by Andrew Palmer. Definition of Future Directions & Research Needs	

2nd ICE SCOUR & ARCTIC MARINE PIPELINES WORKSHOP

15TH INTERNATIONAL SYMPOSIUM ON OKHOTSK SEA & SEA ICE
Mombetsu, Japan, February 7-9, 2000

REGISTERED PARTICIPANTS LIST

<p>Tel: Fax: Email</p>	<p>George N Ahmaogak North Slope Borough PO Box 69 Barrow Alaska USA 99723 907.852.2611 907.852.0337 gahmaogak@co.north-slope.ak.us</p>	<p>Tel: Fax: Email</p>	<p>Denis Blanchet BP Amoco Corp. Westlake 1, Suite 24, 160 501 Westlake park Blvd. Houston Texas USA 77079 281 366 7191 281 366 7983 blanchd1@bp.com</p>
<p>Tel: Fax: Email</p>	<p>Hassan B Ali U.S. Office of Naval Research Asian Office 7-23-17 Roppongi, Minato-ku Tokyo 106 Japan +81-3 3401-8924 +81-3 3403-9670 AliH@onrasia.navy.mil</p>	<p>Tel: Fax: Email</p>	<p>Steve Blasco Geological Survey of Canada Atlantic Bedford Institute of Oceanography, Challenger Drive, P.O. Box 1006 Dartmouth Nova Scotia Canada B2Y 4A2 902 426 3932 902 426 4104 blasco@agc.bio.ns.ca</p>
<p>Tel: Fax: Email</p>	<p>Masaaki Aota Hokkaido University Sea Ice Research Laboratory, 6-4-10 Minamigaoka Mombetsu Hokkaido 094-0013 Japan +81 1582 3 3722 +81 1582 3 5319 aota@pop.lowtem.hokudai.ac.jp</p>	<p>Tel: Fax: Email</p>	<p>Ken Croasdale KR Croasdale & Associates 334, 40th Ave SW Calgary Alberta Canada T2S 0X4 403 243 7787 403 287 7889 krca@cadvision.com</p>
<p>Tel: Fax: Email</p>	<p>Alexander T Bekker Far Eastern State Technical University 10 Pushkirakaya Str. Vladivostok Russia 690600 +7 4232 259 890 +7 4232 259 202 bekker@mail.primorye.ru</p>	<p>Tel: Fax: Email</p>	<p>David F Dickins DF Dickins & Associates Ltd 1660 Cloverdale Road San Pasqual Valley CA USA 92027 - 6717 (760) 746-8688 (760) 746-8488 dfdickins@access1.net</p>
<p>Tel: Fax: Email</p>	<p>Roger J Bergman Chevron Petroleum Technology Company 6001 Bollinger Canyon Road San Ramon California USA 94583-0945 (925) 842-8492 (925) 842-8626 rogb@chevron.com</p>	<p>Tel: Fax: Email</p>	<p>Adolfo Foriero Universite Laval Pavillon Adrien Pouliot Ste. Foy Quebec Canada 418 656 2089 /2163 418 656 2928 adolfo.foriero@gci.ulaval.ca</p>

<p>Tel: Fax: Email</p>	<p>Dennis W Hinnah Minerals Management Service 949 East 36th Ave, Suite 308 Anchorage Alaska USA 99508-4363 907 271 6514 907 271 6504 Dennis.Hinnah@mms.gov</p>	<p>Tel: Fax: Email</p>	<p>Les Owen BP Pipelines (Alaska) Inc 900 E. Benson Blvd. MB11-5 Anchorage Alaska USA 1 907 564 5586 1 907 564 5588 owenl@bp.com</p>
<p>Tel: Fax: Email</p>	<p>Shinji Kioka Hokkaido University, Hydraulic Engineering Laboratory, Division of Environmental Resources Engineering, N-13 W-8 Sapporo Japan 060-8628 81-11-706-6183 81-11-726-2296 kioka@kowanws1.hyd.eng.hokudai.ac.jp</p>	<p>Tel: Fax: Email</p>	<p>Andrew Palmer Cambridge University Engineering Department Trumpington Street Cambridge UK CB2 1PZ +44 1223 332718 +44 1223 332662 acp24@eng.cam.ac.uk</p>
<p>Tel: Fax: Email</p>	<p>Hiromitsu Kitagawa Hokkaido University School Sapporo 06 Hokkaido Japan +81-11-706-7249 kit@eng.hokudai.ac.jp of Engineering</p>	<p>Tel: Fax: Email</p>	<p>Ryan Phillips C-CORE Memorial University of Newfoundland St. John's Newfoundland Canada A1B 3X5 709 737 8354 709 737 4706 ryanp@morgan.uccs.mun.ca</p>
<p>Tel: Fax: Email</p>	<p>Terrence Lyons Asian Office of Aerospace Research & Developmeny 7-23-17 Roppongi, Minato-ku Minatu-ku Tokyo Japan 106-0032 +81-3 5401-4409 +81-3 5410-4407 lyonst@aoad.af.mil</p>	<p>Tel: Fax: Email</p>	<p>Anatoli Polomoshnov Sakhalin Oil and Gas Institute 18 Karl Marx St. Okha Sakhalin Region Russia 694460 424 370 5495 +872 140 4221 ice@smng.com</p>
<p>Tel: Fax: Email</p>	<p>Jim McHale Alaska Clean Seas Pouch 340022 Prudhoe Bay AK USA 99734-0022 (907) 659-3249 (907) 659-2616 JMcHale@AlaskaCleanSeas.org</p>	<p>Tel: Fax: Email</p>	<p>Koji Saka Saka Consulting Inc. Suite 505, Yoyogi Skyheights, Yoyogi 4-23-5 Shibuya-ku Tokyo 151 Japan +81 3 3376 2390 +81 3 3376 2660 ksaka@email.msn.com</p>
<p>Tel: Fax: Email</p>	<p>Shumei Narita Ship Research Institute, Ministry of Transport 6-38-1 Shinkawa, Mitaka Tokyo Japan 181-0004 0422 41 3157 0442 41 3152 narita@srilot.go.jp</p>	<p>Tel: Fax: Email</p>	<p>Hung Tao Shen Clarkson University Department of Civil & Environ. Engrg. Potsdam NY USA 13699-5710 (315)-268-6606 (315)-268-7985 htshen@clarkson.edu</p>

<p>Tel: Fax: Email</p>	<p>Kunio Shirasawa Hokkaido University Sea Ice Research Laboratory, 6-4-10 Minamigaoka Mombetsu Hokkaido 094 Japan +81 1582 3 3722 +81 1582 3 5319 kunio@pop.lowtem.hokudai.ac.jp</p>	<p>Tel: Fax: Email</p>	<p>Gennady A Surkov Sakhalin Oil and Gas Institute 18 Karl Marx St Okha Sakhalin Russia 694460 424 370 5495 (011)872 140 4221 ice@smng.com</p>
<p>Tel: Fax: Email</p>	<p>Charles E Smith Minerals Management Service Technology Assessment Branch, DOI, 381 Elden Street, Mail Stop 4700 Herndon Virginia USA 22070-4817 703 787 1559 703 787 1555 smithc@smtp.mms.gov</p>	<p>Tel: Fax: Email</p>	<p>Greg R Swank Joint Pipeline Office 411 W. 4th Avenue, Suite 2 Anchorage Alaska USA 99501-2343 (907) 271-4412 (907) 272-0690 gswank@jpo.doi.gov</p>
<p>Tel: Fax: Email</p>	<p>Devinder S Sodhi US Army Cold Regions Research & Engineering Lab 72 Lyme Road Hanover NH USA 03755-1290 603 646-4267 603 646-4477 dsodhi@crrel.usace.army.mil</p>	<p>Tel: Fax: Email</p>	<p>Chris Woodworth-Lynas Petra International Cupids Newfoundland Canada A0A 2B0 709 528 4856 709 528 3056 petra@nf.sympatico.ca</p>
<p>Tel: Fax: Email</p>	<p>Igor V Stepanov Arctic & Antarctic Research Institute State Research Centre of Russian Federation, 38 Bering Street St Petersburg Russia 199397 +7 812 352 1003 +7 812 352 2688 / 1557 dspj@aari.nw.ru</p>		

PRESENTATION ABSTRACTS

Offshore Oil Development in the Alaskan Arctic: Who Bears the Risk

George Ahmaogak, *Mayor of North Slope Borough, Alaska*

Gouging in the Context of Critical Issues for Arctic Offshore Pipeline Development

Andrew Palmer, *Cambridge University*

Integrity of Offshore Pipelines: Two Recent Workshops

Charles Smith, *Minerals Management Service*

Development of offshore oil and gas resources has established the subsea pipeline as a reliable, cost effective and safe method for transporting produced hydrocarbons. Today, there are approximately 30,000 miles of pipelines on the U.S. OCS and a like number in state waters. Therefore, a pressing need in the world offshore industry throughout the next decade is felt to be the design, safety assessment and repair/rehabilitation of offshore pipelines, both for new and existing installations. In recognition of the important role that pipelines will play in developing resources in deepwater and the Arctic, the MMS has sponsored a number of international workshops in order to facilitate an improved understanding and assessment of offshore pipeline safety in general. This paper summaries the two most recent workshops undertaken to meet these goals: The International Workshop on Offshore Pipeline Risk Management and the Alaskan Arctic Pipeline Workshop. In addition, the paper presents recommendations for future pipeline needs to ensure that their record on safety and reliability is maintained.

Behaviour of Oil in Ice

David Dickins, *DF Dickins Associates Ltd.*

(paper unavailable)

Oil spills in ice have been studied extensively in U.S., Norwegian and Canadian offshore exploration areas for the past 25 years. Primary data sources include a series of medium to large scale (10's to 100's of barrels) experimental discharges in Canadian and Norwegian waters, tank and basin studies, and empirical modeling. This paper describes the important processes governing the behaviour of oil in ice, and the experience gained not only from experimental spills, but also accidental spills in a wide range of ice conditions in Finland, the United States and Canada.

The discussion will focus on scenarios involving spills from buried arctic pipelines in scour-prone areas. Spills in these environments may involve chronic long term leaks below the limits of routine detection (0.15% of flow) and batch releases from pipeline ruptures (seismic activity, material failures, ice gouging). Processes governing the fate and behaviour of the oil in these scenarios include spreading and natural containment by the ice, encapsulation of the oil in growing ice and vertical migration of the oil through warming ice in the spring. Each of these processes will be discussed in terms of the ice regimes present at the time of the spill: for example, stable fast ice contrasted with broken moving ice. The application of past experience with oil-in-ice in new arctic developments will be presented by using the Northstar offshore field, now under construction in Alaska, as an example.

Oil Spill Response in Ice Infested Waters

Jim McHale¹, David Dickens² and Nick Glover¹

1: *Alaska Clean Seas*, 2: *DF Dickins Associates, Ltd*

Ice conditions, in dynamic stages of development and degradation, are present in the Beaufort Sea adjacent to the operating oilfields on the Alaskan North Slope for over 280 days out of every calendar year. Additionally, wind driven ice invasions may occur for short periods throughout the open-water season, typically July through September. This ice presence, combined with the extreme arctic conditions routinely encountered, presents a

challenge to mounting a safe and effective oil spill response action. In order to overcome this challenge, responders must develop response action plans not only with an understanding of the physical environment but also with a basic understanding of the effect this environment will have on the fate and behavior of the spilled oil. Arctic spill response strategies worldwide have been developed through years of experience with both offshore and onshore drilling and production operations and in all types of sea and ice conditions. Alaska's North Slope oil spill response plans are based on this experience, intense field training, and the ground-truthing of related research and development projects.

Mechanical Oil Recovery In Ice Infested Waters (MORICE)

Hans Jensen and Jim McHale

"Mechanical Oil Recovery in Ice Infested Waters" (MORICE) was initiated to develop technologies for more effective recovery of oil spills in ice. This is a multinational effort that has involved Norwegian, Canadian, American and German researchers.

The program started with an extensive literature review, followed by brainstorming sessions and technical discussions to generate ideas for potential solutions to the problem. As a result, a number of concepts were suggested and discussed in detail. Most of these concepts went through qualitative laboratory testing. The lab experiments provided important insight and reduced the number of concepts that warranted further evaluation and development.

Phase 3 focused on continued development of two concepts. Detailed quantitative testing was conducted on these concepts at a larger scale in the Hamburg Ship Model Basin (HSVA) in Hamburg, Germany. In Phase 4 a complete full-scale harbour-sized prototype was constructed, comprising oil recovery and ice processing units as well as the support vessel. The prototype was tested in ice in the Alaskan Beaufort Sea during freeze-up in October 1999. Oil was not introduced during these tests.

The final phase of the MORICE program is planned to take place in 2000. Following more extensive component testing of oil recovery in ice under controlled conditions, further ice testing will be carried out in the Alaskan Beaufort Sea before the complete prototype is tested in oil and ice, probably at the OHMSETT test facility in New Jersey, USA.

Since the results from the program are proprietary information, the presentation will describe the development and status of the program at a qualitative level.

Ice Scour Morphology, Degradation Processes and Seabed Impact Rates, Resolute Bay, Cornwallis Island, Canadian Central Arctic.

Steve Blasco¹, Robert Harmes¹, Robert Myers² and Rikk Kvitek³

1: Geological Survey of Canada, 2: Canadian Seabed Research Ltd., 3: California State University.

(paper unavailable)

Sea-ice and associated pressure ridges dominate the ice regime in the coastal waters of southern Cornwallis Island near Resolute Bay. Small icebergs and ice island fragments occasionally drift into the area. Deep ice keel impacts with the seabed in water depths ranging from 50 to 10 m were investigated between 1991 and 1999. Using sidescan sonar repetitive mapping techniques, video transects of scours by SCUBA divers and erosion stakes embedded in scour troughs and berms, new scours with depths exceeding 0.5 m were analyzed for size, bathymetric rise-up, impact rates and morphologic changes over time. Analyzed scours ranged from 0.5 to 2.5 m deep, 10 to 400 m wide, and 25 to 1700 m long with rise-ups as great as 3 m. Scour orientation varied considerably from parallel to orthogonal to bathymetric contours. Twenty-six new scours were identified over 8 years of mapping a seabed area of 7 km². Impact rates for the 30 to 10 m water depth interval varied from 1 to 7 events per year with an average of 0.5 impacts per km² per year. No new scours were observed in water depths between 50 and 30 m. Observations of new, recent and relict scours suggest degradation processes are

dominated by current erosion of berms and troughs over time. This process is non-linear with more rapid degradation in the first 20 years and reduced rates over the next 100 years or more as scour relief is lowered.

Seashore Morphology And Lithodynamic Of The North-East Sakhalin Coast

Surkov G.A.¹, Polomoshnov A.M.¹, Zemluk S.V.², Astafiev V.N.^{1,2}, Mikishin Y.A.³, Ribokov V.F.³, Brovko P.F.⁴ and Truskov P.A.⁵

1: Sakhalin Oil & Gas Institute, 2: JSC "Rosneft - Sakhalinmorneftegaz", 3: Coastal Research Center of Far-East State University, 4: Far-East State University, 5: Sakhalin Energy Investment Co.

Coastal lithodynamics is an important phenomenon and its effect should be considered in selecting onshore crossings for subsea pipelines and sites for onshore facilities. Coastal lithodynamics of the north-east Sakhalin coast has been studied by the Oil and Gas Institute "SakhalinNIPImorneft" for several decades. The results of the study are presented.

Can Seabed Gouge Survey Data Be Applied to Prediction of Maximum Depths of Ice Keel Penetration?

Igor Stepanov, *Arctic & Antarctic Research Institute*

Evaluation of maximum depths of penetration of ice feature keels into seabed soil is one of the most important problems which should be solved to provide appropriate protection against ice damages of submarine pipelines on arctic shelf and in other shallow regions of ice-infected waters. Conventional approach to such an evaluation is developing ice gouge survey studies and further statistical analysis of the measured gouge depths. By means of assessment of ice gouge depth probability distribution, the maximum gouge depths corresponding given probability of exceedance are calculated. There are a number of reasons why estimates based on application of this approach can not be considered reliable enough. In particular, measured gouge depth does not always coincide with actual depth of ice keel penetration (this latter value is usually of practical interest for submarine pipeline design). This discrepancy mainly results from the gouge infilling by surrounding soil; rate of such an infilling can hardly be predicted with required accuracy. But even if actual depth of ice penetration is found out somehow, confident assessment of this depth probability distribution scarcely achievable. In fact, a researcher has the following alternative. One of two variants is evaluation of the probability distribution of depth in a given (quite small) area of seabed by means of processing of measurements obtained in this particular area. In such a case, number of observation will be probably not sufficient to get reliable estimate. An attempt to employ data from a larger area (or from other regions) would result in another difficulty. Measurements performed in area(s) with other angles of sea bottom slope, soil properties, direction and velocity of currents, geometry of ice features, etc. are not representative for the particular small area. Simple subdivision of seabed areas depending on only sea depth gradation (as it is done quite frequently) is definitely not sufficient. In accordance with author's understanding, the most appropriate solution of the problem under consideration is employing (and comparative analysis of) not only ice gouge survey data but also results of theoretical consideration including output of numerical simulation the gouging process.

Crushing Failure During Edge-Indentation of Floating Ice Sheets

Devinder Sodhi, *CRREL, US Corp of Engineers*

Small-scale indentation tests were conducted with compliant structures and freshwater ice sheets. Besides measuring forces and displacements, we installed grid-based tactile pressure sensors at the ice-structure interface to measure the pressure generated during an interaction. Similar to the results of earlier studies, the results of the present study with compliant structures show that there is ductile deformation of ice at low indentation speeds and continuous brittle crushing at high indentation speeds. During a typical cycle of the dynamic ice-structure interaction at intermediate speeds, the tactile sensor data indicate that the ice deforms in a ductile manner during the loading phase, and fails in a brittle manner during extrusion phase. Theoretical estimates of global force are given in terms of non-simultaneous local force per unit width during continuous brittle crushing. We find the effective pressure measured during small-scale indentation tests to be close to those measured on full-scale structures, when the indentation rate is high in both situations.

Ice Aspects of Ice Scour

Ken Croasdale¹, Richard McKenna², Ryan Phillips²

1: *KR Croasdale & Associates*. 2: *C-CORE*.

To date, most classical treatments of the ice scour problem either ignore the ice or assume it has infinite strength and driving force. Extreme scour depths and frequencies are developed from the ice scour record. Furthermore, it is generally assumed that pipelines and other sea floor facilities must avoid ice contact by trenching or burial below the extreme depth of scour plus an allowance for sub scour disturbance. These approaches are understandable given the scour evidence which suggests that the forces to create extreme ice scours are likely to be larger than conventional pipelines can resist (Palmer, 1998).

The classical approach to designing for ice scour and avoiding direct ice contact, requires high confidence in being able to define extreme scours from the ice scour record. This can be problematic in regions where the combination of sea floor properties and oceanographic conditions leads to either rapid erosion or in-fill of the scours. In these situations, attempts are made to develop values for scour depths and frequencies from the ice characteristics. This requires a framework for the inclusion of limits to scour depth based on ice strength, driving forces and momentum, as well as soil strengths, ridge depth and ridge frequency statistics. This framework is similar to those developed for ice loads on structures. However, in the case of ice scour it is the strength of the ice at the base of the keel, which is of interest and which is often hard to determine.

Knowledge of ice driving forces and keel ice strengths is also required to assess ice forces on sea floor pipelines and other facilities subject to direct ice contact. This could be either by design - if it is considered more economical to design the facility for direct contact than to bury it, or by accident - if a deeper scour than anticipated occurs. Direct contact by ice can cause local damage (denting or puncturing) or global failure (overall bending and tensile failures of pipelines). On the other hand, a pipeline with sufficient wall thickness or armoring, combined with a suitable distributed anchoring system, may be feasible and cost effective, especially if ice-feature bottom-strengths and driving forces are low enough.

This paper reviews the issues relating to the influence of ice strength and ice driving forces on ice scour processes, and especially on designing pipelines and sea floor facilities for direct ice action. The keel ice strengths of various ice features and ice driving forces are reviewed. Typical calculations are presented for loads due to direct ice action. Uncertainties and future directions for this aspect of the ice scour problem are discussed.

Comparison of Ice Strength and Scour Resistance

Jack Clark and Fanyu Zhu, *C-CORE*

This presentation reviews various ice/soil and ice/structure interaction concepts. The interaction of ice and soil is studied in terms of contact area between the ice and the soil. It is well known that the failure pressure of ice decreases with contact area. This has been demonstrated for level ice and icebergs, The relationships between size of feature and strength for keel of ice pressure ridges is less well known but would logically follow the same trend. The ice surface in contact with the soil is treated as an inclined footing. The bearing capacity of the soil increases with the footing size while ice strength decreases with the size of the contact area. The strengths of ice and soil versus contact area are compared when the friction angle of soil is from 20 to 50 degrees. From the results of analysis, it is concluded that for ice/soil interaction, either ice or soil may fail, depending on contact area. The larger the contact area, the more likely for the ice to fail rather than the soil. For strong soils with friction angles of 40 to 50 degrees, only small ice contact areas can penetrate the seabed.

Discrete Element Simulation of Ridge Keel Resistance During Scouring: A Preliminary Study

Michael Lau¹, Ryan Phillips¹, Richard McKenna¹ and Stephen Jones²

1: *C-CORE*. 2: *IMD-NRC*

Ice scouring is a complex process, which involves the interaction of an ice feature and the seabed soil. Conventional approaches have been focused on deformation behavior of seabed soil while assuming sufficient driving forces transfer through the ice feature to scour the seabed. While this assumption may be valid for solid ice features such as icebergs, validity of its application to ice feature like loosely consolidated first year ridge keels is uncertain. For ice ridges, the keel may deform and fail before sufficient forces required to scour the seabed can be transferred.

This paper reports the preliminary results of a series of discrete element simulations. These simulations looked at the behavior of the ridge keel during idealized ice scouring events, and provided insights on how a scouring ice keel transmits the forces required to scour the seabed. A 2-D discrete element code, DECICE2D, was used. Important parameters include the angle the ice makes with the seabed, the velocity, the degree of confinement, and the shear strength of the ridge keel. Preliminary results suggest that a large confining pressure could develop at the frontal contact between the keel and the seabed. This confinement resulted in keel resistance significantly higher than that predicted from existing analysis.

Behavior of Ridge Ice at a Time of Ice Scouring

Shinji Kioka¹, Yoshikatu Yasunaga¹, Hideyuki Nishimaki² and Hiroshi Saeki¹

1: Hokkaido University, 2: Shimada Kensetu Co,Ltd

Ice scouring is a phenomenon which occurs when ice (pressure ridge, hummock or iceberg) moves in contact with seabed. It has been reported to have caused damage to communication cables and water intake pipelines. In condition that further oil or natural gas exploration projects in offshore areas of the arctic seas is becoming popular, more care must be taken over the design and installation of oil pipelines in such areas in order to avoid accidents due to ice scour. Therefore, it will be very important to estimate rational maximum scour depth due to complicate behavior of ice, and will also be very important to evaluate forces acting on sea bed and stress that is transmitted via the seabed and deformation of soil due to the loads.

In our previous researches, we concluded that local fluctuations in ice forces (bulldozing forces) in the horizontal direction depended on the slope at the corresponding point on the scour curve (the path of motion of the model ice in plane), and in many cases, ice was tend to move upward. If we understand its mechanisms, we could estimate more rational maximum scour depth. So, it is important to acknowledge the behavior of ice at a time of ice scouring.

Now, we have developed the rational experimental device system as compared to previous device system (Kioka and Saeki, 1995,1998), and further approached our experimental conditions(attack angle, travelling velocity and seabed slope) to real conditions. And scour length (travelling distance of the ice) was further lengthened (more than 6 times longer than previous tests). Under the renewal conditions, we conducted a lot of test series, and we revealed relationships between ice forces and behavior of ice , variations of its behavior due to varies condition(attack angle, travelling velocity). And we also revealed the probability distribution of some random variable under the same experimental condition.

Numerical Simulation of Ice Scour using a Static Elastoplastic FEM Analysis and a Steady State Semi-Analytic Power Law Solution

A. Foriero¹ and A. von Keviczky²

1: Université Laval, 2: Concordia University

The knowledge of stress and strain rate associated with plastic flow during ice scouring of marine beds is of great practical importance from the viewpoint of optimally determining the secure burial-depth of pipelines. A complete exact solution of the problem is extremely difficult because the governing equations of plastic flow are highly non-linear due to such common factors as non-linear material behaviour, interface friction and temperature.

Consequently clay flow pattern and velocity field solutions, generally obtained by using simplifying assumptions, provide an interesting approach. An analysis with rate dependent clay, by using the complex stress and stream functions, was proposed by Foriero (1998) and Foriero and Keviczky (1999). In the present study a small strain finite element analysis will be used in order to validate the proposed model. This is possible because the stationary solution corresponds to the conventional static elasto-plastic one.

The horizontal and vertical velocities, strain rate and stress components are found for various strain rate hardening parameters. The analysis illustrates that the velocity and strain rate components are independent of the power law exponent.

FEM simulations of ice scouring in layered seabed profiles are also examined. In particular, limitations of the proposed model with regards to cohesionless layered seabed profiles are discussed. Finally the study ends with the general direction of future studies.

Measuring Sub-Scour Soil Displacements in Different Soil Types Using Examples from the Geological Record

Chris Woodworth-Lynas, *PETRA International*
(paper unavailable)

The vertical extent and amount of displacement of soils affected by ice scour in the zone below the scouring keel can be defined. This knowledge is one of the key determinants for the required trench depth at which a pipeline can be considered safe from the damaging effects of scour events. Small scale and centrifuge physical modelling have been of enormous use in defining the extent and amount of sub-scour soil deformation. Physical model results have been transposed into discrete element models and simulations (e.g. Lau et al. this symposium) that can now be used in the pipeline design process.

Much work has gone into understanding the behaviour of soils such as pure clays, silts and sands, and simple layered soils (e.g. sands and clays). Sub-scour effects in coarser granular soils, and in particular mixed soils (with clay, silt, sand and gravel), is less well known. Granular and mixed soils characterize much of the offshore regions where ice scouring occurs (e.g. Blasco, this symposium).

Thorough study of ice scour-affected granular and mixed soils cannot be carried out offshore due to logistical restrictions. However, scour-affected soils can be studied on land at several localities worldwide where they are exposed to view in a variety of ancient strata from the Ordovician to the Pleistocene. Careful examination and measurement of these preserved examples is an inexpensive way to define the nature and extent of sub-scour displacement in a variety of mixed "natural" soils.

Choosing Optimum Underwater Pipeline Burial Profile on Northeast Sakhalin Shelf

Surkov G.A.¹, Truskov, P.A.³, Zemluk, S.V.², Polomoshnov, A.M.¹ and Astafyev, S.V.¹

1: *Sakhalin Oil and Gas Institute*, 2: *Rosneft – Sakhalinmorneftegaz Company*, 3: *Sakhalin Energy Investment Co.*

The drifting hummocks and stamukhas present main threat for underwater pipelines in the ice seas. The main mode of protection of a pipeline in such conditions is burying them into a sea bottom. In selecting the optimum burial depth, rated probability of damage P_n of a pipeline is taken into account as well the cost of the pipeline for burial depth C .

The choice of the pipeline burial depth is controlled by the following factors:

- a) frequency of penetration of hummocks for the given depth of water;
- b) distribution of depth of hummock penetration into a sea bottom;
- c) length of the pipeline;
- d) type of ground, meteorological conditions etc.

As these parameters can vary along a route of the pipeline, the pipeline is divided into sections and the optimum profile of burial depth is selected: each sections has its own burial depth. The choice of optimum burial depth profile of the pipeline is carried out by trying of all possible options satisfying the following condition:

$$P \leq P_n \quad C \rightarrow \min,$$

where P - probability of damage of the entire pipeline by drifting hummocks. The parameter P_n lies within the limits of 0.001÷0.0001. Despite of the work done under the projects of Sakhalin - 1, Sakhalin – 2, a problem on parameters a) and b) is still not solved. The experience has shown that parameters a) and b) are strongly garbled by lithodynamic processes. The author proposes a technique for obtaining parameters a) and b) based on mathematics modelling with field data on the depth of drift hummock penetration into the sea bottom. The effect of lithodynamic processes on a choice of pipelines burial depth is discussed. The 40-year's experience of a trouble-free operation of the underwater pipeline through the Nevelskoy Strait is discussed.

Response of Buried Arctic Marine Pipelines to Ice Gouge Events

Kenny, S., Phillips, R., McKenna, R.F., Clark, J.I. *C-CORE*

For Arctic marine pipelines, the risk of potential damage due to ice gouges caused by pressure ridges and icebergs is a significant concern. Some fundamental parameters for both ice/soil and soil/pipeline interaction are addressed. Pipeline response to subgouge soil deformations is modelled by fully nonlinear finite element analysis using two-dimensional pipe elements coupled to discrete soil springs. The effects of internal pressure, ice bearing pressure, ice gouge width and depth on the longitudinal strain response of a buried pipeline are investigated. Characteristics of the soil response functions are reviewed and implications on pipeline design are addressed.

Reference:

Kenny, S., Phillips, R., McKenna, R.F. and Clark, J.I. (2000). "Response of Buried Arctic Marine Pipelines to Ice Gouge Events." Proceedings, ETCE/OMAE2000 Joint Conference, Energy for the New Millenium, New Orleans, LA, USA, Paper Number OMAE00-5001.

Welding Challenges for Strain-Based Design

Robin Gordon¹, John Hammond², Greg Swank³

1: Edison Welding Institute. 2: BP Amoco plc. 3: Alaska Dept. of Natural Resources, Joint Pipeline Office

Rigorous engineering analysis utilizing detailed site-specific data can result in acceptable strain-based designs that operate within acceptable integrity, safety, and environmental protection limits. Progress is being made relative to pipeline welding evaluation, however, no prescriptive guidance for strain-based design procedure qualification testing is currently available. A need to develop general pipeline welding procedure guidance when imposing a strain base design exists. The authors suggest that in the interim, designers should use best engineering practices to evaluate the adequacy of the girth welded joint to perform to the intended limit states plus perform full scale demonstration bend tests as required. Further recommendations on weld metal strength, toughness and supplemental weld procedure qualification tests are provided for designer's consideration and evaluation.

To a Problem of Construction of Sea Pipelines in the Freezing Seas

Alexander Bekker, *Far Eastern State Technical University*

Northstar Pipeline Project Beaufort Sea, Alaska, Supplemental Leak Detection System

Les Owen, *BP Pipelines (Alaska) Inc.*

**OFFSHORE OIL DEVELOPMENT IN THE ALASKAN ARCTIC:
WHO BEARS THE RISK
Mombetsu, Hokkaido, Japan**

**ADDRESS OF MAYOR GEORGE N. AHMAOGAK, SR.
NORTH SLOPE BOROUGH, ALASKA, U.S.A.**

Good morning. I am George Nasuayaaq Ahmaogak, and I am an Inupiat Eskimo and the elected Mayor of the North Slope Borough, the regional government in northern Alaska. I want to thank the Alaska Region of the U.S. Minerals Management Service, the workshop organizers, and our gracious hosts here in Mombetsu for the opportunity to speak today at this important gathering. I have always found that the colder the place I visit, the warmer the reception I receive. I think that's because regardless of their home countries, northern peoples share so much in common. Our environment has shaped and continues to enrich us. No matter what modern conveniences we may now finally enjoy, we remain intimately tied to the land and water we depend upon for our traditional foods and for our cultural identity. It's the same everywhere across the northern regions of the world. While we are not in the Arctic now, the conditions here certainly resemble those I left behind in Barrow, my home in Alaska some 330 miles north of the Arctic Circle. I look forward to visiting with all of you while I am here, and especially those of you who call this unique and beautiful region of Japan your home.

I want to speak today about my home, my people, our culture, and our relationship with the increasingly active oil industry in northern Alaska. First, a bit of background to help put my comments in some context. The North Slope Borough was formed in 1972. It is the regional municipal government which encompasses a territory of approximately 88,000 square miles of northern Alaska. The diverse lands of the Borough stretch from the shores of the Chukchi Sea on the west and northwest, to the Canadian border on the east. They reach from the Brooks Mountain Range in the south, to Point Barrow and the shores of the Beaufort Sea in the north. All of the land within the Borough lies above the Arctic Circle. The 7500-plus Borough residents live in eight villages with populations ranging from approximately 230 to 4700. About three-quarters are Inupiat Eskimos. The Prudhoe Bay oil field lies within the North Slope Borough. It is the largest oil field in the U.S. A property tax base that includes Prudhoe Bay has generated sufficient revenues to bring our residents services that did not exist before the incorporation of the Borough. We are still working to bring all of our villages modern sanitation, water, housing, fire protection, education, health care, public transportation, and other services long taken for granted elsewhere in our country.

Despite recent improvements in our standard of living and the introduction of a widespread cash economy, we remain a people whose lifestyle is characterized by the central importance of subsistence. Subsistence is more to us than simply hunting and eating fish and game. It is the cooperative pursuit, harvest, processing, distribution, storage, and consumption of wild foods. It is also the utilization of materials gathered for clothing, tools, crafts, and ceremonial purposes. As a father and grandfather, I also recognize that education of our youth in the great many skills demanded by a subsistence

lifestyle is one of the most important aspects of my culture. All of these subsistence activities bind residents together as a single extended community. The most important of our subsistence activities is the pursuit of the bowhead whale, and I will highlight that activity in the slides I will show in a few minutes.

While it is true that the oil industry is our primary revenue source, the Borough's relationship with oil companies and the agencies which regulate them has not been without conflicts. All of the oil production in our region to date has occurred onshore or in nearshore waters connected to shore by causeways. In the early days of onshore oil exploration and production, the industry was just learning how to function in the harsh arctic environment. Many mistakes were made. Agency oversight was lax. The environment paid the price. Decades later, the tundra still shows the scars of seismic and other vehicle tracks, abandoned drillsites, and gravel mines. Hazardous waste sites await cleanup. Early pipelines, built low to the ground, block the free movement of caribou, other wildlife, and our subsistence hunters.

The good news is that the oil industry in Alaska has made vast improvements in the way it operates onshore. These changes have come with experience, with improved regulations, with more rigorous agency oversight, with better science, and with the aggressive involvement of the Borough and other concerned North Slope organizations. Today, in most locations and with proper oversight, the risks posed by onshore industrial operations are manageable.

Our views regarding offshore industrial operations are different. We continue to have serious concerns about the ability of the oil industry to operate safely in arctic waters. At risk is the arctic marine environment, subsistence and other wildlife resources, and the subsistence lifestyle and culture of my Inupiat people. The Beaufort Sea is a harsh working environment. It is also a unique and vulnerable ecosystem.

Borough residents have experienced the impacts of offshore oil exploration for more than two decades. We now face the potential impacts of offshore oil production. The threats posed by offshore exploration and production activities are of two primary types; noise impacts and oil spill impacts. Noise impacts to wildlife resources and to traditional subsistence harvests have occurred, and will continue to occur even when operations take place as planned. Oil spill impacts to wildlife resources and to subsistence activities could be catastrophic.

This workshop is particularly timely for me and for the residents of northern Alaska who I represent. Two current proposals by British Petroleum would see the first stand-alone offshore production facilities constructed in the Beaufort Sea. Both projects would utilize man-made gravel islands and buried subsea pipelines for transportation of oil to shore-based facilities. As we meet here today, production facilities associated with BP's Northstar Development Project are being constructed in the Beaufort Sea. If BP receives the necessary permits, construction of the Liberty Development Project would begin in two years.

If you understand the central importance of bowhead whaling among all of our subsistence activities, you should understand our great concern over the prospect of oil production facilities and operations expanding offshore into the Beaufort Sea. The noise from a single project in certain locations or from multiple projects has the potential to deflect whales away from their traditional migratory path. The whales could be deflected out of the reach of our whaling crews, or the crews will have to travel greater distances under dangerous conditions to find animals. The Borough, along with the responsible federal agencies, will require monitoring programs associated with these offshore development projects. The monitoring programs will be designed to characterize the noise generated by project facilities and operations, and to assess any impacts on wildlife resources and subsistence activities.

The devastation that would result from a major oil spill is something that we all want to avoid at all costs. That of course means that we should do all we can to prevent a spill. It also means that the industry should have the capability to effectively deal with a spill under arctic conditions if one occurs. We have asked for years for a realistic demonstration of the oil industry's abilities to deal with a spill under the difficult conditions which exist offshore much of the time in the central Beaufort Sea. We have yet to see such a demonstration, and remain unconvinced that a significant spill could be effectively responded to in anything but near ideal conditions. I look forward to hearing what you experts have to say during this workshop about the design of marine pipelines, and their ability to function under arctic conditions. I only ask you to remember that if one of these pipelines fails in the Alaskan Beaufort Sea, it is my people, my children, my culture, and the wildlife resources we respect and depend upon which will suffer.

I now have some slides which I hope will give you a better appreciation for the environment, the resources, and the traditional Inupiat subsistence culture at risk as the oil industry directs increasing attention offshore in the Arctic. Photographer Bill Hess, who we have allowed to document our activities for the past fifteen years, took these photos. Bill has shown a great respect for our culture, and has captured in these and other images many of the things we consider most precious about our homeland in Alaska. I will be available to answer questions after we view the slides. I hope you enjoy them.

GOUGING IN THE CONTEXT OF CRITICAL ISSUES OF ARCTIC OFFSHORE PIPELINE DEVELOPMENT

Andrew Palmer (Engineering Department, Cambridge University, Cambridge, England)

Introduction

The objective in this paper is to examine decisions about gouging in the broader context of the design of Arctic submarine pipelines. A design inevitably involves many decisions: they interact in complex ways, and none of them can be considered in isolation.

This is naturally well known to engineers generally, and of course to the designers of pipelines. They know, for example, that many pipelines have to be buried. Among the reasons for burial are to hold the pipeline down against the possibility of upheaval buckling (in which the pipeline arches upward out of the seabed), to protect the pipeline against fishing gear, and to give the pipeline additional thermal insulation to help maintain the temperature of the contents. Each of these objectives can be accomplished in other ways. It follows that a designer concerned with one objective has to see that objective in the context of all the others. If she decides that the pipeline has in any event to be buried to protect it against upheaval, then that decision in turn influences choices between insulation options. An additional complication is the fact that if the pipeline runs hotter because of better insulation by the rock or soil it is buried in, then the driving force for upheaval is greater, because it is the axial compressive force induced by temperature and pressure. This is of a simple instance of the 'design spiral'.

The overall context, as George Ahmaogak eloquently points out in his keynote address to this meeting, is that the Arctic offshore is a precious and vulnerable environment, important to the fauna and flora, to the local human community, and to the wider human community. The petroleum industry can operate safely in the Arctic environment, but on a zero-defect basis: one error will not be forgiven.

This paper examines the different problems that arise in the design of Arctic pipelines. Intentionally, it starts with the easier problems, and goes on to those that create greater difficulties and might become 'show-stoppers'. It leaves aside decisions that are routine and understood parts of marine pipeline engineering, and that are not greatly different in the Arctic from elsewhere: corrosion and stability design are examples.

Some of the technical aspects of these ideas are developed more fully in a paper [1] at the Offshore Technology Conference, and in earlier papers on gouging [2,3].

Problems other than gouging

Strudel scour occurs in areas close to the mouths of Arctic rivers. In the spring, the rivers thaw while the sea is still frozen, and river water floods out over the sea ice. If the river water encounters a hole or a crack, the water pours downwards through the hole, and forms a rotating jet ('strudel'), which in extreme cases can excavate a large hole in the seabed. If that hole should happen to intersect a trench or buried pipeline, the pipeline might be overloaded by hydrodynamic forces, or might be set into vortex-excited oscillation and might fail by fatigue.

Damage by this mechanism is certainly conceivable, but it requires a coincidence of a number of conditions:

- 1 the strudel has to coincide with the pipeline; and
- 2 the strudel jet has to be powerful enough, and at the same time the water shallow enough, for the seabed to be eroded; and
- 3 the seabed has to be eroded deeply enough for a buried pipeline to be exposed over a substantial length; and
- 4 the jet has to reach the pipeline, and still have a high enough velocity to cause damage (and, in the cause of vortex-excited oscillation, to persist long enough for damage to occur).

Point 1 is important, and the probability of the required coincidence is rather low. Strudel scour is a point phenomenon: for damage to be possible, the point where the strudel forms has to coincide with the line of the pipe. In contrast, gouging is a line phenomenon, and gouging damage requires the intersection of two lines, the gouge line (a random walk driven by current and wind, and modified by interaction with the seabed) and the line of the buried pipe.

Most strudel scours are rather shallow. A pipeline in an area subject to strudel scour would almost certainly in any event be buried to a substantial depth to protect it against gouging. Only a small proportion of strudel scours are simultaneously deep enough to meet condition 3 and wide enough to meet condition 4. Simple calculations [1] for a typical large-diameter line suggest that any credible combination of water depth, burial depth, strudel diameter and jet velocity would not be enough to lead to either a deformation and rupture limit state or to a fatigue limit state.

A second possible problem is leak detection. Leak detection in the Arctic is centrally important, because of the sensitivity of the environment to even very small amounts of oil (though much less so to gas), the possibility that oil might be trapped and spread under sea ice but not be observed on the surface, and seasonal constraints on the deployment of inspection equipment such as remotely-operated vehicles. Leak detection based on mass balance is inherently of limited sensitivity, and much work is being done on acoustic and chemical methods, which are capable of extraordinary sensitivity. Because leak detection

is important to petroleum operations everywhere, not just in the Arctic, it is reasonable to conclude that high-performance leak detection technology will be available when the industry and the regulators demand it. Compatibility between leak detection and other aspects of the pipeline system might prompt a change in configuration. One idea that has been put forward is a pipe-in-pipe system, which allows the annulus to incorporate leak sensors, and allows the annulus to be continuously sniffed to detect leaks, while the outer pipe provides a second containment barrier.

A third possible problem is permafrost in shore crossings [4,5]. Some shore crossing design concepts are indeed potentially very vulnerable to thaw by heat conducted from a pipeline. Other design concepts are much less vulnerable, and the optimal strategy is to select a design which minimises the problem. Horizontal drilling has many other advantages – not least in minimisation of environmental impact – and allows extensive experience of well drilling through permafrost to be brought to bear. Without discounting the careful engineering that needs to be carried out, this seems to be a containable problem that can be overcome by design.

The more difficult and challenging problems relate to construction and gouging.

Construction

Construction is a harder subject to get right than design is. There are good reasons for that. The development of new kinds of construction equipment, and trials of new construction methods, are orders of magnitude more expensive than design studies or research in the laboratory, or even some kinds of field experiment. Contractors are understandably and correctly extremely reluctant to invest in research and development of new techniques, unless they have a high degree of confidence that their investments will pay back within a reasonably short time. There are many examples of contractors who burned their fingers with over-confident investment which did not pay off. It is occasionally suggested that only the bad ideas fall by the wayside, and that survival of the fittest governs technological development. There is no justification for this complacent view: many good ideas get lost as well [6].

In the past, 20 or 30 years ago, oil companies recognised this, and were prepared themselves to invest, or more or less to promise that investment would be rewarded with contracts. Several worthwhile and successful technological developments can be traced back to that willingness [6]. The current climate, particularly since the new fashions forced on oil companies by two sudden collapses in the oil price, has led oil companies to take the position that they are not prepared to invest in technology, and to say to would-be developers “we will not invest now: develop it and get it working, and then we might possibly be interested”.

Even in better-understood fields such as deepwater pipelaying, bold moves forward in technology have needed deep pockets and iron nerves. What may happen in the Arctic is that the understandable absence of investment in the past will combine unhappily with

lack of experience, risk aversion and the absence of R&D, to lead to troubled construction projects, linked to cost overruns and long delays. It is difficult to see what can be done to resolve this.

Several areas are potentially troublesome. One is construction from the winter ice, which has been applied extensively in the Canadian Arctic. In the Drake F76 flowline construction project [7], long ago off Melville Island, ice-based construction worked very well, but it has to be said that at that time the potential difficulties of using ice as a construction material were not fully understood. At that sheltered location the winter ice was extremely stable, moved less than 1 m during the on-ice construction period (February through April), and was not adversely affected by the cutting of a 1000 m slot, a large hole, and several smaller holes. However, sea ice is quite extraordinarily brittle, has a fracture toughness about one-tenth of that of glass [8,9], is inhomogeneous and full of pre-existing cracks and brine channels, creeps, is within a few degrees of its melting point, and is pushed around by very large environmental forces. It is not completely unfair to think of an analogy of marine construction based on a floating sheet of heavily-cracked glass loaded by large edge forces, which suggests that it will not be without problems.

Almost certainly, Arctic marine pipelines will need to be trenched into the seabed, often to a depth of several metres. That is not beyond the reach of dredging techniques, but it is beyond conventional pipeline trenching equipment, because pipeline trenches are normally required to have depths only between 1 and 2 m. Trenches will also need to be backfilled. The potential demand for very deep Arctic trenches has been recognised for a long time, but it has suffered from the lack of investment mentioned above.

Gouging

Gouging has been recognised as a potential ‘show-stopper’, at least since it was understood that gouging is a contemporary process and estimates were made of the ice forces that must have been applied to cut the large gouges that are frequently observed. The problem became more serious still with the realisation that large deformations occur beneath gouges [3], so that a pipeline trenched below the maximum gouge depth is not necessarily safe.

A complete solution to this problem is still some way away. The prudent strategy that has been adopted in at least one current project is to select the trenching depth very conservatively, so that the top of the pipe is set at a depth below the mudline equal to several times the maximum observed gouging depth. That strategy is straightforward in a relatively benign gouging environment, but would be expensive in an aggressive gouging environment with temporally and spatially frequent gouges several metres deep.

Only limited information is available about the extent of subgouge deformations, which have been measured in centrifuge model tests [3] and in field observations on relic gouges. Most of the tests were on a model clay, and little is known about how the

deformations depend on the type and geotechnical history of the soil. From the mudline to the level of the deepest significant subgouge deformations, the seabed soil has been repeatedly remoulded by previous gouges, over a timescale which is very short geologically (in comparison with major changes in sealevel, for example) but long by comparison with the interval between extreme gouging events. It follows that the gouges important in design are invariably gouges in soil which has been remoulded into a critical state. This aspect of the problem has not been represented in model tests. It has also been suggested [10] that geotechnical data ought to reveal the depth of remoulding, and that this may be a better way of getting at the extreme subgouge deformation depth, rather than extrapolation from observed gouge depth statistics combined with a subgouge deformation model.

Though the geotechnics are extremely interesting, the response of the pipeline itself is more important to decisions about safe strategies to protect the pipeline against gouging. Modern design methods for pipelines are based on a limit-state philosophy [11], which concentrates attention on states which directly threaten the environment and continuing safe operation. The limit state that most concerns us is any rupture which allows the contained fluid to escape. Yield, local wrinkling, large deformations and buckling are not themselves limit states, and experiments show that pipelines can be buckled without leaking (though buckling is undesirable for other reasons, such as obstruction to flow and to the passage of pigs).

Conclusion

This suggests the unsurprising conclusion that analysis should focus on rupture limit states, and that it can usefully apply methods developed in other contexts, such as pipeline resistance to landslides in mountainous terrain. Some preliminary work indicates that these limit states are not necessarily sensitive to the details of the subgouge deformation. That in turn suggests that the most useful experiments will be those that incorporate pipelines. Full-scale trials are better still, but they are expensive and may encounter regulatory and environmental difficulties.

Acknowledgment

The writer's research is supported by the Jafar Foundation.

References

- 1 Palmer, A.C. Are we ready to construct submarine pipelines in the Arctic? In
press, Proceedings, Thirty-second Annual Offshore Technology Conference,
Houston, OTC12183 (2000).
- 2 Palmer, A.C., Konuk, I, Comfort, G. and Been, K. Ice gouging and the safety of
marine pipelines. Paper OTC6371 in Proceedings, Twenty-second Offshore
Technology Conference, Houston, 3, 235-244 (1990).
- 3 Woodworth-Lynas, C.M.L., Nixon, J.D., Phillips, R. and Palmer, A.C. Subgouge
deformations and the security of Arctic marine pipelines. Paper OTC8222 in
Proceedings, Twenty-eighth Annual Offshore Technology Conference, Houston,
4, 657-664 (1996).
- 4 Walker, D.B.L., Hayley, D.W. and Palmer, A.C. The influence of subsea
permafrost on offshore pipeline design, Proceedings, Fourth International
Conference on Permafrost, Fairbanks, National Academy Press, 1338-1343
(1983).
- 5 Marcellus, R.W. and Palmer, A.C. Shore crossing techniques for offshore
pipelines in Arctic regions, Proceedings, Fifth International Conference on Port
and Ocean Engineering under Arctic Conditions, Trondheim, 3, 201-215, (1979).
- 6 Palmer, A.C. Innovation in pipeline engineering: problems and solutions in search
of each other. Pipes and Pipelines International, 43, 5-11 (1998).
- 7 Palmer, A.C. , Baudais, D.J. and Masterson, D.M. Design and installation of a
submarine flowline in the Canadian Arctic Islands, Proceedings, Eleventh Annual
Offshore Technology Conference, Houston, 2, 765-772 (1979).
- 8 Palmer, A.C., Goodman, D.J., Ashby, M.F., Evans, A.G., Hutchinson, J.W. and
Ponter, A.R.S. Fracture and its role in determining ice forces on offshore
structures, Annals of Glaciology, 4, 216-221 (1983).
- 9 Sanderson, T.J.O. Ice mechanics: risks to offshore structures. Graham & Trotman,
London (1988).
- 10 Palmer, A.C. Geotechnical evidence of ice scour as a guide to pipeline burial depth.
Canadian Geotechnical Journal, 34, 1002-1003 (1997).
- 11 Palmer, A.C. The limits of reliability theory and the reliability of limit-state
theory applied to pipelines. Paper OTC8218 in Proceedings, Twenty-eighth
Annual Offshore Technology Conference, Houston, 4, 619-626 (1996).

Integrity of Offshore Pipelines: Two Recent Workshops



by
Charles E. Smith
 Research Program Manager
 Minerals Management Service
**2nd Ice Scour & Arctic Marine
 Pipeline Workshop**
 Mombetsu, Hokkaido, Japan
 February 7, 2000

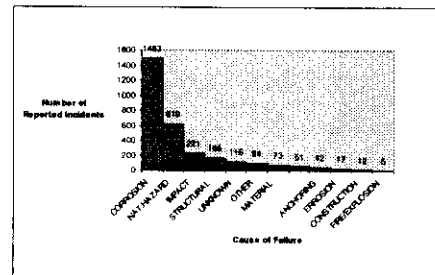
Introduction

- * Development of offshore oil and gas resources has established the subsea pipeline as a reliable, cost effective and safe method of transportation of produced hydrocarbons.
- * The need for subsea pipelines systems will continue as future oil and gas exploration results in discovery of resources in more hostile areas in the Arctic and deep waters of the oceans.
- * Integrity of pipeline systems, both during installation and throughout the operating life, is an important element for operators to improve reliability and service for economical, operational and environmental reasons.
- * In many countries, pipeline safety is now recognized as a critical public issue and failures are not acceptable.

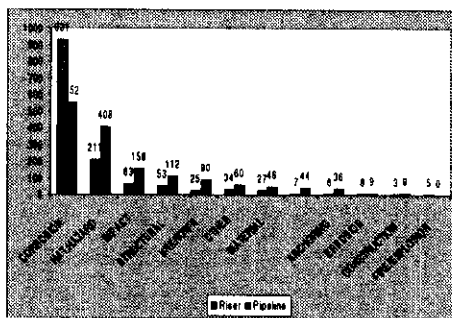
Introduction (cont.)

- * Today, there are approximately 30,000 miles of pipelines on the U.S. OCS and a similar number in state waters.
- * These pipelines have had a remarkable record of safety and reliability, and both industry and researchers are cooperating to maintain this record.

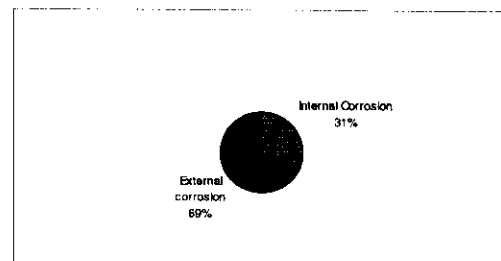
Distribution of Reported Incidents by Cause of Failure



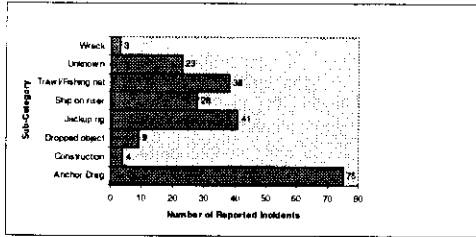
Breakdown of Failures by Cause and Location



Failures due to corrosion



Breakdown of failures due to impact by sub-category



Recent Pipeline Workshops

SUMMARY OF PROCEEDINGS FOR THE 1998 INTERNATIONAL WORKSHOP

Proceedings of the 1998 International Workshop on Offshore Pipeline Risk Assessment & Management

OFFSHORE PIPELINE RISK ASSESSMENT & MANAGEMENT

Edited by: T. G. ...

MMS

C-COAR

ALASKAN ARCTIC PIPELINE WORKSHOP

Capital Bank Hotel - Anchorage, Alaska

November 8-9, 1999



International Workshop on Offshore Pipeline Risk Assessment & Management

Two key objectives:

1. Compare alternative pipeline Risk Assessment and Management (RAM) systems, with emphasis on the analytical modeling aspects of these systems; and
2. Define ways forward that can lead to improved applications and developments of these systems for offshore oil and gas pipelines.

RAM Workshop (cont.)

- * Eight keynote presentations summarized the current state-of-practice and state-of-the-art in RAM of onshore and offshore pipelines. One keynote paper addressed maintenance and the integrity of offshore platforms (as a comparison as to what might be developed for pipelines).
- * Five presentations addressed RAM of refinery pipeline systems and other onshore transmission pipelines to seek possible applications to offshore pipelines.
- * Three presentations addressed modeling of mitigation impacts including corrosion, third party damage and determination of optimum RAM strategies.
- * Three panels addressed key aspects of pipeline RAM including applicability of the three alternative approaches (Qualitative, Quantitative, and mixed Qualitative/Quantitative), links between the approaches and ways forward in utilizing and implicating the approaches.

RAM Workshop (cont.)

The keynote presentations indicated:

- * A variety of methods and approaches can be used to help maintain the safety and reliability of existing pipelines, variations of Qualitative, Quantitative, and mixed Qualitative/Quantitative approaches; and
- * A substantial body of existing technology has been and is being implemented at the present time to maintain pipeline systems, each has its advantages and limitations.

RAM Workshop (cont.)

The presentations indicated:

- * Protection against corrosion, third-party damage, and natural hazards appear to be the primary challenges for both onshore and offshore pipelines; and
- * Active work is underway within the industry to improve corrosion and third-party damage prediction, detection, characterization, assessment and protection.

RAM Workshop (cont.)

The panel discussions indicated:

- * Important differences exist between onshore and offshore pipelines, including inspectability, consequences of loss of containment, the products transported, and the pipeline environment; and
- * Because of these difference, it is expected that there will be some important differences in details of RAM for onshore pipelines compared to RAM for offshore pipelines, especially for those in Arctic/deepwater environments.

OFFSHORE PIPELINE INTEGRITY

Title: Performance of Offshore Pipelines (POP)

Principle Investigator: Winmar Consulting

Purpose:

With the resources of Winmar, Rosen, Pipeline Integrity International and the University of California at Berkeley, several pipelines over a two-year period will be smart pigged, then overpressured to failure. The failed sections will be identified and brought to shore for actual measuring of the defects. The inspection data and actual measurements will be inputted into assessment methods such as DNV 99, B31G, and RAM Pipe Requal to compare their accuracy. The accuracy of the smart pig measurements will be compared to the actual onshore measurements as well.

Alaskan Arctic Pipeline Workshop

Key objectives of the workshop:

- * To bring together members of the public and a group of experts with skills related to offshore pipeline design, operation maintenance and inspection to examine the current state of practice for pipeline alternatives under consideration for Alaska offshore oil and gas reserves.
 - ** Robust single wall design (all steel)
 - ** Pipe-in-pipe design (all steel)
 - ** Flexible pipe system
 - ** All steel carrier pipe, polyester jacket pipe-in-pipe design
- * A key aspect of the workshop was that it was open to the public and the speakers were urged to avoid highly technical discussions, formal lectures and commercial overtones, and with their expertise, to address the concerns and interest of the public sector, the regulators, the designers and the operators.

Arctic Workshop (cont.)

- * Composed of 27 invited presenters in 6 sessions
 - ** Opening session
 - *** Keynote address - "Challenges for Arctic Offshore Pipeline Developments" by Dr. Andrew Palmer
 - *** Key presentation - "Arctic Offshore Pipeline Comparison Assessment Project" by Dr. Jack Clark
 - ** Pipeline Design, Construction and Operations
 - ** Pipeline Technology
 - ** Pipeline Operational Monitoring Technology
 - ** Pipeline Risk Analysis
 - ** Regulations Panel Discussions
- * Composed of 3 breakout sessions
 - ** Design of Arctic Pipelines
 - ** Construction
 - ** Operation and Maintenance
- * 155 people attended the workshop which indicates the level of interest in Arctic Pipeline Safety

Arctic Workshop (cont.)

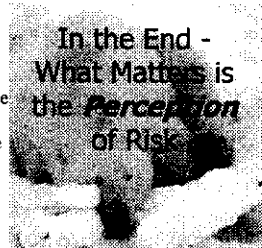
Presentations indicated:

- * Importance of regulatory aspects related to the design, construction and operation of Arctic offshore pipelines.
- * Underlined the importance of Arctic ecosystems for both physical and cultural systems - need to work together to ensure that oil spills under any circumstances should not occur or be mitigated without harm to the environment.
- * Overviews focusing on pipeline design, construction, and operations as well as operation and maintenance of the Trans-Alaska Pipeline.
- * Overview of popular pipeline risk assessment and management approaches with particular emphasis on pipeline corrosion.
- * Overview of designs of pipe-in-pipe, flexible pipe, and other related topics/applications. Typically, designs were discussed along with key issues for such systems.

Arctic Workshop (cont.)

Concluding observations: (Dr. Andrew Palmer)

- * Workshop served as a good example on how to create an informed community
- * 25 pipe-in-pipe systems in the GOM/N.S., some operated for more than 15 years with satisfactory performance providing confidence and indicating confidence for Arctic offshore pipelines
- * No consensus was reached on the "Optimum" system for Arctic offshore pipelines
- * Observed that the regulatory process like all human activities isn't perfect, but events such as the workshop are very important in expanding knowledge and involvement of the whole community



OFFSHORE PIPELINE INTEGRITY

Title: An Engineering Assessment of Double Wall Versus Single Wall Designs for Offshore Pipelines in an Arctic Environment

Principle Investigator: C-CORE, Memorial University of Newfoundland

Purpose:

The objective of the C-CORE project is to accurately document the advantages and disadvantages (technical and non-technical) of either a robust single thick walled design to a pipe-in-pipe design considering the constraints associated with an offshore Arctic pipeline project, i.e. ice cover, permafrost, scouring of the seafloor by ice, etc. and based on supporting quantitative information.

Electronic Files Available

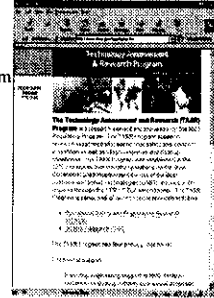
Both the RAM and Arctic Workshop Proceedings can be downloaded at the following sites:

Ram Workshop

<http://www.mms.gov/eod/tarproj/Proj282.htm>

Arctic Workshop

<http://www.mms.gov/tarp/workshop25.htm>



Closing Comments

- * With increasing environmental awareness and strengthening of regulations worldwide, the industry has been required to develop new operating procedures and technologies at an unprecedented rate.
- * To date, the oil industry has met this challenge.
- * Future promises to bring new and more challenging situations.
 - ** Aged platforms and pipelines
 - ** Arctic operations (ice scour, etc.)
 - ** Deepwater operations (slope stability, etc.)
- * To continue conducting safe and pollution free operations, industry and regulators must work as partners to formulate solutions.

Future Pipeline Needs

- * Acceptable design mitigation for Arctic/deepwater hazards (ice scour, soil movements, etc.)
- * Reliable methods to assess integrity of existing pipeline systems
- * Standardization issues for internal monitoring (smart pigs, coupons, other NDE techniques)
- * Acceptable reliability based design method (limit state criteria)
- * Improvement in the leak detection technologies and emergency shut down systems to improve response capabilities (for both abnormal and emergency situations)
- * Reliable repair methods should the need arise

Oil Spill Response in Ice Infested Waters

James E. McHale
Alaska Clean Seas
Prudhoe Bay, Alaska, USA

David F. Dickins
DF Dickins Associates, Ltd
Salt Spring Island, B.C., Canada

Nick W. Glover
Alaska Clean Seas
Prudhoe Bay, Alaska, USA

ABSTRACT

Ice conditions, in dynamic stages of development and degradation, are present for over 280 days out of every calendar year in the Beaufort Sea nearshore environment adjacent to the operating oilfields on the Alaskan North Slope. Additionally, wind driven ice invasions during the open water season, typically July through September, may also occur for periods of seven to ten days, each with concentrations of 2/10 to 4/10 (concentration refers to the area of surface water covered by ice and is described by an ice-to-water ratio expressed in tenths). This presence, combined with extreme arctic conditions routinely presents a challenge to mounting safe and effective oil spill response actions. In order to overcome this challenge, responders must develop response action plans, not only with an understanding of the physical environment of the response operations area, but also with a basic understanding of the effect this environment will have on the fate and behavior of the spilled oil. Arctic spill response strategies, worldwide, have been developed through more than twenty years of experience with both offshore and onshore drilling and production operations in all types of sea and ice conditions. Alaska Clean Seas (ACS) has based North Slope response action plans on this experience, intense field training, and investigation and ground truthing of related research and development projects.

1.0 INTRODUCTION

Oil and ice interactions have been the subject of many oil spill response research and development projects over the last 20 years.

Beginning with the research conducted offshore in the Canadian Beaufort Sea and followed by projects in the Alaskan and Norwegian arctic, scientists and responders have studied oil behavior, developed and tested methods and tools to mitigate the effects of an oilspill in, on, or under ice. Arctic spill research projects have explored, under various ice conditions, aspects including oil weathering characteristics, spreading under ice, encapsulation and migration, remote sensing, trajectory modeling, and the testing of in-situ burning, dispersants, and conventional containment and recovery equipment.

Alaska Clean Seas (ACS) was originally established in Prudhoe Bay in 1979 under the name of ABSORB, an acronym for Alaskan Beaufort Sea Oilspill Response Body, to support offshore exploration ventures in the Alaskan Beaufort Sea. This support was defined by the following organizational objectives (Shafer, 1990):

- 1) to develop spill response technology for the area;
- 2) to acquire an appropriate inventory of the best available countermeasure equipment and materials;
- 3) to maintain the equipment and materials in a high state of readiness; and
- 4) to provide spill response training for personnel of member companies and their contractors.

The organizational objectives of ACS did not include the provision of manpower and management to conduct oil spill response operations until 1990 when the ACS ownership elected to expand the mission of the organization to include response operations both offshore and onshore. The new onshore operating area (Figure 1-1) included all of the producing (North Slope) oilfields and the Trans Alaska Pipeline System (TAPS) corridor north of the crest of the Brooks Range (Shafer, 1990).

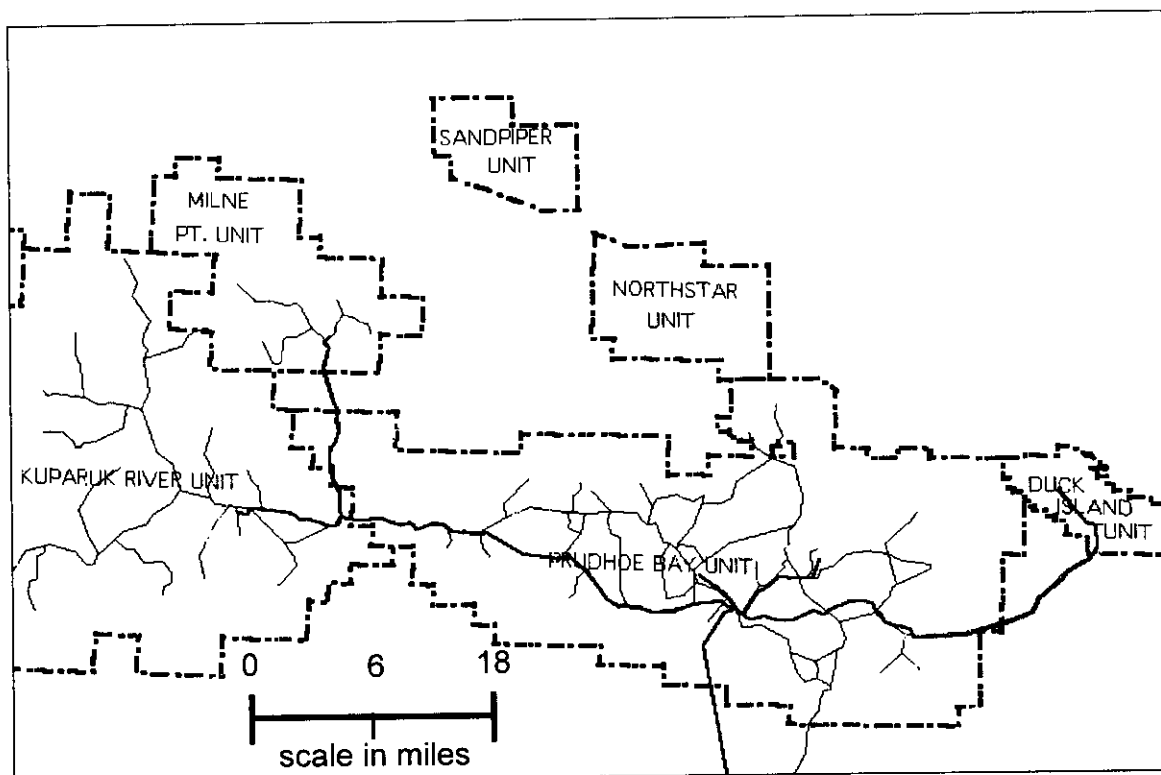


Figure 1-1
Alaska Clean Seas North Slope Area of Operations

In recent years, the level of awareness for spill responders has grown with an increased number of coastal exploration and development projects. In addition to the existing facilities within the ACS area of operations, the development of on-line facilities at Niakuk, Pt. McIntyre and Milne Point with direct exposure to the coastal waters of the Beaufort Sea put additional demands on ACS. These included the need to maintain, disseminate, and train themselves and their member companies with a common set of response action plans to protect the marine and coastal environment under a variety of oil and ice conditions. Figure 1-2 indicates areas of direct coastal exposure from current production and pipeline operations.

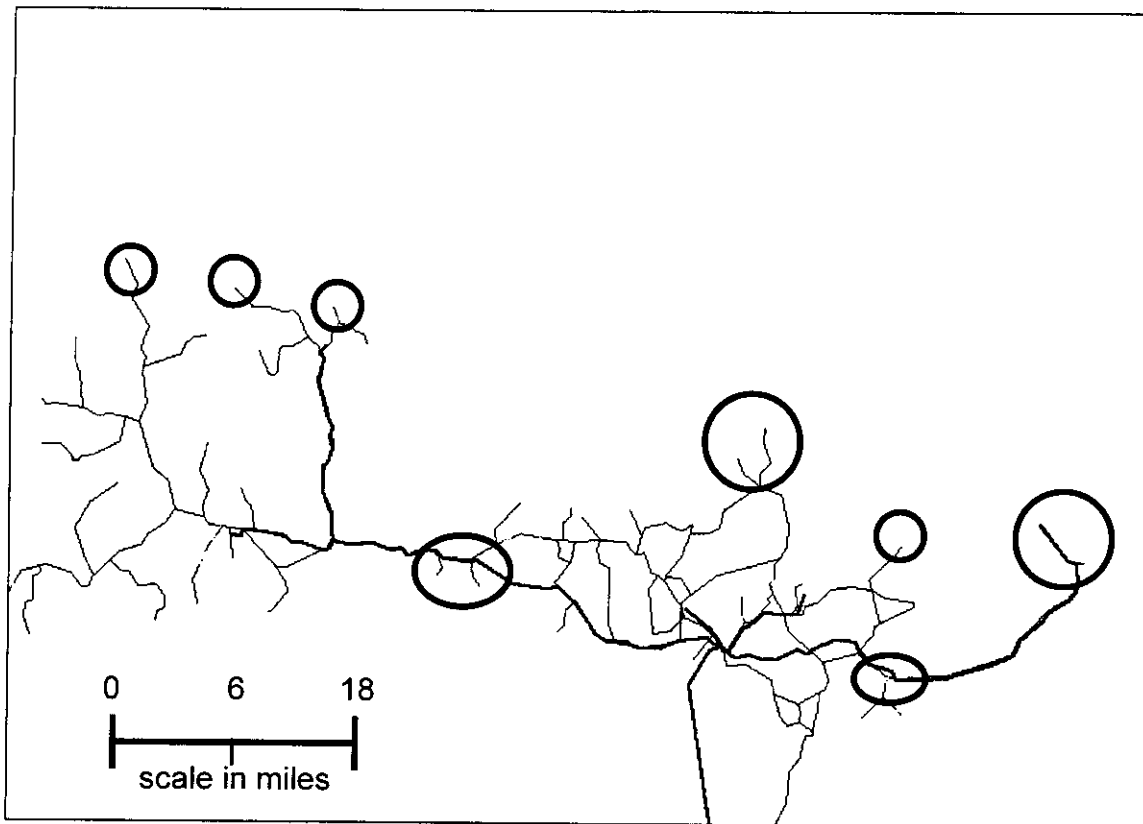


Figure 1-2
Areas of Direct Coastal Exposure from North Slope Oilfields

The primary purpose of this paper is to present the operational spill response strategies that would be employed in the Beaufort Sea environment during different seasons and ice conditions. Much of the validity of these plans rests in the additional information provided on response planning, oil fate and behavior in various ice conditions, and the influence of ice conditions on clean-up strategies. Since there are currently no exploration or production projects seaward of the barrier islands this paper will concentrate on the coastal waters between the barrier islands and shore. It is important to note that an recent discovery (North Star) will alter these facts and Alaska Clean Seas has been working with Member Companies to design response tactice for the offshore environment. A synopsis of the history of events and knowledge that has built the framework for oilspill response under the challenging oil and ice conditions on the North Slope is provided as the final section.

2.0 RESPONSE ORGANIZATION AND PERSONNEL RESOURCES

ACS is an oil industry-sponsored, not-for-profit organization that provides oil spill response functions in support of petroleum-related activities on the North Slope and in the coastal and outer continental shelf waters off the coast of the North Slope of Alaska.

ACS provides manpower and equipment resources from its main base at Deadhorse and from within each of the operating oilfield units to assist in spill containment and recovery. The U.S. Coast Guard has certified ACS as a Class E Oil Spill Response Organization in nearshore and river environments. This is the highest certification available.

The North Slope operating companies coordinate with ACS to ensure a pool of trained manpower is available for an extended spill response. Under the current agreement to consolidate spill response resources (1995), there are approximately 115 trained employees and contractors (± 15 percent) available for immediate response in the event of a spill incident per shift from the various operating areas on the North Slope. All on-shift members of the North Slope Spill Response Team (NSSRT) are available for call-out through dedicated paging systems within each of the units. ACS also manages existing contracts with several spill response and service contractors (VECO, Alaska Petroleum Contractors, CCI, etc.) to provide additional personnel within hours from their initial callout.

Within the State of Alaska, there are four other spill response organizations, each with its respective area of operation and commitment. Close working relationships have been established with each of these organizations in order to facilitate immediate support of a major spill response effort anywhere within Alaska.

ACS also manages over forty additional contracts and personal service agreements to provide support for all facets of a spill response effort. These services include, but are not limited to, aviation support, telecommunications services, veterinary services, computerized mapping, catering and security.

3.0 NORTH SLOPE EQUIPMENT INVENTORIES

ACS has purchased and maintains a spill response equipment inventory valued well in excess of 20 million dollars. This equipment is designed to respond to spills within the defined area of operation, under all environmental conditions. Over the years, each of the ACS operating members have built corresponding inventories capable of meeting the immediate response needs of their respective unit. The North Slope Operators Mutual Aid Agreement for Spill Response (1999) enables each of the operating Member Companies, BP Exploration, Alaska (BPXA), ARCO Alaska, Inc., (ARCO), and Alyeska Pipeline Service Company (APSC), to share equipment resources in the event of a significant spill within any of the North Slope operating units.

To assist with this task ACS manages the combined inventory of all dedicated North Slope spill response assets in a single computerized maintenance and job order system. Additional equipment is also available through other cooperatives and industry sources.

4.0 RESPONSE TIMES

ACS personnel are on call seven days a week, 24 hours a day while on-shift. The time necessary to arrive at a spill site with the appropriate equipment depends on a number of variables. As a general guide, immediate response to small spills in the nearshore area of the Beaufort Sea will be available within the first few hours using pre-staged spill response resources and personnel from within the responsible parties unit. With offshore boom, vessels and skimmer systems pre-staged at West Dock, an offshore first-response task force consisting of ACS personnel and equipment could be on site in the vicinity of Prudhoe Bay within hours of notification, depending on weather conditions. In the event of a catastrophic spill requiring full mobilization of North Slope resources, oil spill response barges would be equipped and placed into service to assist with containment, recovery, transfer and lightering operations.

5.0 OIL FATE AND BEHAVIOR IN ICE COVERED WATERS

The following section provides an overview of oil behavior in broken and solid ice. This background is intended to provide a better appreciation for the choice of spring, winter and fall response options in subsequent discussions. The physical distribution and condition of spilled oil under, within, or on top of the ice plays a major role in determining the most effective response strategies at any time of the year.

5.1 Overview

Strategies and techniques for dealing with oil in ice have been studied intensively in the United States, Canada and Norway during the past twenty years. The most significant scientific knowledge was gained through a number of Canadian field studies aimed at gaining approvals for offshore Beaufort Sea exploration beginning in 1976. These field studies and others in Alaska and most recently in Norway, have looked at the behavior of fresh and emulsified crude oil, with and without gas, in a variety of ice conditions including landfast and broken pack ice (e.g., McMinn, 1972; Norcor, 1975; Buist and Dickins, 1981; Nelson and Allen, 1982; S. L. Ross, 1987; Vefsnmo and Johannessen, 1994). Dickins and Fleet (1992) contains a comprehensive summary of all known references on the subject of oil-in-ice fate and behavior, including analytical studies, tank and basin tests, spills of opportunity, and experimental spills at sea.

The fate and behavior of oil in ice covered waters is governed by a number of important processes, several of which are illustrated in Figure 5-1 (after Bobra and Fingas, 1986) and discussed below:

- **Spreading.** In Arctic waters during early and late summer, oil spills tend to spread less and remain slightly thicker than in temperate waters (such as the Gulf of Mexico) partly because oil is more viscous in cooler waters, but mostly due to the presence of broken ice and brash ice, respectively. In high concentrations (greater than 5/10), oil spreading tends to be limited to the spaces between the floes. There are a number of models that predict the spreading of oil as a function of ice concentration. These are based largely on the results of a field trial off the east coast of Canada (Ross and Dickins, 1987). In general, oil spilled under stable landfast ice will not spread beyond hundreds of feet from the spill source, based on currents and projected under-ice storage capacity (see ice storage below). The maximum expected under-ice currents in the Beaufort Sea nearshore are extremely low. In a March 1996 study inside the barrier islands, no currents were detected under the ice over a period of five days (Intec, 1996a). In the extreme case, any tidal currents present are expected to be much lower than the minimum threshold of 0.5 feet per second (ft/sec) necessary to initiate and maintain any transport of oil under solid ice (Cox and Schultz, 1980). A new study is currently underway in the vicinity of Seal Island in the off shore Prudhoe Bay area. The results of this US Minerals Management/University of Alaska-Fairbanks study should be published in early 2000.
- **Evaporation** of volatile components occurs with any oil resting on the water or ice surface. Evaporation rates of oil slicks are influenced by wind speed, slick thickness and environmental temperatures. Laboratory testing of oils from the North Slope indicate that the initial evaporative loss by volume, within the first 48 hours, can be expected to range between 16 and 30%, depending on the oil tested. (Buist, 1994)
- **Dispersion** is a process by which small oil droplets are driven under the surface by waves and turbulence and remain suspended in the water column. Dispersion rates depend largely on sea state, oil viscosity, interfacial tensions, and the tendency of the oil to emulsify. The formation of stable water in oil emulsion generally stops the natural dispersion of a slick.

- **Entrainment and rapid immobilization** of oil spilled beneath growing ice essentially stops all weathering processes (Buist and Dickins, 1981; Norcor, 1975; Allen and Nelson, 1981). The implications of this are significant.
When response crews pump or burn oil brought to the surface from a trapped layer under or within the ice, they will be dealing with almost fresh crude, even months after the spill occurred.
- **Ice Storage.** Natural variations in first-year ice thickness provide huge natural “reservoirs” to effectively contain oil spilled underneath the ice within a small area. From surveys in late winter near West Dock, under-ice storage capacities have been estimated to be as high as one million barrels per square mile (Kovacs et al., 1981). The implication here is that any mid-winter spill that may occur beneath the ice would be naturally contained within a relatively small area when compared to an identical volume spill on open water
- **Vertical migration** of oil through the melting ice starts in the spring (Norcor, 1975; Buist and Dickins, 1981). Beginning as early as the last week in May and continuing through breakup, oil will naturally rise to the surface from wherever it is trapped within or beneath the ice. The timing of this process will dictate appropriate response strategies to deal with any accidental spill that may have become trapped within the ice during the previous winter months.

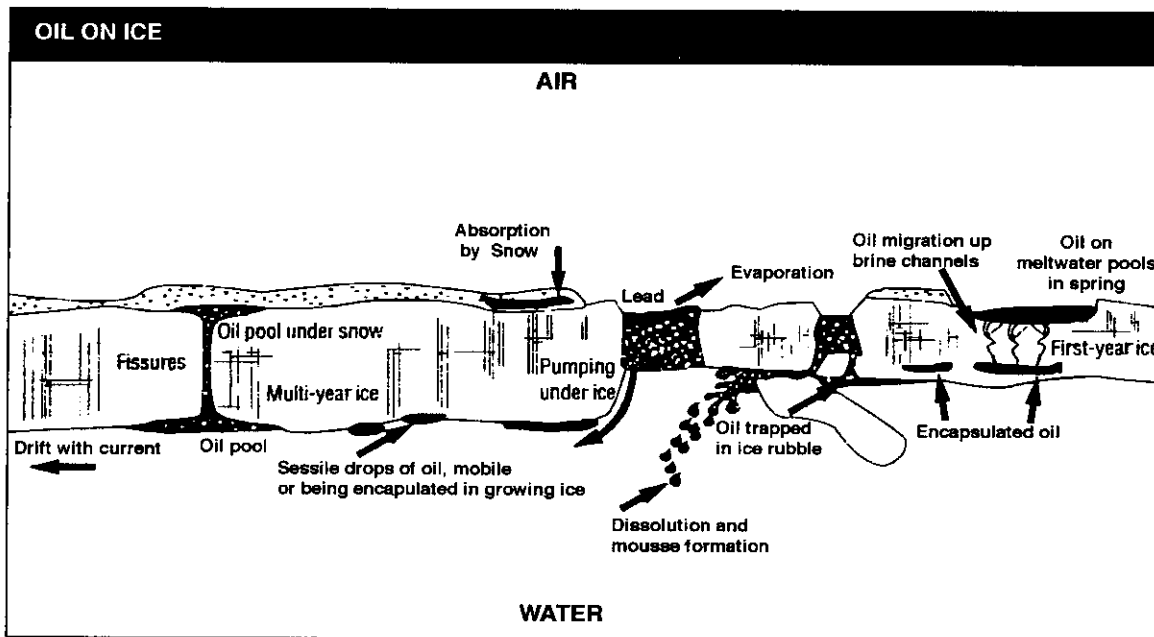


Figure 5-1
Illustration of Oil and Ice Processes

5.2 Oil Spills Beneath Floating Solid Ice

The subject of the behavior of oil spilled under solid ice cover has been the subject of numerous field, laboratory, and analytical studies. The two largest field experiments took place in the Canadian Beaufort Sea in 1974-75 and 1980 (Norcor 1975; Dickins and Buist, 1981). The Norcor project involved eight spills of two different crude oils totaling 330 barrels under ice ranging from 17 to 70 inches in thickness. An experiment sponsored by Dome Petroleum and supported by ABSORB (Dickins and Buist, 1981) simulated a subsea blowout by injecting compressed air and Prudhoe Bay crude oil under landfast ice. One of the Dome releases was predominantly oil alone and can be used in conjunction with the Norcor results to accurately describe the interaction of oil with the ice during winter and spring conditions right up to breakup. It is convenient to separate the discussion seasonally into:

- Winter ice contamination and oil encapsulation (October to April), and
- Spring oil migration and surface appearance (April to July).

While current oil production facilities within the ACS area of operation pose little risk, if any, of a release of crude oil under solid floating ice, the proposed future winter exploration drilling projects and the North Star Island sub-sea pipeline route warrant inclusion of this information into the response strategy discussion.

5.2.1 Winter Ice Contamination And Oil Incorporation

Oil released into the water column under a floating solid ice cover will rise and gather in pools or lenses at the bottom of the ice sheet. Based on Stokes Law, the terminal rise velocity of a 0.4-inch diameter oil particle, with a density of 0.850 g/ml, is about 0.75 ft/sec in seawater. Typical under-ice currents within the barrier islands are unlikely to exceed 0.5 ft/sec. As a result, almost all of the oil will contact the ice under surface within a few feet of the center of a release.

Winter under-ice currents, in the coastal area of the Beaufort Sea will not spread spilled oil beyond the initial point of contact with the ice under surface. Several studies have determined that with roughness values typical of undeformed first-year sea ice, the threshold current speed needed to initiate and sustain movement of an oil lens or pool along the ice under surface is approximately 0.7 ft/sec, well over the highest currents anticipated in the near coastal areas of ACS operation (Cammaert, 1980; Norcor 1975; Rosenegger, 1975).

Two physical factors that act to naturally limit the area contaminated by oil under ice are natural depressions related to variability in snow depth, and rapid incorporation of the oil by new ice growth around and beneath the oil layer. Ice naturally develops an undulating bottom surface in response to snow drift patterns on the surface. Researchers have investigated the holding capacity of ice cover by mapping the under-ice topography and calculating the potential for oil containment (e.g., Kovacs et al., 1981). Results indicate that typical under-ice containment capacities for first-year landfast ice (representative of the Prudhoe Bay area within the barrier islands) range from 0.012 barrels per square foot (bbls/ft²) for 25-inch thick ice in December to 0.026 bbls/ft² for 60-inch thick ice in April, equivalent to about one million barrels per square mile. As the natural containment increases with ice thickness, the area needed to contain a given spill volume decreases steadily throughout the winter, as shown in Figure 5-2.

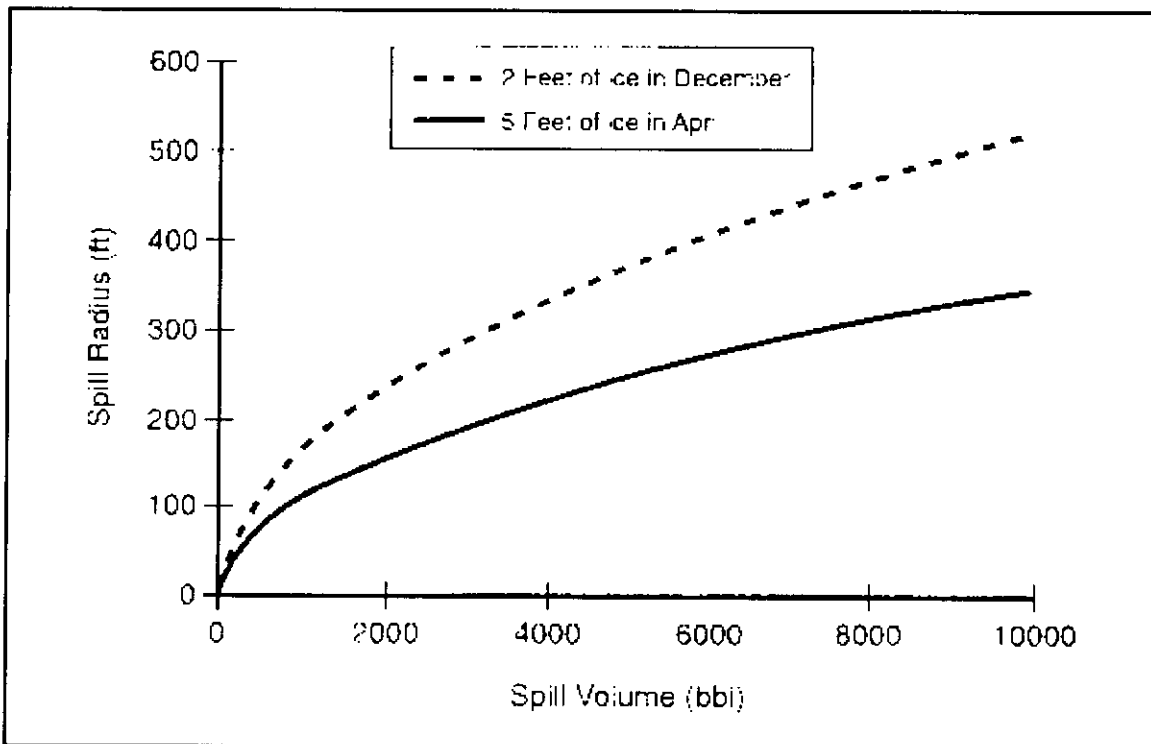


Figure 5-2
Predicted Radii of Spills of a Given Volume Spilled Under Landfast Ice
(Dickins, 1985)

Based on these containment capacities, a 1,325-barrel spill from a source beneath the ice surface in December would be contained within a diameter of approximately 380 feet, decreasing to a diameter of approximately 260 feet for spills of equal volume in April or May. The associated average oil layer thickness in the ice would range from three inches in early winter to seven inches in April, with the maximum thickness in the deepest pools varying from five to 14 inches, respectively.

Natural variations in ice thickness comprise the most important physical characteristic limiting the spreading of oil from a sub-surface release. In the case of a small leak, the formation of a lip of new ice at the outer perimeter of the spilled oil will also act to further limit spreading in the case of unusually smooth ice.

In a batch release, new ice will completely encapsulate the oil layer within 18 to 72 hours, depending on the time of year, December to late April (Dickins and Buist, 1981). Oil spilled under the ice after May 1 may not become encapsulated due to insufficient new ice growth.

With a chronic leak that occurs over a long period of time, new ice is prevented from immediately growing directly as a hard layer beneath the oil pocket due to the continuing arrival of fresh oil. Ice crystals present in the water at the oil/ice interface will probably be incorporated to provide a slush/oil mixture that gradually thickens the longer the spill source remains undetected. At the same time, new ice growing around the perimeter of the contaminated area will progressively contain the oil. The end result for most of the winter will be a cylinder of liquid oil and slush, deepening as the surrounding ice grows. In the case of a chronic leak spanning the April to June period, the contaminated area will increase as the ice growth rate slows down. The final trapped oil geometry in this situation would be similar to chronic leaks in mid-winter, except that the oil pocket will assume the shape of an inverted truncated cone, with the largest diameter at the deepest depth and the angle of the cone increasing as new ice growth diminishes. Once the spill source is detected and the flow stopped, new ice will begin to form beneath the oil within several days (December to April).

5.2.2 Spring Oil Migration And Surface Appearance

After the oil has spread under the ice and been encapsulated, it will remain trapped until around March, at which time a process of vertical migration will begin with the gradual warming of the ice sheet.

The rate of vertical migration depends on the degree of brine drainage within the ice (a function of internal temperature), oil pool thickness, and oil viscosity. During the period from November to February when the sheet is cooling and growing rapidly, there are very few passages for the oil to penetrate. Vertical migration of the oil in this period is limited to several inches of initial penetration through the porous skeletal layer of individual ice crystals at the ice/water interface. The internal ice temperature reaches a minimum in late February. As ice temperatures gradually increase in March and April, brine trapped between the columnar ice crystals begins to drain out of the ice, leaving vertical channels for the oil to eventually rise to the surface.

The first evidence of natural oil appearance on the surface can be observed in the last week of May or may be delayed until the first week in June, depending on air temperatures. Oil released under six feet of ice in one experiment on May 21 reached the ice surface within one hour (Norcor, 1975).

The rate of oil migration increases rapidly once daily air temperatures remain consistently above freezing. During the same experiment mentioned above, up to 50 percent of the oil originally trapped within the ice became exposed on the ice surface between June 10 and June 20. Oil slick thickness in the melt pools on the surface increased from 0.04 inches to over 0.4 inches during a one-week period.

Natural melt of the ice from the surface down acts as a competing process to expose encapsulated oil. When this melt reaches the level where the ice was growing at the time of the spill, the oil is exposed. In most situations of a concentrated thick oil layer in the ice, natural migration will bring most of the oil to the surface before the surface melts down to meet it.

Once the oil reaches the ice surface, it lies in melt pools or remains in patches on the melting ice surface after the surface waters have drained. Winds act to herd the oil into thicker layers against the edges of individual pools. Spring observations during experimental spills in landfast ice in the Canadian Beaufort have shown the following size distribution of melt pools containing oil which has naturally migrated to the surface. This type of information is important in determining how much of the oil can be effectively burned through ignition of individual pools by either Heli-torch or manual ignition (refer to discussion in Section 6.3).

Table 5-1
Average Oil Pool Size Distribution, McKinley Bay NWT (Buist and Dickins, 1981)

	All	10 ft ²	50 ft ²	100 ft ²	200 ft ²	1000 ft ²
Number of pools per acre greater than a given size	32	24	12	6	1.6	0.8
Percent of oil in pools greater than a given size	100	95	85	75	45	40

Any oil remaining on the ice at final breakup and disintegration of the ice cover will be released slowly into the water as thin slicks and sheens.

5.3 Oil Spills Within or Beneath Broken Ice

In this case, oil would rise to the surface and either collect in the interstices or openings between individual floes or be trapped underneath the floes themselves. During the primary period of broken ice in the spring, oil released beneath the floes will naturally migrate through the rotting ice and appear on the ice surface within a matter of hours (refer to the above discussion of the spring oil migration process). Oil released into spring broken ice conditions would be contained in the openings between floes and coat the surrounding ice surfaces. As spring melt continues the area of contamination would correspondingly increase. For the case of oil trapped within or under newly forming pancakes or sheet ice in the fall, the likely fate will be rapid entrapment, with new ice quickly growing beneath the oil as already discussed. The fate of oil trapped between floes will depend largely on the ice concentration and time of year.

During freezeup, the oil will most likely be entrained in the solidifying grease ice and slush present on the water surface prior to forming sheet ice. Storm winds at this time often break up and disperse the newly forming ice, leaving the oil to spread temporarily in an open water condition until incorporated in the next freezing cycle (within hours or days depending on the air and water temperatures at the time). Ice drift rates at this time of year are highly variable, but a daily average of five nautical miles per day can be expected in October decreasing as the ice thickens and stabilizes through November.

At breakup, ice concentrations are highly variable from hour to hour and over short distances. In high ice concentrations (greater than 5/10), the oil is effectively prevented from spreading and is contained by the ice. As the ice cover loosens, more oil is able to escape into larger openings as the floes move apart. Eventually, as the ice concentration decreases to less than 3/10, the oil on the water surface behaves essentially as an open water spill, with localized oil patches being temporarily trapped by wind against individual floes. Any oil present on the surface of individual floes will move with the ice as it responds to winds and nearshore currents.

5.4 Spreading Oil on Top of the Ice

The resulting area of contamination from a release of oil on top of ice will be influenced by a number of site specific factors, such as, wind speed, surface roughness and the amount of snow cover in the area of the release. Other factors associated with an individual release may have an even greater potential to influence the total area of contamination. For instance, a release from a high pressure pipeline versus a tank rupture has a greater potential to spread the contamination to a larger area.

Likewise, if a breach of a high pressure pipeline directed the escaping oil toward the ground, the overall impacted area would be less than if the breach directed the escaping oil high into the air where wind conditions could potentially spread the contamination for miles.

A number of process equations are available to predict the spreading behavior of oil in snow (Belore and Buist, 1988). Key behavioral factors associated with oil spilled on snow can be summarized as follows (after Wotherspoon, 1992):

- Oil evaporation rates in snow are substantially reduced compared with oil slicks on open water;
- Oil mixed with snow does not readily form emulsions; and
- Once ignited, there are no appreciable differences between burning oil in snow or oil in water.

6.0 PLANNING AND RESPONSE STRATEGIES

Response planning and strategies for oil spills in ice have been developed over twenty years of actual experience with North Slope drilling and production operations. The techniques discussed in this document have been demonstrated and applied in real spill situations. The following sections describe:

- methods and applicability of surveilling and monitoring oil spills in various ice and open water conditions;
- the influence of various ice conditions on the logistics of mounting an effective response operation and determining the best cleanup strategies;
- the effective use of in-situ burning as a response option in various oil and ice conditions; and
- a summary of seasonal response strategies based on ice conditions.

6.1 SURVEILLANCE AND MONITORING

Surveillance and monitoring involves the techniques and systems available to detect, map, and track oil spilled into the Beaufort Sea from any source connected with the current North Slope production facilities and pipelines.

6.1.1 Surveillance and Monitoring Systems

One of the initial actions that must be implemented for any oil spill is to determine the initial extent of contamination and, in the case of spills on water or in moving ice, to continually locate and track oil as it migrates.

Numerous systems and specific equipment have been developed to detect and track oil spills on open water and ice, mostly through experience in sub-Arctic areas, arctic field trials, and laboratory research (summarized in Wotherspoon, 1992). Common techniques and equipment available to ACS include a combination of the following:

- **Satellite tracking buoys** are designed to follow the movement of the oil slick in response to winds, surface currents, and ice movements. Using the Global Positioning System (GPS), these "Slicktrackers" are capable of delivering real-time positions to computers in the command center with accuracy of better than 150 ft. (Costanzo, 1994). ACS maintains an inventory both the Trimble Sliktrak buoys and Metocean satellite ice beacons in their existing inventory. The Metocean beacons are capable of being deployed under virtually all ice conditions and providing a location signal for months after their initial release.
- **Radio tracking buoys** are similar in design and use to the satellite tracking systems but utilize a small radio transmitter built into the buoys to emit signals. These signals are then tracked by the receiving equipment which can be placed onboard vessels of opportunity, fixed wing or rotary wing aircraft. An inventory of Orion radio tracking buoys are maintained by ACS on the North Slope.
- **Airborne reconnaissance** is conducted with visual observers, still and video cameras, infrared and ultraviolet sensors, laser fluorosensors, and radar. Trained visual observers are used, together with more sophisticated remote-sensing equipment to enhance the information (helping to differentiate between natural "slick-like" targets such as silt on the ice, cloud shadows on water, and wind patches, and to map both the thick and thin parts of the slick).
 - Optical methods (still and video cameras) are useful for recording overall spill location and slick boundaries in reasonable light conditions. They do not provide a good indication of slick thickness and can cause confusion in low light conditions.
 - Infrared (IR) systems are highly effective in documenting offshore slicks through temperature differences between the oil and water. UV systems are more expensive and used primarily in conjunction with IR to differentiate between thick and thin sections of the slick.
 - ACS has immediate access to a variety of helicopters and fixed wing aircraft to map any slicks observed on the water in the project area.
 - The ARCO Twin Otter, located on the North Slope, is equipped with a Forward Looking InfraRed (FLIR) thermal imaging system.

The system is a gyro-stabilized, microprocessor-based system that provides state-of-the-art digital image processing. An onboard computer system is capable of processing the digital information and combining these images with environmental data and GPS information simultaneously collected by other shipboard instruments. The images shown below, in Figure 6-1, depict two (2) crude oil storage tanks on the North Slope. The image on the left shows two tanks of which the tank on the right is full and thus give a brighter image. The image on the right is a close up of the other tank in the left hand image and clearly indicates the tank is approximately 25% full. In addition, the U.S. Coast Guard operates specialized UV/IR and Side Looking Airborne Radar-equipped aircraft for surveillance of large spills over wide ocean areas (known as the "Aireye").

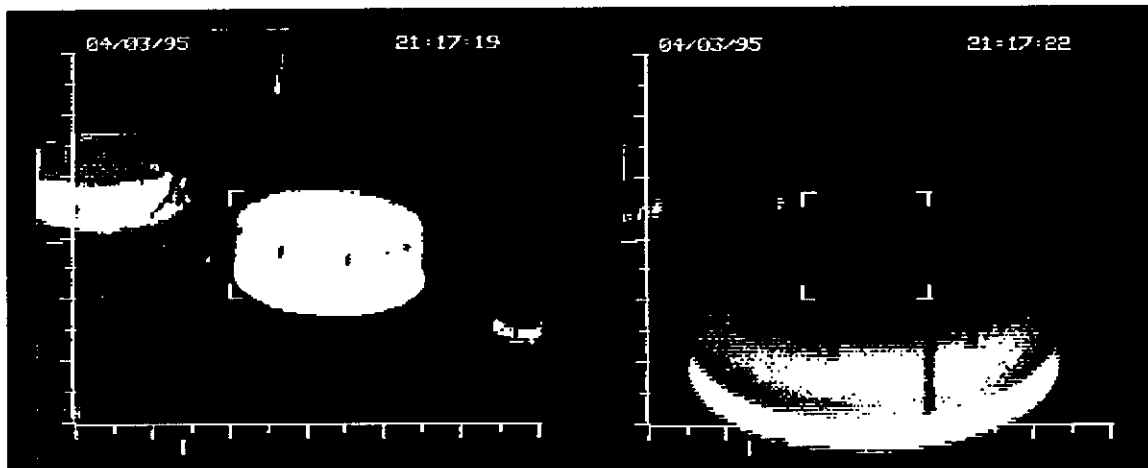


Figure 6-1
Infrared Photography of Crude Oil Storage Tanks
(Source: ARCO Aviation, 1995)

- **Handheld GPS** units are used extensively on the North Slope to document locations and extent of spill sites. ACS maintains an inventory of Garmin 45 handheld GPS units at each of the operating oilfields on the North Slope. Responders are trained in the use of these units and as such they are used frequently to support daily work activities. During previous spill events GPS data has been used in conjunction with survey crews to delineate areas of contamination under extreme winter conditions.

- ***Portable Current Meters*** are available and have been used to determine both current speed and direction under both summer and winter conditions. Information gathered by current meters is extremely important to produce accurate computer modeling.
- ***Underwater Lights*** have been researched, field tested and found to be very effective in locating oil under ice. The systems utilized by the NSSRT consist of a high intensity quartz halogen light fixture attached to a long handle. The assembly is lowered through a hole augered through the ice and illuminated once it is placed in the water. Once the snow cover is removed the lighting clearly indicated areas of oil accumulation.

6.1.2 Shoreline Surveillance

Aerial surveillance and mapping of oil on shore is more difficult than on water, largely because of the difficulty in separating the oil from background biogenic materials. Considerable progress has been made recently in this area, and multispectral scanners have been developed and tested in this role on real spills. In practice, the most reliable and effective approach to shoreline mapping of oil contamination is still to rely on ground crews trained to document the degree of oiling and penetration into the shorezone. Procedures for this mapping process are well developed through the Shoreline Cleanup Assessment Team (SCAT) process. Key specialists have been identified to lead a SCAT in the event of any oil spill on the coastline or in the marine environment on the North Slope.

6.1.3 Surveillance During Arctic Ice Season

When drifting ice concentrations are less than 5/10, the process of detection and mapping is basically the same as open water. As ice concentrations increase to greater than 6/10, visual detection of oil in small openings and leads becomes more difficult. These problems are magnified in October and November by conditions of frazil ice, thin moving ice and decreasing daylight. There are a number of possible approaches to tracking and mapping oil under these conditions. Experimental airborne systems such as the laser fluorosensor and IR sensors have shown potential for detecting oil on or amongst ice floes. Satellite beacons are available for airborne deployment and do not require aircraft to land on the ice. As of April 1996, daily satellite coverage is now available for offshore ice conditions independent of daylight, cloud cover, or fog (Canadian Radarsat). The satellite lacks the resolution to detect small oil slicks directly, but it can provide a clear picture of the ice conditions in the vicinity of the oil when used in combination with tracking buoys.

As the ice sheet stabilizes and thickens, a number of resources may be utilized to approach an offshore spill site. Small one and two man All Terrain Vehicles (ATV's) (i.e., snowmachines, 4-wheelers, ARGO tracked vehicles) are available across the North Slope to support reconnaissance and survey teams. In December, as thicker ice forms, it is possible to land helicopters on the ice and confirm any sightings of oil. Once the ice is stabilized and landfast out to the barrier islands, any oil spilled will either lie trapped within, under, or, in the case of a coastal blowout incident, lie mixed with snow on top of the ice surrounding the island.

The primary techniques for detecting oil on top of the ice are visual observation or optical cameras.

During the winter, oil on the ice surface may be covered by drifting snow, and it may become necessary to map any suspected contaminated area with radial trenches or a grid pattern shoveling down to the bare ice. This process will clearly reveal the extent of snow contamination through visual inspection of the trench walls.

In May and early June, optical and visual methods work well in mapping oil on the surface. Oiled snow will melt faster than the surrounding snow due to the increased heat absorption. As the melt progresses, sediment on the ice (particularly in the river overflow area) and the light and dark patterns, characteristic of a deteriorated ice surface appearance, can easily be confused with weathered oil. Oiled ice tends to melt slightly faster than the surrounding ice, and these differences can still provide visual clues to the location and extent of oiling (Norcor, 1975; Dickins and Buist, 1981).

Oil remaining trapped beneath or within the ice at the end of the growth cycle becomes mobile as the ice sheet warms in April. For a known area of trapped oil, the rate of vertical migration of the oil within the ice can be monitored by regular core samples (starting weekly in April and progressing to daily by mid-May). At the same time, the degree of weathering of the surfaced oil can be monitored by collecting samples for lab analysis.

6.2 Influence of Ice Conditions on Cleanup Strategies

Ice in one form or another can be encountered in the vicinity of the North Slope oilfields at any time of the year. Of all the factors affecting the choice of response actions to deal with a marine spill originating from coastal facilities or pipeline river crossings, ice and weather conditions largely determine workable strategies and control the eventual outcome. Examples of important ice conditions include thickness, stability, bearing capacity and concentration.

Ice thickness dictates the available site access and load-bearing capacity for staging equipment and surface travel to and from the spill site. Depending on location and time of year, sea ice will support heavy equipment, such as trenchers, end-dumps, backhoes, ditch witches, and bladders for temporary storage and/or transport of liquid oil pumped from within the ice. Figure 6-2 illustrates the correlation between ice thickness and loading capacity.

During a typical winter, ice roads will be available or can be constructed to support oil spill recovery operations from late December to late April. By early May the ice surface is usually too deteriorated to maintain the ice road in a usable state.

The ice sheet itself usually retains enough stability and thickness until early June to support heavy loads at the spill site itself; the problem during this period becomes one of access to and from shore. On-ice operations from early June to breakup will depend on day to day conditions and may require continuous helicopter or Air Cushion Vehicle (ACV) support to ensure the safety of work crews.

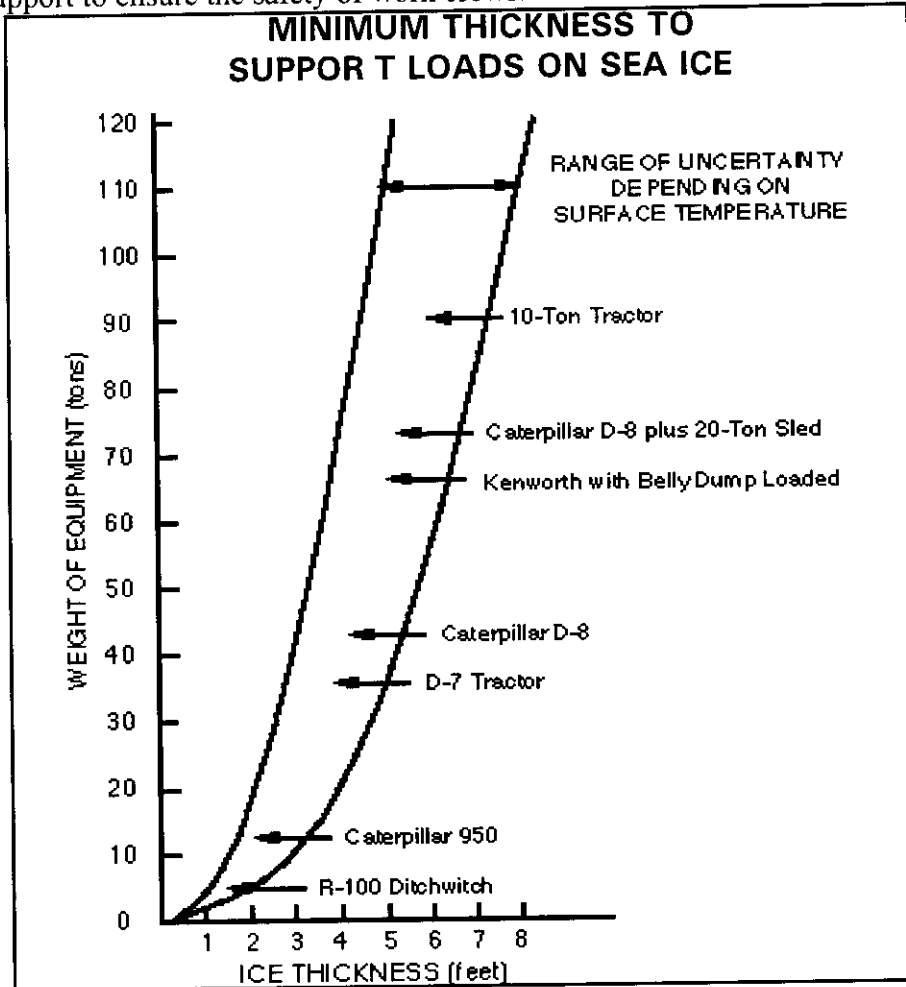


Figure 6-2
Load Bearing Capacities of Sea Ice (Source: ACS Training Manual)

Helicopters, ACV's and airboats can be used during the shoulder seasons of freezeup or breakup to transport limited payloads of personnel and equipment to an offshore spill site. ACS has a contract in place to utilize a high speed, turbine powered ACV currently located at West Dock in Prudhoe Bay. The unit has a cargo payload of 30 tons and can be operational within four (4) hours of crew arrival in Prudhoe Bay.

Bottom founded ice refers to the condition where a portion of the fast ice becomes thick enough to rest on the bottom in shallow water.

This condition is commonly encountered between the shore and the barrier islands after mid-February. Winds have a great effect on water levels throughout the study area, even in the winter; westerly storms can create a one to two foot increase in water levels and temporarily lift the ice sheet off the bottom during mid-winter (Coastal Frontiers in Intec, 1996a). After March, much of the ice in Simpson Lagoon rests firmly on the seabed with an attached layer of frozen sediment at the ice/bottom interface. Figure 6-3 shows a typical transitional cross-section for arctic sea ice. It is important to note that in the nearshore area of Prudhoe Bay, the bottom founded condition could extend for 2 - 5 miles offshore to contact the barrier islands. The implications of this "bottom-founded" condition are that crews may have to trench completely through the ice and recover oiled sediments encapsulated within or lying under the ice. The capability to perform this operation was demonstrated by BPXA during a trenching test in April 1996.

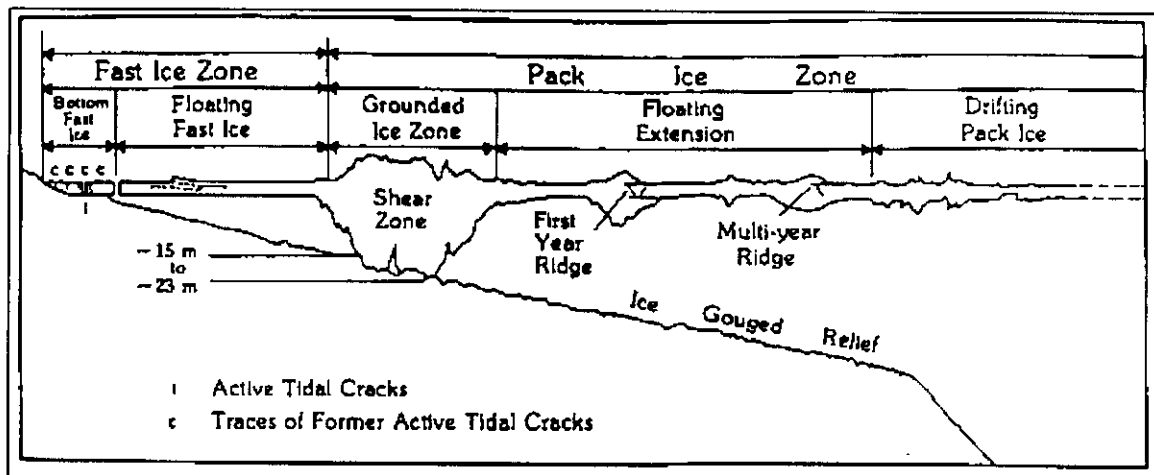


Figure 6-3
Typical Arctic Sea Ice Cross Section

Ice Stability is closely linked to thickness and refers to the potential for large ice movements in response to storm winds. Periods of most concern for oil spill response are freezeup from October through December, and breakup in June and July. During October and November, the ice is less than two feet thick and easily broken up by sustained storm winds predominantly from the east-northeast (Vaudrey - internal project memorandum, May 1996). By late December, once the first-year ice has reached approximately three feet in thickness, ice becomes relatively stable and remains so until late June. There are exceptions, such as February 1989 when 90- to 100-knot southwesterly winds drove most of the landfast ice from inside the barrier islands 20 to 30 nautical miles offshore (Vaudrey, 1996).

Once the ice has deteriorated during spring melt, another short period of instability occurs during the transition from a continuous ice cover to predominantly open water.

The ice normally melts in-situ in the shallow waters near the coastline by mid- to late June. Further offshore the fast ice becomes unstable and susceptible to wind-induced breakup in early July (Vaudrey, 1996).

During these "unstable" months, response operations may encounter the possibility of oil trapped in, or on top of the ice, moving 10 miles or more in a 24-hour period of sustained storm winds. The oil location can be tracked accurately on an almost real-time basis by deploying Global Positioning System (GPS) beacons reporting to satellites. During dynamic broken ice conditions following freezeup and preceding breakup, helicopter-supported burning operations with the Heli will likely be the most effective response strategy.

Ice concentration refers to the area of surface water covered by ice, and is described by an ice-to-water ratio expressed in tenths. Ice concentrations dictate not only the extent to which conventional open water oil recovery systems can be used in deeper water, but also the extent to which the natural containment offered by the ice will limit spreading and allow direct *in-situ* burning (S. L. Ross and D. F. Dickins, 1987). The period when the choice of cleanup strategy will be most affected by drifting ice stretches from approximately July 4 (± 2 weeks), the average dates when breakup occurs in the vicinity of the barrier islands, to July 22 (± 7 days), the average dates when ice concentrations fall to less than or equal to 3/10. The value of 3/10 is significant in that it represents a generally accepted upper limit for deploying conventional booms and skimmers without unacceptable interruption from drifting ice (S. L. Ross, 1983; Shell et al., 1983).

The period from first breakup in early July to approximately mid-July provides a two-week window when the ice cover is likely to remain in concentrations of 7/10 to 9/10; high enough to support natural burning with aerial ignition from helicopters. Ice concentrations between 3/10 and 6/10 represent the greatest problem for oil spill cleanup. Conventional booms may be collapsed, overrun, or damaged by drifting ice. At the same time, there is insufficient ice to naturally contain the oil into sufficiently thick patches to burn *in-situ* without firebooms. Fortunately this troublesome range of concentrations is short lived; concentrations normally fall from 5/10 to 3/10 in less than one week during breakup (Vaudrey, 1996).

The period of **ice overflow** introduces a special set of circumstances in modifying the oil behavior and complicating cleanup efforts for a period of 10 days to two weeks. From late May to mid-June, a large proportion of coastal waters within the ACS area of operation is incorporated within the spring overflow from the Sagavanirktok, Putuligayuk, and Kuparuk Rivers (Vaudrey, 1996). Figure 6-4 represents the areas of spring overflow.

Not only is surface access difficult at this time, but any oil surfacing through the ice is potentially free to spread on the surface waters. After a short period of five to 10 days, the overflow waters drain through natural holes in the ice (in some cases creating pits called *strudel scours* in the seabed). Some surface oil, if not contained or recovered, may be redistributed under the ice during the process of surface drainage. As the overflow drains, the sea ice lifts off the bottom and quickly melts to provide open water nearshore a month or more ahead of the offshore areas.

6.3 In-situ Burning, A Response Option

Mechanical recovery is considered a primary means of response for both fresh crude and emulsified oil in calm to moderate seas with ice concentrations of less than 3/10. For spills over solid ice, response actions are very similar to terrestrial spills and therefore mechanical recovery is also considered the primary response option. The actual efficiencies of mechanical recovery are highly variable, depending on skimmer design, oil viscosity, pour point, and degree of emulsification. Environmental conditions also play an important role in determining efficiencies of mechanical recovery operations. In some cases, such as the periods of freezeup and breakup, the environmental conditions limit the use of mechanical containment and recovery. Recent developments and greater understanding of the residual effects of *in-situ* burning have increased the window of opportunity for *in-situ* burning and gained acceptance within the federal and State of Alaska regulators as a viable response option.

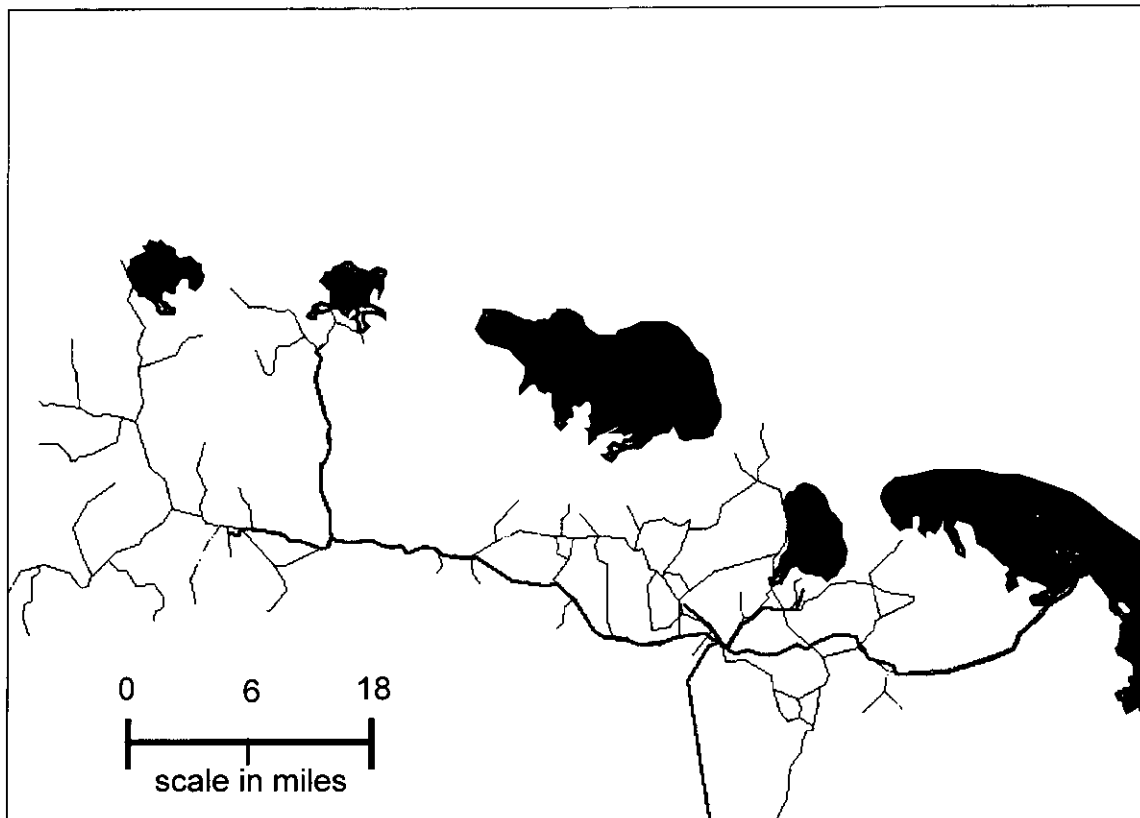


Figure 6-4
Areas of Spring Overflow Near North Slope Oilfields

In-situ burning in open water, using fireproof booms already in the ACS inventory, offers the potential of achieving almost complete oil removal from the water under a wide range of conditions (fresh to lightly-emulsified oil, seas less than three to five feet, and winds less than 20 knots). Burning is considered as a proven response technique that, depending on circumstances, would be used together with mechanical recovery to substantially increase the overall oil removal rate. Comprehensive guidelines are available to establish procedures for requesting, evaluating, and authorizing the use of *in-situ* burning during an actual response (Alaska Regional Response Team, May 1994).

In-situ burn efficiencies in the range of 95 to 98 percent have been demonstrated in a wide variety of tests and field trials in Alaska, Alabama, Norway, and the Canadian East Coast, and have involved test basins, experimental crude oil spills in ice, and open ocean trials with actual oil (summarized in Buist et al., 1994). High removal rates of 60 to 80 percent have also been achieved in more extreme conditions with up to 50 percent oil/water emulsions, stronger winds and oil on slush ice in leads. A fire boom was used successfully during the *Exxon Valdez* response to remove an estimated 360 barrels of crude in 75 minutes (Allen, 1991).

Two successful burns were recently carried out in the United Kingdom using harbor fire boom under adverse conditions of five-foot seas and 15-knot winds (Allen pers. comm. June 1996).

Extensive scientific measurements of large scale burns at sea by U.S. and Canadian scientists in 1993 have conclusively demonstrated that with appropriate guidelines and safe distances, *in-situ* burning poses no significant human health or other environmental risk, either from smoke inhalation or toxic compounds associated with the smoke (Fingas et al., 1995). There are three emissions of possible concern to regulatory agencies and local residents:

- ***Respirable particulates in the smoke.*** Measurements have found that the ground level concentrations fall below human health limits within a thousand feet downwind of the burn. Concentrations in the plume fall below ambient air quality standards within several miles (Buist, per. comm. September 1996)
- ***Volatile Organic Compound (VOC)*** levels have been found above normal background as far as 1,500 feet from the fire, but even those slightly elevated VOC levels were still lower while burning than when the oil slick was left on the water.
- ***Polycyclic Aromatic Hydrocarbons (PAH).*** Extensive monitoring of large scale oil burns has shown that *in-situ* burning actually removes PAHs and that the soot contains PAHs at lower levels than the original oil. Results from water analyses similarly showed that *in-situ* burning did not adversely affect the underlying water column beyond those effects already associated with the unburned oil slick in the Newfoundland trials (Daykin et al., 1994).

In addition to removing almost all oil present from the water surface, burning eliminates the need for storage and disposal. The taffy-like residue survives in small volumes (typically one to ten percent of the original oil volume). The residue can be manually recovered from the ice surface and deposited in open top barrels or portable tanks with shovels and pitchforks (Norcor, 1975; Dickins and Buist, 1981). Concerns have been expressed about residues sinking after the burn, and this subject is being studied. It is not likely that residues from naturally contained slicks, such as in melt pools or win-herded against ice edges, will sink (Buist et. al., 1995; Trudel et. al., 1996). A comprehensive summary and evaluation of the state of knowledge surrounding the burning of oil spills at sea is provided by Buist et al. (1994).

ACS currently maintains in excess of 14,000 feet of fire boom on the North Slope, and six Heli-torches (Figure 6-5) for airborne ignition of oil either within a boom, trapped in broken ice, or lying in melt pools on the ice surface.

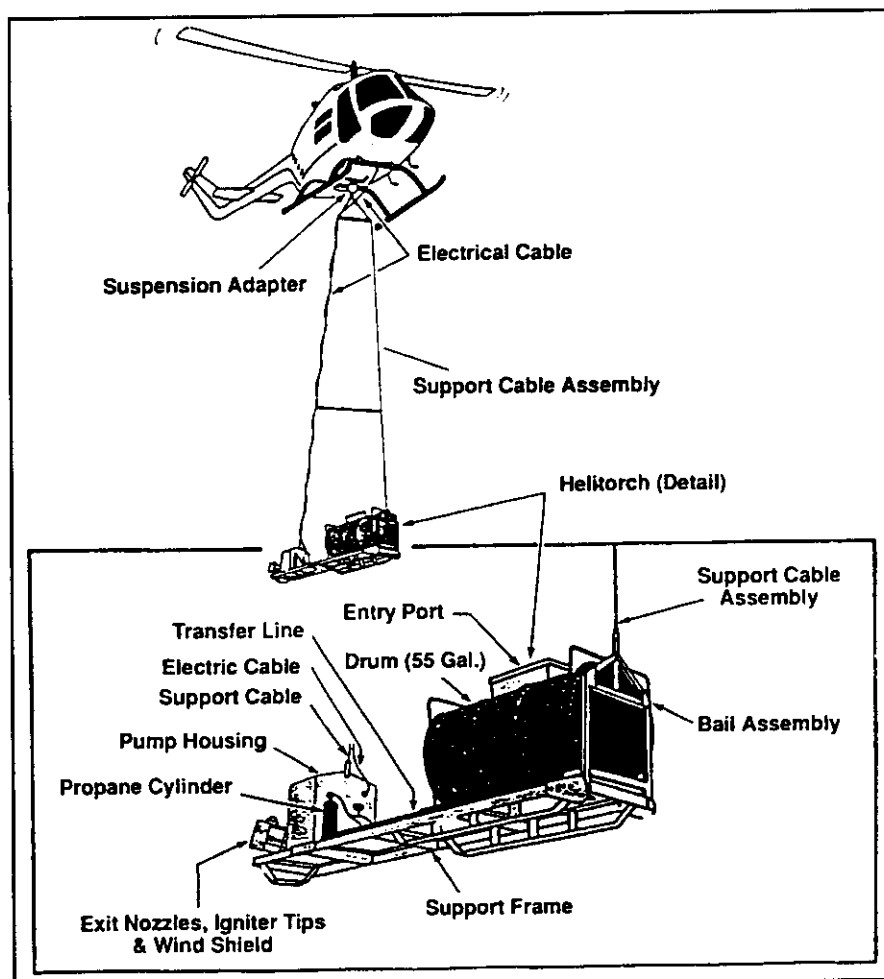


Figure 6-5
Heli-torch Ignition System

Figure 6-6 (Allen, 1988) compares achievable volume recovery rates for different open water cleanup strategies. The broad bands reflect the ranges in recovery rates expected under actual operating conditions. The graphs demonstrate the dramatic differences in likely recovery rates between the two primary cleanup strategies of mechanical recovery and in-situ burning. When compared with the most optimistic example of mechanical recovery using a large offshore skimmer with a V-boom, a single 1,000 foot section of fire boom in a U configuration is still capable of removing five times as much oil per unit time in slicks thicker than 0.1 inches.

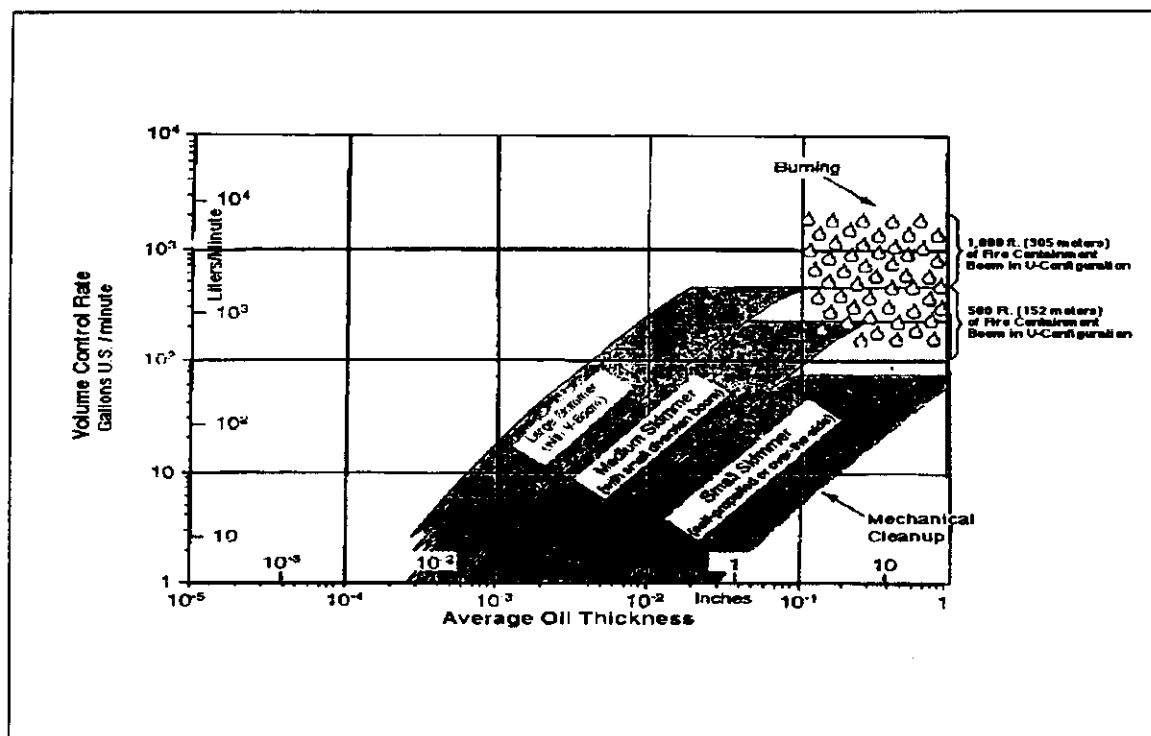


Figure 6-6
Selected Volume Recovery Rates for Primary Open Water Cleanup Techniques
Over a Range of Oil Film Thickness' (after Allen, 1988)

In summary, the expected removal effectiveness for an offshore open water or broken ice response is highly variable and depends on a large number of factors including timing, weather and sea conditions, degree of emulsification, and slick conditions. Very few historical response operations have achieved better than five to 15 percent using mechanical systems (excluding natural processes). Increased levels of preparedness and equipment resources can improve on these numbers.

Using a combination of mechanical recovery and burning downwind of a surface blowout, Gulf Canada (1990) calculated removal rates of up to 80 percent of the oil present under ideal conditions. When environmental factors (visibility, waves, ice, and response times) were included in the final analysis, the expected effectiveness fell to between 30 and 40 percent. Given the high level of readiness on the North Slope, it is possible that crews can achieve equivalent or even better, especially with the growing acceptance of *in-situ* burning as a response option.

6.4 Seasonal Response Techniques

The following sections describe strategies and techniques for dealing with oil spilled in different combinations of ice and open water, drawing on experience with past spills (both accidental and experimental) and knowledge of the expected fate and behavior of oil in ice.

6.4.1 Fall and Early Winter Response (October to December)

There are limited mechanical options for recovering large volumes of oil spilled under or among new and young ice in the fall months of October and November. A "Foxtail" rope mop style skimmer can be deployed by crane over the side of a response barge or vessel to recover localized oil patches trapped in water and slush between floes. This is one of the few skimmers able to recover oil from leads and openings in heavy ice conditions (Counterspil, 1992). Additionally there are 37 portable rope mop skimming systems within the North Slope response equipment inventories that could be placed into service as required. In areas of heavy oil concentration near the coastline or in available open water leads, other portable skimming systems could be utilized. These would include vacuum, drum and disc type skimmers. It is possible to utilize weir type skimmers under building ice conditions as long as the skimmers are equipped with mechanical systems to handle debris and ice. Any skimming operation will likely be curtailed by thicker, more concentrated ice within one to two weeks of initial freezeup.

In the beginning of the ice growing season, many of the spill response vessels would remain operational. Jet powered vessels will become inoperative as the brash ice and slush thickens and begins to interfere with the exposed mechanical parts of the jet systems. Outboard powered vessels will also be taken out of service when the thickness of the forming ice begins to clog the water intake ports on the lower units. Screw driven vessels along with the tug and barge systems have the longest sustainable operational period.

The most effective sustainable strategy during freezeup conditions will likely utilize *in-situ* burning, with the ice providing natural containment and Heli-torches providing a remote ignition source. A number of tests have shown the feasibility of burning oil trapped in leads with and without the presence of brash ice and slush (Brown and Goodman, 1987; SL Ross and D. F. Dickins, 1987). Depending on conditions, removal efficiencies over 90 percent are readily achievable. Weathering the oil up to 20 percent had no significant effect on the results. As the ice growth continues, oil spreading and conveyance processes will decelerate and eventually cease. Ultimately the oil will be incorporated into the new ice formation.

The oiled ice may move short distances (thousands of feet) in October before becoming landfast. Oil, during this time, is effectively trapped within the ice and contained from spreading until response teams can gain access. During the early stages of freezeup, the fringe of new landfast ice protects the shoreline from oiling.

Satellite tracking beacons would be deployed at the spill source to monitor the drift of any oiled ice away from the spill site. If this ice subsequently becomes incorporated as part of the landfast zone some distance from the original spill location, conventional winter response procedures can be followed by using helicopters, ATV's, and ACV's to ferry personnel and equipment to the site. Due to the temperatures, remote locations and darkness involved in these type of operations, personnel safety considerations will require additional attention. Resources such as personnel shelters, portable lighting, portable heaters and restroom facilities will be required along with the initial response resources.

The contaminated area would be located through visual observation of surface oiling and boring holes in the ice on a grid pattern to locate sub-surface accumulations of oil. Using underwater lighting the extent of contamination will be marked and recorded. It may become necessary to auger additional holes, in a radial pattern, from a known contaminated location to complete the delineation process. Handheld GPS units will be used to record the exact locations of both surface and sub-surface pools.

Recovery operations on early season, but landfast ice, are very similar to remote terrestrial spill response actions once the oil is brought to the surface. Teams would be set up to trench, slot and bore into sub-surface oil pools to gain access to the oil. Surface oil would be bladed into bermed recovery trenches. Skimmers will recover oil into portable tanks or into small, 500 gallon, airliftable bladders for helicopter transport to shore. Ice blocks cut from the landfast sheet could also be used to build containment reservoirs until surface transportation becomes feasible. Figure 6-7 represents a typical recovery operation on solid ice. Logistics constraints may demand that *in-situ* burning be utilized as the primary recovery option. If there were concerns over the ability to muster adequate resources to the site or if the recovered product could not be transported back to shore within acceptable timeframes, burning operations would be the most effective option. In all recovery operations, mechanical or *in-situ* burning, the site would be thoroughly cleaned during the demobilization operations.

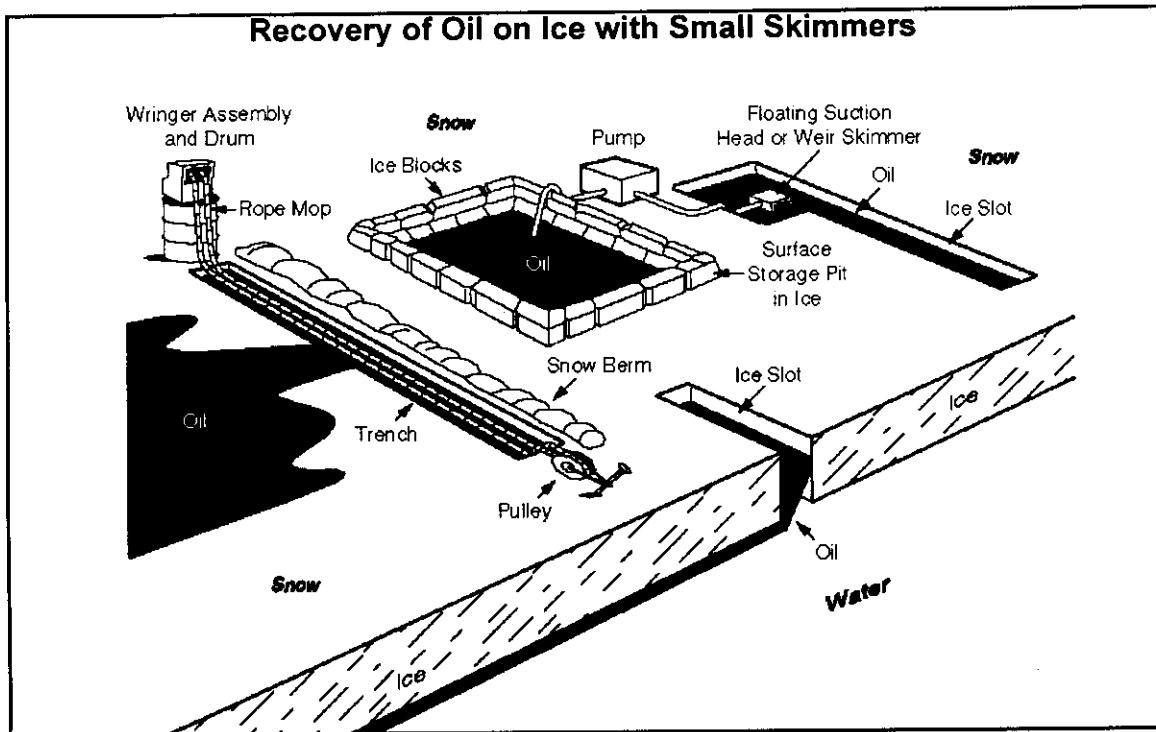


Figure 6-7
Typical Solid Ice Recovery Operations

6.4.2 Mid-winter Response (January to April)

Current technology is considered capable of successfully cleaning up oil spilled onto solid ice. Although more difficulties are expected in terms of initial detection, a similar successful outcome is expected for oil spilled under the ice from offshore winter exploration (MMS, 1996) and proposed pipeline projects.

By late December, the landfast ice is normally stable along the entire length of the route out to the barrier islands (Vaudrey, 1996). From this time until late May, cleanup operations dealing with spills originating from either offshore exploration or a shoreline production facility can utilize the ice cover as an secure operating platform for support equipment, including trucks, bladders and portable trenching equipment. Depending on location, in some years this period of on-ice operation can be extended. For example, the ice cover in the near shore areas can often support lightweight vehicles by November, and in many years the ice near the barrier islands (although deteriorated) can still support substantial loads and work crews into late June. While stable winter ice allows for greater access winter arctic conditions may control feasibility of cleanup operations. Extreme low temperatures present a hazard to operating heavy equipment and other hydraulic systems.

In order to maintain personnel safety and reduce the risk of further contamination through hydraulic systems failures, the North Slope operators have set the temperature limits shown in Figure 6-8 for safe operation.

Operator Criteria for Stopping Work in the Cold		
OPERATING AREA	EQUIPMENT	SHUTDOWN TEMPERATURE
ARCO Prudhoe Bay Eastern Operating Area (EOA)	Cranes and Man-lifts	-35°F
	Loaders, Vacuum Trucks	-40°F
ARCO Kuparuk	All Equipment	-35°F
BP Endicott	No Unnecessary Equipment Use	-35°F
	All Equipment	-40/-50°F
BP Milne Point Unit (MPU)	All Equipment	-45°F
BP Prudhoe Bay Western Operating Area (WOA)	All Equipment	-45°F

Figure 6-8
Safe Working Limits for Arctic Equipment Operations

In the case of a known reservoir of oil trapped within the ice sheet in mid-winter, direct pumping and ice road haul operations will result in almost complete removal of the spilled oil. Larger equipment would be utilized to gain access to sub-surface pools. In order to eliminate the volume of contaminated ice, the upper layer of ice can be removed prior to exposing the oil pool. Ice roads and pads can be built to allow heavy equipment and vacuum trucks direct access to the oil pools. These trucks would recover oil directly into attached 300 barrel insulated tankers for transportation to waste disposal facilities. During extremely cold periods it may be necessary to use steam wands on the oil pools to facilitate recovery. Additionally, it may become necessary to load 200 to 300 gallons of hot water into the vacuum tanks from shoreside facilities to maintain internal tank temperatures during recovery and transport periods.

The logistics are also quite feasible, even without the benefit of an ice road. For example, four Rollagons hauling bladders for 20 hours per day could transport 20,000 barrels in 15 days from a site 10 miles from shore. This sample calculation assumes a five mph average vehicle speed and a one-hour turnaround. Larger trucks operating on an improved ice road or high speed ACV's could achieve over five times as much productivity through greater speeds and loads.

Even greater volumes could be dealt with by adding more equipment over a longer period, or by burning at the site. Final cleanup in June will use selective burning of oil on melt pools followed by manual recovery of any residue. It is estimated that the remaining oil available to enter the marine environment (after all mechanical recovery and evaporation) be less than 10 percent of the original spill volume.

The choice and application of the two primary winter waste handling options of burning in-situ or removal to shore (Figure 6-9) depend on both time of year and water depth. Once an encapsulated oil layer is delineated drilling or trenching would be conducted to expose the oil layer for recovery. Snow melters can be placed on site or at shoreside positions to melt contaminated snow and ice. Recovered oil can then be trucked to designated disposal wells for reinjection or to a designated production facility for reprocessing. Burning on-site could become the preferred option late in winter when there may be insufficient time to transport the recovered oil to shore prior to breakup.

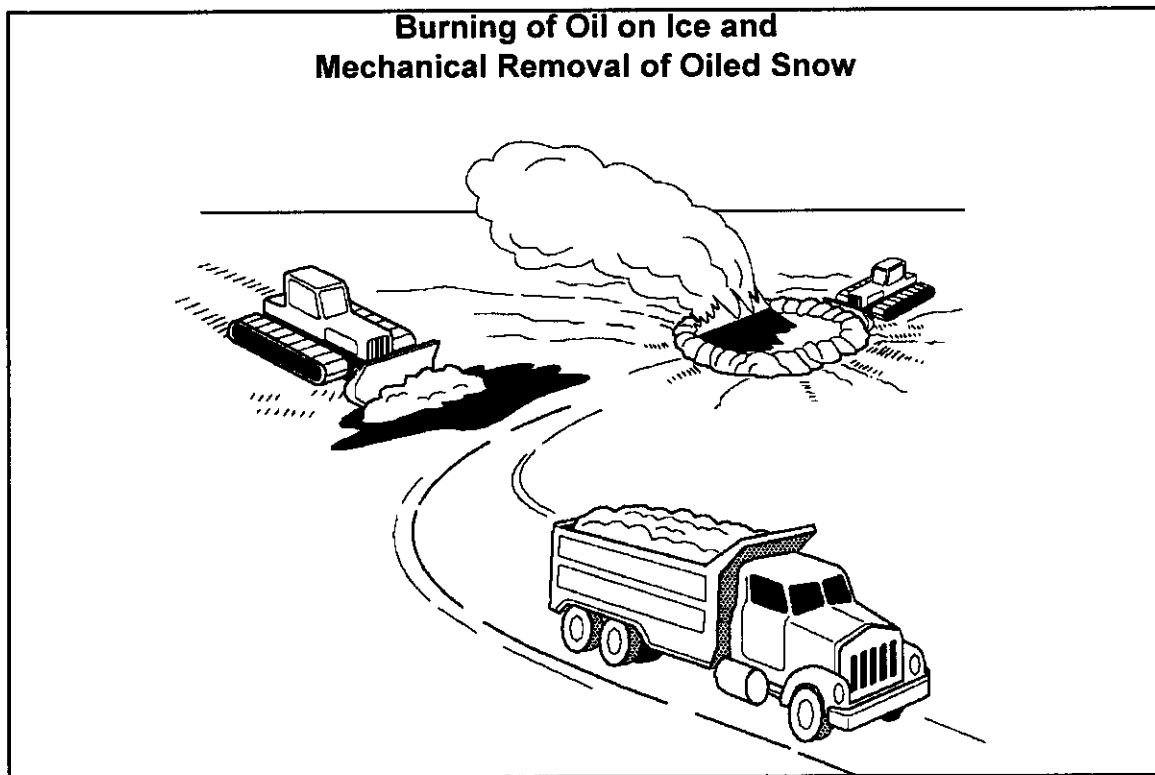


Figure 6-9
Winter Oilspill Waste Handling Operations

In the case of bottom founded ice encapsulating an oil pool, responders could trench and remove all of the ice blocks and cuttings in very shallow water (zero to four feet). After March, it may be possible to operate within a dry trench in many areas. There may still be a thin layer of frozen soil at the ice/seabed interface.

It may be necessary to penetrate this icy soil layer to release any oil accumulated within the sediment. Recovered oiled seabed or trench material can be trucked to shore for interim storage and final disposal.

A mid-winter blowout or pipeline rupture from either a coastline production facility or an offshore project could produce significant areas of surface contamination. Given the predicted oil plume height and droplet size, the oil concentration on much of the surface area may be insufficient for successful burning. Exceptions would be: (1) where surface procedures did not achieve well control and the flow continued for more than a number of days; and (2) within a few thousand feet of the island where up to 4 mm of oil could accumulate over ten days during periods of light winds. In order to limit the spreading of thicker oil accumulations close to the well site, a snow berm will need to be constructed as close as safely possible (figure 6-10), with the priority being the east-northeast and west-southwest quadrants (matching the predominant winds).

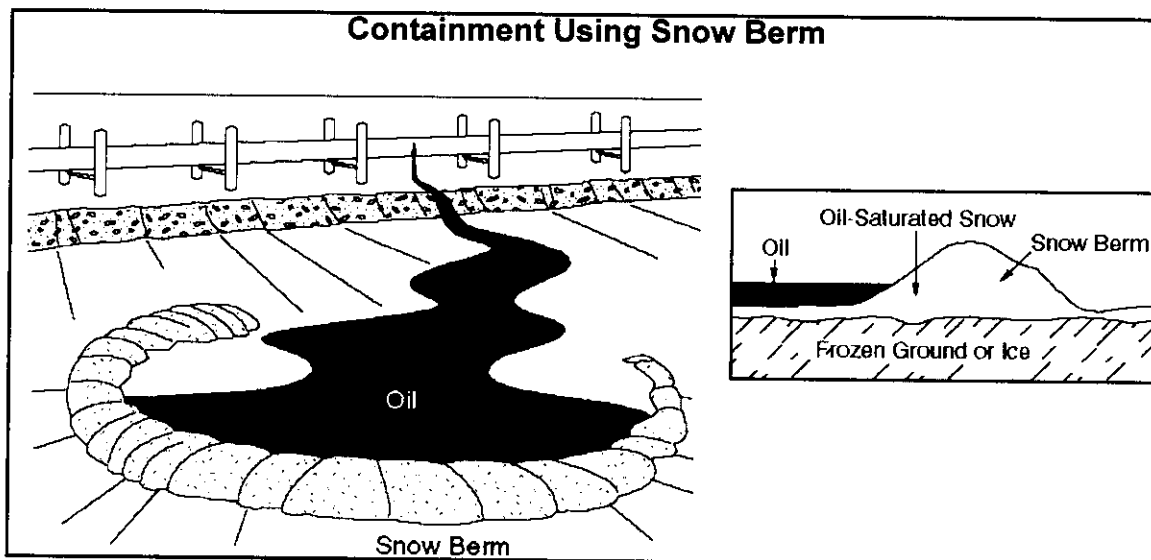


Figure 6-10
Snow Berm Construction for Winter Oilspill Containment

Plowing surface materials and removing the uppermost ice layer (2 - 4 inches) in the areas of gross contamination would be conducted utilizing heavy equipment. In areas of lighter contamination hand recovery operations would be conducted to reduce the total volume of solids recovered. Previous winter on-shore responses and experiments on the North Slope have proven this method to be very effective in recovering all visible traces of crude oil.

As long as the ice remains stable and strong enough to support heavy equipment, the cleanup operation becomes an exercise in materials handling.

In order to recover the oil, it is necessary to plow and recover the contaminated snow from the ice surface. If the oil is not too weathered, it can be recovered for reprocessing at onshore facilities. Otherwise, contaminated snow and ice can be melted and reinjected through approved disposal wells.

In rougher ice ridging and rubble, oil cleanup is still feasible, although more labor intensive. Experiences in Canada with offshore flare burner malfunctions have resulted in minor spills in rough ice close to the drilling structure. In those cases, a combination of local melting with torches and manual chipping and removal of the oiled ice was used to achieve a high percentage of overall recovery.

6.4.3 Spring Response (May to June)

The period between the first onset of surface snow melt and final deterioration of the landfast ice provides the best opportunity for *in-situ* burning of oil that naturally appears on the surface, or remains on the surface following a winter cleanup operation. However, this period also marks the end of easy site access with any heavy equipment.

In-situ burning is an efficient and effective method of removing oil from a solid ice cover in late May and early June timeframes, after ice roads have been closed to traffic. Tests have demonstrated that the oil on the surface of the ice can be successfully ignited and burned even after weathering for several weeks. Wind herding of the oil in small pools enables much thinner oil films to be burned than would otherwise be possible (Dickins and Buist, 1981). Fresh crude must be approximately 0.04 inches thick for ignition to take place, and weathered crudes in the range of 0.1 to 0.2 inches are readily ignitable. Weathering of the oil is not as critical as once thought. Ongoing work by SINTEF Norway has demonstrated that it is possible to effectively burn fresh crudes with up to 40 percent emulsification (water in oil), albeit at a reduced efficiency (Guenette and Sveum, 1995). ACS has conducted similar studies in the last few years concentrating on emulsions made of Alaskan risk oils and seawater. During these studies bench testing was conducted utilizing various emulsion breakers and gelled fuel mixtures to enhance ignition of emulsions. Promising techniques from the laboratory were then re-evaluated during both small scale and meso-scale testing, producing similar results to the SINTEF studies (Buist et. al., 1994)

Work in Alaska and elsewhere has proven that the Heli-torch is a highly effective tool in igniting multiple oil pools over large areas (Allen, 1987). Slung beneath a helicopter, the Heli-torch is safe and efficient. Approved hand-held igniters can still be used by helicopter-transported field crews to ignite isolated pools of oil.

Burning efficiencies of approximately 97 percent have been achieved in numerous large scale and meso-scale experiments.

In practical applications, values tend to be lower because a proportion of the oil is contained in pools too small and numerous to burn (refer to pool sizes shown in Table 5-1), and not all of the oil is available in sufficiently thick films. As a general rule, it is considered practical to burn 80 percent of all oil present in pools greater than 50 square feet, amounting to 68 percent of the total oil exposed on the surface (Norcor, 1975; Buist and Dickins, 1981, Gulf Canada, 1990). Manual recovery of any burn residue or thin unburned oil films on the ice may increase the overall recovery effectiveness by up to 10 percent. In addition, natural evaporation will remove an additional 30 percent of any oil lying on surface melt pools prior to burning. Realistic estimates for the amount of residual oil remaining after all cleanup and natural processes up to the point of final ice breakup range from 10 to 20 percent. With appropriate safety precautions and a helicopter or amphibious vehicle in attendance, surface operations on the ice can continue until within a few days of breakup.

The small amount of residue left after burning (typically a few percent of the oil available for burning) can be recovered manually with crews on the ice and transported to shore with helicopter buckets.

As the ice begins to break up nearshore in mid-June, and near the barrier islands in early July, the response options will depend on the ice concentration as discussed earlier. There will be a period of several weeks when response operations will need to apply a mix of strategies over short periods as conditions allow: Oil containment booms and skimmers operated from shallow draft barges in light to moderate ice, *in-situ* burning of thick oil trapped between the floes in heavier ice, and manual cleanup and pumping from any ice rubble remaining attached to the island, as well as cleanup of any shoreline or gravel pad surfaces that may have been affected.

As ice concentrations diminish to less than 3/10 in the nearshore areas by mid-June and offshore by mid-July, response operations will become increasingly less restricted by ice and more able to rely on traditional open water mechanical containment and recovery techniques (Figure 6-11).

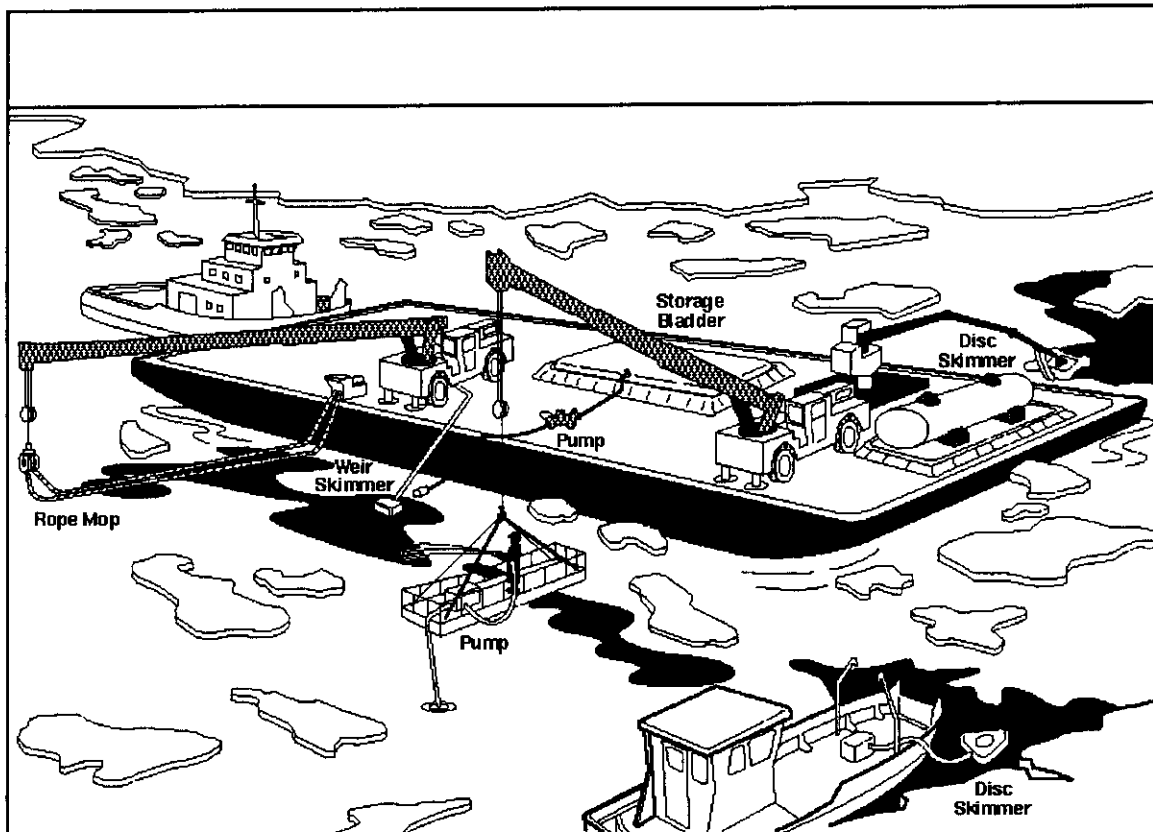


Figure 6-11

Broken Ice Mechanical Containment and Recovery Operations

7.0 SYNOPSIS: OIL AND ICE SPILL RESPONSE IN THE BEAUFORT SEA

In summary, the knowledge gained through actual spills, drills, experimental field spills, tank tests, and analytical studies has led to the evolution of a number of practical response strategies and options to deal with a wide range of nearshore and offshore conditions expected in the North Slope oilfields adjacent to the Beaufort Sea. Today's arctic spill contingency plans focus on multiple countermeasure options to cope with different spill situations. *In-situ* burning in ice and with fire-resistant booms in open water are proven techniques, as is mechanical recovery with the latest generation of containment and recovery equipment.

Each season presents different drawbacks and different advantages for spill response. During freezeup and breakup, drifting ice and limited site access tend to restrict the possible response options and significantly reduce recovery effectiveness. Mid-winter involves long periods of darkness and cold temperatures but provides a stable ice cover that not only naturally contains the oil within a relatively small area but also provides a safe working platform for oil recovery and transport.

The summer open water period provides the advantage of familiar response techniques but introduces the variability of wind and waves and the challenge of containing an extremely mobile target.

For seven to eight months of the year, ice aids oil spill response in the Beaufort Sea. Solid ice naturally contains and immobilizes oil for an extended period of time in the winter (up to 230 days corresponding to the period of stable ice cover nearshore). The presence of solid landfast ice allows response teams to mobilize the necessary resources and plan a coordinated winter response effort with a high probability of recovering a large percentage of the spilled oil. At the same time, the environmental conditions present during the summer months are also much more favorable to offshore cleanup when compared with many more temperate areas. For example, broken ice during breakup tends to limit oil spreading and maintain the oil in thick patches amenable to burning *in-situ* with a Heli-torch. The generally low to moderate sea states during the open water period increases the effectiveness of booms and mechanical recovery systems.

Response planning supported by detailed sensitivity assessments, coastal classifications, computer tracking models, and regular training of the North Slope Spill Response Team and ACS staff provides the foundation for an organized and timely response at any time of the year. This foundation is augmented with continuous development of working relationships with other spill response organizations and response contractors within the State of Alaska. Further efficiencies will be attained as ACS, and its Member Companies, continue to support and participate in ongoing research and development of new or enhanced response methodologies, systems and equipment dedicated to mitigating the effects of oilspills in the arctic environment.

Recently, a great deal has been learned about Arctic offshore oil spill response through practical experience and research. In many respects, the Arctic offshore is a more favorable environment to carry out an effective oil spill cleanup than many ice-free waters. This is not to say that spill cleanup in an Arctic environment will ever be a simple operation, or that the impacts of spills in ice covered waters can be dismissed. There are, however, many aspects of the natural ice environment that, if properly understood, can be made to work in favor of a successful offshore oil spill cleanup.

Mechanical Oil Recovery in Ice Infested Waters (MORICE)

Hans V. Jensen, SINTEF
hans.v.jensen@chem.sintef.no

Jim McHale,
Alaska Clean Seas
Prudhoe Bay, Alaska, USA

Abstract

In 1995 the R&D program “Mechanical Oil Recovery in Ice Infested Waters” (MORICE) was initiated due to the lack of efficient techniques to clean up oil spills during winter conditions.

The overall objective of MORICE is to develop technologies for more effective recovery of oil spills in ice. MORICE is a multinational effort that has involved Norwegian, Canadian, American and German researchers. Financial contributions from oil companies, private as well as governmental oil spill responders, governmental agencies and research funds have secured the funding.

Each phase of the program has been organized as a separate project with its own objective:

Phase 1 started with an extensive literature review to identify available information from previous efforts to develop oil-in-ice recovery equipment. Following this, a series of brainstorming sessions and technical discussions were held to evaluate past ideas and generate new ideas for potential solutions to the problem. As a result, ten concepts were suggested and discussed in detail by a Technical Committee.

Phase 2 of the program involved qualitative laboratory testing of six of the concepts from Phase 1. The lab tests in Phase 2 were carried out in a test tank where oil in ice-infested water conditions could be prepared. This phase of the study provided important insight and reduced the number of concepts that warranted further evaluation and development.

Phase 3 focused on continued development of two concepts that were selected from Phase 2, the lifting grated belt (ice processing/deflection) and the brush-drum system (oil recovery). Detailed quantitative testing was conducted on these concepts at a larger scale in the Hamburg Ship Model Basin (HSVA) in Hamburg, Germany.

In Phase 4 a complete full-scale harbor-sized prototype was designed and constructed, comprising oil recovery and ice processing units as well as the support

vessel. The prototype was tested in the Alaskan Beaufort Sea during freeze-up in October 1999. Oil was not introduced during these tests.

At present Phase 5 is planned to take place in 2000 and will probably be the final phase of the MORICE program. Following more extensive component testing of oil recovery in ice under controlled conditions, further ice testing will be carried out in the Alaskan Beaufort Sea before the complete prototype is tested in oil and ice, probably at the OHMSETT test facility in New Jersey, USA.

1 INTRODUCTION

Several countries on the Northern Hemisphere face the risk of an oil spill in waters where ice is present permanently or during parts of the year. Among these countries are Canada, USA, Sweden, Finland, Norway, Germany and Russia, all of which have pursued certain R&D activities in the past to improve their capability to remove oil in ice-infested waters.

The recovery of oil in ice was studied extensively in the 1970s. This work mainly involved evaluations of modified and unmodified off-the-shelf equipment. In the early 1980s, brainstorming and laboratory studies were conducted on this topic. However, few concepts were developed to an operational or prototype stage. In 1992, a state-of-the-art review was published by the Canadian Association of Petroleum Producers that summarizes the status of mechanical oil-in-ice recovery and identifies the most promising approaches in terms of seven existing oil removal principles (Solsberg et al, 1992). This report represented a starting point for the MORICE technical process.

Despite the similarities of the problems faced by several of the northern nations, the R&D activities on mechanical oil recovery in ice have rarely been coordinated internationally. Rather, they have been conducted on an individual basis according to the objectives and criteria determined to be priorities in each country. MORICE was initiated with the understanding that an international cooperative effort is both a cost-beneficial and effective way in which to work out new techniques for oil removal in ice. MORICE is a multinational effort involving Norwegian, Canadian, American and German researchers. The present paper is presenting a qualitative description of the program towards the end of Phase 4. Most of the results from the work cannot be presented though due to confidentiality clauses.

1.1 Organisation of the program

Before the program could be started it took some time to find out how to organize the work.

Funding

For a program that most likely would take several years to finalize, it was not realistic to secure the funding for the whole period from the start. Hence the work had to be divided into phases, small enough that each phase could be treated as a separate project, with its own objective and its own funding. Furthermore it was clear that each project had to be funded as a joint project. It had to be expected that the participants or sponsors typically would join in for one or more phases, but that few sponsors, if any, would stay in throughout the whole program.

Although some funding from official sources like research funds would be expected, it was also realized that financial contribution had to come from private industry like oil companies and response organizations. This led to the conclusion that the results from the work had to be considered proprietary information within a certain period after the reporting.

Literature review

The members of the project team had different background and experience from working with mechanical oil recovery equipment some way or another. It was considered necessary that all the Technical Committee members had an overview of the R&D work that had taken place over several decades, and it was decided to spend the time required to go through all information that could be found on the issues of interest. Each member would be assigned to reviewing a number of these documents in depth, while the other members would read through the same documents more superficial. After reviewing some documents, the team would go through them in telephone conferences. This way the more valuable documents could be identified fairly effectively and studied more thoroughly by all the team members.

Brainstorming sessions were held several times. One first session was held before the literature review started, based on ideas from each member of the group. Later more sessions were held to continue the process after reviewing the literature, and after the different team members had the chance to “digest” the ideas from previous meetings. This process was exhausting, partly because the discussions would be heated when persons had different views or interests, partly because such a process requires that all the persons be focused during the discussions. However, these meeting were also very fruitful.

Define scenario

Even during the first meetings it was obvious that due to different background and experience, discussions would be difficult because different persons had different perception of the issues currently discussed. It was realized that a set of conditions, a scenario, had to be defined as a common background for the discussions. This way the MORICE scenario came about.

2 OBJECTIVE

The overall objective of MORICE is to develop more effective technology for recovery of oil spills in ice-infested waters.

The program relies on a stepwise approach involving brainstorming, laboratory studies and field evaluations and has the commercialization of effective equipment as the ultimate goal. It is organized in several phases, allowing funding parties to evaluate the outcome of each phase throughout the process.

PHASE 1 – PILOT STUDY

A Technical Committee that engaged in extensive technical discussions conducted the Phase 1 work. The committee considered the applicability of existing methods as well as the potential of new concepts conceived during the technical sessions. As a result, ten concepts were proposed involving both ice processing and oil recovery techniques.

A database was compiled containing both the available information on previous efforts to develop oil-in-ice recovery equipment as well as information on historical spills and oil behavior in ice.

Here the main activities and conclusions of Phase 1 of the study are presented, and six recommended concepts for oil-in-ice recovery are briefly described.

Phase 1 had the following objectives:

- To identify and address the fundamental problems related to the recovery of oil spilled in ice.
- To identify the potential applicability and limitations of existing oil spill clean-up equipment for use in ice.
- To suggest technical solutions with a potential for oil-in-ice clean-up, considering both existing and new concepts.
- To recommend an approach for the development of more efficient methods to clean up oil spills in ice, and to define the elements essential in the subsequent phases in the program.

3 PHASE 1 ACTIVITIES

A Technical Committee consisting of 5 members representing the participating institutions performed the work in Phase 1. As the initial step, the Technical Committee members conducted an extensive and coordinated review of the literature describing any past efforts to develop oil-in-ice recovery equipment. Also literature relating to oil behavior in ice and case histories was reviewed. As a result, more than 200 references were examined in depth by the study team. The comprehensive set of literature formed the basis for all subsequent technical meetings. In the Phase 1 report

it is summarized in a set of cross-referenced tables to allow easy access to the documents of interest.

As a next step, an oil spill scenario, describing both oil and ice conditions, was selected and the specific problems involved in oil-in-ice recovery were identified based on the collective experience of the work group and a study of past oil spills in Arctic areas.

A brainstorming session was held at the commencement of the project in which approximately 20 concepts were proposed for possible application to mechanically recover oil in broken ice. At a later stage, the Technical Committee reconvened to re-examine the concepts in detail so that the less feasible ones could be discarded in favor of more practical approaches. This was followed by a workshop at which the Technical Committee presented the suggested technical solutions to a larger group consisting of experienced representatives from Norway, Canada, Germany and Sweden.

MORICE Scenario

An oil-in-ice spill can involve a wide variety of ice conditions. In very light ice conditions, the presence of ice can be treated as a simple debris problem, similar to situations frequently encountered in open water. In other cases the oil may be trapped between floes or may be intermixed with small ice forms making it virtually inaccessible for recovery. Before addressing the problems of oil-in-ice recovery on a technical level, it was essential to define one or more oil spill scenarios on which to focus the discussions, since different environmental conditions or spill circumstances may call for completely different approaches. Once the spill situation was defined, the various problems involved in oil recovery under such conditions could be addressed in a systematic manner.

The spill scenario was selected to represent the environmental conditions within the geographical areas of the participating countries to the greatest extent possible. A situation with relatively light ice conditions was considered to be the most relevant to all the participants involved. It was agreed to focus on the following scenario for the technical work:

-
- Broken ice
 - Up to 70% ice concentration on a large scale; locally up to 100%
 - 0 - 10 m ice floe diameter
 - Small brash and slush ice between ice floes
 - Mild dynamic conditions (current, wind)
 - A wide range of oil viscosity
-

These conditions imply that the recovery operation be marine-based (on-water operations). The selected environmental conditions imply an ice field that is open enough to maneuver a ship to the spill site. However, due to pile-up in front of the recovery unit, the ice concentration can be up to 100% in its immediate vicinity, even if the

overall ice concentration (for example within a 1 km x 1 km square) is much lower. It must be noted that larger ice floes can be present but will not be processed in any way by the unit. In this case the recovery process would circumnavigate these larger ice floes.

4 DIFFERENT APPROACHES FOR DEVELOPING OIL RECOVERY TECHNOLOGY

The problem of recovering oil in a broken ice field characterized by ice forms of various types and dimensions can seem overwhelming. One way to attack the problem in a systematic manner is to break it down into separate tasks according to the scale of the ice present, see Figure 4.1.

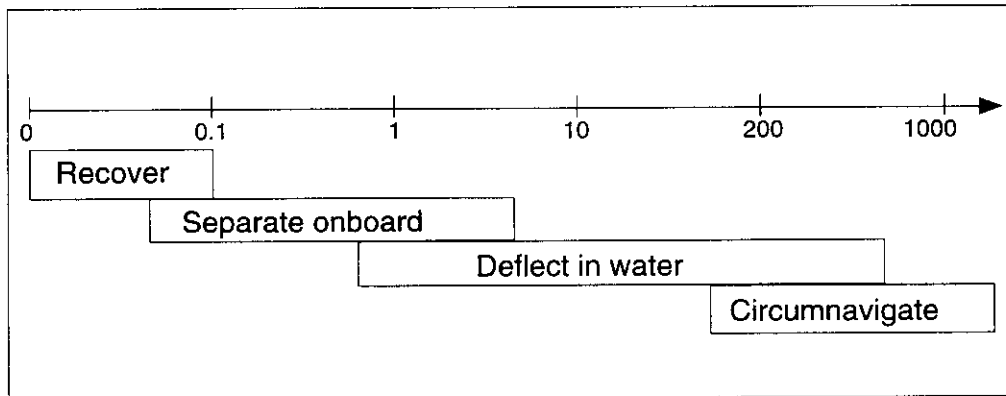


Figure 4.1 Response method according to ice dimensions

Small ice pieces like slush and small brash ice will most likely be collected together with the oil. The only way to separate this ice from the oil may be after melting it in a storage tank. Depending on the scale of the unit, ice forms with dimensions up to a couple of meters may be possible to bring onboard the recovery unit in order to access the oil or clean the ice actively. However, if collected, such ice pieces will require an enormous storage capacity, and the recovery system must incorporate some means of separating these ice floes from the oil and finally re-deploy the ice back into the water. Ice floes larger than this can not be processed onboard and may have to be deflected in the water to avoid interaction with the recovery unit. A challenge for the recovery operation is to selectively deflect these floes while minimizing the amount of oil diverted simultaneously. It may not be practical to deflect large ice floes, and the recovery operation may be required to circumnavigate these floes rather than attempting to deflect them.

The concepts that were discussed address different tasks along the process line illustrated in Figure 4.1. Some concepts are solely ice/oil separation devices, conceived to transform the conditions from one with a wide variety of ice forms to a more uniform small brash ice situation, assuming that this is easier to handle. Other concepts, on the other hand, are solely recovery devices with no means of deflecting

ice. In many cases, the problem of oil recovery in a mixed ice field may require a combination of several methods, unless some recovery system is identified that is able to recover oil directly without deflecting ice. This reasoning leads to the identification of two different approaches that can be applied to address the problem of oil recovery in broken ice:

Approach 1 - Ice-deflecting oil recovery systems

An ice deflecting system for recovery of oil in broken ice will have to incorporate four components:

-
- 1 A mechanism to recover oil intermixed with small brash ice, preferably with a minimum of ice in the recovered product.
 - 2 A means of separating small floes from oil and small brash ice either onboard or in the water.
 - 3 A method for selectively deflecting larger floes while minimizing the movement of oil with the ice.
 - 4 A working platform that is capable of moving alongside and/or over very large ice floes.
-

Components 2-4 are intended to transform the conditions from the complicated oil in broken ice situation to the more simple oil in small brash ice mixture. The term "small brash ice" as used refers to ice with dimensions up to maybe 20 cm. Oil recovery is effected by component No. 1 only. The four components are prioritized in the sense that solving a problem on the bottom of the list will not improve the recovery capability unless the problems higher up are also solved. However, solving problem No. 1 will always be useful since environmental conditions exist where only brash ice is present. This may indicate a preferred priority of the development efforts.

Approach 2 - Non ice-deflecting oil recovery systems

A non ice-deflecting recovery system will have to incorporate:

-
- 1 A recovery device that can recover oil intermixed with small brash ice, with a minimum of ice in the recovered product.
 - 2 A working platform that can position the recovery device anywhere in the spill and can operate with a minimum deflection of the larger ice.
-

Such a system will have to attack the oil slick from above and must be able to move on top of or through various ice forms as well as in water. Clearly, Approach 2 involves fewer elements than Approach 1 and may represent the simpler solution to the problem.

5 CONSIDERATIONS AND POTENTIAL PROBLEMS FOR OIL-IN-ICE RECOVERY

Discussions were undertaken to identify the main problems and considerations that should be addressed for an oil recovery operation in ice infested waters. These factors, addressed below, were considered when assessing the feasibility of the various suggested concepts.

Reduced flow of oil to the recovery device

In ice-free open water conditions, natural spreading of the oil as well as the relative velocity of the recovery device are factors that ensure more oil to be encountered. Depending on the ice concentration and the viscosity/density of the oil, this effect is reduced or completely eliminated for oil spills in ice. This poses special requirements of the recovery system since it must be able to move to the spilled oil or, alternatively, be able to deflect the ice in order to recover the oil. In ice concentrations up to 20-30%, oil is assumed to spread freely without any significant limitations due to the ice.

Limited access to the oil

Moving a recovery unit to the spilled oil can be very complicated due to the presence of ice. This depends on a series of parameters such as the ice concentration, floe sizes, ice thickness and the dynamics of the ice field. The ice conditions impose special requirements on the operation platform with respect to strength, maneuverability, crane working range etc. Depending on the temperature, wave conditions and weather since the spill occurred, the spill can be frozen into the ice or heavily mixed with brash and slush ice. A common problem when operating a skimmer from a ship is that the vessel opens up the ice field and oil that initially was concentrated between floes spreads and forms a much thinner layer that is less recoverable.

Unintentional deflection of oil during ice deflection

Ideally, the recovery of oil in ice should entail collecting the oil while leaving the ice behind. This usually implies that a form of ice processing or ice deflection is required. However, deflecting the ice without also deflecting the oil is difficult since oil and ice may be intimately mixed, pools of oil may be trapped in clusters of ice or oil may adhere to the edges of ice floes. During all ice deflection operations, a certain amount of unwanted oil deflection is to be expected. The key objective would be to reduce this oil deflection to the greatest extent possible.

Separation of oil from ice after recovery

Oil-in-ice recovery methods will collect varying amounts of small ice forms with the oil. In addition to the common oil/water separation problem, oil-in-ice recovery systems must address separation of oil from ice and water onboard the recovery vessel. The complexity of this problem will vary depending on temperature, to what degree the oil is intermixed with the ice, the efficiency of the recovery equipment, oil properties etc.

Contamination of ice /cleaning of ice

During the recovery process, some recovery principles are likely to increase the visible oiling of ice. An example is the mop concept which often may leave the ice apparently more contaminated after recovery. In addition to being a visual pollution problem, the oil may be more hazardous to wildlife when spread over the top of the ice as opposed to being concentrated between the ice floes. Incorporation of an ice cleaning method into the oil-in-ice recovery system may be considered to reduce this problem.

Changing oil properties

Oil viscosity increases with decreasing temperature. Since temperatures could be below the pour point of the oil, the recovery device may have to be able to recover oils of very high viscosity. Presence of ice intermixed with the oil may highly reduce the efficiency of recovery by adhesion. One reason for this is that the adhesion between oil and ice might be just as strong as adhesion between oil and recovery material.

Icing /freezing of equipment

A variety of operational problems may be experienced due to low temperatures and ice. Examples may include the freezing of hoses and moving parts and jamming of skimmers and pumps due to the accumulation of ice. Scrapers for adhesion skimmers may also work less effectively due to ice pile-up, jamming by ice, stiffening of rubber compounds, etc. Low temperature operation can present various other difficulties with hydraulic fittings and controls, gratings, screens and water spray systems. At low temperatures, storage of an oil/water/ice mixture could cause serious problems if no system to avoid further freezing is incorporated.

Strength considerations

Operating in ice infested waters will require that both the operation platform and the recovery unit be designed to withstand impacts with ice. Exceptions are amphibious type platforms that can operate on top of the ice.

Other problems/challenges

Cold conditions tend to lower the efficiency and performance of the response personnel. All equipment should be designed with this in mind and be made with robust parts and adjustments that can be readily made in cold climate. Cold weather operations pose health and safety risks to the response crew. Appropriate measures must be included in any response operation to provide protection from the elements. Problems may also be encountered relating to the detection and monitoring of oil spills, especially in poor light conditions.

6 POTENTIAL OIL-IN-ICE RECOVERY CONCEPTS

More than 20 concepts for oil-in-ice recovery were suggested at the first MORICE brainstorming meeting. A number of concepts were, after the initial discussions, not found to warrant detailed assessment and are only briefly described in the Phase 1 report.

In this section, some of the concepts that were subjected to in-depth assessment by the Technical Committee are described. Some of these are variations of well-known principles used in open water. Others are based on old but unrealized ideas conceived for ice-infested waters whereas some are completely new ideas. Each principle is discussed in the report in terms of:

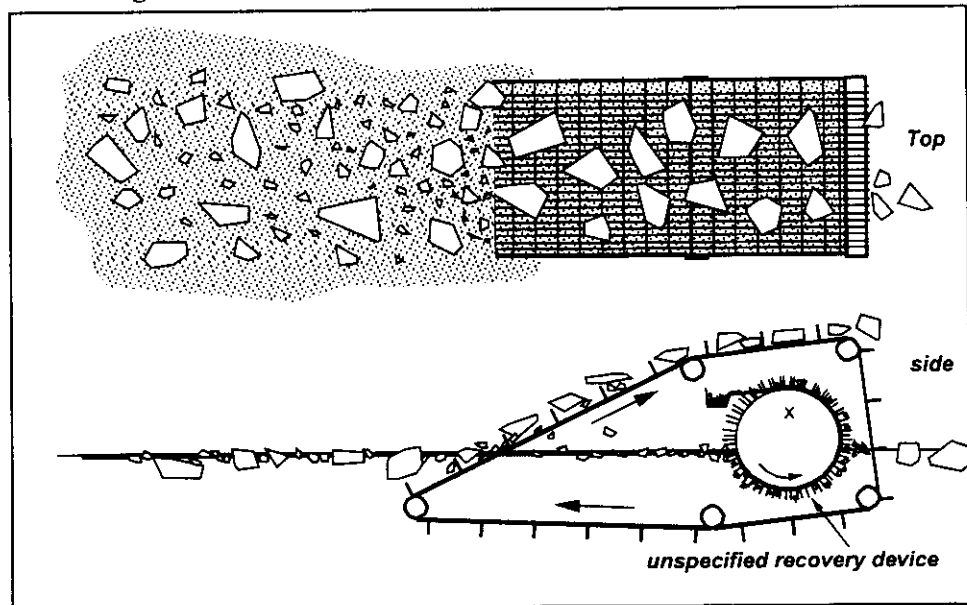
- Operating principle
- Possible variations to the general principle
- Potential problems and considerations
- Advantages
- Status of development and overall potential

The concepts are categorized according to their principle of operation as follows:

Oil Recovery Principle	Adhesion, Lifting, Suction, Unspecified
Ice Processing Principle	Ice Deflecting, Lifting, Submerging, Lateral displacement, Non Ice Deflecting
Ice Cleaning Principle	Active, Passive, None
Operating Platform	Incorporated, Unspecified

Most concepts address only one or two of these functions, and the concepts are only briefly described here. For an in-depth discussion of each concept the reader is referred to the MORICE Phase 1 report.

6.1 Lifting Grated Belt

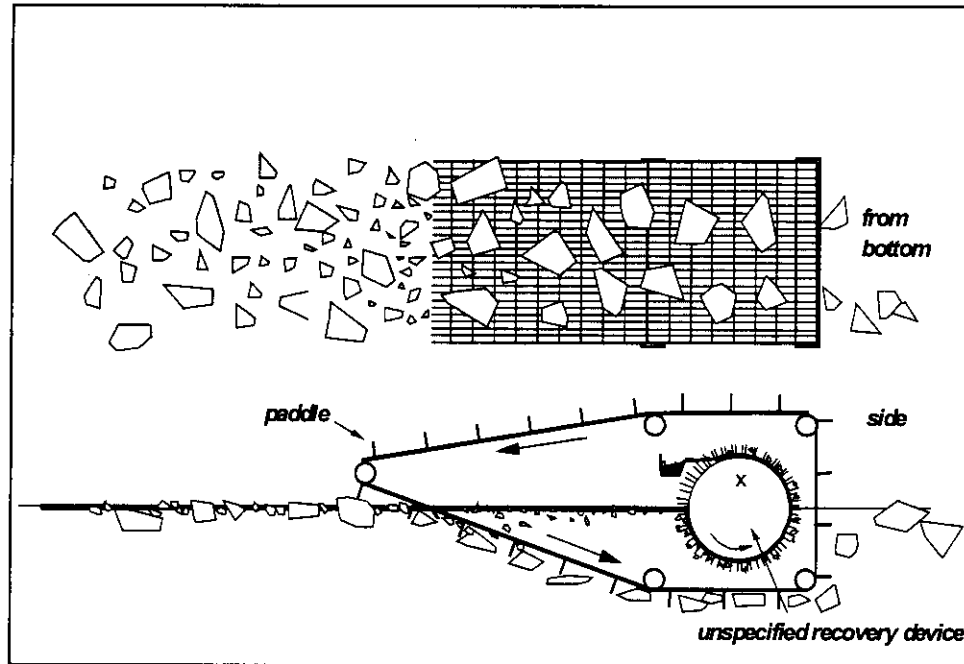


Oil Recovery	Unspecified recovery method inside the belt.
Ice Processing	Deflection by lifting of small ice floes. Larger ice floes must be circumvented or deflected sideways by separate mechanism.
Ice Cleaning	None. Although not specified, an ice cleaning system can easily be incorporated, using water spraying or brushes.
Operating Platform	Unspecified

This concept is an ice deflecting principle that prevents larger ice pieces from entering the recovery area, leaving a mixture of oil and small brash ice on the water surface. Spiked paddles mounted on a chain raise encountered ice along longitudinally oriented rails. It is critical that the spacing between the rails is such that the amount of ice deflected is maximized and the oil quantity lost with the disposed ice is minimized. Most of the oil should pass through the lifting portion of the belt at the water line. Oil that is unintentionally carried up the belt together with the ice may drip off or can be actively removed with the use of water flushing. Smaller ice pieces will pass through the grating and enter the recovery area together with the oil. The concept depends on a recovery device capable of recovering oil in small brash ice operating in the area inside the belt. Brash ice may be evacuated through openings in the unit after oil has been recovered. Alternatively the entire ice/oil volume inside the belt may be transferred to storage if the required storage and/or separation capacity is available.

Excessively large ice pieces must be deflected sideways in the water by a separate method. Some oil will be lost, adhering to the ice re-deployed into the water behind the belt. The concept differs from existing belt skimmers in that the belt is used solely as an ice deflection mechanism without the intention to recover oil by adhesion.

6.2 Submerging Grated Belt

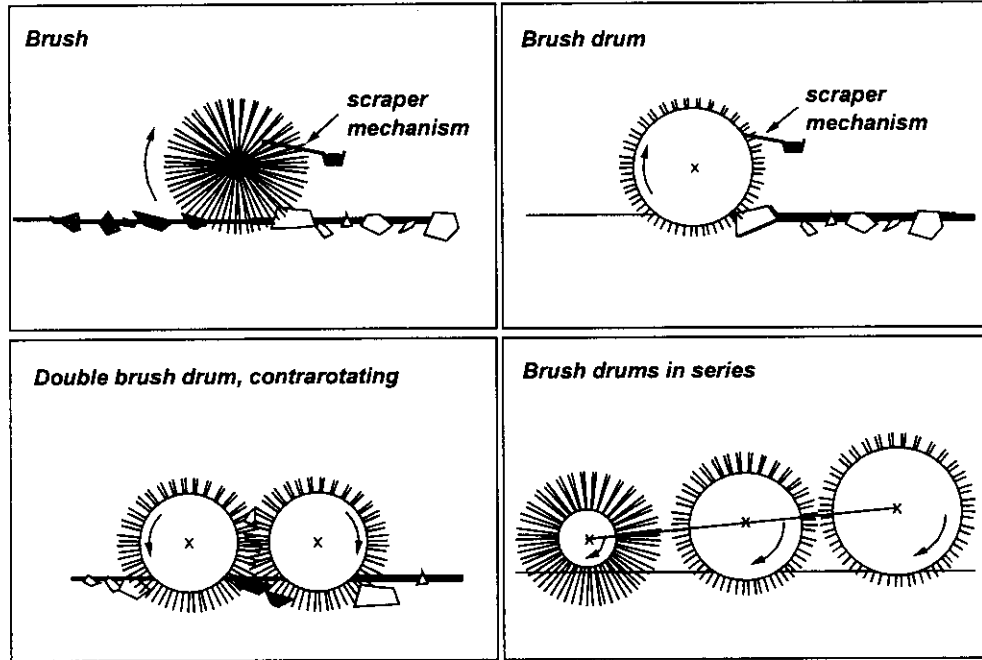


Oil Recovery	Unspecified recovery method inside the belt.
Ice Processing	Deflection by submergence of small ice floes. Larger floes must be circumvented or deflected sideways by separate mechanism.
Ice Cleaning	Passive - by flushing with water as ice is submerged.
Operating Platform	Unspecified.

This ice deflection principle uses a grated belt to depress ice as the unit advances. The grating allows oil and small ice pieces to pass through the descending portion of the belt at the water line or rise from the submerged section to the water surface inside the belt where recovery of oil takes place by an unspecified method. The deflected ice floes will re-surface behind the unit. The belt can be equipped with paddles or spikes, similar to the Lifting Grated Belt. The opening of the grating is decisive for the performance of the unit. Openings that are too narrow will reduce oil passage through the grating, hence large amounts of oil will be lost behind the unit. Wide openings, on the other hand, will allow large amounts of ice to pass into the collection area. This problem is expected to be more and more noticeable with increasing density and viscosity of the oil. The separation process may be aided by ice tumblers, shaking action, brushes etc. The device must have a considerable weight if large amounts of ice are to be submerged. However, the force required is much lower compared to the lifting belt concept. On the other hand, buoyancy forces that are important for separation of oil from ice are similarly lower compared to the gravity forces utilized for separation by the lifting belt.

Similar to the lifting belt, this concept is based on the assumption that oil recovery is simplified in the absence of large ice floes. Methods to deal with the oil and ice mixture in the recovery area may be similar to those considered for the Lifting Grated Belt.

6.3 Brush and Brush-Drum

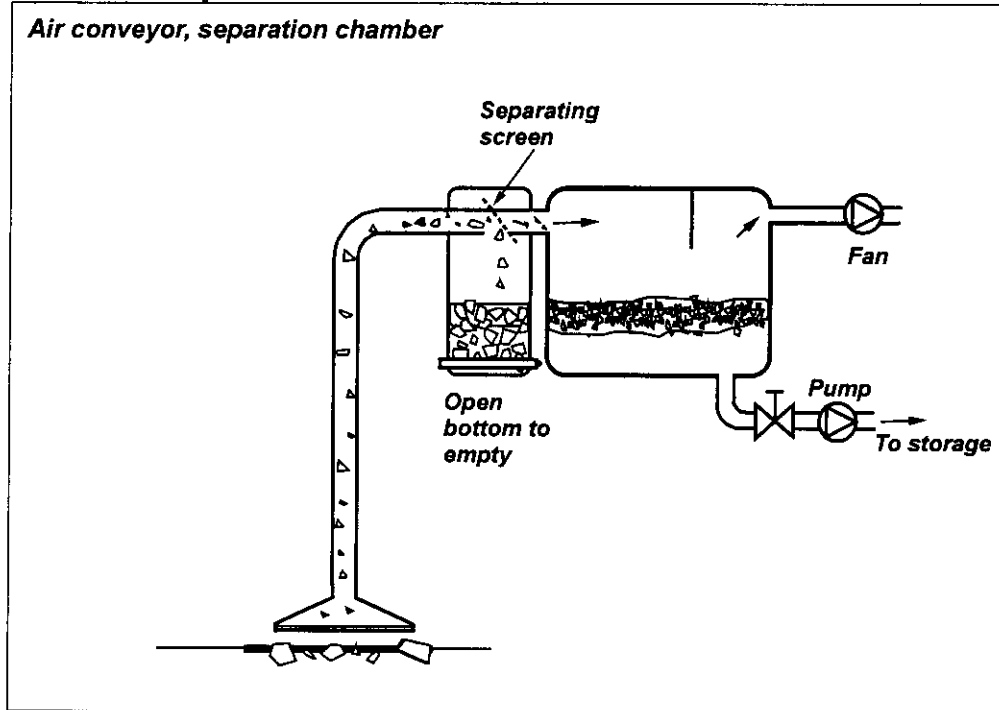


Oil Recovery	Adhesion and mechanical lifting by bristles and spikes. Adhesion to smooth part of drum.
Ice Processing	Submerging of small ice pieces. Rolls over larger ice.
Ice Cleaning	Active by brushing, Passive by submersion.
Operating Platform	Unspecified. Can be floating or attached to a vessel.

This concept attempts to combine the potential of the brush to contact oil that is intermixed with small ice forms with the advantages of the drum, primarily its light weight and large buoyancy. Oil is collected by adhesion to the smooth part of the drum and to the bristles that are installed on the surface. The oil is removed by a comb mechanism and/or a scraper. Small ice forms are deflected under the brush/drum by the bristles and spikes. Several alternatives were discussed including a system with two or more brush/drums, one after the other. The brush/drums have different bristle stiffness, where each stiffness is designed to serve a specific function, i.e. remove oil on the ice and water surface, recover oil between ice pieces or convey ice away from the recovery device. Bristles must be fabricated from a flexible and very durable material to prevent them from being permanently damaged when encountering ice. Evenly distributed spikes between the bristles may protect the brushes from excessive bending. Parameters like bristle length and stiffness, drum diameter, angle of attack between brush drum and surface, number of brush drums

and rotational speed are expected to be important factors for both oil recovery and ice processing.

6.4 Air Conveyor

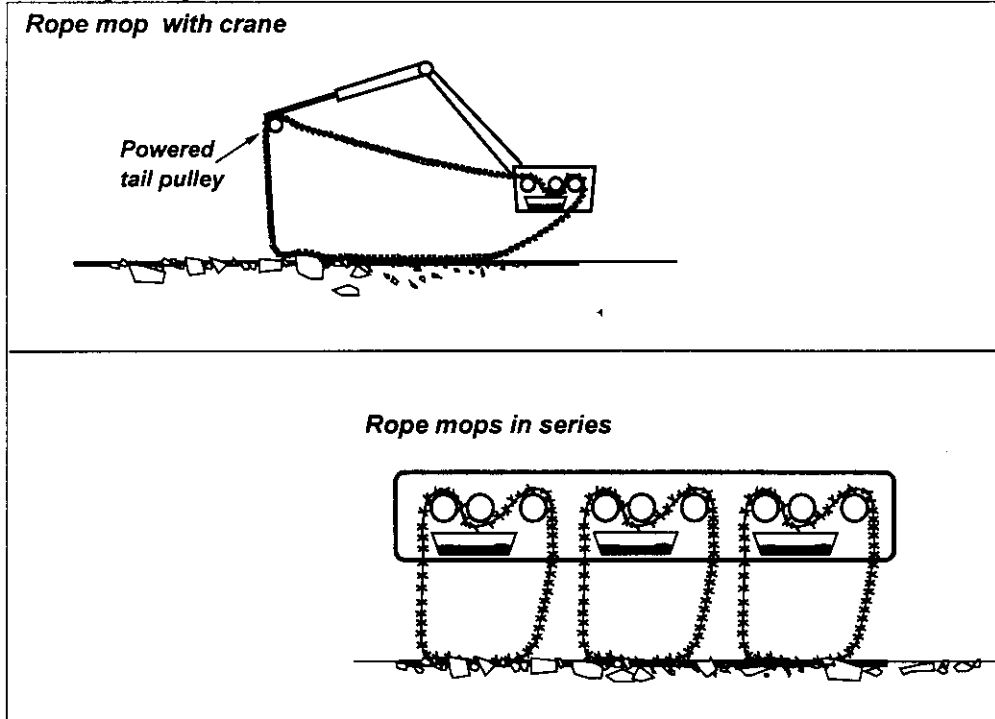


Oil Recovery	Suction. Air at high speed pulls oil and small ice into a hose and moves it to a collection tank.
Ice Processing	No ice deflection. Collects small ice pieces.
Ice Cleaning	Active by suction
Operating Platform	Unspecified

An air conveyor creates high air flow at the suction end of a hose connected to a recovery head. Oil, water and small ice are drawn into the hose and transferred to a separation chamber installed at the end of the line. The separation chamber consists of an ice compartment, an oil/water compartment and a separation screen or grating between the two. Ice pieces above a certain size will be stopped by the screen and fall into the first chamber. Fluid will pass through the grating to the second chamber. The recovery head will work from above the oil slick and may therefore avoid extensive ice deflection. Several versions of the skimmer head were discussed including brushes, drums or a plain suction head with a continuously cleaned screen.

A common problem with air conveyors in low temperatures is freezing of the hoses. This may be avoided with steam injection or other heating methods. Ice pieces that are jammed in the grating can be removed continuously with some combing/scraping mechanism. One advantage of this system is its low weight at the recovery end since any material recovered will be conveyed away from the recovery head instantly.

6.5 Rope Mop

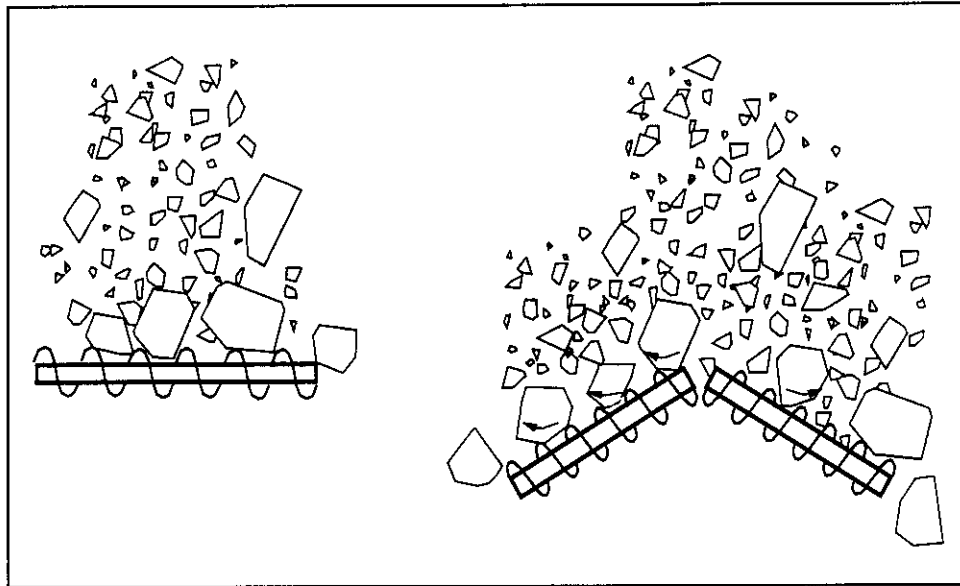


Oil Recovery	Adhesion to mop material.
Ice Processing	Non ice deflecting. The concept operates from above without need for ice deflection.
Ice Cleaning	Active by mop action
Operating Platform	Unspecified

The rope mop concept is one of the oil recovery principles that has been used most frequently and with the most success in oil-in-ice situations. It is included here for its possible improvement potential and/or for possible combination with other oil skimming and ice deflection principles. Existing rope mop skimmers include versions that are integrated into catamaran vessels, suspended from a drive/wringer head operated by crane and those with anchored tail pulleys. A number of improvements have been proposed to adapt the rope mop skimmers to Arctic conditions. These improvements include hot pressurized water spraying of mops, installation of a pump in the sump, improvements to the wringer mechanism, development of mops for recovery of high viscosity oils, reduced exposure to cold air etc. Additional changes discussed include replacing the commonly used single long mop between hulls on catamaran type skimming vessels with several shorter ones in series. This will increase the throughput efficiency of the system. A great advantage of the vertical mop system is that no ice processing is required and the mop can be selectively positioned to the areas of high oil concentration. The mop skimmer is a proven device for brash ice conditions (Jensen et al, 1993).

Although the rope mop concept was considered to have a high potential for improvement, it has not been studied in later phases of the program. This is probably due to the fact that several members of the project team earlier have studied this concept carefully, also under oil in ice conditions. In other words, the absence of rope mop concepts in the following phases does not mean that rope mops have been ruled out as a useful recovery method in a broken ice situation.

6.6 Auger Deflector



Oil Recovery	Adhesion to auger or; None
Ice Processing	Deflection by lateral displacement of ice.
Ice Cleaning	None
Operating Platform	Unspecified

The concept consists of a drum with auger flights incorporated on the surface. The unit is operated horizontally and partially submerged in the water. As the rotating auger advances through the ice field in a direction perpendicular to its longitudinal axis, the auger flights deflect the encountered ice pieces laterally. The oil that adheres to the auger flights and the drum is scraped off. This idea evolved from the discussion on drum skimmers which, due to their smooth surfaces, are incapable of displacing ice pieces. The auger device can be used solely as an ice deflector or as a combined deflection/recovery method. It represents an active deflection method that allows the residence time to be controlled to enable sufficient time for a separate recovery method, e.g., a brush, prior to ice deflection. If used only as an ice deflector, the auger does not have to incorporate a drum. However, using a drum as the core in the auger may still be advantageous as a means of providing flotation. The auger is likely to deflect oil together with the ice and because the recovery body also acts as a deflection device, problems could be encountered matching deflection rate with

necessary residence time for recovery of all the oil between the floes. A system incorporating a second recovery method would be more controllable. A relatively complex scraping mechanism is required to remove oil from the auger.

7 CONCLUSIONS AND RECOMMENDATIONS FROM PHASE 1

Two principally different approaches were suggested for recovery of oil in ice. The first approach involves an initial separation of ice floes from oil to obtain a situation with oil in small brash ice, using different deflection methods depending on the scale of the ice present. In addition, the approach requires a method to recover oil in small brash ice. The second approach is predicated on the development of a non-ice deflecting oil recovery system which, similar to the first approach, features a recovery device capable of recovering oil in small brash ice and oil in between floes when positioned directly in the spill. Furthermore, the system must include a working platform that is able to position the recovery device anywhere in the oil spill.

It was recommended that the development of an oil-in-ice recovery system should focus on the following aspects:

Development of a recovery device for operation in small brash ice

Both approaches identify the need to develop a device capable of recovering oil in small brash ice. Several concepts were discussed for this purpose. It was concluded that the Brush-Drum and the Rope Mop have the highest potential of success in this kind of operation. To our knowledge the combination of brush and drum as proposed here had not been evaluated before. It was suggested that this concept be investigated as a recovery method for oil-in-brash-ice applications. In several past studies mop type recovery devices have been confirmed to have a good recovery potential. It was believed that mops may be a key component in a recovery system in ice and that several improvements to the wringer mechanism, method of deployment and mop material can greatly enhance its performance.

Recovery of oil in brash ice will inevitably lead to the recovery of small ice forms together with the oil. The development of a recovery system for operation in ice will have to address this issue and investigate methods to separate ice from oil after recovery.

Ice deflection

Several methods of separating oil and ice have been discussed. These methods include lifting or submerging the ice using grated belts, or the lateral deflection of ice by augers or grated plough-shaped deflectors. The capacities of the vertical deflection methods are limited by the weight and dimensions of the ice forms, while lateral deflectors can deflect larger ice floes. Several of these techniques were believed to have the potential to separate oil from ice. It was recommended that the proposed deflection methods be further evaluated and compared through physical testing in a laboratory. Such tests should focus on methods to deflect ice while minimizing the deflection of oil away from the recovery device. The non ice-deflecting oil recovery methods will not have to incorporate the means to overcome this concern.

Operating platforms

Since a main problem is the access to the oil, the operational platform is a vital element in an oil-in-ice recovery system. It was believed that the performance of several of the recovery methods presently available could be greatly improved by an operating platform capable of positioning the recovery unit anywhere in the polluted area. It was recommended that platforms available for use in an ice-infested environment be evaluated. Archimedean Screw Vehicles in particular are potentially useful in an oil-in-ice response operation since the vehicle can operate on ice as well as in water and brash ice, and was believed to be able to move to the spill site with a minimum of disturbance of the ice field. In this way, the natural oil containment by the ice could be maintained and utilized.

PHASE 2 – QUALITATIVE LABORATORY EVALUATIONS

The objective for Phase 2 was to evaluate, at a qualitative level, the feasibility of the concepts recommended in Phase 1. This was achieved through testing and evaluation of the concepts in ice-infested water conditions in a Cold Environment Laboratory at the SINTEF. Testing involved both oil recovery and ice processing concepts.

The test units consisted of only the principal components that provide the ice deflection or oil recovery. Floatation structures, power drives, control systems and other secondary components were left out or simplified to focus the testing on the primary function of each concept.

Three separate laboratory sessions took place to evaluate the concepts in the test tank with simulated oil spills in ice-infested water. Assessments focused on ice processing and/or oil recovery capabilities of the test units. Careful evaluations were undertaken for each test while visual observations and video were recorded. Modifications and improvisations were essential elements during the lab activities.

At different stages throughout Phase 2, Steering Committee meetings and Technical meetings were held to provide progress updates to the funding participants and to receive their technical input.

8 TESTING METHODS

Phase 2 evaluations focused on providing a basic understanding of the operational characteristics for each of the selected oil-in-ice response concepts. To assess a reasonable number of concepts without incurring prohibitively costly testing, these evaluations were kept at a qualitative level. The assessments of the units focused primarily on oil recovery and ice deflection capabilities.

The following sections describe some general preparations and methods used for testing of the units:

Phase 2 test facility

Evaluations of the concepts took place in a test tank that measures 8 meters in length, 5 meters in width, and 1.2 meters in depth. The water level in these tests was 0.9 meters. The tank is located in a cold room. Under favorable conditions this enables control of the air temperature down to -20°C , with an accuracy of $\pm 0.5^{\circ}\text{C}$. Most of the tests were performed in air temperatures ranging from -5°C to 0°C . Ice was prepared by freezing an ice sheet of a desired thickness. Subsequently, the ice sheet was broken into sizes of ice floes required for the testing. Wave makers or current generating systems were not used. A motorized carriage extends across the tank and can travel the length of the tank with speeds adjustable up to 0.20 m/s. The carriage is equipped with a movable crane that was used to hold the tested units in position.

Tanks used for storage and preparation of test oils were located outside the cold-room. Four storage tanks measuring 12, 7, 6 and 1.2 m^3 are available to hold test oils and waste products after testing. For this testing program a non-emulsified oil was used with a viscosity of approximately 1500 cP at the temperature of the water in the test basin.

A calibrated measuring tank (CMT) was constructed for the test program, with a volume of 1.2 m^3 and with an inspection window for accurate reading of the quantity of recovered fluid and the location of the oil/water interface. The tank is sealed and is connected to a vacuum unit that creates a lower pressure within it. A flexible hose connected to the tank was used to transfer recovered products to it from the various recovery units.

Ice Preparation

Salt water with salinity of 2.0 % was prepared for the tests. The refrigeration unit was operated until an ice cover of 10-15 cm thickness was formed, Then the ice sheet was broken to form ice pieces of sizes ranging from small brash to one-meter ice floes. Some slush was inevitably formed during the ice-breaking process. When required to perform tests in conditions with only slush present in the recovery path, ice pieces were lifted out of the water, crushed manually, and the slush formed was transferred back to the basin.

The amount of slush was fairly high during the whole test series.

Preparation of Test Oil and Distribution in the Tank

A non-emulsified oil was used in the tests and was prepared by blending prescribed proportions of heavy fuel oil (IF240, similar to Bunker C) and diesel to form an oil with viscosity about 1500 cP at a shear rate of 10 s^{-1} and 0°C . The oil was manually poured into the tank prior to each test. Typically, 10-30 liters of oil were available for recovery along the 6-meter long testing path. After pouring in the oil, the ice and oil were lightly mixed to result in a relatively even distribution of oil between and on top of the ice pieces.

Towing, positioning and operation of tested units

The test basin was equipped with a motorized carriage extending across the width of the tank. Except for the Air Conveyor that was manually operated over the water

surface the test units were secured to the carriage to permit the units to advance through the ice field. The Lifting and Submerging Belt units were equipped with wheels to roll on the tank floor when pulled by the tow bridge through the basin. Most other units were supported on the bridge by means of a crane to allow the vertical position in the water to be varied. Advancing speeds were kept low in most tests to allow for careful examination of the interaction between oil and ice. Typical tow speeds ranged from 1 to 3 m/min. In many instances, test units were examined at various tow speeds to observe for any possible variations in performance.

All the units, except the Grated Plough, were operated hydraulically. Hydraulic adjustment valves were controlled from the tow bridge. Parameters that were varied were belt speed, drum rotation speed, draft etc. The recovered material was conveyed to collection troughs from where it was transferred by means of an air conveyor unit to a storage tank.

Qualitative assessments

Testing included visual examination and careful assessment of the operation of each unit. Video recordings permitted the Technical Committee to immediately review the individual tests if required. Testing procedures and the test matrix sequence remained flexible to allow for variations based on review of the preceding tests.

Ice deflection performance was assessed solely through visual observations of the unit-ice interaction and the ability of a device to separate large ice features from smaller ice pieces. Oil recovery performance was evaluated through visual observations of oil adhesion to the skimmer surfaces and through the rate of oil accumulation in the test unit's collection trough. Qualitative assessments were also made of throughput efficiency by observing the oil removal apparent in the path along which the skimmer had advanced.

Quantification of performance

Testing was of a qualitative nature and few attempts were made to quantify the performance of the units. However, in a few cases, estimates were made of oil recovery and slush pickup by collecting samples of the recovered product for visual inspection in 20-liter sampling containers.

9 TESTED CONCEPTS

Most of the concepts from MORICE Phase 1 referred were selected for evaluation in this phase. These include oil recovery concepts, ice processing devices and concepts that integrate these two functions in the same unit. The selection was based primarily on the recommendations from the Phase 1 study. Table 1 shows the evaluated concepts along with their functions in an oil-in-ice recovery system.

Concept	Function
Lifting Grated Belt	Ice Deflection
Submerging Grated Belt	Ice Deflection
Grated Plough	Ice Deflection
Brush/Drum	Oil Recovery/ Ice Deflection
Air Conveyor	Oil Recovery/ Transfer
Auger Drum	Oil Recovery /Ice Deflection

Even though the Air Conveyor was tested for its oil recovery ability it was primarily used throughout the laboratory tests as a means of conveying recovered material from the other recovery units. In the following, brief descriptions of the testing of five of the concepts are given.

9.1 Lifting Grated Belt

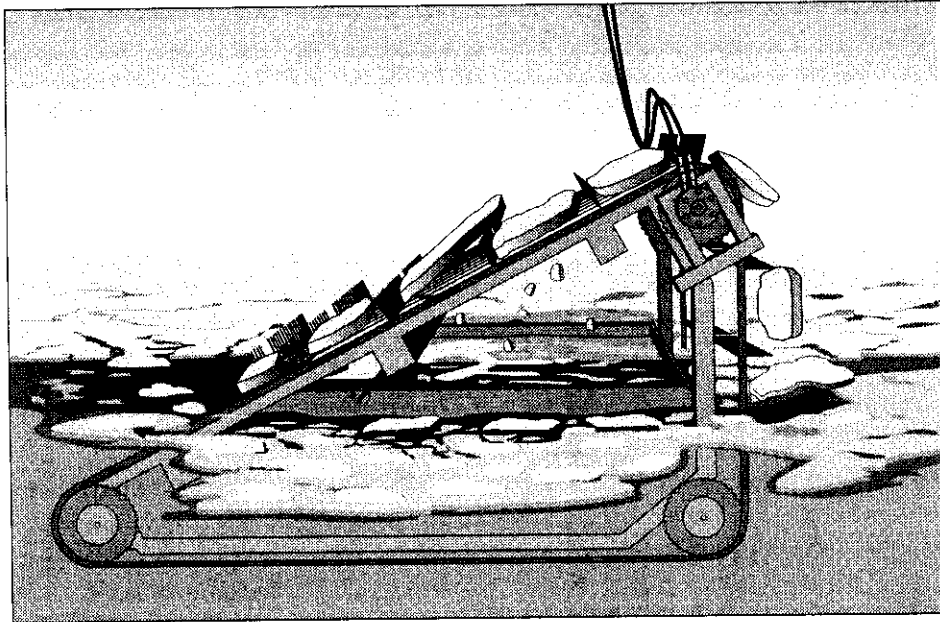


Figure 9.1 Lifting Grated Belt - Phase 2 version

The test unit consisted of three shafts mounted on a triangular steel frame. Lifting paddles were mounted on two chains, each of which moves along the outer perimeter of the frame on sprockets mounted on each shaft. The paddles, driven by a hydraulic motor connected to one of the three shafts, slide along parallel fixed glider rods. The collection reservoir consisted of a wooden frame constructed to fit under the lifting grated belt to provide an enclosed area in which to contain the collected oil, slush and small ice pieces. For the purpose of these tests, the unit was moved along the tank floor by means of wheels mounted on the frame, and the unit was pushed through the ice field in the tank by the motorized carriage.

The Lifting Grated Belt proved to be an effective ice-deflecting concept that moves large ice pieces out of the recovery path and thus provides a simplified condition for oil recovery operations. The Lifting Grated Belt concept was recommended for further development.

9.2 Submerging Grated Belt

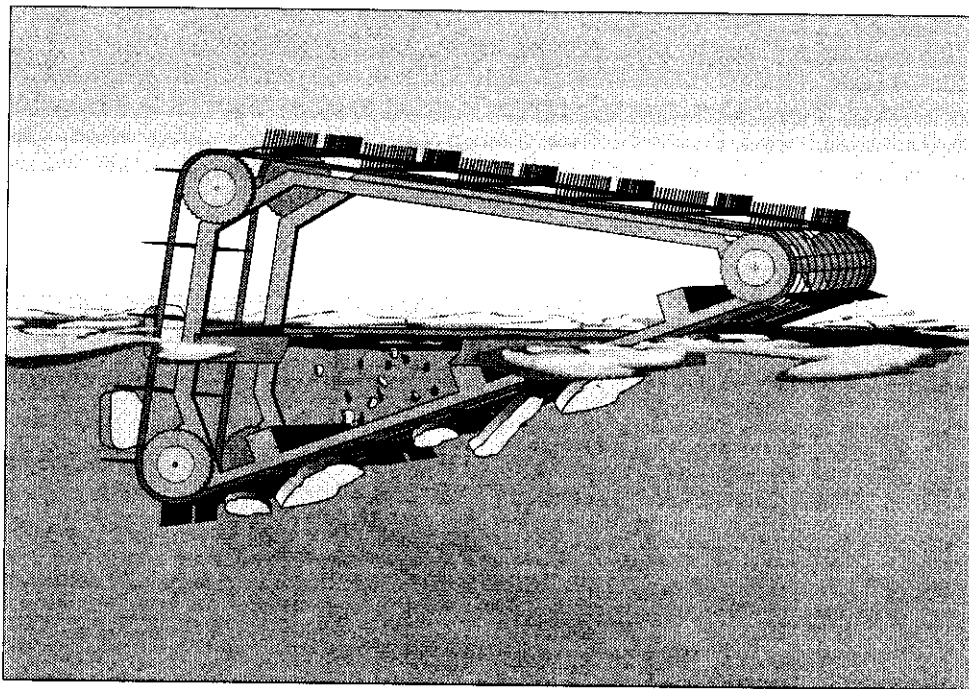


Figure 9.2 Submerging Grated Belt - Phase 2 version

Similar to the lifting belt, this concept is based on the assumption that oil collection is simplified in the absence of large ice floes. Methods to deal with the oil and ice mixture in the collection area may be similar to those considered for the Lifting Grated Belt. The test unit was the same as in the Lifting Grated Belt tests but inverted to submerge the ice. The unit was equipped with wheels rolling on the tank bottom, allowing it to be pulled through the ice basin by the motorized platform across the

tank. The area under the belt was enclosed by sidewalls within the unit frame to keep the collected product contained for subsequent observations.

The belt submerged ice effectively. However, the rakes on the belt, used to submerge and deflect the ice, inadvertently carry oil down and behind the unit. Also submerged ice carries some oil with it. Oil/ice separation was ineffective. Resolving these problems requires some type of underwater cleaning mechanism. Recovery of the oil in the collection area is also difficult since oil does not appear to form a distinct layer on top of the slush ice. Several of these inherent problems did not seem to have any clear or simple solutions and a high level of effort was expected to be required to overcome these difficulties. The concept was therefore not found to warrant further investigation in the subsequent development phase.

9.3 Brush/Drum

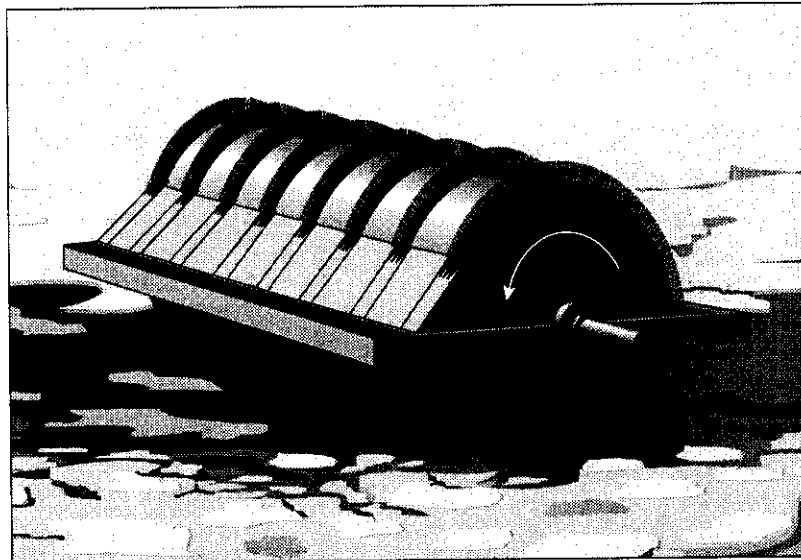


Figure 9.3 One of several Brush/Drum config. in Phase 2

The Brush/drum concept includes a range of combinations of the brush and the drum principles, both of which are widely used in oil recovery operations. The concept seeks to combine the advantages of each principle to produce a unit suitable for ice conditions. The brush skimmer can be an effective oil recovery device that performs well in viscous oils and has the ability to operate relatively undisturbed in debris. Drum skimmers, on the other hand, get easily obstructed by debris but have a higher oil recovery efficiency and can have a high buoyancy, thus reducing the need for additional flotation.

Tests were performed with a variety of combinations of the brush and the drum recovery principles, from a smooth drum to a full brush unit. In all cases, oil that was scraped off the collector surface drained to a trough from which it was pumped using an air conveyor. The units were held in position by a crane mounted on the motorized

carriage. Both brush and drum principles collected oil in ice effectively. As expected, smooth drums had very little ice deflecting ability. However, ice may be pushed under a unit by ice pressure or water current. Units with brush arrangements deflected ice effectively, depending on brush type and configuration. Sometimes brushes also deflected substantial amount of oil together with the ice (throughput efficiency < 100%). Some of the units effectively combined ice deflection and oil recovery, potentially eliminating the need for an additional ice deflector.

It was recommended that the development of the Brush/Drum concept be continued.

9.4 Air Conveyor

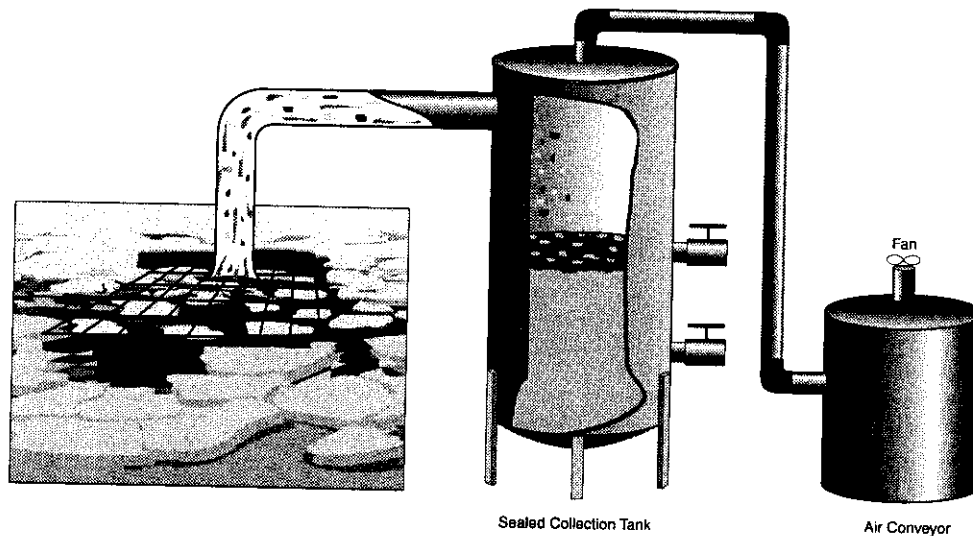


Figure 9.4 Air Conveyor used as recovery device

Testing during this phase evaluated the Air Conveyor's viability for recovering oil from between ice pieces when operated from above the surface of the water. It was considered that this system might eliminate the need to deflect or process the encountered ice during recovery operations. The suction head was operated manually to observe the performance of the unit at various locations and heights above the ice/water surface. Parameters such as oil, water and ice recovery rates were observed and assessed.

For proper operation of the Air Conveyor, the unit needs good airflow at all times. This requires that the inlet hose not be allowed to submerge or fill up so that its entire cross section is blocked. The laboratory evaluations found that controlling the suction hose inlet location and jerking motion can be very difficult even in these controlled conditions and would likely get worse in actual field conditions. The Air Conveyor recovers oil, water and ice indiscriminately, and large quantities of water are easily recovered along with the oil. Problems are associated with maintaining the suction inlet at a constant distance to the water surface. Also, a reliable method to prevent ice pieces from plugging the hose inlet was not devised. Although not experienced in the

laboratory tests, freezing of the suction line can be a major problem with these systems.

No further work was recommended on the Air Conveyor as an independent oil recovery unit. On the other hand, the Air Conveyor system was effective as a fluid transfer method for conveying oil, water and small ice pieces to a storage tank, and it may provide a feasible alternative for use as a fluid or material transfer system in oil-in-ice recovery operations.

9.5 Auger Drum

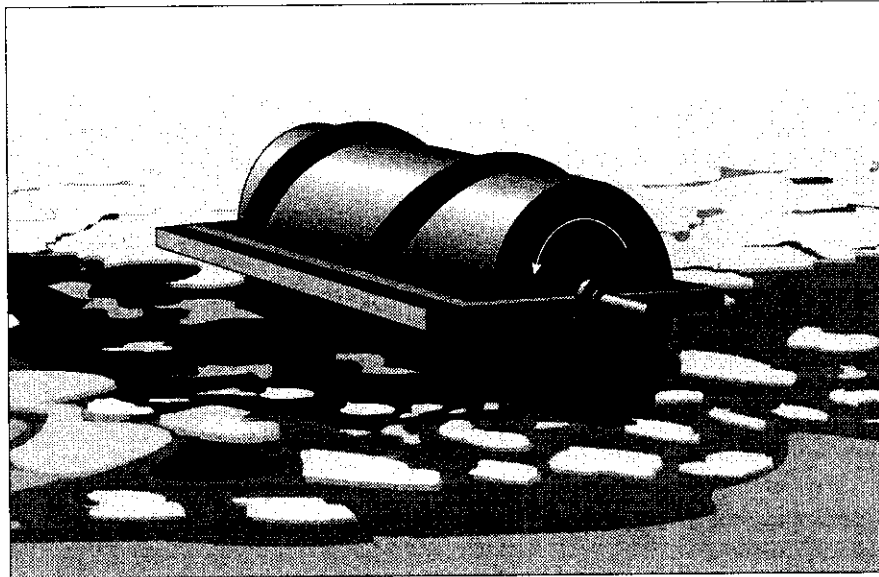


Figure 9.5 Auger Drum

The laboratory tests on the Auger Drum focused on evaluating the concept's ability to deflect ice laterally without deflecting a significant quantity of oil, and to evaluate the potential for oil recovery on the auger surface. Three units with different auger flights were tested.

As intended, the auger deflected ice laterally, off to the side of the unit. The Auger concept collected a substantial amount of oil both on drum and on auger flights. The auger flights appear to enhance oil movement around the ice pieces and to the drum surface by providing subtle agitation at the waterline as the flight passes.

In high ice concentrations, the Auger Drum concept ceases to operate as intended. Lateral ice deflection can no longer take place and ice is instead pushed under the unit. A main problem with this concept is the sideways deflection of oil together with the deflected ice. Also problems are associated with the relatively complex scraper required for this type of unit.

Although the concept appeared to offer an innovative method of deflecting ice and recovering oil, it remains uncertain as to the overall advantage of this concept. Further testing and development of this concept is not recommended in subsequent phases of MORICE.

PHASE 3 – QUANTITATIVE TESTS

The main objective in Phase 3 was to evaluate two concepts, the Lifting Grated Belt and the large Brush/Drum system, through quantitative testing and assessment in the Arctic Environmental Test Basin at the Hamburg Ship Model Basin (HSVA).

Testing was expected to give estimates as to the oil recovery capabilities and the oil/ice separation performance of the units. As in the previous phases, evaluations continued to focus on the oil recovery and ice deflection components of the concepts, not on complete recovery systems. Hence, issues such as support structures and flotation were not major considerations at this stage.

10 TEST SET-UP AND METHODS

With the intention of carrying out quantitative experiments, more carefully designed and constructed models were required compared to earlier experiments. It also called for a slightly more sophisticated test set-up, although still only concept components, not complete prototypes, were tested.

The following sections describe preparations and methods used for testing of the units at the HSVA facility.

The Arctic Environmental Test Basin

Evaluations of the concepts took place in the Arctic Environmental Test Basin at the Hamburg Ship Model Basin. This test tank is a former ice testing tank and measures 30 meters in length, 6 meters in width, and 1.2 meters in depth, see Figure 5. The water depth in these tests was 1.1 meter.

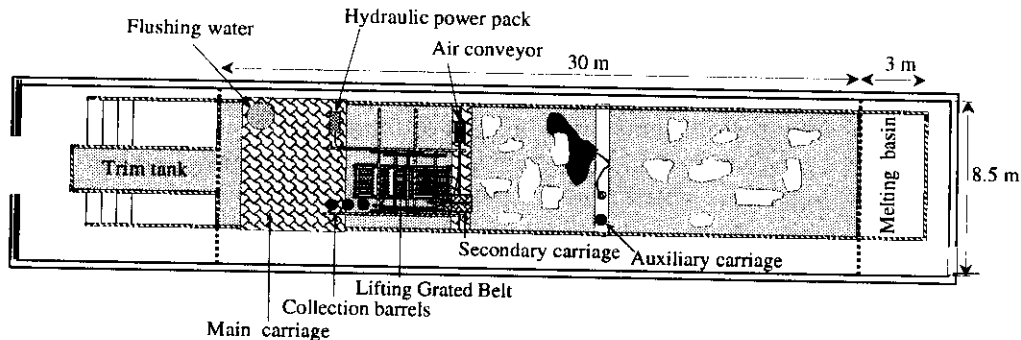


Figure 10.1 Overview of the HSVA facility used for Phase 3 tests

The tank is located in an insulated room that is cooled by heat exchangers covering the entire ceiling. Under optimum conditions this enables control of the air temperature down to -25°C . Most of the tests were performed in temperatures just below 0°C . The test tank can be equipped with wave makers and a current generating system. However, none of these systems were required for our tests. A motorized main carriage extends across the tank and can travel the length of the tank with speeds adjustable from 0 up to several m/s. The main carriage was also equipped with a crane which was very useful.

The models to be used were fairly large for the test tank, hence the dimensions and weight of the units had to be matched to the capacity of the test tank. The models were supported by two I-beams connecting a smaller carriage with the main carriage. Due to the size of the support system for the models, the walls to the main tank area could not be properly closed during the freezing of the ice sheet. This meant that the temperature was -15°C instead of -25°C , and the time to prepare the ice sheet of approximately 20 cm thickness took much longer than foreseen.

A more detailed description of this HSVA facility is given by Wessels (1992).

Ice Preparation

Using the same ice for carrying out experiments during two to three weeks required that the ice had sufficient strength to resist the grinding due to mechanical wear and tear. Although the hardest ice is made of freshwater, we wanted to have ice with the typical porosity found in saltwater ice, since oil has a different affinity or adhesion to such ice.

In Hamburg we used water with a salinity of 0.85%, pumped directly from a much larger ice tank into our test tank. This made it possible to install the Lifting Grated Belt as the first model in the tank before water was filled. Water with this salinity proved to be working very well for our purposes.

After filling of water in the tank to the design water level for the Lifting Grated Belt, the ice making was started. The insulating end wall of the lab could not be closed due to the size of our test set-up. This caused the temperature in the room to stay at about -15°C during the freezing, and it took about one week to prepare the ice sheet of approximately 20 cm thickness. The ice sheet was cut by chain saw and broken up manually, to form ice with size ranging from small brash to ice pieces of maximum 1.5 m. Some slush was inevitably formed during this ice-breaking process. This mixture of ice with different size was used during all the tests.

A straight path in the ice sheet about 4 m wide was cut to form a broken ice situation in the test tank, leaving about 2 m of level fast ice along one side of the tank. To reduce the ice concentration in the path, some of the broken ice was pushed underneath this fast ice.

Preparation of Test Oil and Distribution in Tank

Two tanks for storage of prepared test oil and used oil were located outdoors. A non-emulsified oil was used in the tests. It was decided to use a similar type of oil used in the previous phase, a blend of heavy bunker and gas oil called IFO30 (Intermediate Fuel Oil 30), with a viscosity of 30 cP at 50°C. This oil was delivered from a bunker station and stored in a tank at the lab. Most of the tests were carried out with the IFO30 oil as it was delivered, but at the end of the test period some of the IFO30 oil was blended in a 70/30 ratio with diesel to reduce the viscosity.

The viscosity of the IFO30 was around 12000-14000 cP at 10s^{-1} and 0°C, the temperature of the water in the test basin. Although the trade name of this oil is the same as for the oil used in the previous phase, the viscosity measured at the freezing point proved to be very different for the two oils.

The oil was deployed through a hose and manually distributed between the ice pieces from a service carriage in the tank. Typically, 130 liters of oil was deployed prior to every test along a 20 meter long testing path. Overnight when there was no work done in the tank, a very thin sheet of ice would form. In the morning, prior to distribution of oil, we would therefore move along the path and break this thin ice to make sure the conditions would be similar from one test to another.

Operation of Tested Units

The test tank is equipped with a large motorized carriage extending across the width of the tank. A smaller carriage was connected to the main carriage by two strong I-beams, forming a rectangular area where the units were supported. With this arrangement we had access, although sometimes a bit difficult, to the models from all the sides.

Advancing speeds were kept low in all the tests (typically 2-4 cm/s) to allow for careful examination of the interaction between oil and ice. The intention was to increase the advancing speed after the first few tests. However, after realizing that operation in the field probably would be performed at a similar relative speed as we had in the tank, the low speed was maintained throughout all the tests.

The small drums for the LGB recovery unit were operated electrically, and the rotational speed of each drum could be varied individually and very accurately. The Lifting Grated Belt and the large Brush Drums were operated hydraulically. Hydraulic adjustment valves were controlled from the main carriage. Parameters to be varied were belt speed, drum rotation speed, unit draft etc.

The recovered material slid into collection troughs. The air conveyor from Phase 2 was used to transfer recovered fluid from the troughs to the temporary storage. A number of standard 200 l steel drums with detachable top were used as temporary storage containers during the tests, one for each drum. On the suction line of the air conveyor, flexible hoses were connected to the top of the container covers. By using a manifold with ball valves for each container top, product could be transferred from one trough to its storage container at a time. This was necessary since the capacity of the air conveyor did not allow for transfer of product from all troughs simultaneously.

Quantitative Assessments

Testing included visual examination and careful assessment of the operation of each unit. Video recordings permitted the team to review the individual tests when required. Testing procedures and the test matrix sequence remained flexible to allow for variations based on preceding tests.

Ice deflection performance was assessed only through visual observations of the interaction between unit and ice, and the ability to separate large ice features from smaller ice pieces. Oil recovery performance was evaluated through visual observations of oil adhesion to the skimmer surfaces and through the rate of oil recovered and measured for each individual drum.

After each test the temporary storage containers were replaced by new empty ones, while the used containers were moved out to the workshop for proper measurement of oil, ice and water. Total volume of recovered material and volume of ice were recorded just after each test. Then the ice was melted and the volume of water measured again to find out how much ice was collected together with the oil and water.

11 CONCEPTS TESTED IN PHASE 3

11.1 Lifting Grated Belt (LGB)

Figure 11.1 shows an artist impression of the Lifting Grated Belt (LGB) with the recovery unit used in Phase 3. The unit was suspended by two I-beams fixed to the inside of the LGB frame. These two beams again were suspended under two larger I-beams that spanned between the main and secondary carriages.

Figure 11.2 shows the Lifting Grated Belt unit with the flushing booms above the front inclined plane and the oil recovery unit within the frame. The unit advances to the right as ice pieces are lifted and deflected over the grated inclined planes by means of the moving rakes. Oil at the water surface is intended to pass through the grating into the collection area. Some oil that adheres to and is lifted with the large ice pieces may be removed from the ice by the flushing operation. A flushing tray just below the front section of the moving belt prevents the flushing water from interfering with the oil recovery operation below. A trough at the end of this tray was available to contain and pump the flushing product into a separate container for evaluation of oil removal by the flushing system.

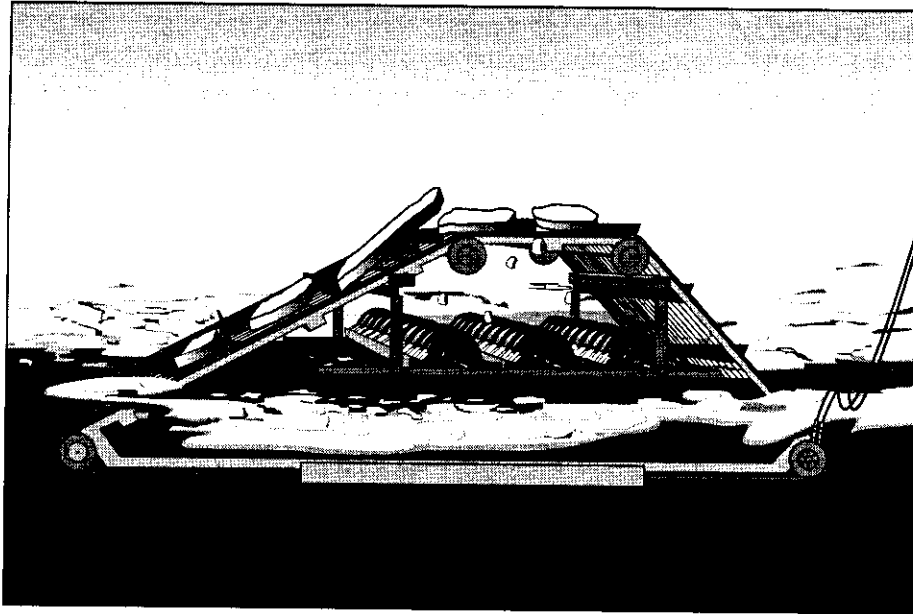


Figure 11.1 Lifting Grated Belt with Recovery Unit

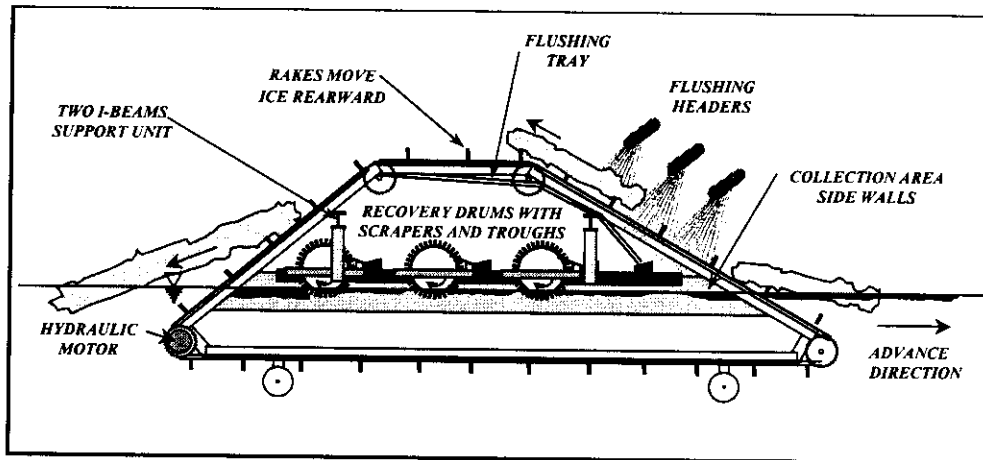


Figure 11.2 Lifting Grated Belt with Flushing System and Recovery Unit

An oil recovery unit may then recover oil contained in the collection area. In the present phase, an oil recovery unit for the LGB collection area consisting of three small brush/drums was used for the first time. Other oil recovery units may be considered for use under the LGB. In this unit, as oil passes from the front to the rear of the collection area due to the action of the rotating brush drums, oil adheres to and is lifted by each drum. The oil is then scraped off, slides into the drum's respective trough and is subsequently sucked out by an air conveyor and transferred to a separate collection barrel for analysis.

11.2 Brush/Drum System

The Brush/drum concept includes a range of combinations of the brush and the drum principles, both of which are widely used in oil recovery operations. The concept seeks to combine the advantages of each principle to produce a unit suitable for ice conditions. The brush skimmer is an effective oil recovery device that performs well in viscous oils and has the ability to operate relatively undisturbed in debris. Drum skimmers, on the other hand, get easily obstructed by debris but have higher oil recovery efficiency and can have a high buoyancy, thus reducing the need for additional flotation.

Tests were performed with essentially two different configurations of the concept. One configuration uses a smaller drum placed just behind the larger first drum and rotated in the reverse direction to contain and pool oil in the area between the two drums, see Figure 11.3. The other Brush/Drum configuration has two large drums rotating in the same direction, see Figure 11.4. Both configurations were tried with different combinations of the brush and the drum recovery principles, using a range of surfaces from a smooth drum to a full brush unit.

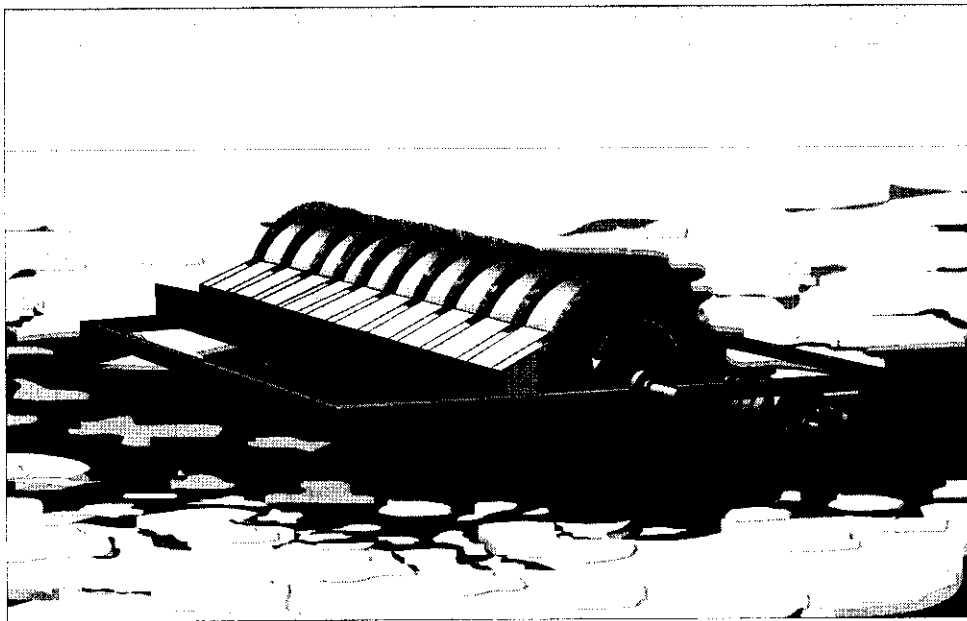


Figure 11.3 Brush/Drum with drums of different size

Tether lines fastened to a support frame held the units in position. This support frame was fixed to the two I-beams that spanned between the main and secondary carriages, similar to the operation of the LGB. The lengths of the tether lines were adjusted to obtain the desired operating draft and to provide an effective angle of incidence between the drum and the water surface.

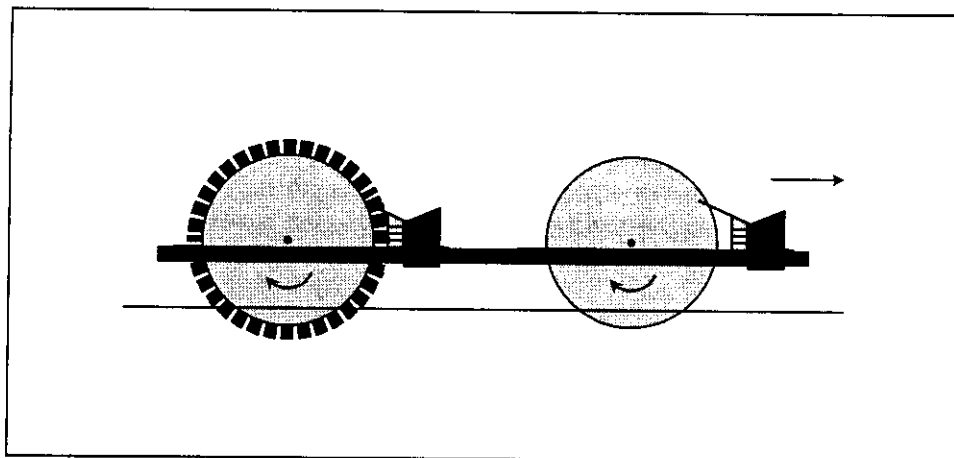


Figure 11.4 Brush Drum configuration with two large drums

The ice encountered was deflected under the Brush/Drum by bristles or spikes. The oil collected by the drums and/or the bristles was scraped or combed off the collector surface and drained into a trough from which it was transferred using an air conveyor.

12 CONCLUSIONS FROM PHASE 3

Due to confidentiality considerations only some general comments can be referred regarding the overall results of the Phase 3 laboratory experiments:

The Lifting Grated Belt and the Brush Drum concepts have both been further developed and evaluated at a larger scale than previously in Phase 2. Quantitative results have been achieved through tests carried out in the cold test facility at the Hamburg Ship Model Basin. The oil that was provided for these tests had other physical properties than the oil used in previous experiments. These oil properties presented new challenges that were solved in a satisfactory way.

Throughout the testing period both the concepts and the operation have undergone modifications and refinements. Under the given conditions, both concepts were considered to provide effective methods to deal with oil spills in ice. Recovery rates were good for the conditions and the amount of oil present, and recovery rates would be expected to increase with a greater amount of oil present under similar conditions.

PHASE 4 - PRESENT STATUS

At present Phase 4 is nearly finalized, and at the same time the next phase is under planning. Since the results are proprietary information it is possible to give only some very brief comments regarding Phase 4 and the plans for the continuation of the program.

In Phase 4 a complete full-scale prototype was designed and constructed. The units were at the same scale as the ones tested in Phase 3. As a matter of fact, some of the components tested in Phase 3 were modified and used in the prototype. In addition to oil recovery and ice processing units, the prototype had to include a support vessel. Such a vessel or work platform was designed and built. Most of the construction work to build the prototype was carried out by the Alaska Clean Seas at their base in Prudhoe Bay, Alaska.

The prototype was tested in the Alaskan Beaufort Sea during freeze-up in October 1999 where ice up to 37 cm in thickness was processed without problems. Oil was not introduced during these tests.

Phase 5 is planned to start as soon as the funding is in place. This will probably be the final phase of the MORICE program. Following more extensive component testing of oil recovery in ice under controlled conditions, further ice testing will be carried out in the Alaskan Beaufort Sea before the complete prototype is tested in oil and ice. The field testing with oil and ice under real conditions, initially planned to take place in the Barents Sea, will probably be carried out at the OHMSETT test facility in New Jersey, USA.

13 ACKNOWLEDGEMENT

The authors would like to thank the participants for their financial support and valuable input throughout the four phases of the program carried out so far. The following companies or institutions have contributed to the funding of one or more phases:

- Saga Petroleum
- Norsk Hydro
- Statoil
- Exxon Production Research Company
- US Minerals Management Service
- Alaska Clean Seas
- Norwegian Pollution Control Authority (SFT)
- Canadian Coast Guard
- Environment Canada
- Norwegian Ministry of Industry and Energy
- The Research Council of Norway
- Hamburg Ship Model Basin
- The European Communities DG XII Science, Research and Development under the "Access to Large Scale Facilities Activities of the TMR Programme"
- SINTEF

14 REFERENCES

Jensen, H., T. Lorenzo, L. Solsberg, The Program for Mechanical Oil Recovery in Ice-Infested Waters (MORICE) Phase 3, SINTEF report STF22 F99213, 1999.

Jensen, H. and Johannessen, B.O., "Muligheter og begrensninger for eksisterende oljevernustyr ved bruk i is" (Tests of Foxtail Skimmer in Ice), SINTEF NHL report (in Norwegian) STF60 F92127, 1993.

Johannessen, B.O., H. Jensen, L. Solsberg, T. Lorenzo, Mechanical Oil Recovery In Ice-infested Waters (MORICE), Phase 1, SINTEF report STF22 F96225, 1996.

Johannessen, B.O., T. Lorenzo, H. Jensen, L. Solsberg, The Program for Mechanical Oil Recovery In Ice-Infested Waters (MORICE), Phase 2, SINTEF report STF22 F98206, 1998.

Solsberg, L.B., McGrath, M., "State-of-the-Art Review: Oil in ice recovery". Canadian Association of Petroleum Producers, 1992.

Wessels, E., "New Test Basin for Experimental Studies on Oil Spill in Ice", Proceedings of the 15th Arctic and Marine Oilspill Program (AMOP) Technical Seminar, pp. 271-279, Edmonton, Alberta, June 1992.

SEASHORE MORPHOLOGY AND LITHODYNAMIC OF THE NORTH-EAST SAKHALIN COAST

Surkov G.A.¹, Polomoshnov A.M.¹, Zemluk S.V.², Astafiev V.N.^{1,2},
Mikishin Y.A.³, Ribokov V.F.³, Brovko P.F.⁴, Truskov P.A.⁵

1 - Sakhalin Oil & Gas Institute, Okha, 2 - JSC "Rosneft - Sakhalinmorneftegaz", Okha,

3 - Coastal Research Center of Far-East State University, Vladivostok

4 - Far-East State University, Vladivostok

5 - Sakhalin Energy Investment Co., Moscow

INTRODUCTION

Coastal lithodynamics is an important phenomenon and its effect should be considered in selecting onshore crossings for subsea pipelines and sites for onshore facilities. Coastal lithodynamics of the north-east Sakhalin coast has been studied by the Oil and Gas Institute "SakhalinNIPImorneft" for several decades. The results of the study are given below.

DIVISION OF THE SEASHORE INTO SECTIONS

The seashore in the region can be divided into 19 morphodynamic sections (Fig. 1).

1. Piltun. This section extends for 15 km. It is a typical depositional shore with a rather broad sand beach formed on the seaward margin of the Piltun sandbar. The sandbar is 200 m to 1 km wide and can be divided into two zones: a 2 to 4 m terrace with rolling and crestal aeolian landforms (on the side facing the lagoon) and two 2-m high shore bars (Remenets and Klimov, 1981). No field data on erosion rate are available; by analogy with the neighboring, well-known shores of the Chaivo sandbar, it may be 2 to 5 m a year (mpy).

The basic lithodynamic processes in this segment are moderate deposition, that do not exceed several meters a year, and sediment transit, the latter being the dominating process. Occasional erosion affects an insignificant segment.

2. Piltun-Astokh (3.3 km long) is a permanent lagoonal strait connecting the Piltun and Astokh lagoons with the Sea of Okhotsk with adjacent depositional spits. At present, the strait tends to shift southward as a result of an active growth of the northern-spit distal end, which is induced by the movement of shore sediments from north to south and, accordingly, by erosion of the southern sandbar segment. The rate of strait shift is nonuniform. Between 1920 and 1975, the mean rate was 22 mpy; it dropped to 10 mpy by the late 1970s; and, in 1980, the location of the strait temporarily stabilized. In 1981-1982, it again started shifting at a rate of 10 mpy, to increase the rate rapidly to 84 mpy in the 1983-1984 and decrease it to 57 mpy in 1984-1985 (Surkov, 1998). Thus, the strait has been shifting at rates differing by a factor of 5 to 8 during 3 to 5 years.

The major lithodynamic processes in this segment are as follows: active sedimentation on the northern shore and intensive erosion on the southern shore of the strait. Also, deposition of sediments takes place in the wave shadow of the tidal fan, these sediments being moved in the summer by southward waves from the seaward side of the southern shore of the strait.

3. Astokh (13 km long) is represented by a depositional shore generated on the seaward margin of the Astokh Spit, which separates a narrow (200 to 800 m wide)

strait of the same name from the Sea of Okhotsk. Geomorphologically, it is nearly identical to the Piltun section. A 1.6-km long fresh erosion bench in ancient shore bars can be noted in the northern part of the spit, 3.8 km from the lagoonal strait. However, here, erosion is not so widespread. It seems to proceed only during autumn gales.

The major lithodynamic processes are a moderate deposition in the beach zone, which does not exceed several meters a year, and a transit of sediments.

4. North Chaivo (32.6 km long) is on the whole a depositional shore that tends to recede steadily. Moderate sedimentation occurred here until 1955. The shore built up at a rate of 4 to 7 mpy. Erosion has activated here since 1955. Within some lengths, the shore backed out 70 to 150 m between 1955 and 1985. Hence, the rate of erosion varied between 2.5 and 5 mpy. According to field observations performed between 1982 and 1987, the shore benches in easily eroded fine sand recede at the maximum rate of 13 mpy. The major lithodynamic processes are a moderate deposition, an erosion of 30% of the section shoreline and a transit of sediments.

5. South Chaivo (9 km long) represents a shore with active sedimentation and absence of erosion benches. The section exhibits a broad (60-170 m wide) full-profile fine sand beach. The shore is building up at rates in the range from 5.5 to 12 mpy, increasing southward. The deformation of the beach profile does not exceed 2 to 2.5 m (Brovko et al., 1984; Brovko, Volodarsky, Mikishin, 1985).

6. Kleie (3 km long) is represented by the permanent lagoonal Kleie Strait connecting the Chaivo lagoon with the Sea of Okhotsk and the adjacent ends of the depositional Chaivo and Arkov (to the south) spits. The history of the strait has been traced out since 1927 (Buzlaev, 1982; Brovko et al., 1984; Surkov, 1998). The segment basically tends to shift southward as the result of an active growth of the distal end of the Chaivo spit (Cape Aiash) and, as a consequence, an intensive erosion of the opposite shore of the strait by strong tidal currents. Between 1927 and 1955, the land on Cape Ayash was built up at an average of nearly 11,000 m² a year, while in the north of the Arkov spit, it was eroded at a rate of 18,000 m² a year, the maximum recession (475 m) having taken place at Cape Kambrulbash. Throughout the period of observations, the rate of the southward shift of the strait varied between 13 mpy in 1981-1983 and 35 mpy in 1984-1985.

The major lithodynamic processes in this section are as follows: an active deposition on the north shore of the strait and an intensive erosion, on the south shore. Moreover, on the seaward side of the south shore, in the wave shadow generated by the fan of the strait, sediments are transported and moderately deposited by southward waves.

7. Chaivo-Dagi (22 km long) is a depositional body of the sandbar that isolates the narrow northern part of the Dagi Bay affected by intense aeolian processes. The morphodynamic processes on the seaward margin of the sandbar are to a large extent similar to those in the North Chaivo section. Here, the tendency of erosion of the generally depositional shore is stronger. The episodically eroded lengths total at 16.1 km.

The major lithodynamic processes are a moderate sedimentation (within several meters a year) and, from time to time, erosion of shore benches at a rate of max. 2 to 5 mpy.

8. Dagi (4 km long) is represented by a permanent lagoon strait connecting the Dagi Bay with the Sea of Okhotsk and adjacent depositional spits. The lithodynamic processes in this section are similar to those in the Kleie and Piltun Astokh Straits, namely an active build-up of a spit on the north shore and erosion of the south spit with the resulting southward shift of the entire morpholithodynamic system. A

comparison of aerial photos of different years revealed that the mean rate of the shift was 23 mpy between 1952 and 1979. No appreciable changes in the outlines of the shores of the strait were noted for the period from 1981 to 1985 (Buzlaev, 1982; Surkov, 1998). This fact suggests a temporary break in the shift, rather than shore stabilization. The best proof of this conclusion is a very large length of the distal end of the northern spit (3 km).

9. Gafovicha (10.4 km long) is represented by a depositional shore with a broad full-profile beach. The shore show no traces of erosion.

10. Anuchina (4 km long) is represented by a permanent lagoonal strait with adjacent distal ends of spits. Connects the Nyi Bay (Nyivo Lagoon) with the Sea of Okhotsk. Contrary to the northern straits, this is shifting in an opposite direction due to the resultant northward movement of sediment along the shore. A comparison of aerial photos of different years revealed that the mean rate of strait shift was 22 mpy between 1952 and 1979, the shore-forming processes stabilized between 1979 and 1981, the shift rate increased to 17 mpy from 1981 to 1984, and decreased to 12 mpy from 1984 to 1985.

The major lithodynamic processes: active deposition on the south shore of the strait, erosion of the north shore, and slight sedimentation on its seaward side, in the wave shadow of the fan of the strait.

11. Nyivo (11 km long) is a depositional shore of the Plastun Spit, which separates the Nyivo Lagoon from the Sea of Okhotsk and grows northward. Since the spit and its sea-facing beach are narrow (max. 60 m wide), sedimentation appears to be slow on most of the section, within 1-3 mpy, sediment transit being predominant.

12. Nyivo-Nabil (12.4 km long) is represented by a wave-cut shore spotted with quite short depositional lengths confined to stream mouths. The wave-cut benches, 8-13 to 20 m high, with landslides developed on their sides, give way, owing to landslides, to narrow (10-20 m wide) adjacent beaches underlain by sandy-gravelly-pebbly sediments. Until 1985, the shores receded at a rate of 1-2 mpy, more rarely 5 mpy (Buzlaev, 1982; Surkov, 1998). According to the Seashore Research Center, the mean rate of cliff abrasion was quite variable in the south of the segment and did not exceed 1.4 mpy in the period from 1987 to 1998

13. Aslanbekova (3.5 km long) is represented by the permanent lagoonal Aslanbekova Strait connecting the Nabil Strait with the Sea of Okhotsk and adjacent shores: the distal end of the Aslanbekov Spit, and Cape Tamary with a small fragment of the depositional shore on the north margin. The segment basically tends to shift rapidly northward because the depositional body of the Aslanbekov Spit grows while the opposite shore is eroded at Cape Tamary. The mean rate of the strait northward shift was 13.3 mpy between 1952 and 1978, a temporary stabilization was noted in 1978, and it was 19 mpy from 1979 to 1984. A temporary stabilization of lithodynamic processes occurred again in 1984-1985. Over the period 1952-1986, the strait had shifted 505 m northward (Buzlaev, 1993).

14. Nabil (6.6 km long)) is represented by an accumulative shore formed on the sea edge of the sand bar separating the Nabil lagoon and Aslanbekov strait from the Sea of Okhotsk. In this area, morphological processes are similar to those on the South Chaivo section, therefore, one may assume that, here, the wash accumulation rate is also several meters a year. According to repeated level surveys, over the summer, the beach deformation varies between 1.5 and 2.5 m (Brovko et al., 1977) The south segment of the section reveals more moderate accumulation rates. This fact is proved by a smaller width (max. 50 m) of the beach. A transit of hirsts and occasional scour of ancient embankments of the sand bar predominates.

15. Stary Nabil (18.8 km long) is represented by an narrow accumulative sand bar separating a narrow lagoon – Stary Nabil bay from the Sea of Okhotsk. In the period 1985–1989, the mean scour rate varied from 2 to 22 mpy, increasing southward and peaking 1.5 km north of the Stary Nabil township latitude (Surkov, 1998; Buzlayev, 1993). Somewhat to the south, it decreased down to 3-4 mpy. Abrasion also abates altogether 1.5 km south of the stated latitude. In addition, this section reveals a strong deflation. It threatens the surface of the accumulative form.

16. Lunskiy–Stary Nabil (17.7 km long) is represented by a low accumulative terrace of wave origin built up by sand-gravel materials. At the time being, the main litological processes are a transit and a weak accumulation of detritus. Ablation is occasional (when festoons shift) and on limited segments of the shore. Buzlaev (1982) reported that this section is stable.

17. Lunskiy (5 km long) is represented by a lagoon strait connecting the Lunskiy with the Sea of Okhotsk and adjacent narrow (100-200 m wide) forelands. This strait moves as all other straits of the northeastern coast. However, in contrast to the other, it does not show a tendency to a stable shift to one side. During 1952-1980 it was shifting northward with a mean rate of 20 mpy. From 1980 to 1983, the south shore shifted north with a mean rate of up to 30 mpy, while from 1983 to 1985, it started shifting south at a rate of 100–176 mpy. In these years, the northern shore of the strait moved either north or south by 20–30 m (Surkov, 1998). In 1985-1986, it shifted north by 70 m and found itself in the boundaries of 1983 (Buzlaev, 1993). Unstable behavior of the strait and a narrow width of accumulative forelands prove the absence of a sufficiently strong resultant flow of detritus in this site of the coast. It is more probable that instead an insignificant migration of detritus takes place. The strait migration zone is limited by a 5-km length where narrow 2-3 km long forelands can be found.

18. South-Lunskiy (7 km long) is represented by a 100-500 to 1500 m wide sand bar separating the southern part of the Lunskiy bay from the Sea of Okhotsk. Multiple aerial photography surveys fail to reveal changes in the outlines of the section (Surkov, 1998). An abrasion bench in the northern half of the section suggests a periodic scour of the shore at a rate max. 1-2 mpy.

19. Kongi (24.5 km long) is represented by a typical shore with a fossil scar and an adjacent sea terrace. The benches are 6-10 m high in the northern part of the section and 18-26 m in the south part (outside the considered region). The terrace is at most 100 m wide. Repeated aerial survey indicated this shore section is stable. Taking into account recently eroded benches extending 18 km southward from the influx of the Machngi river almost to the Nampi river, one may assume occasional shore erosion at a rate of 1-2 mpy.

Upon consideration of morphological and litological processes on the section of the northeastern Sakhalin shore confined between 51°N and 53°N we conclude that, beginning with the middle of the 20th century, the tendency to scour predominates in shore evolution. The proportion of retreating shore is almost 40% (Table 1).

CONCLUSIONS

Table 1. Modern tendency in coastal evolution of the northeastern Sakhalin (disregarding segments of lagoon straits and internal lagoon shores)

Morphodynamic section	Coastal length/proportion, km[%]			
	Total	Increasing	Stable	Eroded
Piltun	15.0	4.5/30.0	9.5/63.4	1.0/6.6
Astokh	13.0	6.0/46.2	5.4/41.5	
North Chaivo	32.6	7.0/21.5		
South Chaivo	9.0	9.0/100		
Chaivo-Dagi	22.0		6.5/29.0	15.5/70.5
Gafovicha	10.4	7.7/74.0	2.7/26.0	
Nyivo	11.0	2.5/22.7	7.1/64.6	1.4/12.7
Nyivo-Nabil	12.4		4.4/35.5	8.0/64.5
Nabil	6.6	2.5/37.9		4.1/62.1
Staro-Nabil	18.8			18.8/100
Lunskiy–Staro Nabil	17.7		17.7/100	
South Lunskiy	7.0		3.2/45.8	3.8/54.2
Kongi	24.5		13.0/53.1	11.5/46.9
Total length	200.0	39.2/19.6	84.3/42.2	76.5/38.2

If we take into account that the morphological processes in the region were poorly studied in the recent decade, we cannot exclude that a substantial proportion of the shore treated is currently subject to erosion. The modern rise of the ocean level should be recognized without any doubt as the main cause of the intensifying scour of the generally accumulative lagoon coast.

REFERANCES

- Brovko, P.F., MIkishin, Yu.A., Volodarsky, A.N., Rybakov, V.F., et al., 1977, Dynamic behavior of the lagoon shore of the Aslanbekova strait. Report on engineering and geomorphological and hydrological studies in the Aslanbekova strait (Nabil bay), Available from the Beach Research Center at the DVGU.
- Brovko, P.F., MIkishin, Yu.A., Volodarsky, A.N., Rybakov, V.F., et al., 1984, Morphology and dynamic behavior of the northeastern Sakhalin shore near the Chaivo bay. An interim report under a contract between the DVGU and SakhalinNIPIneftegaz on the shore morphology and dynamics in the region of the construction of shore facilities and offshore ice-resistant foundations, Vladivostok.
- Brovko, P.F., Volodarsky, A.N., and MIkishin, Yu.A., 1985, Dynamic behavior of the Sakhalin lagoon coast, in: *Exogenic Relief Formation in the Far East*, DVNTs AN SSSR, pp. 102–111. (in Russian)

- Buzlaev, V.A., 1982, Report on aerogeological and engineering geological studies of shore scars that were conducted during 1978–1981 with the purpose to evaluate the intensity of abrasion processes and predict landslide phenomena on the northeastern Sakhalin shore, Integral dedicated expedition of Sakhalingeologiya. Available from SakhalinNIPImorneft.
- Buzlaev, V.A., 1993, New data on Sakhalin shore ablation rate, in: Geographical Studies of the Shelf of the Far East Seas, pp. 78–86. (in Russian)
- Surkov, G.A. “Development of Design Criteria for the Optimal Burial Profile of Underwater Pipelines for the Sakhalin 2 Project”. Report. Research and Engineering Center, Closed-End Joint Stock Company, Okha, 1998. –150 P.
- Remenets, A.I. and Klimov, I.N., 1981, Evolution of the Piltun-bay lagoon shore in the Holocene, in: *Evolution of the environment in the Pleistocene*, Vladivostok: DVNTs AN SSSR, pp. 123–126. (in Russian)

Can Seabed Gouge Survey Data Be Applied To Prediction Of Maximum Depths Of Ice Keel Penetration?

Igor Stepanov

State Research Centre of the Russian Federation – Arctic and Antarctic Research
Institute, Saint Petersburg, Russia

Introduction

The evaluation of maximum depths of penetration of ice feature keels into seabed soil is one of the most important problems which should be solved to provide appropriate protection against ice damages to subsea structures (e.g. submarine pipelines) on the Arctic shelf and in other shallow regions of ice-infected waters. In fact, the ultimate objective of the investigation has to be the prediction of the conditions under which the structure would be damaged by an ice feature. Sometimes structural failure may happen even if the lowest point of the keel passes above the structure. This is more to be expected in the case of a relatively strong ice feature (like an iceberg) and a hard seabed soil due to sub-gouge soil deformations. (There were a number of studies done which were aimed at a better understanding of sub-gouge deformation phenomenon; see for example, overview by Clark et al, 1998 and description of the original research along with a comprehensive list of references by Woodworth-Lynas, 1998.) On the other hand, a structure can resist a direct impact of an ice feature if the ice/structure contact area is comparatively small and/or the ice keel is weak. This is more likely to occur in the case of interaction between a drift first-year ice ridge and a structure.

Anyway, the solution of the problem in both the above mentioned variants requires an answer to the following question: What are the maximum depths of the ice feature keels' penetration into the seabed soil in the planned installation site? Because of the apparent stochastic nature of the gouging process, the answer should be given in probabilistic terms. An approach to the finding of a rational answer which is widely used and seems quite natural, is the statistical processing of seabed gouge survey data. The measurements are usually performed by means of side scan sonars and/or echo sounders. There were a number of such surveys developed in various geographical regions. The most comprehensive data base was collected on Beaufort Shelf (see Blasko et al, 1998). There is also data on Lake Erie (Comfort et al, 1982 and Grass, 1984), Baydaratskaya Bay of the Kara Sea (Klepikov et al, 1997 and Stepanov et al, 1998), and other regions. Surveys ordered by Exxon of the offshore Sakhalin Island in 1997 and 1998 can be mentioned among the latest studies of such a kind (Klepikov et al, 1999).

Conventional approach to evaluation of maximum depths of ice keel penetration basing on gouge survey data

The conventional approach to employing gouge survey data for the prediction of maximum depths of ice keel penetration can be presented based on comprehensive and specific description given by Weeks et al, 1983. There are a number of peculiarities in the implementation of this approach but the basic ideas are similar.

The main input for the analysis is usually information about gouge depths and widths, spatial gouge frequency, and predominant gouge orientation. All these data are given with reference to particular geographical region(s) and accompanied with bathymetry data. The gouge depth is conventionally defined as a measured vertical distance “from the level of the (presumably undisturbed) adjacent sea floor to the lowest point of the gouge” (Weeks et al, 1983). As a rule, spatial gouge frequency is estimated by counting gouges per particular length of sampled track (e.g. the number of gouges per kilometre). Even if a set of gouges have been created by the same pressure ridge (these gouges run in parallel) they are counted as separate. Sometimes there is no possibility of estimating the depth of the gouge (e.g. because the gouge depth is less than the resolving capacity of the measuring device) but it is possible to ascertain that a gouge exists. Micro-seismic investigation provides the possibility of even detecting old gouges that due to infill do not now exist.

Conventional statistical analysis of gouge depth population results in a frequency histogram for this value. This histogram is usually approximated by exponential distribution (Weeks et al, 1983) or more generally, Weibull distribution (Klepikov et al, 1997 and Stepanov et al, 1998). The latter one provides a better approximation of the distribution of shallower gouges. The measured number of gouges with smaller depths (less than about 0.4 m) is frequently less than it should be in correspondence with the exponential distribution. This difference is due to the cutting-off of the measuring devices, and/or gouge infill brought about by natural causes.

Another important distribution is the distribution of gouge spatial frequency (number of gouges per kilometre) or spatial-temporal frequency (number of gouges per kilometre for a year). The latter one is ultimately necessary in any case to get maximum gouge depth corresponding to a given exceedance probability for a given return period. The problem is that a direct evaluation of temporal frequency requires repeated mappings for rather a long period of time in order to detect new (appeared during a known interval of time) gouges. There is no such information apart from probably the Beaufort Shelf. Gouge frequency distribution may be approximated by Poisson or gamma distributions (Weeks

et al, 1983) or by exponential distribution which is a special case of the gamma distribution (Blasko et al, 1998). Consequently, after estimating the parameters of the required probability distributions, one can calculate the probability that the maximum gouge depth in the area under consideration (e.g. along whole length of the pipeline) would not exceed a given value (or predict gouge depth corresponding to given exceedance probability).

The described approach looks quite promising and natural. But there are a number of factors that give doubt as to the reliability of this method. Three objections against the application of this approach are presented below.

Objection #1: Ice keel penetration does not necessarily coincide with measured gouge depth

It is well known that following the formation of an ice gouge from an ice keel, the gouge can be infilled with soil. The ploughed sediment may slide back into the gouge immediately behind the ice keel under the influence of gravity. Wind-induced waves and currents (tidal, wind-driven, etc.) can also cause gouges to backfill over longer periods of time. Such a seabed sediment movement is an extremely effective erasure mechanism (Palmer, 1998 and Niedoroda & Palmer, 1986). At the same time, it is in principle possible, that due to currents, gouges can become deeper than they were originally.

The rate of gouge infill is greater in the case of higher waves, and/or stronger currents, and/or non-cohesive soils (sand, sandy silts, etc.). But the problem is that reliable quantitative predictions of the infilling rate is unlikely achievable at present. The influence of infill is most pronounced in an ice gouge study conducted in Lake Erie (Comfort et al, 1982). The lake bottom was examined both near the northern shore not far from the city of Nanticoke, Ontario and near the U.S. south shore near Girard, Pennsylvania. The studies in both cases were carried out simultaneously in the same water depths. The natural conditions of these two regions are quite similar. The main difference is that near the Canadian shore, the prevailing seabed soil is comprised of boulders, gravel, cobbles and clay whereas near the U.S. shore, the soil is weaker (predominantly loose sand, dense sand, loose, silty sand and dense silt). Near the Canadian shore, the average gouge depth was 1.23 m with a maximum depth of 1.7 m whereas near the U.S. shore, it was only 0.3 m and 0.4 m, respectively. (This was observed in spite of the fact that based on an analysis of the drifting ice ridge/soil interaction mechanics, other conditions being equal, the maximum penetration of the ridge keel into the weak soil should have been greater.)

Consequently, in general, ice gouge survey can provide information about depths of gouges in a region of survey at the time of measurements but NOT about actual depths of penetration of ice keels into seabed soil.

Objection #2: Available gouge survey data on the geographical region under consideration is practically always not sufficient for adequate statistical analysis

Although gouge surveys can not provide appropriate information on depths of ice keel penetration, reliable statistics of gouge depths (at least) would be helpful. A natural solution is to measure the depths in the area in which the structure is planned to be installed. As an example, let us restrict ourselves further by considering linear structures like pipelines, cables, etc. If an area of survey is limited by a narrow corridor (e.g. 30-50 m width) along the pipeline route then the total number of the observed gouges (in average) would be equal to the mean number of gouges per kilometre multiplied by the route length. In accordance with (Weeks et al, 1983), the average spatial frequency on the Alaskan shelf is less than 10 gouges/km. Consequently, the total population for a route of 30 km length would be less than 300 gouges. Such a size of the sample would probably be sufficient to reliably fit the histogram by a particular distribution within a range of frequent events (typical gouges). But it should be noted that the deepest gouges of small probability of exceedance (which are of the most practical interest) appear quite rarely. Due to this reason, an approximation of the distribution “tail” will hardly be any good. Moreover, it is well known that gouge distribution is usually not the same for different segments of the pipeline route. In particular, both average gouge depth and gouge frequency are conventionally considered as functions of water depth. Consequently, the total sample has to be subdivided into a number of sub-samples; each of the sub-samples would correspond to a smaller water depth range. But water depth is not the only parameter that influences the gouging process. It means that further clustering is required. Following this procedure, one will come to the situation when the number of observations within each class is insufficient, not only for estimation of the probability distribution, but even for finding the mean value of the gouge depths.

Objection #3: Gouge survey data obtained in other geographical regions are usually not statistically representative for the region under consideration

A possible solution of the above stated problem can be obtained by a radical enhancement of the analysed sample of gouges. For example, it may be achieved if ice

gouge survey is performed in a much wider corridor along the pipeline route (let us say, 3-5 km instead of 30-50 m). A more radical solution is to employ survey data from other geographical regions. Ultimately, it may be all events recorded in any region in the past. Such an imaginary data base would consist of many thousands of records. But even in this case the problem would not be resolved due to the following reasons: As was mentioned above, gouge depth, gouge frequency and other characteristics of the gouging phenomenon depend on a number of parameters. The list of these parameters includes (at least but not only) water depth, angle of seabed slope, soil properties (at least, cohesion and angle of internal friction), current and wind directions and speeds, ice conditions (types of drift features, their dimensions and shape, strength of ice constituting these features). Let us assume that the total number of scalar parameters that influence gouging is 10 (it is an optimistic estimate) and each parameter may be presented by four range classes (quite a rough subdivision). Applying the mentioned clustering procedure one would obtain the average size of (relatively homogeneous) sub-samples, 40 times less than that of the original sample. But it is not the only difficulty. The problem is that the gouge depth in a given point on a seabed depends not on water depth, soil properties, etc. in this point, but on water depth, soil properties, etc. in the surrounding area within the length of the gouges. This statement can be illustrated by the following example. Let us imagine that the considered point is located in a natural cavity surrounded by an almost horizontal surface of sea bottom formed of hard soil. In such a case, there will be no gouging in the point under consideration (no matter which parameters of soil, angle of seabed slope, etc. are in this point); all ice features would stop far from this point. For example, if a pipeline is laid on the bottom of a relatively narrow and deep enough natural gully than the seabed itself provides effective protection of the pipeline against ice keels. Unfortunately, all these conditions cannot be taken into account by conventional statistical processing of ice gouge survey data.

Any alternative?

A possible alternative may be the theoretical and/or physical modelling of gouging. But no one model is perfect. Any model is based on a number of assumptions, employed simplifications, etc. Consequently, verification of a model is of critical importance. One of the most obvious methods for such verification is a comparison of predictions (model output) with actual data. This comparison can be made relatively simple if a deterministic model of a given interaction event is under consideration. In such case, ice feature and seabed surface geometry, soil and ice properties, and all the initial conditions are assumed as known. The output of the theoretical model that is compared with experimental data could be depth and length of the gouge, time-history of ice feature kinematics (and consequently, forces acting on the ice feature, if its inertial

characteristics are measured), etc. Obtaining such full-scale data that is associated with the observation of an interaction event is very money and time consuming. For this reason experiments on a smaller scale would be helpful. As far as the theoretical models are concerned, it seems that the most advanced numerical solutions of general equations of soil mechanics, coupled with the simulation of ice feature failure can give quite realistic predictions. Such models employing computer software for finite element analysis can be developed in the nearest future and promising achievements have been reached up until now.

The task becomes more complicated if the objective is to compare statistical characteristics of gouges in a geographical area under consideration. The making of this comparison requires that the output of the model would be similar to those parameters which are observed in the field (i.e. spatial distributions of ice gouge depth, width, orientation etc. in the particular area with all the peculiarities of its bathymetry, soil properties, ice conditions). Such a model was elaborated and practically implemented by the Arctic and Antarctic Research Institute in cooperation with specialists from other Russian institutions in 1990-1998. The model was developed with reference to the design of an underwater crossing of Baydaratskaya Bay (Kara Sea) for a system of pipelines «Yamal-Europe». The methodology is described briefly as follows (a more detailed description is presented in a paper by Stepanov et al, 1998).

At the first stage, information about the investigated region is processed. Such data includes the topography of the seabed, soil characteristics, velocity and directions of currents and other parameters. Additionally, as far as possible, a statistical evaluation of the laws of probability distribution and regression dependencies between fundamental parameters of ice features is carried out according to the results of the observations.

The second stage involves formulating a deterministic model of the seabed gouging by the ice feature which has known characteristics, moves with a definite velocity, and gouges the soil which has known properties. In this case, the shape of that part of an ice feature which interacts with the ground is assumed to be simplified.

At the third stage, in the course of the computer Monte Carlo simulation, ice features and other objects, processes and values of random character are simulated (or generated). The results of statistical analysis of the first stage are used for this purpose. Using these data in addition to deterministic values (e.g. topography of the seabed, properties of the soil) as input (and with the help of the dependencies obtained at the second stage), the process of gouging is modelled. Statistical processing of the simulation results allows us to evaluate the long-term probability distributions of the ice keel penetration depths.

The model as it exists at present can definitely be improved. In particular, a more advanced procedure (deterministic approach) for calculation of force acting on an ice feature is obviously required. Meanwhile, the approach in general looks quite promising. Its main advantages are providing statistical characteristics of ice keel penetration depths in dependence on two spatial coordinates, and the capability of direct comparison of the simulation results with survey data.

Conclusion

In conclusion the following statements can be formulated: Conventional statistical analysis of ice gouge survey data will probably not result in reliable estimates of statistical characteristics of depths of ice keel penetration. Meanwhile, such data have valuable information that can be employed for the validation of theoretical models of gouging. Special requirements to the simulation procedure used in making direct comparisons of simulated and observed data are needed. Approaches based on time-domain stochastic simulation meet these requirements.

Acknowledgment

The author gratefully acknowledges Alexander Klepikov for his helpful comments on the paper.

References

1. Blasko, S.M., Shearer, J.M., and Myers, R. (1998) Seabed scouring by sea-ice: scouring process and impact rates: Canadian Beaufort Shelf. Proceedings of Ice Score and Arctic Marine Pipeline Workshop, 13th Okhotsk Sea & Sea Ice Symposium, Mombetsu, Japan, February 1998, 53-58.
2. Clark, J.I., Philips, R., and Paulin, M.J. (1998) Ice scour research for safe design of pipelines: 1978-1998. Proceedings of Ice Score and Arctic Marine Pipeline Workshop, 13th Okhotsk Sea & Sea Ice Symposium, Mombetsu, Japan, February 1998, 1-7.
3. Comfort, G., Abdelnour, R., Trak, B., Menon, B., and Graham, B. (1982) Lake Erie ice scour investigation. Submitted at NRC Workshop on Ice Scour, Montebello, Quebec, February 1982.

4. Grass, J.D. (1984) Ice scour and ice ridging studies in Lake Erie. Proceedings of IAHR Ice Symposium, Hamburg, 1984, 33-43.
5. Klepikov, A.V., Malek, V.N., Stepanov, I.V., Timofeev, O.Ya., Spichkin, V.A., and Egorov, A.G (1997) Sea ice and its impact on seabed in the area of submarine pipeline crossing of Baydaratskaya Bay. Proceedings/Abstracts of the 3rd International Conference "Development of Russian Arctic Offshore" RAO-97, St.Petersburg, September 23-26, 1997.
6. Klepikov, A., Malek, V., Finkelshtein, A., Poplin, J. P., Wang, A. T., and Beketsky, S. (1999). Ice gouge mapping survey off the northeastern coast of Sakhalin Island. Proceedings of the 2nd ISOPE European Offshore Mechanics Symposium: Pipelines, Moscow, 1999, 93-95.
7. Niedoroda, A.W. and Palmer, A.C. (1986) Subsea trench infill. Proceedings of 18th Offshore Technology Conference, Houston, OTC 5340, 4, 445-452.
8. Palmer, A. (1998) Alternative paths for determination of minimum burial depth to safeguard pipelines against ice gouging. Proceedings of Ice Score and Arctic Marine Pipeline Workshop, 13th Okhotsk Sea & Sea Ice Symposium, Mombetsu, Japan, February 1998, 9-16.
9. Stepanov, I.V. Timofeyev, O.Y., Klepikov, A.V., and Malek V.N. (1998) An approach to the optimisation of the burial depth of underwater pipelines on the arctic offshore. Proceedings of Ice Score and Arctic Marine Pipeline Workshop, 13th Okhotsk Sea & Sea Ice Symposium, Mombetsu, Japan, February 1998, 59-69.
10. Weeks, W.F., Barnes, P.W., Rearic, D.M., and Reimnitz, E. (1983) Statistical aspects of ice gouging of the Alaskan Shelf of the Beaufort Sea. CRREL Report 83-21.
11. Woodworth-Lynas, C.M.T. (1998) Sub-scour soil deformations and the development of ideas from field work in the last decade. Proceedings of Ice Score and Arctic Marine Pipeline Workshop, 13th Okhotsk Sea & Sea Ice Symposium, Mombetsu, Japan, February 1998, 33-41.

CRUSHING FAILURE DURING EDGE-INDENTATION OF FLOATING ICE SHEETS

Devinder S. Sodhi

U. S. Army Cold Regions Research and Engineering Laboratory
72 Lyme Road, Hanover, 03755-1290, USA
e-mail: dsodhi@crrel.usace.army.mil

ABSTRACT

Small-scale indentation tests were conducted with compliant structures and freshwater ice sheets. Besides measuring forces and displacements, we installed grid-based tactile pressure sensors at the ice–structure interface to measure the pressure generated during an interaction. Similar to the results of earlier studies, the results of the present study with compliant structures show that there is ductile deformation of ice at low indentation speeds and continuous brittle crushing at high indentation speeds. During a typical cycle of the dynamic ice–structure interaction at intermediate speeds, the tactile sensor data indicate that the ice deforms in a ductile manner during the loading phase, and fails in a brittle manner during extrusion phase. Theoretical estimates of global force are given in terms of non-simultaneous local force per unit width during continuous brittle crushing. We find the effective pressure measured during small-scale indentation tests to be close to those measured on full-scale structures, when the indentation rate is high in both situations.

KEYWORDS

Ice crushing, Ice forces, Ice mechanics, Edge indentation, Ice–structure interaction

1 INTRODUCTION

Structures placed in an environment where the presence of ice can be a threat to their safety need to be designed and built strong enough to resist any ice action. To achieve this objective, an accurate estimate of the ice forces and their variation with respect to time is necessary. Examples of structures that commonly encounter ice actions are lighthouses, channel markers, bridge piers, dam walls, offshore drilling platforms in the Arctic regions, etc. The force required to fail an ice feature against a structure generally limits the interaction force resulting from a relative motion between them. An ice sheet may fail against a structure in bending, buckling, crushing, or a combination of these failure modes. However, a thick ice feature, e.g. an iceberg, is likely to fail in the crushing mode or in large-scale fracturing during an interaction with a structure. During the full-scale ice force measurement program at the Molikpaq structure (Wright et al. 1986, Wright and Timco 1994, Hardy et al. 1998), the observers recorded the failure modes in which the moving ice cover failed against the structure. They found that, although the ice crushing

occurred only 1% of the time of observations, it caused some of the highest forces on the structure, which at times vibrated the 110-m-wide structure.

Floating ice sheets exist on the surface of rivers, lakes, and seas at a temperature very close to ice's melting point. The behavior of most solid materials is very ductile when their temperature approaches their melting point. However, ice also fails easily in a brittle manner when subjected to stresses from a high rate of loading. The ductile and brittle characteristics of ice are manifestations of its creep and elastic properties, making the prediction of ice behavior very complex from the point of view of mechanics.

Topics included in this paper are results from previous and recently conducted indentation tests, derivation of global ice force in terms of local ice forces, and comparison of ice forces from full-scale measurements and small-scale indentation tests. The results of recently conducted indentation tests include data from tactile sensors placed between an ice sheet and a vertical indenter plate. The tactile sensor data provide magnitudes of the actual contact area and the ice-structure interfacial pressure, and insights into the processes taking place during ice crushing. The results of the present study confirm there is ductile deformation of ice during the loading phase and non-simultaneous brittle crushing during the extrusion phase of a dynamic ice-structure interaction cycle. This results in a saw-tooth pattern in the time-history plots of ice forces and an intermittent advance of the structure into the ice at highly variable speeds that differ by one or two orders of magnitude.

There are two types of ice indentation encountered in ice-structure interaction according to the size and shape of ice feature: (1) indentation into an ice wall, and (2) indentation against the edges of floating ice sheets. Indentation into an ice wall entails an ice-structure contact area whose width and height are nearly equal. The crushed ice flows in all radial directions within the contact area, such as what happens during the impact of icebergs against a structure or the ramming of an icebreaker against a multi-year ice floe. Edge indentation involves a large floating ice sheet moving against a nearly vertical structure, in which the contact area is much wider than its height. The crushed ice flows mainly up and down during an ice-crushing event. As a result of differences in the geometry of the contact areas, there is a significant difference in confinement experienced by crushed ice as it extrudes out of the region being crushed. In this paper, we discuss the results of edge-indentation of floating ice sheets, an interaction commonly encountered by structures in an ice environment.

2 RECENT SMALL-SCALE INDENTATION TESTS

For most practical applications, the ice interaction with compliant structures is of interest, and it is appropriate to develop an understanding of this interaction from the point of view of ductile and brittle failure modes of ice. The main objective for conducting a set of small-scale indentation tests, to be discussed in next section, is to develop an understanding of the processes taking place during dynamic ice-structure interaction, in which the indentation rate into the ice can vary by two orders of magnitude. Data on effective pressure, measured during small-scale indentation tests (Sodhi 1991b), indicate that there is ductile deformation and brittle failure of ice during the loading and extrusion phases, respectively, of a dynamic ice-structure interaction event.

2.1 Experimental Setup and Procedure

The indentation apparatus (Fig. 1) used in the present series of tests is the same used during the indentation tests conducted in 1988–89 (Sodhi 1991a). The structural support consisted of two horizontal plates attached to each other with four hinged links. The top plate was mounted under the carriage of a high-force module, which in turn was installed under the main carriage that spans the test basin of the Ice Engineering Facility of the Laboratory. Between the two plates, we bolted two brackets, one to each plate, and mounted a spring between these brackets, as shown in Figure 1. The spring consisted of two rectangular aluminum plates, and was held together by bolting them to 25-mm-diameter aluminum cylinders at a spacing of 50 mm. By removing or installing these cylinders, we could change the effective stiffness of the spring from about 0.9 to 2.5 MN m⁻¹. We determined the stiffness of the spring during low-speed indentation tests or special tests to measure the creep properties of the ice. We installed a displacement transducer to measure the relative displacement between these two plates, and we call this measurement a structural deflection. We also installed two string-type displacement transducers to measure the carriage position and the indenter position. Underneath the bottom plate, we attached the support for the indenter plate and about a 300-kg mass of lead weights. As shown in Figure 1, we mounted the indenter plate on three load cells, each having a capacity of 22.24 kN and bolted on the indenter supports. We used interchangeable indenter plates having widths of 100 and 146 mm, as shown in Figure 2. We obtained the total force or load on the indenter by adding the forces measured by three load cells. We also installed an accelerometer, but the measured acceleration exceeded the transducer range of ± 3 g (29.43 m s⁻²) during dynamic ice–structure interaction.

During each test, we tried to hold the speed of the carriage constant, whereas the speed of the indenter varied considerably, according to the response of the structure to interaction forces. We conducted the indentation tests by either moving the indenter carriage of the high-force module in the transverse direction or the main carriage in the longitudinal direction of the 9-m-wide and 36-m-long test basin. For low-speed indentation, we mounted the high-force module in the transverse direction, parked the main carriage in place at a different position along the basin, and moved the screw-driven indenter carriage in the module with a direct current (DC) electrical motor. By changing the gear ratio, we obtained two ranges of indentation speed: 0.5–7.5 and 8–38 mm s⁻¹. For indentation speeds greater than 40 mm s⁻¹, we mounted the high-force module in the longitudinal direction, did not move the screw-driven indenter carriage of the high-force module, and moved the main carriage with either the DC motor within a speed range of 62–125 mm s⁻¹ or an alternating current (AC) electric motor within a speed range of 50–500 mm s⁻¹.

We conducted all indentation tests with freshwater ice, as in the previous series of tests (Sodhi 1991a). Before growing an ice sheet in the basin, we mixed the water by bubbling it with air to obtain a uniform temperature close to 0°C. We started the ice growth process by spraying a fine mist of air and water into the –10°C ambient air above the basin, and letting the ice grow at an ambient temperature of –20°C to the desired thickness. By this process, we obtained small-size, columnar-grained ice sheets.

We changed the following parameters during the course of this program: ice thickness, indenter width (100 and 146 mm), indentation speed, and spring stiffness. Table 1 lists the parameters either set or measured during the present testing program. To obtain the stiffness of the spring and creep properties of the ice sheets, we conducted either indentation tests at very

low speeds or relaxation tests, which consisted of loading the edge of an ice sheet, locking the carriage in that position, and measuring the slow relaxation of the interaction force for a few minutes.

We connected all transducers to a signal conditioner, which also provided the excitation signal to the load cells and displacement transducers. We powered the accelerometer and the structural deflection transducer from external sources. We installed 481-Hz, low-pass electrical filters to filter all signals. The sampling rates were 1200 Hz during all indentation tests and 100 Hz during all relaxation tests.

A significant difference between the present series of tests and those conducted earlier (Sodhi 1991a) is that we installed tactile sensors to measure the interfacial pressure and the actual contact area between the indenter and the ice sheet. There have been many attempts to make these measurements during ice–structure interaction (Tanaka et al. 1987, Joensuu and Riska 1989, Frederking et al. 1990). Some of these measurements gave good data on interfacial pressure, but it was not possible to obtain a complete distribution of the interfacial pressure. Using the grid-based tactile pressure technology utilized in this study, Izumiyama et al. (1998) and Sodhi et al. (1998) reported distributions of interfacial pressure measured during indentation tests in Japan at various speeds.

The grid-based tactile pressure technology is a combined system of hardware and software components (Paikowsky and Hajduk 1997). The hardware system comprises three physical units: a sensor, a data acquisition board, and a connection unit between the data acquisition board and the sensor. The sensor software allows recording, analysis, and replaying of the collected data. In each sensor used in this study, there were 44 rows and 44 columns of conductive material, separated by semi-conductive ink and encased in thin plastic sheets. The intersection of these rows and columns formed a grid of sensing areas. Changes in resistance of the semi-conductive ink in response to an applied pressure or force provided the data on interfacial pressure, and the data acquisition board recorded the resistance at each grid point. The thickness of sensor was extremely thin (about 0.1 mm) in comparison to the size of sensing areas, which were 56×56 mm, 84×84 mm, and 112×112 mm in this study. The actual unit sensing area changed with the sensor size, but the number of rows and columns remained the same. We inserted the end of a tactile sensor into a handle and cable unit, which was connected to a data acquisition board in a computer. The handle contained 88 connection points, and a software-controlled test verified the connection of all points between the sensors and the acquisition board. The board recorded data by sequentially scanning the rows and the columns, and measuring the electrical resistance at each grid point. The sensor software recorded data from all rows and columns at a maximum scanning rate of 137 frames per second, while displaying the data in a variety of graphical forms. After recording a set of frames in a movie, the software can playback a recorded movie either continuously or intermittently, one frame at a time, while moving forward or backward in time. The software has the ability to generate graphs of force, contact area, or pressure with respect to time. It is also possible to determine the location of the resultant force. We can select specific zones within the sensing area to generate these graphs, allowing detailed analysis of the recorded pressure distributions. The analysis pertaining to a frame or a movie can be done either using the software or exporting the data in ASCII format for processing in a spreadsheet. The sensor software allows pre- or post-calibration of the sensor by specifying the total force applied on the sensing area at a particular point in time (I-Scan 1999).

The basis of calibration is the change in resistance of each sensing element in inverse proportion to the applied normal force on that sensing element. According to the user's manual (I-Scan 1999), some variation exists between sensitivities of individual elements on any sensor, and this variation is acceptable in a majority of applications. The software provides a method, called equilibration, to minimize this source of error. However, we did not conduct this procedure, which requires application of hydrostatic pressure across a thin membrane over the sensing area. Upon our request for the data on variation of sensitivities, the sensor manufacturer conducted a test on a sensor from the same batch as those supplied to us by applying a hydrostatic pressure across a thin membrane on the sensing area. The standard deviation of measured pressure had an error of $\pm 5\%$. Therefore, the maximum error in values of tactile pressure reported here is $\pm 15\%$, assuming normal distribution of error and a probability of exceedance equal to 0.0013. To reduce the effects of variation in sensitivities and other noise on the results, the data in each frame were averaged to reflect the values in neighboring grid points, while keeping the contact area the same. This is known as the fixed-area averaging, a feature available in the software (I-Scan 1999).

Under the assumption that the sensor output is linearly proportional to applied pressure, the sensor software allows calibration between a known force applied over the entire sensing area and the computed raw sum at one point in time. During the indentation tests, we inserted the tactile sensors in-between a folded plastic sheet (an overhead-projection transparency) to protect it from ice abrasion during the tests. To account for the effect of the plastic sheet and other factors affecting sensor measurements, we calibrated the tactile sensor data from each test with the forces measured with the load cells. Because the sensor width was smaller than the indenter width, we reduced the total force measured by the load cells by the ratio of the two widths and applied the proportionately reduced load on the sensor during calibration. Taking the width ratio into account for a particular test, we can relate the total force measured across the entire indenter width with the load cells to those measured with a tactile sensor, and vice versa.

2.2 Results

As in previous small-scale indentation tests (Sodhi 1991a, 1992), we observed here that the mode of ice failure depended mainly on the indentation rate: ductile deformation of ice during a low-indentation rate, brittle failure during a high-indentation rate, and 'intermittent' crushing during indentation at intermediate speeds. In the present study, we obtained data on contact area and interfacial pressure from the tactile sensors. These data provide important insights into the processes taking place during indentation tests at various rates. In the following, we present data from a few selected tests conducted in the three regimes of indentation rate to highlight important differences in the failure modes of ice crushing.

During most low-speed indentation tests, the contact area between an indenter face and the edge of an ice sheet grew from a small value to almost full sensor width and almost full ice thickness. We define here the 'contact area ratio' as the ratio of actual contact area to nominal contact area, which is the product of ice thickness and sensor width. During these tests, the interaction force gradually increased to a magnitude large enough to buckle the ice sheet, which was the final failure mode in most low-speed indentation tests. During Test 10, the carriage speed was 0.33 mm s^{-1} , but the actual rate of indentation into the edge of the ice sheet was 0.08 mm s^{-1} , because the structure deflected at a rate of 0.25 mm s^{-1} . Figure 3 shows plots of the

interaction force, as measured by the load cells and the tactile sensors, and the contact area ratio with respect to time. We calibrated the tactile sensor data by matching the maximum force on the sensor with the proportionately reduced maximum load from the load cells at one point in time only. Though the time-history plots of the total force measured by the load cells and tactile sensor are close to each other, there are some differences between the two plots, which can be attributed to the visco-elastic response of the tactile sensor. Figure 4 shows plots of interfacial pressure and its distribution, as measured in one frame with the grid-based tactile pressure technology, at a time when the force was near the maximum value of 15.73 kN. The pressure distribution is fairly uniform, having a mean value of 6.9 MPa and a standard deviation of 2.7 MPa. As mentioned earlier, some of this variation in pressure can be attributed to the variations in sensitivities of the individual sensing elements of the tactile sensor.

During most high-speed indentation tests, the ice failed continuously in the brittle mode, and the severity of structural vibrations was low compared to those encountered during intermittent crushing. Movies of the tactile sensor data show that the contact areas, over which the interfacial pressure was high, were in the middle of the ice sheet, and that high interfacial pressure persisted over these areas for a short time because the location of high-pressure zones shifted to a different location in each frame. The rate of frame acquisition being 137 Hz indicates that the duration of each high-pressure zone was less than 7.3 ms. Figure 5 shows time-history plots of total force, as measured by the load cells and the tactile sensor, and the contact area ratio during Test 93. During an interval of time between 4.5 and 9.5 s in Fig. 5, the interaction force was the results of brittle failure of ice. During that time, the carriage and the indenter moved at the same speed, whereas the average structural deflection and the average interaction force were 6.73 mm and 13.74 kN, respectively. We calibrated the tactile sensor by matching the total force from the tactile sensor with that from the load cell at the time of highest force (≈ 9.813 s in Fig. 5). There is a good agreement between the two sets of data at all times in that test, and the differences between the two data sets may be attributed to the noise in the tactile sensor data. Figure 6 shows plots of typical interfacial pressure and its distribution at a time (≈ 6.592 s in Fig. 5) when ice failed continuously in brittle crushing. As described earlier, we applied the fixed-area averaging to reduce the noise in the data of each frame. The zones of high-pressure are randomly distributed within the nominal contact area, and their area is small compared to the actual contact area, which is in the range of 60–80% of the nominal contact area (Fig. 5). The pressure distribution is non-uniform, having a mean value of 1.6 MPa and a standard deviation of 1.5 MPa.

The distribution of interfacial pressure shown in Fig. 6b is quite different from that shown in Fig. 4b for a low-speed indentation test. The pressure is more uniform over the actual contact area during a low-speed indentation (Fig. 4a), and it is non-uniform during high-speed brittle crushing (Fig. 6a). The average pressures of these two pressure distributions differ significantly, leading to a significant difference in the total force on the indenter during these two modes of ice crushing.

During intermediate speeds, the ice-structure interaction takes place in a manner that the interaction force plots have a typical ‘saw tooth’ pattern. This happens during interactions in a range of relative speeds for a given structural stiffness and ice thickness. The main characteristic of this interaction is that the actual indentation rate into an ice sheet varies by one or two orders of magnitude, while the relative speed between a distant point on the ice sheet with respect to a fixed datum remains constant. Adjacent to the structure, the ice sheet appears to stop against the

structure and then move suddenly, giving an appearance of an intermittent motion. Hardy et al. (1998) made the following comment in their report on the full-scale monitoring of ice forces on Molikpaq: "Drift measured by radar was approximately 0.05 m/s. However, locally, the ice was moving in the start-stop manner." It is for this reason that Sodhi (1991a) called this type of interaction as 'intermittent' crushing. Though this is a commonly encountered interaction, the exact reasons for its development have not been known. Sodhi (1991c) presented a detailed account of energy transfer during a typical dynamic ice-structure interaction cycle. He also presented data on the measured effective pressure with respect to the actual indentation speed into the ice (Fig. 17), and proposed that the ice effective pressure decreases with increase in indentation rate (Sodhi 1991b). In the present study, we obtained all of the above results, as well as the data on interfacial pressure and contact area with the help of the grid-based tactile pressure technology. The data on interfacial pressure shed new light on the processes taking place during dynamic ice-structure interaction.

Figure 7 shows time-history plots of the positions of the carriage and the indenter, interaction force measured by the load cells and the tactile sensor, and the contact area ratio for a typical cycle during Test 88. During the test, the ice thickness was 25 mm, the indenter width was 146 mm, the average speed of the carriage was 55 mm s^{-1} , and the spring stiffness was 0.92 MN m^{-1} . Overall, there is a good agreement between the forces measured by the load cells and the tactile sensor. The data in Figure 7 show that a typical interaction cycle can be divided into three phases: (1) the loading phase when the interaction force and the structural deflection increase with time until ice failure takes place, (2) extrusion phase when the structure moves forward at a very high indentation speed while extruding ice in its path, and (3) separation phase when the interaction force is nearly zero and there is no contact between the structure and the ice. During Test 88, the average indentation speed was about 7.8 mm s^{-1} during the loading phase, and it reached a maximum value of about 750 mm s^{-1} during the extrusion phase. The sudden unloading of the structure at the end of a loading phase leads to transient motion of the structure, and the separation phase starts at the end of the forward indentation of the structure, resulting in loss of contact as shown in Figure 7. Sodhi (1995) presented a theoretical model for dynamic ice-structure interaction, incorporating the three phases of a dynamic ice-structure interaction cycle.

Figures 8 and 9 show plots of interfacial pressure over a grid that covers an area of 84 by 84 mm, and the distribution of the pressure at two time instants during Test 88: (a) near the end of the loading phase ($\approx 14.903 \text{ s}$ in Fig. 7), and (b) near the middle of extrusion phase ($\approx 14.976 \text{ s}$ in Fig. 7). In Figure 7, the contact ratio approaches 1 at the end of the loading phase, and it is greater than 1 during the extrusion phase, which can be attributed to the enlargement of contact area as a result of the vertical movement of crushed ice. The distributions of interfacial pressure in Figures 8 and 9 are different, and the mean values differ significantly. The mean value at the end of the loading phase (Fig. 8b) is 5.1 MPa, which is close to the mean pressure of 6.9 MPa at the end of low-speed indentation (Fig. 4b). The mean value in the middle of the extrusion phase (Fig. 9b) is 1.9 MPa, which is close to the mean pressure of 1.6 MPa during high-speed indentation (Fig. 6b).

We will put a segment of the video movie of the tactile sensor data at the CRREL internet site: www.crrel.usace.army.mil/?. Replaying the tactile sensor data frame by frame, we can see that the pressure increases in magnitude simultaneously at all high-pressure zones across the width of the sensor during the loading phase, as in ductile deformation of ice. On the other hand,

the locations of high-pressure zones change continuously during the extrusion phase, as in brittle crushing. Thus, the dynamic ice–structure interaction is a sequential failure of ice in the ductile and brittle modes. The structural compliance causes variable rates of indentation into the ice, resulting in a ‘saw-tooth’ pattern in ice force records. Because of the two modes of ice crushing, we now call this type of interaction with a compliant structure as intermittent ductile-brittle crushing.

To show the effect of structural stiffness on ice–structure interaction, we conducted two tests under nearly the same conditions, except that we changed the structural stiffness from 2.45 MN m^{-1} in Test 26 to 1.12 MN m^{-1} in Test 27 (Table 1). Figure 10 shows the time-history plots of the interaction force and the structural deflection from these two tests. As listed in Table 1, the indenter width, the ice thickness, and the average indentation rate were almost the same during these two tests. Significant differences between the two interactions as a result of stiffness difference are: (a) the structural deflections were larger in Test 27 compared to those in Test 26, and (b) the frequency of intermittent ductile and brittle crushing was higher in Test 26 than that in Test 27. Though the failure load at the end of loading phase is variable, the average of peak values is approximately 25 kN during both tests. As a consequence of this, the frequency of intermittent crushing events should be in proportion to the structural stiffness, as postulated by Määttänen (1975) and Sodhi and Nakazawa (1990). However, the ratios of failure frequencies and structural stiffness are, respectively, 1.85 and 2.15, which are different. This difference can be attributed to the presence or absence of the separation phase during transient vibrations at the end of each loading phase. In Figure 10, the interaction force in Test 26 does not reach the value of zero, indicating absence of separation phase, and it reaches the zero value after most peak-force events in Test 27, indicating presence of separation phase. We can determine the ice crushing frequency from an ice–structure simulation program (e.g., Sodhi 1995), because an explicit expression for the frequency of an intermittent ductile-brittle crushing cycle has not yet been found.

To summarize the results from small-scale and medium-scale indentation, Figure 11 shows a map of ice crushing failure during interactions with rigid and compliant structures. During an ice interaction with a rigid structure, the ice fails in the ductile and brittle modes, and there is a sharp transition at an indentation speed, which has been found to be close to 3 mm s^{-1} . During an ice interaction with a compliant structure, the failure modes are ductile and brittle at low and high rates of indentations, respectively. At intermediate indentation speeds, the ice fails in the intermittent ductile-brittle mode as a result of variable indentation rates into the edge of an ice sheet. Because of this, there are two transition speeds, ductile to intermittent and intermittent to continuous brittle crushing, during interactions with compliant structures.

3 LOCAL AND GLOBAL FORCES

From the data presented above and from other indentation tests (Joensuu and Riska 1989, Sodhi et al. 1998), it is evident that the areas of high pressure regions during brittle crushing events are narrow regions in the middle of an ice sheet, and that the ice fails non-simultaneously across the width of a structure or an indenter. Kry (1978) and Ashby et al. (1986) proposed models for non-simultaneous crushing by dividing the width of a structure into an arbitrary number of zones. However, they did not consider the correlation of ice forces generated in different regions of an indenter. There is a need for a theoretical model to define the local forces,

and to include the correlation of non-simultaneous local forces with the forces generated in neighboring points. Dunwoody (1991) presented the following model for non-simultaneous failure of ice across the width of a structure to estimate the global force from the local force per unit width. He considered the global force to be given by:

$$g(t) = \int_w f(x, t) dx, \quad (1)$$

where $f(x, t)$ is the local force per unit width of a structure, x is the position of a point across the width of the structure, t is the time, and w is the width of the structure. The variation of local force across the width as well as with respect to time depends on the number of contacts, the size of crushing zones, and the duration of the high pressure zone at a point. The local force varies with respect to both t and x . To obtain $f(x, t)$ from measurements of interfacial pressure $p(x, y, t)$ with a tactile sensor, we integrate the pressure over rows in each column of a grid to get:

$$f(x, t) = \int_h p(x, y, t) dy \approx \sum p(x, y, t) \Delta y, \quad (2)$$

where x and y are the coordinates of a point in the contact area, Δy is the height of each sensing area in the grid, and the summation is over all rows across the ice thickness h . Sodhi et al. (1998) have given three-dimensional plots of $f(x, t)$ with respect to t and x for ductile and brittle crushing of ice, showing simultaneous and non-simultaneous variations of $f(x, t)$.

Under the assumption that the ice failure process is uniformly the same across the width of the structure, the average local force per unit width $\mu_{f(t)}$ is independent of the position of a point on the structure, implying the average global force $\mu_{g(t)} = E[g(t)] = wE[f(t)] = w\mu_{f(t)}$.

From the tactile sensor data obtained during Test 93 of this study, we obtained $f(x, t)$ by the summing the interfacial pressure over all rows in each column of each frame for a duration of 2 seconds. The average value $\mu_{f(t)}$ of $f(x, t)$ was found to be 89.446 kN m⁻¹. Dividing $\mu_{f(t)}$ by h , we get the average global effective pressure $\mu_{g(t)}/wh$ equal to 2.13 MPa. The average global effective pressure $\mu_{g(t)}/wh$ from load cell data for continuous crushing is equal to 2.28 MPa, as listed in Table 1. These two average values of the global effective are close to each other, but differ slightly (Fig. 5) because of two different force-measuring systems.

Dunwoody (1991) proposed a spatial correlation function in terms of a negative exponential function:

$$R_{f(t)}(x_2 - x_1) - (E[f(t)])^2 = \sigma_{f(t)}^2 \exp\left(-\frac{|x|}{L}\right), \quad (3)$$

where $R_{f(t)}(x_2 - x_1)$ is the auto-covariance function of the local force $f(t)$, x is the distance between two points at x_2 and x_1 on the structure, $\sigma_{f(t)}$ is the standard deviation of the local force $f(t)$, and L is a length parameter in the above equation to express correlation of forces over a distance and may be related to the size and density of the crushing zones. Figure 12 shows plots of correlation coefficient of $f(x, t)$ with respect distance x for Tests 10 and 93, in which the indentation rates were, respectively, 0.33 and 502 mm s⁻¹. We generated the data on $f(x, t)$ as per equation 2 for a certain duration of time. The correlation coefficient plot for Test 93 decreases to a low value with an increase in distance x during high-speed indentation, whereas the same plot for Test 10 decreases slowly with an increase in distance x . Approximations of these plots in the form of negative exponential function leads to estimates of the correlation length parameter L , as shown

in Figure 12. These trends indicate that the correlation length L changes significantly with the mode of ice crushing: large values for ductile crushing, and small values for brittle crushing. The high-pressure zone during Test 10 covered the entire sensor area, whereas it varied between 4 and 24 mm with an average value of about 10 mm during brittle crushing in Test 93. These observations indicate that we can relate the correlation length to the size of crushing zones. However, we need to conduct a detailed study for verification of this assumption.

From the tactile sensor data on continuous brittle crushing during Test 93, the standard deviation of local force $f(x, t)$ is $\sigma_{f(t)} = 36.134 \text{ kN m}^{-1}$. If we divide $\sigma_{f(t)}$ by h , we obtain the standard deviation of local effective pressure to be 0.86 MPa. An estimate of the correlation length L during continuous crushing is about 4 mm, as indicated by the plot of $\exp\{-x/(4 \text{ mm})\}$ vs. x in Fig. 12.

The standard deviation of the global force (Dunwoody 1991, Sodhi 1998) is given by:

$$\sigma_{g(t)}^2 = 2L\sigma_{f(t)}^2 \left[w - L \left\{ 1 - \exp\left(-\frac{w}{L}\right) \right\} \right]. \quad (4)$$

We divide $\sigma_{g(t)}$ by wh , the nominal contact area, to obtain the standard deviation of global effective pressure. For Test 93, we substitute for $\sigma_{f(t)} = 36.134 \text{ kN m}^{-1}$, $w=0.146 \text{ m}$, $h=0.042 \text{ m}$, and $L=0.004 \text{ m}$ in eq.4, and get a value of $\sigma_{g(t)}/wh$ equal to 0.199 MPa. From the force record obtained by summing all pressure values in each frame of the tactile sensor data movie, the standard deviation of global effective pressure during continuous crushing is 0.252 MPa, which is close to 0.199 MPa obtained from eq. 4. but much smaller than the standard deviation of local effective pressure $\sigma_{f(t)}/h$ (0.86 MPa). The same value from the load cell data is 0.125 MPa, which is about half the values of 0.199 and 0.252 MPa. We discuss below the reason for this discrepancy.

Figure 5 shows plots of total force $g(t)$ measured during Test 93. In the plot, the ice force is approximately constant with random variations, indicating crushing in the brittle mode during the time interval of 4.5–9.5 seconds. Figure 13 shows distributions of the total forces, measured by the load cells and obtained from the tactile sensor data, during time interval of 5–7 seconds. Though the average values of the total force are close to each other, the standard deviation of the force data from tactile sensor is about two times larger than that from load cell measurements. The difference between the values of the standard deviation can be attributed to the difference in inertia of the two measuring systems and the electromagnetic noise recorded by the tactile sensor. As shown in Figure 2, the force measuring system consisted of a 25-mm-thick steel plate, which was supported on three load cells. Though the rigidity of this system was high, it could have acted as a filter to high-frequency forces generated at the ice-structure interface. As discussed earlier, the tactile sensor measurement system picked up some signal when we moved the carriage using the big AC motor. However, the record generated by summing all the data due to this noise source had very small variation superimposed on a constant value. We believe that the variations in the force records from tactile sensor data are due to the ice failure process because of the use of the fixed-area averaging of the tactile sensor data before the summation process to generate the ice force records. Figure 13 also shows that the assumption of a Gaussian distribution of global force is reasonable for high-speed indentation during brittle crushing of ice.

Assuming a Gaussian distribution for the global force $g(t)$, we can obtain an estimate of the maximum global force on the structure :

$$F_{\max} = \mu_{g(t)} + 3\sigma_{g(t)}, \quad (5)$$

where the factor 3 relates to a probability of exceedance equal to 0.0013 for a Gaussian distribution. It may be necessary to use a value other than 3 for a non-Gaussian distribution. Dividing both sides by wh and rearranging the expression, we get the following expression for the relative pressure ratio (A_r) of maximum effective pressure to average local pressure:

$$A_r = \frac{p_{\max}}{\mu_{f(t)}/h} = 1 + 3 \frac{\sigma_{f(t)}}{\mu_{f(t)}} \sqrt{2 \frac{L}{h} \frac{h}{w} \left[1 - \frac{L}{h} \frac{h}{w} \left(1 - e^{-\frac{wh}{hL}} \right) \right]}, \quad (6)$$

where $\mu_{f(t)}/h$ is the average local effective pressure, and $\sigma_{f(t)}/\mu_{f(t)}$ is the coefficient of variation of the local load per unit width. Figure 14 shows plots of the relative pressure ratio A_r with respect to aspect ratio w/h for three values of the coefficient of variation ($\sigma_{f(t)}/\mu_{f(t)} = 2.0, 1.0, \text{ and } 0.5$) and for two values of the ratio of correlation length to ice thickness ($L/h = 1 \text{ and } 0.1$). It is not meaningful to plot the aspect ratio effect for values of L/h greater than 1, because a large value of L in comparison to ice thickness h would mean that simultaneous failure of ice is occurring during low-speed indentation. For those cases, the assumption of a Gaussian distribution of $g(t)$ may not be valid.

The plots in Figure 14 show a trend of decreasing relative pressure ratio with increasing aspect ratio. It is important to account for this effect when comparing the effective pressure from small-scale tests with those measured on full-scale structures, because of the higher effective pressure measured on narrow structures. Afanasyev et al. (1972) were the first to report this effect on the basis of the results from small-scale indentation tests. Others (Michel and Blanchet 1983, Sodhi and Morris 1984, Timco 1987, Sodhi 1992) have also found this effect in their results from small-scale indentation tests.

To estimate maximum global force on a structure for brittle crushing of ice, we propose the following expression:

$$F_{\max} = A_r w \mu_{f(t)} = A_r w h p_w, \quad (7)$$

where $p_w (= \mu_{f(t)}/h)$ is the average effective pressure of the local force, which is the same as the effective pressure on a wide structure when the value of $A_r = 1$ for $w \gg h$. Though this expression appears similar to that given by Korzhavin (1962), the basis for arriving at this expression is the non-simultaneous brittle crushing of ice at high-indentation rates. This equation includes the average local force per unit width or the effective pressure on a wide structure instead of ice strength in Korzhavin's expression. To use this expression, one needs to know $\mu_{f(t)}$ or p_w , which can be obtained from either full-scale measurements or small-scale indentation tests, and the correlation length L with respect to either ice thickness or structure width. Measurement of both these parameters is not simple, but this appears to be a rational approach to reconciling the measurements of ice forces on full-scale and small-scale structures. At present, Dempsey et al. (1999) have proposed a theoretical formulation to determine the high pressure to fail an individual zone of ice that forms during non-simultaneous, brittle failure. There is still theoretical and experimental work to be done to sort out the scaling issues of continuous brittle crushing of ice sheets. In the next two sections, we discuss the applicability of the similarity principle according to replica modeling for scaling the results of small-scale tests to full-scale situations.

4 COMPARISON OF ICE FORCES MEASURED AT DIFFERENT SCALES

In the plots of measured effective indentation pressure versus contact area presented by Sanderson (1988), the range of small-scale data is large (1–20 MPa), whereas the range of full-scale data is comparatively small (0.5–3 MPa). Comparing the maximum values of the indentation pressure from small-scale tests and full-scale measurements, Sanderson (1988) attributed the trend of decreasing effective pressure with increasing contact area to non-simultaneous failure of ice (Ashby et al. 1986) and also to the ‘size effect.’ The results of present and previous indentation tests indicate that the mode of ice crushing is highly dependent on the indentation rate, even during dynamic interaction with a compliant structure. Therefore, consideration of indentation rate is very important because different modes of ice crushing cause different magnitudes of effective pressures.

As discussed above, there are theoretical and empirical relationships (Michel and Toussaint 1977, Ponter et al. 1983) to estimate the edge indentation force during ductile deformation of ice at low speeds. These relationships produce results that are close to experimental results. However, verification of these models has been done using the small-scale indentation data. There are no data available on full-scale, ductile indentation force, because creep buckling takes place when the ice speed is low. Wright and Timco (1994) and Hardy et al. (1998) describe various modes of ice failure (such as, crushing, flexural, buckling, fracture, and mixed mode) during ice force monitoring program at the Molikpaq structure, and they state that creep buckling was a frequent failure mode at very low drift speeds. In the fjords of Spitzbergen, advancing glaciers against a first-year ice sheet cause the ice sheet to buckle in creep (Løset, personal communications). This is a possible reason for the lack of data on indentation pressure for large structures.

Sjölin (1985) presented visco-elastic, finite-element results on creep buckling of floating ice sheets. Sanderson (1988) discusses creep buckling of floating ice beams and finds the size of half-wave lengths from theoretical results for an in-plane pressure of 0.5 and 0.25 MPa to be close to those observed in the field around large structures. Luk (1990) conducted a creep buckling analysis of floating ice sheets, which were thought to become unstable when the vertical deflections of the ice sheet suddenly increased after a long period of slow in-plane deformation. The results of his analyses indicate that an effective pressure for creep buckling depends on the indentation rate. For slow rates, the effective pressure is less than 1 MPa. If creep buckling can occur at low indentation pressure, one is not likely to encounter in-plane ductile indentation of an ice sheet, which is expected to take place at much higher indentation pressure. Moreover, any non-uniformity in thickness and structure of an ice sheet would lead to buckling instead of in-plane ductile deformation of floating ice sheets at very low indentation speeds.

During the ice force-monitoring program on Molikpaq, there were occasions when the structure vibrated from cyclic loading. Most of the dynamic ice–structure interactions took place at intermediate ice drift speeds in the range of 30 and 70 mm s⁻¹. The ice sheet appeared to move in jerks adjacent to the caisson, pausing a duration of about 1 second or less, and then moving instantly a distance of 20–30 cm. In April and May of 1986, multi-year ice floes impacted Molikpaq, and the structure vibrated to such an extent that part of its core liquefied. Because the data from those interactions have not been fully released, we are unable to comment on those events in detail. However, some of the published data (Jefferies and Wright 1988) show that there was simultaneous generation of ice forces across the width of the structure. The ‘saw-tooth’ pattern of these forces indicates that there was ductile deformation and brittle failure of ice

during the loading and extrusion phases, similar to that found in the present and previous indentation tests with compliant structures. It is only during the loading phase that ductile deformation of ice takes place, leading to high forces.

Figure 15 shows plots of effective pressure from small-scale indentation tests and full-scale measurements with respect to indentation rate, as presented by Blanchet (1998). Most of the small-scale data are from tests with a 50-mm-wide indenter, and some from tests with a 100-mm-wide indenter (Sodhi 1991a,b). In Figure 15, the highest full-scale effective pressure is about 1.5 MPa at an indentation rate of about 150 mm s^{-1} . Blanchet (1998) compared the two sets of data presented in Figure 15 by proposing that each data set has a maximum value similar to the increasing and decreasing trends of uniaxial strength with respect to increasing strain rate (Michel 1978). He conjectured that the maximum effective pressure and the speed at which the maximum effective pressure occurs differ because of scale effects. In the discussion below, we offer a different comparison of the two sets of data, based on ductile and brittle failure of ice.

As shown in Figure 16, Wright et al. (1986) and Wright and Timco (1994) presented data on effective pressure measured at the Molikpaq structure during interactions with first-year level ice. Though details of these measurements are not readily available, it appears that most of the data on crushing failure of first-year ice were obtained during ice drift speeds greater than 100 mm s^{-1} (Blanchet 1998). Because no severe structural vibrations were reported during those interactions, it appears that the ice failed in continuous brittle crushing. Thus, the comparison of full-scale data on effective pressure should only be made with small-scale data when ice fails in the brittle crushing mode, which is active during high-speed indentation tests.

To relate the effective pressure measured during small-scale tests to full-scale situations, Sodhi (1992, 1998) proposed similarity principles according to replica modeling for brittle crushing during edge indentation of ice sheets at high speeds. A replica model is a model of a dynamic system or structure of exactly the same geometry and material as the prototype, but scaled in size alone (Baker et al. 1973). The gravitational and creep effects are not scaled in replica modeling, but the velocity, pressure, stress, modulus of elasticity, and strain are the same at homologous times and locations in small-scale and full-scale situations. Thus, the effective pressure measured during full-scale tests can only be compared to those in small-scale tests if the indentation speed is the same. Validation of replica modeling for brittle crushing is achieved by comparing the effective pressure measured in the two situations.

Figure 17 shows plots of maximum effective pressure vs. aspect ratio from small-scale indentation tests at speeds greater than 100 mm s^{-1} . The data shown in this figure are from the present study as well as from previous indentation tests conducted at CRREL during 1991–92 with segmented indentors (Sodhi 1992, 1998). In Fig. 17, the effective pressure decreases with increase in aspect ratio, but it remains constant for aspect ratios greater than 8. As required by replica modeling, we did not conduct the small-scale tests with geometrically similar structure. To satisfy this requirement to some extent, we choose the data from tests with aspect ratios greater than 8 for comparison with full-scale data. The effective pressure, measured during small-scale tests at high speeds and having high aspect ratio, is between 1.5 and 2.5 MPa. The range of pressure measured during full-scale measurement and shown in Fig. 16 is between 1 and 3 MPa. The range of the two sets of data being close to each other is a validation of the replica modeling, meaning the absence of any scale or size effect on effective pressure during brittle crushing.

As discussed above, Figure 15 shows plots of measured effective pressure from small-scale indentation tests and full-scale measurements (Blanchet 1998). The symbols in these plots refer to the maximum and average effective pressure measured at particular times during small-scale indentation tests (Sodhi 1991b). The small-scale data are in two groups: a high-pressure range from 8 to 14 MPa for low-speed indentation, and a low-pressure range from 1 to 4 MPa for high-speed indentation. Among the high-speed ($>100 \text{ mm s}^{-1}$) indentation test data, the symbol 'C' in Figure 15 denotes the average pressure measured during continuous brittle crushing of ice, and these data can, therefore, be directly compared with full-scale data after taking into account the effect of aspect ratio. The aspect ratio during those indentation tests (Sodhi 1991a) was in the range of 1.5 and 5.3, with an average value of 2.6. Assuming a ratio of L/h equal to 10, the aspect ratio effect A_r for a value of w/h equal to 2.6 is about 1.82. If the effective pressures from small-scale tests are divided by a factor of A_r ($=1.82$), there is a good agreement between the two sets of data shown in Fig. 15.

5 CONCLUSION

To observe the modes of ice crushing during ice–structure interaction, we conducted a new series of indentation tests with freshwater ice. During the testing program, we varied the indenter width, ice thickness, indentation speed, and structural stiffness. We installed tactile sensor at the ice–structure interface to measure the indentation pressure, which provide insights into the ice failure process in ductile and brittle modes. The results of these tests indicate that there is ductile deformation of ice, resulting in the simultaneous generation of pressure across the indenter width during low rates of indentation, and brittle failure leading to non-simultaneous generation of forces across the indenter width during high rates of indentation. At intermediate rates of indentation, we observed dynamic ice–structure interaction because of variable indentation rates during each cycle. Time-history plots of the interaction force have a ‘saw tooth’ pattern. Each cycle of dynamic ice–structure interaction can be divided into the loading, extrusion, and separation phase. The tactile sensor data on interfacial pressure indicate that there is ductile deformation of ice during the loading phase at low indentation speed, and brittle failure of ice during the extrusion phase at high indentation speed. This is a significant finding because a satisfactory explanation with experimental evidence did not exist for the saw-tooth pattern of ice force.

Based on measurements of interfacial pressure with tactile sensors, we discuss a statistical method to estimate the global ice force on a structure in terms of the average, the standard deviation, and correlation length of the local force per unit width. Using this methodology, we derive the aspect ratio effect, which has been observed by many researchers from their indentation test results.

Lastly, we compare the effective pressure measured during small-scale indentation tests for brittle crushing with those measured on Molikpaq and other full-scale structures. Full-scale data are not available for in-plane ductile failure of ice, and we propose that the possibility of encountering an in-plane ductile deformation of an ice sheet is small because it is possible for the ice sheet to buckle in creep at lower effective pressure. It is for this reason that full-scale data on ice crushing are only available for brittle crushing of first-year ice sheets at drift speeds greater than 100 mm s^{-1} . We find a good agreement between full-scale data on brittle crushing to that from small-scale tests having high aspect ratios and the same indentation speed as in full-scale.

Some data on dynamic ice–structure interaction from the ice measurement program on Molikpaq have been published. We find similarity in the saw-tooth patterns of ice force and the simultaneous generation of force across the width of Molikpaq to that found in small-scale indentation tests.

Acknowledgements

This work was conducted with In-house Laboratory Independent Research funding at CRREL and leverage funding from Exxon Production Research Company under a Cooperative Research and Development Agreement. The author gratefully acknowledges the help from Mr. Christopher J. Donnelly of CRREL in conducting the ice indentation tests, repairing the apparatus after breakdowns, and attaching the tactile sensors with duct tape in front of the indentors by leaning from above to the water level with his long arms. The author thanks Dr. Gordon F. N. Cox and Mr. Denis Blanchet for providing an unpublished report by Prof. A. B. Dunwoody to the author, and Mr. Chuck McWilliams and other persons at Tekscan, Inc. for providing support in interpreting the tactile sensor data.

REFERENCES

- Afanasyev, V.P., Dolgopolov, Iu.V., and Shvashteyn, Z.I. (1972) Ice pressure on separate supporting structures in the sea. Draft Translation 346, U. S. Army Cold Regions Research and Engineering Laboratory, Hanover, New Hampshire.
- Ashby, M.F., Palmer, A.C., Trouless, M., Goodman, D.J., Howard, M.W., Hallam, S.D., Murrell, S.A.F., Jones, N., Sanderson, J.O., and Ponter, A.R.S. (1986) Non-simultaneous failure and ice loads on structures. In Proceedings, Offshore Technology Conference, Houston, Texas, p. 399–404.
- Baker, W.E., Westine, P.S. and Dodge, F.T. (1973) Similarity Methods in Engineering Dynamics. Spartan Books, Hayden Book Company, Inc., Rochelle Park, New Jersey.
- Blanchet, D. (1998) Ice loads from first-year ice ridges and rubble fields. *Canadian Journal of Civil Engineering*, 25: 206–219.
- Dempsey, J. P., Palmer, A. C. and Sodhi, D. S. (1999) High pressure zone formation during compressive ice failure. In Proceeding, 18th International Offshore Mechanics and Arctic Engineering Conference, St. John's, Newfoundland, Canada, OMAE99/P&A1155.
- Dunwoody, A.B. (1991) Non-simultaneous ice failure. A report to Amoco Production Company, Tulsa, Oklahoma.
- Frederking, R.M.W., Jordaan, I.J., and McCallum, J.S. (1990) Field tests of ice indentation of medium scale Hobson's Choice Ice Island, 1989. In Proceedings, 10th IAHR Symposium on Ice, Espoo, Finland, vol. 2, p. 931–944.
- Hardy, M.D., Jefferies, M.G., Rogers, B.T., and Wright, B.D. (1998) DynaMAC: Molikpaq ice loading experience. PERD/CHC Report 14-62, Kohn-Crippen, Calgary, Alberta, Canada.
- I-Scan (1999) Pressure measurement system: user's manual. Tekscan, Inc. South Boston, Massachusetts.
- Izumiyama, K., Wako, D. and Uto, D. (1998) Ice force distribution on a flat indentor. In Proceedings, 14th International Symposium on Ice, Edited by Hung Tao Shen, Vol. 2, Balkema, Rotterdam, pp. 917–922.
- Jefferies, M.G., and Wright, W.H. (1988) Dynamic response of "Molikpaq" to ice–structure interaction. In *Proceedings, 7th International Conference on Offshore Mechanics and Arctic Engineering (OMAE)*, Houston, Texas, vol. IV, p. 201–220.
- Joensuu, A., and Riska, K. (1989) Contact between ice and structure (in Finnish). Laboratory of Naval Architecture and Marine Engineering, Helsinki University of Technology, Espoo, Finland, Report M-88.
- Korzavin, K. N. (1962) Action of ice on engineering structures. CRREL Draft Translation No. 260.
- Kry, P.R. (1978) A statistical prediction of effective ice crushing stress on wide structure. In Proceedings, 4th IAHR Symposium on Ice Problems, Lulea, Sweden, p. 33–47.
- Luk, C.H. (1990) Creep buckling of floating ice sheets moving against a vertical cylindrical structure. In Proceedings, 9th International Conference on Offshore Mechanics and Arctic Engineering (OMAE), Houston, Texas, vol. IV, p. 103–110.

- Määttänen, M. (1975) Experiences of ice forces against a steel lighthouse mounted on the seabed, and proposed construction requirements. Proceedings, 3rd International Conference on Port and Ocean Engineering under Arctic Conditions (POAC), Fairbanks, Alaska, USA, Vol. II, pp. 857-869.
- Michel, B., and Toussaint, N. (1977) Mechanisms and theory of indentation of ice plates. *Journal of Glaciology*, 19(81): 285–300.
- Michel, B. (1978) *Ice Mechanics*, Les Presses de L'Université Laval, Quebec, Canada.
- Michel, B., and Blanchet, D. (1983) Indentation of an S2 floating ice sheet in the brittle range. *Annals of Glaciology*, 4: 180–187.
- Nakazawa, N. and Sodhi, D.S. (1990) Ice forces on flat, vertical indentors pushed through floating ice sheets. USA Cold Regions Research and Engineering Laboratory, Hanover, New Hampshire, Special Report 90–14, p. 70.
- Paikowsky, S. G. and Hajduk, E. L. (1997) Calibration and use of grid-based tactile pressure sensors in granular material. *Geotechnical Testing Journal*, June, pp. 218-241.
- Ponter, A.R.S., Palmer, A.C., Goodman, D.J., Ashby, M.F., Evans, A.G., and Hutchinson, J.W. (1983) The force exerted by a moving ice sheet on an offshore structure. *Cold Regions Science and Technology*, 8:109–118.
- Sanderson, T.J.O. (1988) *Ice Mechanics: Risks to offshore structures*. Graham and Troutman, London.
- Sjö Lind, S.–G. (1985) Viscoelastic buckling analysis of floating ice sheets. *Cold Regions Science and Technology*, 11: 241–246.
- Sodhi, D.S., and Morris, C.E. (1984) Ice forces on rigid, vertical, cylindrical structures. CRREL Report 84–33, U.S. Army Cold Regions Research and Engineering Laboratory, Hanover, New Hampshire.
- Sodhi, D. S. and Nakazawa, N. (1990) Frequency of intermittent ice crushing during indentation tests. Proceedings, 10th IAHR Symposium on Ice 1990, Espoo, Finland, August 20-24, Vol. 3, pp. 277-290, Discussions, pp. 446-449.
- Sodhi, D.S. (1991a) Ice-structure interaction during indentation tests. In *Ice-Structure Interaction: Proceedings of IUTAM-IAHR Symposium*, Edited by S. Jones et al. Springer-Verlag, Berlin, p. 619–640.
- Sodhi, D.S. (1991b) Effective pressures measured during indentation tests in freshwater ice. In Proceedings, 6th International Cold Regions Engineering Specialty Conference, Hanover, N.H., February 26–28, Edited by D.S. Sodhi. American Society of Civil Engineers Publications, New York, p. 619–627.
- Sodhi, D.S. (1991c) Energy exchanges during indentation tests in freshwater ice. *Annals of Glaciology*, 15: 247–253.
- Sodhi, D.S. (1992) Ice-structure interaction with segmented indentors. In Proceedings, 11th IAHR Symposium on Ice 1992, Banff, Alberta, Canada, vol. 2, p. 909–929.
- Sodhi, D.S. (1995) An ice–structure interaction model. In *Mechanics of Geomaterial Interfaces*, edited by A.P.S. Selvadurai and M.J. Boulon. Elsevier Science B.V., Amsterdam, p 57–75.
- Sodhi, D.S. (1998) Non-simultaneous crushing during edge indentation of freshwater ice sheets. *Cold Regions Science and Technology*, 27:179–195.
- Sodhi, D.S., Takeuchi, T., Nakazawa, N., Akagawa, S., and Saeki, S. (1998) Medium-scale indentation tests on sea ice at various speeds. *Cold Regions Science and Technology*, 28: 161-182.
- Tanaka, S., Saeki, H. and Ono, T. (1987) The distribution of ice pressure acting on offshore pile structure and the failure mechanics of ice sheet. *ASME Transactions, Journal of Offshore Mechanics and Arctic Engineering*, 1: 85–92.
- Timco, G.W. (1987) Indentation and penetration of edge-loaded freshwater ice sheets in brittle range. *Journal of Offshore Mechanics and Arctic Engineering*, 109(3): 287–294.
- Wright, B., Pikington, G.R., Woolner, K.S., and Wright, W.H. (1986) Winter ice interactions with an arctic offshore structure. In Proceedings, 8th IAHR Symposium on Ice, Iowa City, Iowa, vol. III, p. 49–73.
- Wright, B.D. and Timco, G.W. (1994) A review of ice forces and failure modes on the Molikpaq. In *Proceedings, 12th IAHR Symposium on Ice, Trondheim, Norway*, vol. 2, p. 816–825.

LIST OF SYMBOLS

A_r	Ratio of global effective pressure to average local effective pressure
$E[f(t)]$	Expected value of $f(t)$
F	Estimate of ice force on a structure
F_{\max}	Estimate of maximum global ice force on a structure
$f(x,t)$	Local force per unit width of the structure
$g(t)$	Global force on a structure
h	Ice thickness
L	Correlation length parameter used in spatial correlation function
p	Pressure at the ice-structure interface
p_{\max}	Maximum effective pressure
p_w	$\mu_{f(t)}/h$, average local effective pressure
$R_{f(t)}$	Auto-covariance function
w	Width of a structure
t	Time
x	Position of a point or distance across the width of a structure
y	Vertical position of a point in the contact area
$\mu_{f(t)}$	Mean of the local force per unit width at a point
$\sigma_{f(t)}$	Standard deviation of the local force per unit width at a point
σ	Uni-axial strength of ice

Table 1. List of parameters either set or measured during the indentation tests. Various symbols denote the following parameter or variable: w the indenter width, h the ice thickness, v the average carriage speed, K the structural stiffness. Symbols to denote the failure modes are: D for ductile deformation, B for buckling, I for intermittent ductile-brittle crushing, C for continuous brittle crushing, and R for relaxation tests Effective pressure listed below is the force divided by the product of ice thickness and indenter width.

Test	w mm	h mm	v mm s ⁻¹	K MN m ⁻¹	Failure Mode	Effective Pressure (MPa)					Aspect Ratio w/h
						Buckling Maximum	Intermittent Maximum	Brittle Average	Brittle Std. Dev.	Brittle Maximum	
1	146	30.0	0.32	0.78	D	-	-	-	-	-	4.87
2	146	30.0	7.40	0.00	I	-	6.221	-	-	-	4.87
3	146	30.0	7.40	0.00	I	-	6.799	-	-	-	4.87
4	146	33.0	7.50	1.34	I	-	6.077	-	-	-	4.42
5	146	34.0	0.63	1.44	$D\&B$	5.977	-	-	-	-	4.29
6	146	34.0	4.30	1.41	I	-	5.359	-	-	-	4.29
7	146	24.0	7.50	1.33	$I\&B$	-	6.601	-	-	-	6.08
8	146	23.5	4.30	1.35	$I\&B$	-	6.274	-	-	-	6.21
9	146	23.0	0.35	1.41	$D\&B$	5.230	-	-	-	-	6.35
10	146	23.0	0.33	0.92	$D\&B$	4.683	-	-	-	-	6.35
11	146	22.5	4.30	0.91	$I\&B$	-	6.085	-	-	-	6.49
12	146	22.0	7.50	0.91	$I\&B$	-	6.634	-	-	-	6.64
13	100	35.0	0.34	0.91	$D\&B$	6.339	-	-	-	-	2.86
14	100	35.0	7.50	0.83	$I\&B$	-	7.606	-	-	-	2.86
15	100	34.5	0.30	1.46	$D\&B$	6.501	-	-	-	-	2.90
16	100	33.5	7.50	1.44	I	-	8.060	-	-	-	2.98
17	100	34.0	15.70	1.38	I	-	8.235	-	-	-	2.94
18	100	34.0	37.10	1.31	I	-	10.000	-	-	-	2.94
19	100	35.0	35.00	0.83	I	-	9.429	-	-	-	2.86
20	100	35.0	14.50	0.82	I	-	8.000	-	-	-	2.86
21	100	37.0	14.20	0.82	I	-	8.649	-	-	-	2.70
22	100	38.0	32.00	0.94	I	-	9.474	-	-	-	2.63
23	100	39.0	37.00	2.10	I	-	9.300	-	-	-	2.56
24	100	36.6	0.00	2.75	R	-	-	-	-	-	2.73
25	100	36.0	15.80	2.50	I	-	7.854	-	-	-	2.78
26	100	36.0	37.10	2.45	I	-	9.322	-	-	-	2.78
27	100	38.0	36.30	1.12	I	-	8.780	-	-	-	2.63
28	100	36.0	16.20	1.12	$I\&B$	-	7.959	-	-	-	2.78
29	100	36.0	0.00	1.18	R	-	-	-	-	-	2.78
30	100	36.0	0.00	1.19	R	-	-	-	-	-	2.78
31	100	37.5	0.00	1.18	R	-	-	-	-	-	2.67
32	100	27.0	37.90	1.10	$I\&B$	-	7.574	-	-	-	3.70
33	100	25.0	16.00	1.15	$I\&B$	-	7.504	-	-	-	4.00
34	100	27.0	15.80	2.50	I	-	8.716	-	-	-	3.70
35	100	28.0	38.00	2.40	$I\&B$	8.180	-	-	-	-	3.57
36	100	28.0	0.00	2.60	R	-	-	-	-	-	3.57
37	146	35.5	0.00	2.60	R	-	-	-	-	-	4.11
38	146	35.5	37.70	2.40	$I\&B$	-	6.326	-	-	-	4.11
39	146	36.0	16.25	2.40	$I\&B$	-	6.333	-	-	-	4.06
41	146	27.5	112.40	2.50	I	-	7.558	-	-	-	5.31
42	146	26.5	406.30	2.50	C	-	-	1.682	0.0670	1.913	5.51
43	146	27.5	51.40	2.70	I	-	4.981	-	-	-	5.31
44	146	26.0	206.80	2.30	$I\&C$	-	-	1.353	0.0806	1.669	5.61
45	146	25.5	308.00	2.10	C	-	-	1.516	0.0610	1.748	5.72
46	146	26.5	508.00	2.20	C	-	-	1.607	0.0863	1.784	5.51
47	146	26.0	157.00	2.70	I	-	8.736	-	-	-	5.61
48	146	26.0	0.00	2.50	R	-	-	-	-	-	5.61

50	146	21.0	0.00	2.70	<i>R</i>	-	-	-	-	-	6.95
51	146	21.0	128.00	2.70	<i>I&C</i>	-	-	1.037	0.0678	1.220	6.95
52	146	21.0	113.00	2.70	<i>C&I</i>	-	-	1.079	0.0753	1.368	6.95
53	146	21.0	228.00	2.70	<i>C&I</i>	-	-	1.172	0.1138	1.433	6.95
54	146	21.0	57.20	2.70	<i>I</i>	-	5.120	-	-	-	6.95
55	146	20.2	101.00	2.70	<i>I&C</i>	-	4.313	-	-	-	7.23
56	146	20.2	-	2.70	<i>R</i>	-	-	-	-	-	7.23
57	146	20.7	121.00	1.22	<i>I&C</i>	-	7.400	1.020	0.0761	1.195	7.05
58	146	21.0	94.00	1.22	<i>I&C</i>	-	7.295	-	-	-	6.95
59	146	21.0	57.20	1.22	<i>I</i>	-	7.011	-	-	-	6.95
60	146	21.0	-	1.22	<i>R</i>	-	-	-	-	-	6.95
61	146	21.0	-	1.22	<i>R</i>	-	-	-	-	-	6.95
62	146	28.3	70.40	1.17	<i>I</i>	-	7.694	-	-	-	5.16
63	146	28.6	52.60	1.17	<i>I</i>	-	6.430	-	-	-	5.10
64	146	28.7	-	1.17	<i>R</i>	-	-	-	-	-	5.09
65	146	28.7	205.00	1.17	<i>I</i>	-	10.820	-	-	-	5.09
66	146	28.5	509.00	1.17	<i>C</i>	-	-	1.749	0.0735	1.945	5.12
67	146	28.6	358.00	1.17	<i>C</i>	-	-	1.568	0.0520	1.706	5.10
68	146	29.0	283.00	1.17	<i>I&C</i>	-	6.511	1.464	0.0524	1.608	5.03
69	146	29.3	470.00	2.05	<i>C</i>	-	-	1.699	0.0538	1.875	4.98
70	146	29.4	268.00	2.05	<i>C</i>	-	-	1.555	0.0538	1.733	4.97
71	146	30.0	206.00	2.05	<i>C</i>	-	-	1.324	0.0680	1.575	4.87
72	146	30.0	152.00	2.05	<i>I</i>	-	7.824	-	-	-	4.87
73	146	29.5	0.00	2.05	<i>R</i>	-	-	-	-	-	4.95
74	146	29.5	51.60	2.05	<i>I</i>	-	6.845	-	-	-	4.95
75	146	29.5	50.50	2.05	<i>I</i>	-	6.499	-	-	-	4.95
76	146	25.7	72.10	2.20	<i>I</i>	-	7.275	-	-	-	5.68
77	146	27.5	54.10	2.20	<i>I</i>	-	5.514	-	-	-	5.31
78	146	26.5	204.00	2.20	<i>I&C</i>	-	7.071	1.676	0.0879	1.914	5.51
79	146	26.0	351.00	2.20	<i>C</i>	-	-	1.849	0.0867	2.135	5.61
80	146	25.2	501.00	2.20	<i>C</i>	-	-	2.010	0.0617	2.183	5.79
81	146	25.2	0.00	2.20	<i>R</i>	-	-	-	-	-	5.79
82	146	25.4	503.00	0.90	<i>C</i>	-	-	1.805	0.0569	1.926	5.75
83	146	25.5	354.00	0.90	<i>I&C</i>	-	5.770	1.786	0.0747	1.998	5.72
84	146	25.3	205.00	0.90	<i>I&C</i>	-	7.642	1.541	0.0939	1.826	5.77
85	146	25.5	0.00	0.90	<i>R</i>	-	-	-	-	-	5.72
86	146	25.5	0.00	0.92	<i>R</i>	-	-	-	-	-	5.72
87	146	25.0	113.00	0.92	<i>I</i>	-	7.083	-	-	-	5.84
88	146	25.0	53.80	0.92	<i>I</i>	-	6.164	-	-	-	5.84
89	146	40.2	500.00	0.95	<i>C</i>	-	-	2.537	0.1225	2.842	3.63
90	146	40.5	353.00	0.95	<i>I&C</i>	-	6.910	2.185	0.1255	2.491	3.60
91	146	40.5	0.00	0.95	<i>R</i>	-	-	-	-	-	3.60
92	146	40.0	204.00	0.95	<i>I&C&I</i>	-	7.630	1.482	0.0854	1.705	3.65
93	146	42.0	502.00	1.64	<i>C</i>	-	-	2.280	0.1246	2.646	3.48
94	146	42.0	0.00	1.64	<i>R</i>	-	-	-	-	-	3.48
95	146	37.1	354.00	1.64	<i>C</i>	-	-	2.153	0.0942	2.344	3.93
96	146	39.0	203.00	1.64	-	-	-	-	-	-	3.74

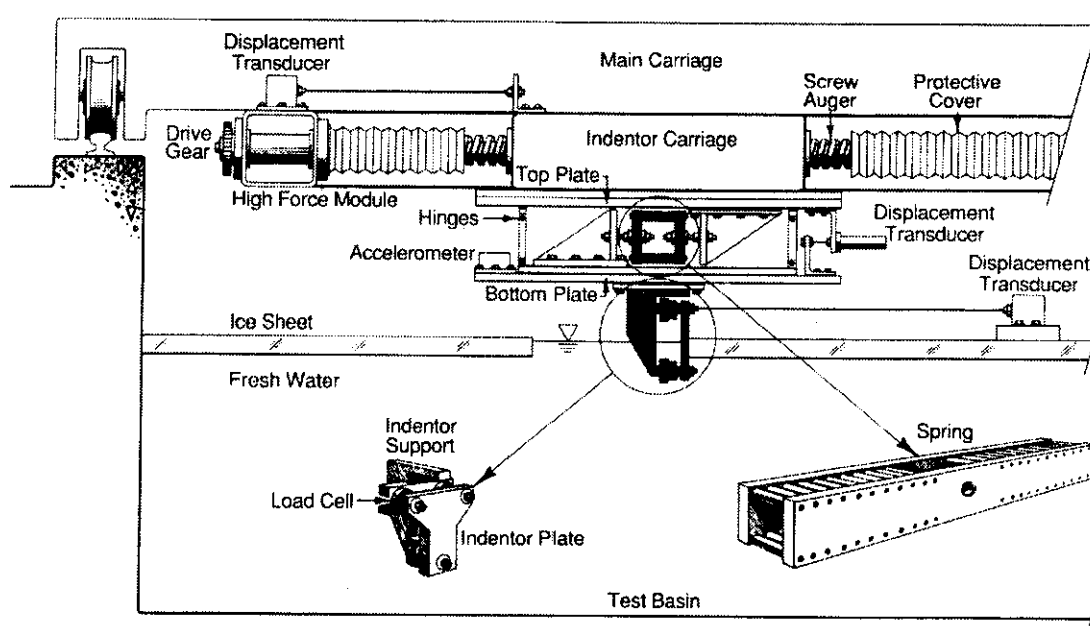
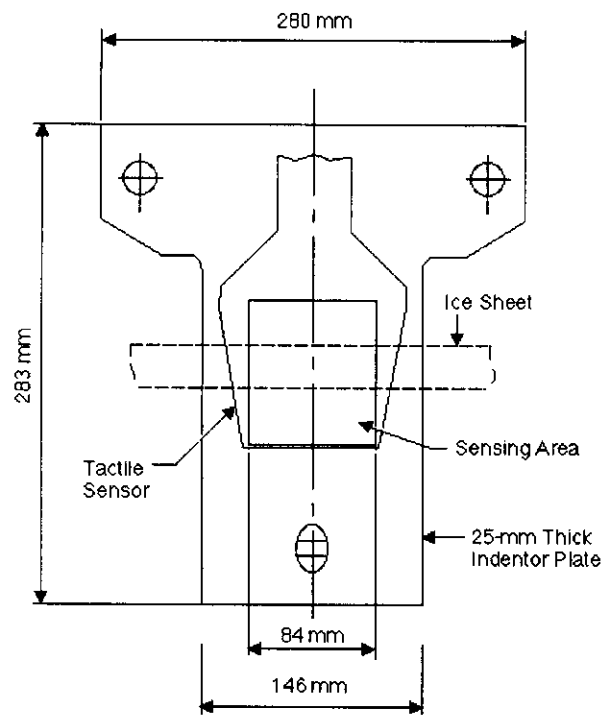


Figure 1. Experimental setup and indenter support system



104

Figure 2. Position of a tactile sensor on an indenter.

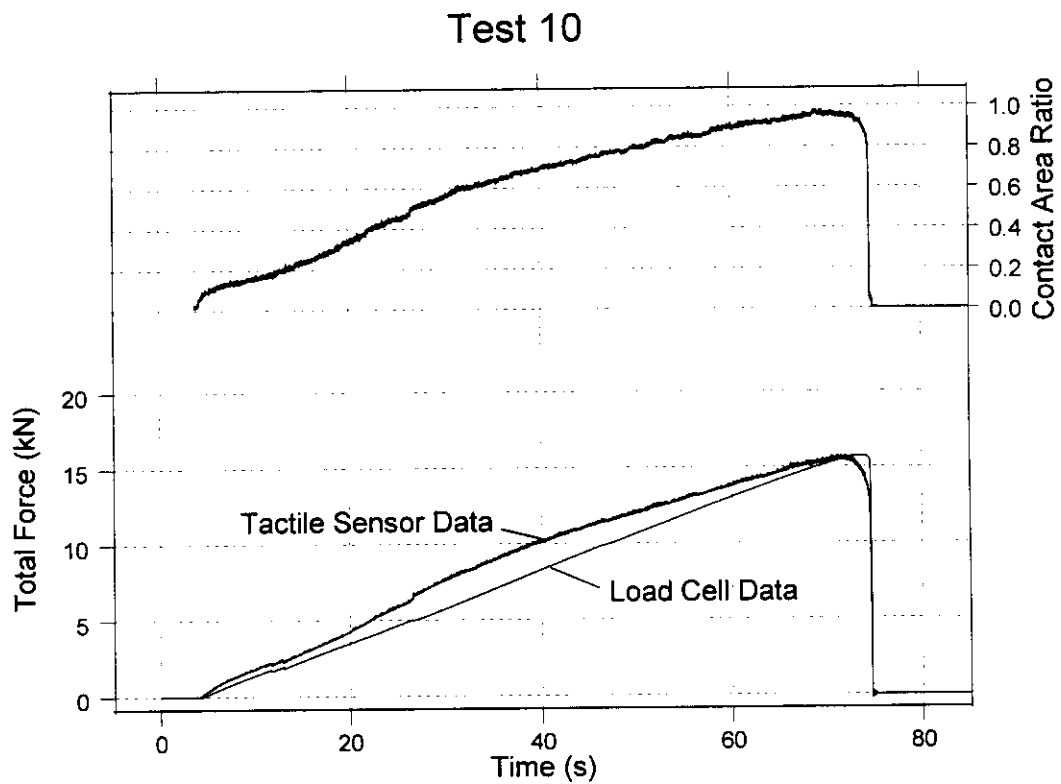
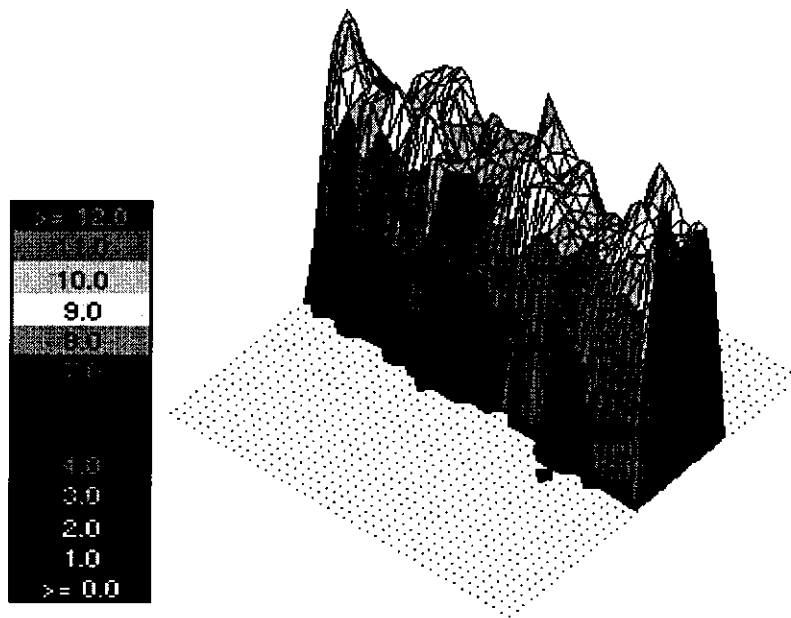
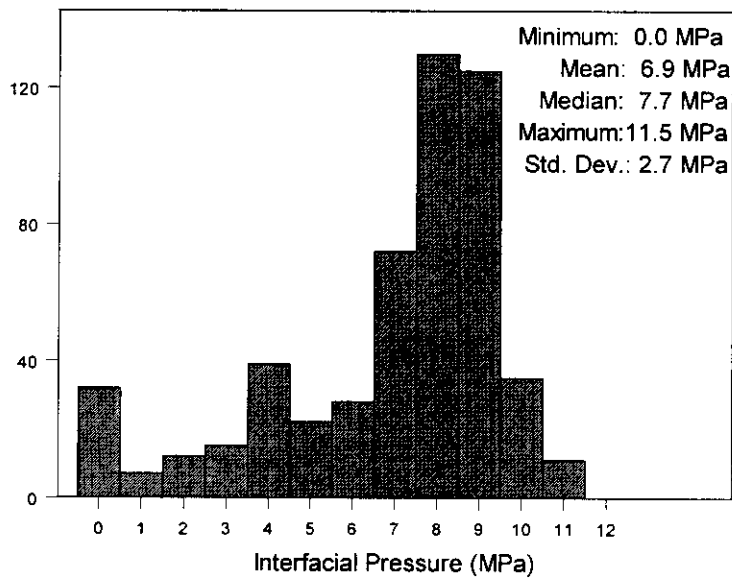


Figure 3. Time-history plots of total force and contact area ratio from a low-speed indentation test.



(a)



(b)

Figure 4. Interfacial pressure measured with a tactile sensor at a time when ductile deformation of ice took place during Test 10, which was conducted at an indentation speed of 0.33 mm s^{-1} : (a) plot of the pressure on a grid area that covers a width of 84 mm and a height of 84 mm, and (b) distribution of the pressure. The ice thickness was 23 mm.

Test 93

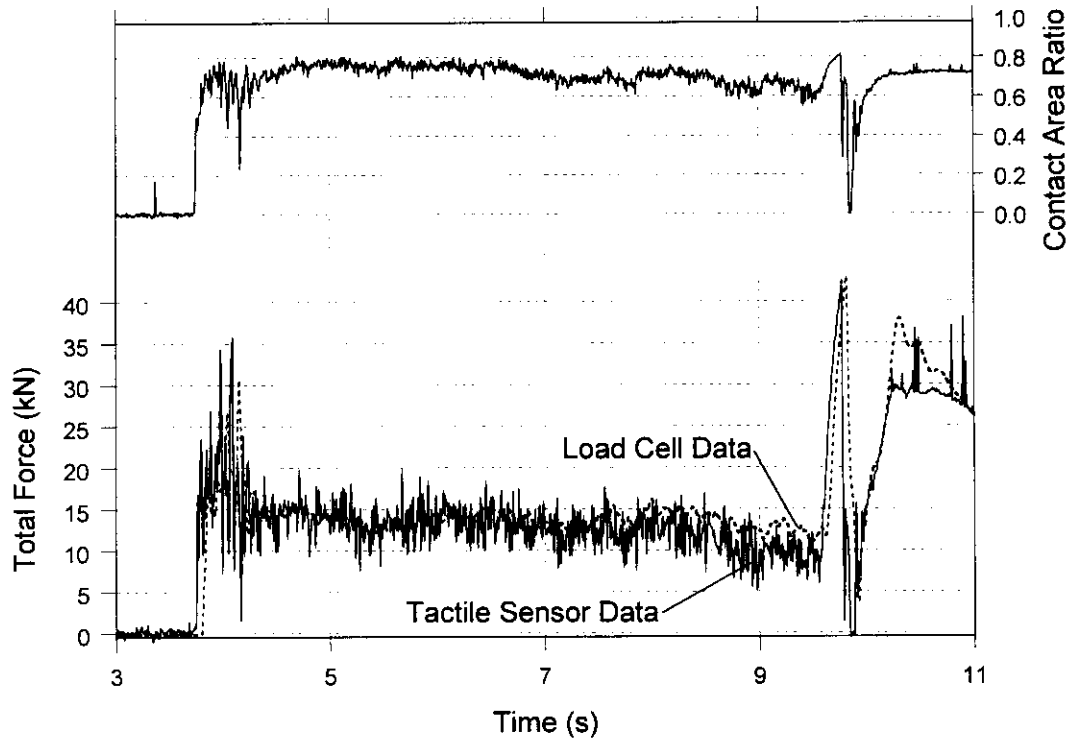
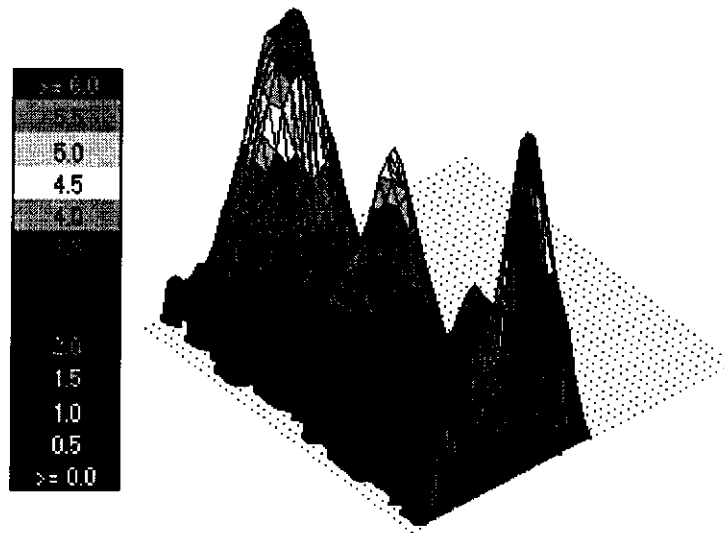
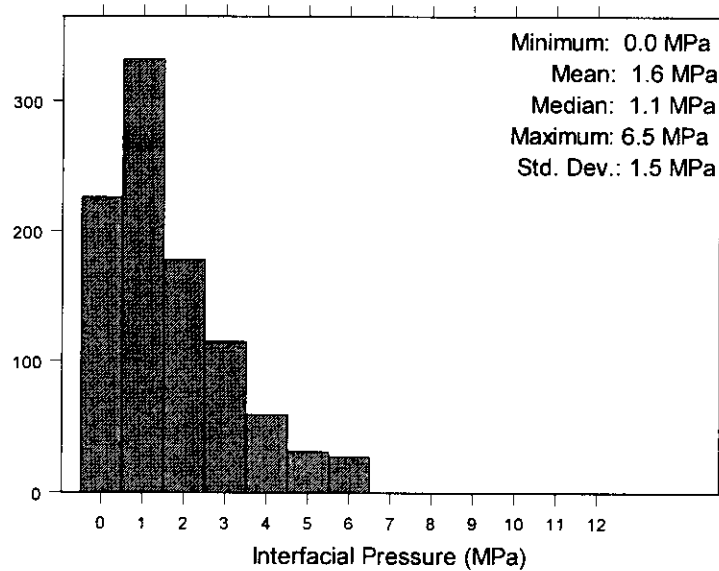


Figure 5. Time-history plots of total force and contact area ratio from a high-speed indentation test.



(a)



(b)

Figure 6. Interfacial pressure measured with a tactile sensor at a time when continuous brittle crushing of ice took place during Test 93, which was conducted at an indentation speed of 500 mm s^{-1} : (a) plot of the pressure on a grid area that covers a width of 84 mm and a height of 84 mm, and (b) distribution of the pressure. The ice thickness was 42 mm.

Test 88

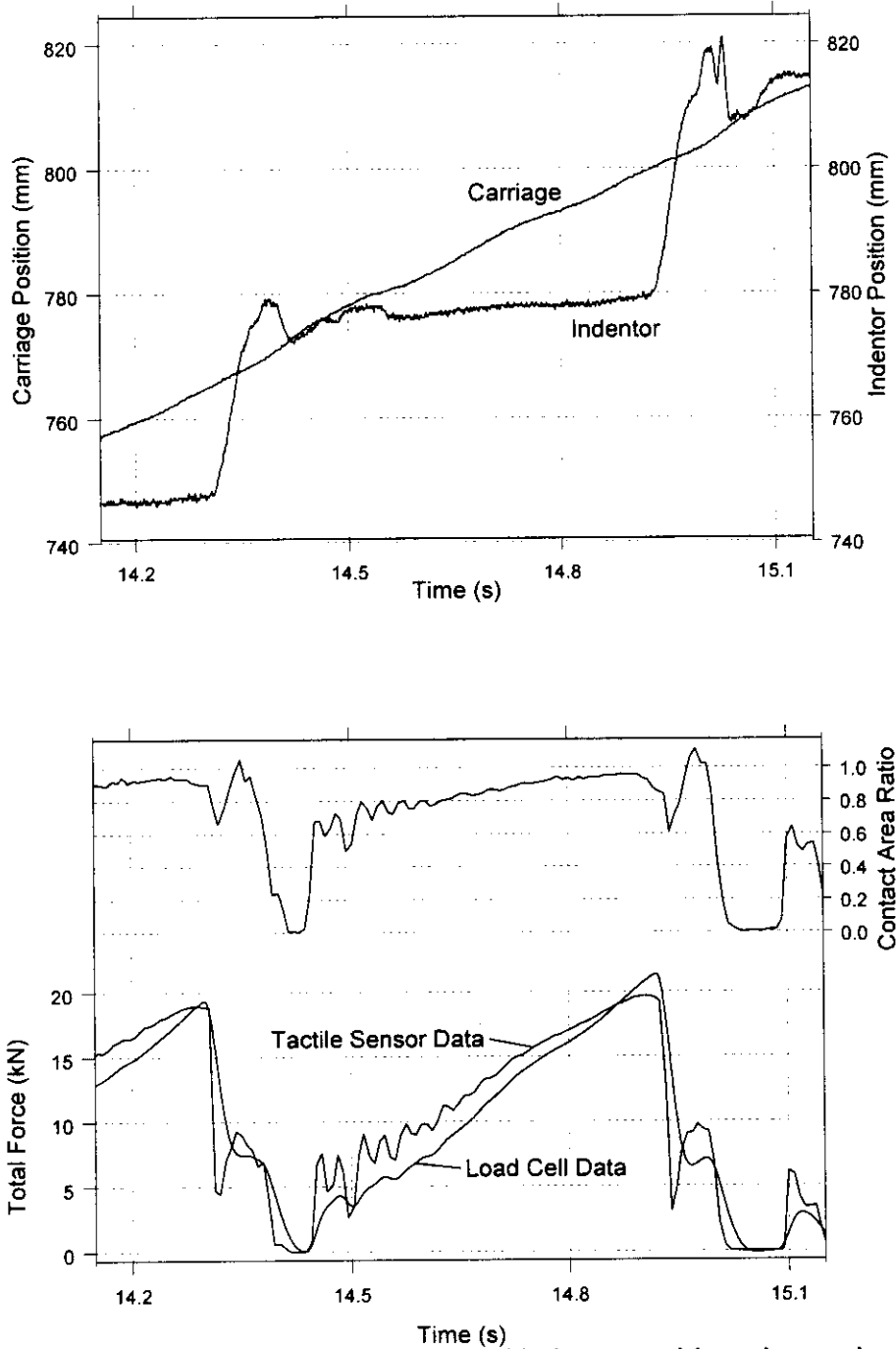
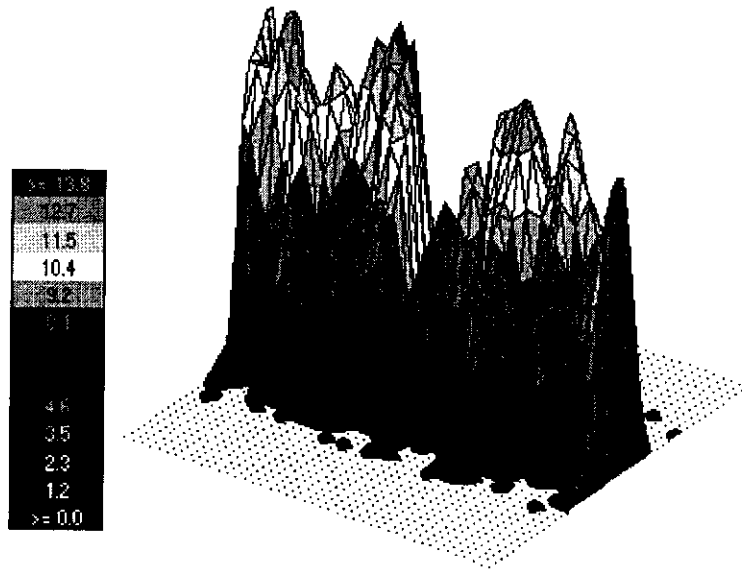
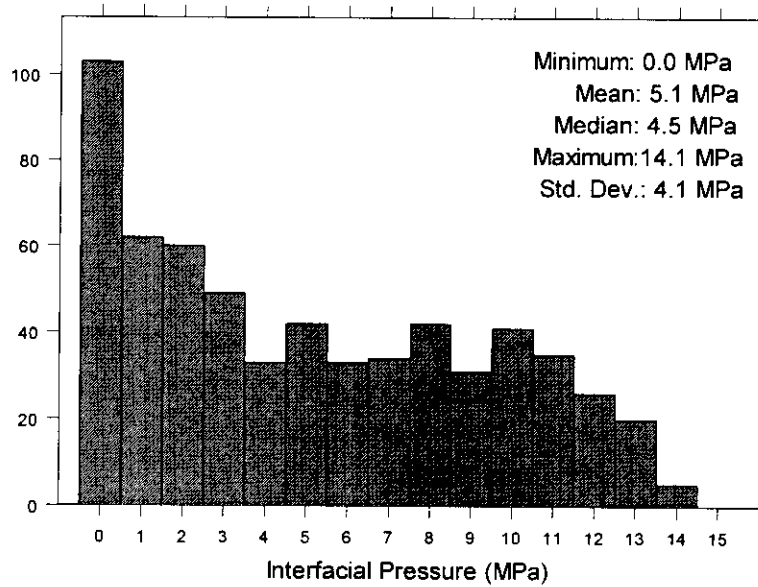


Figure 7. Time-history plots of carriage and indenter positions, interaction forces from load cell data and tactile sensor data, and contact area ratio during Test 88, when the ice failed intermittently in ductile and brittle manner. During the test, the ice thickness was 25 mm, the indenter width was 146 mm, the average indentation speed was 54 mm s^{-1} , and the spring stiffness was 0.92 MN m^{-1} .

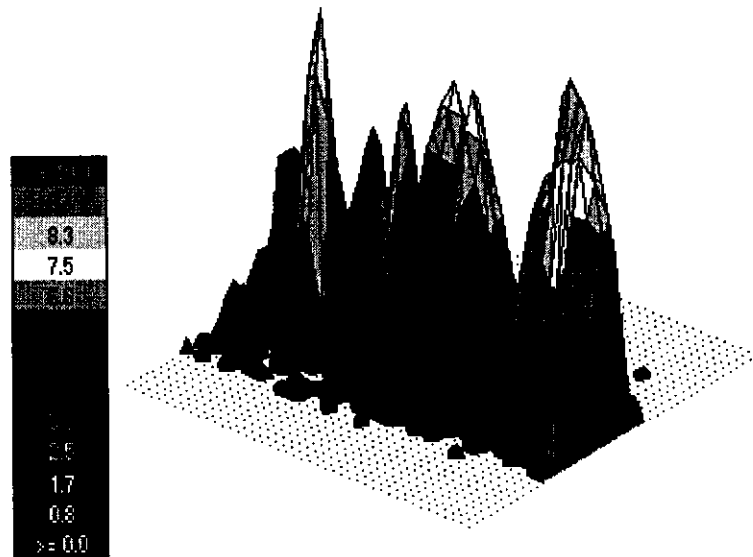


(a)

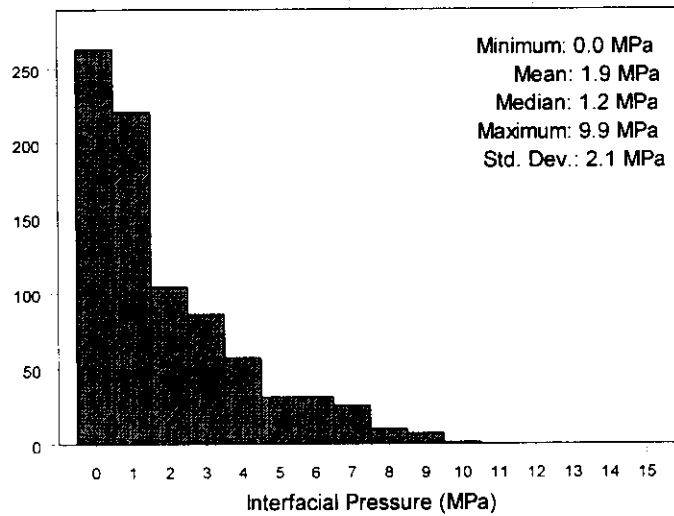


(b)

Figure 8. Interfacial pressure measured with a tactile sensor near the end of loading phase during Test 88, which was conducted at an average indentation speed of 55 mm s^{-1} : (a) plot of the pressure on a grid area that covers a width of 84 mm and a height of 84 mm, and (b) distribution of the pressure. The ice thickness was 25 mm.



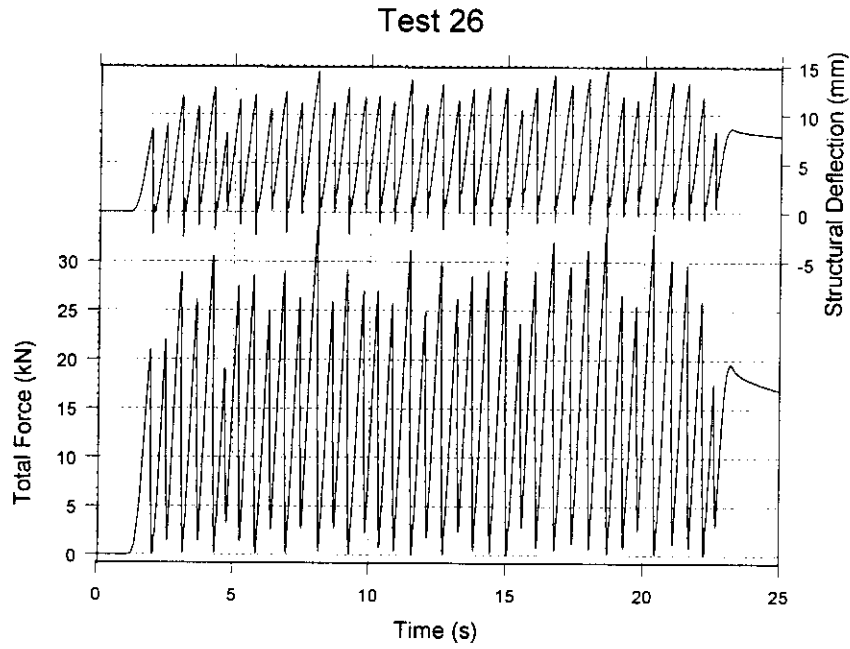
(a)



(b)

Figure 9. Interfacial pressure measured with a tactile sensor near the middle of extrusion phase during Test 88, which was conducted at an average indentation speed of 55 mm s^{-1} : (a) plot of the pressure on a grid area that covers a width of 84 mm and a height of 84 mm, and (b) distribution of the pressure. The ice thickness was 25 mm.

(a)



(b)

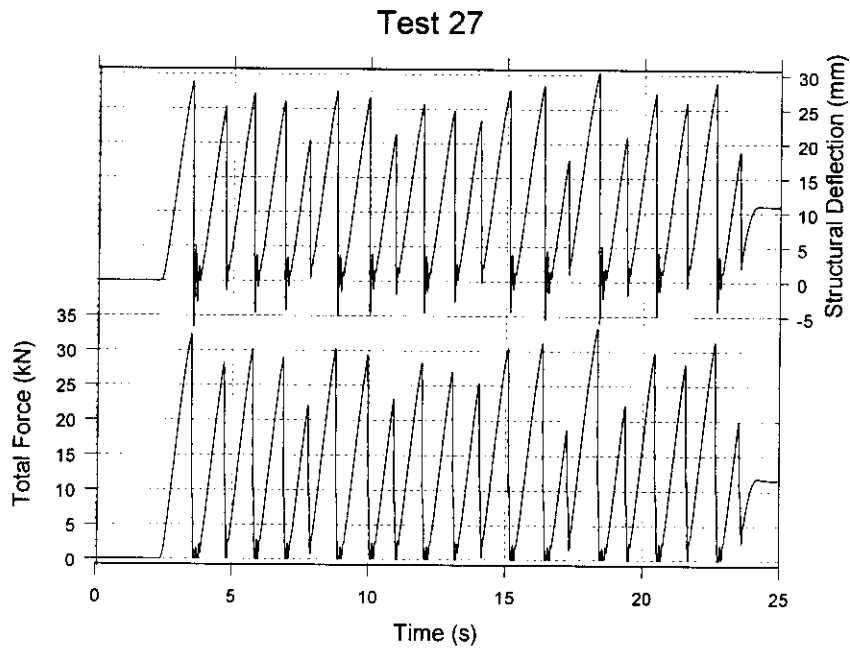


Figure 10. Time-history plots of interaction force and structural deflection from Tests 26 and 27, in which all other variables were nearly the same except the structural stiffness, which were 2.45 and 1.12 MN m^{-1} , respectively.

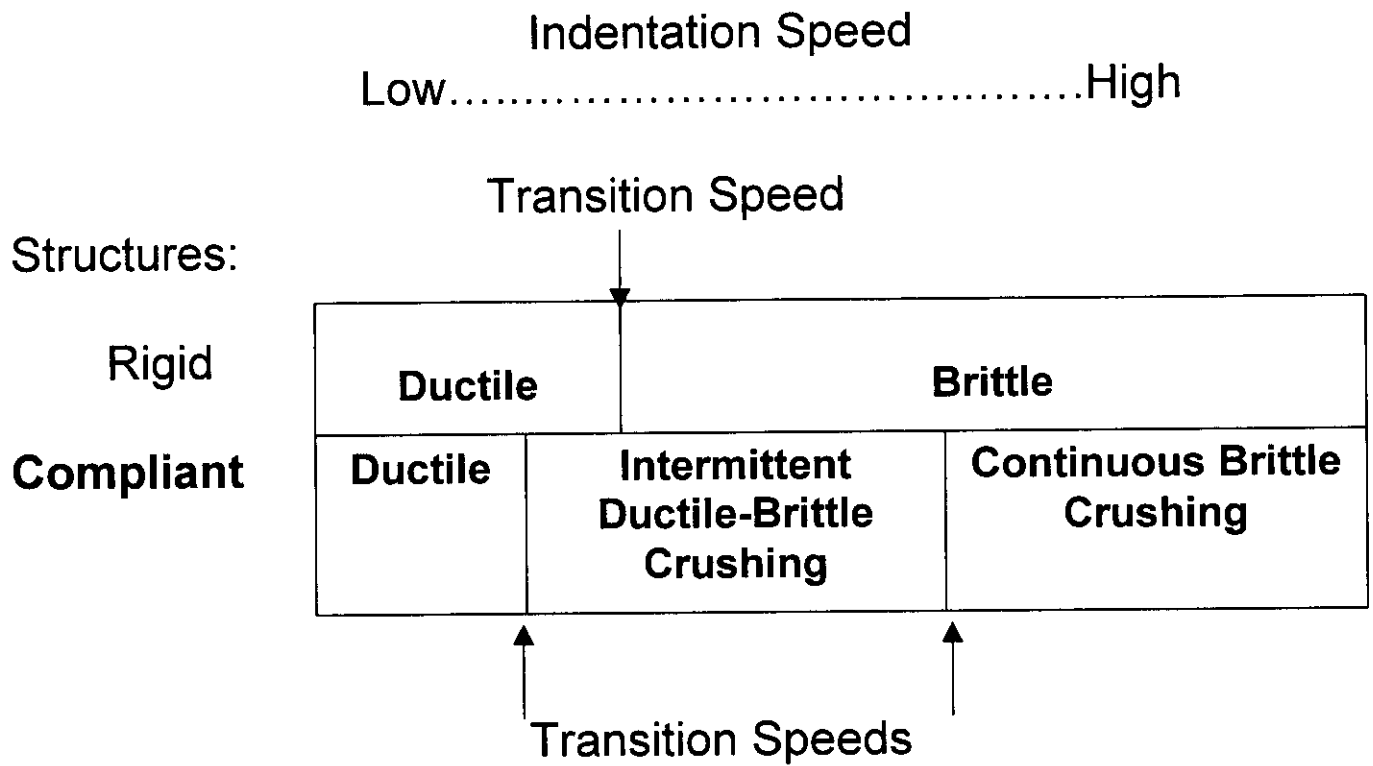


Figure 11. Failure map for ice crushing failure mode in terms of indentation speed and type of structure.

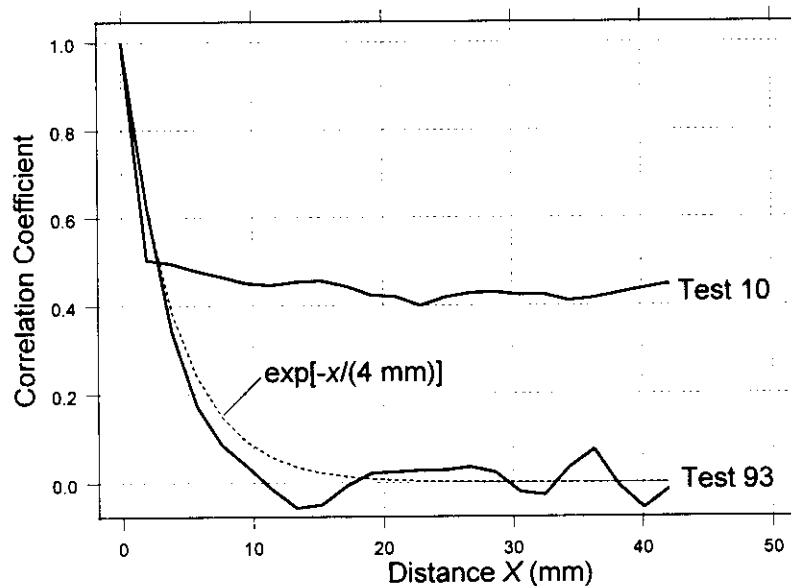


Figure 12. Plots of correlation coefficient from Test 10 and 93, during which the indentation speeds were, respectively, 0.3 and 502 mm s⁻¹.

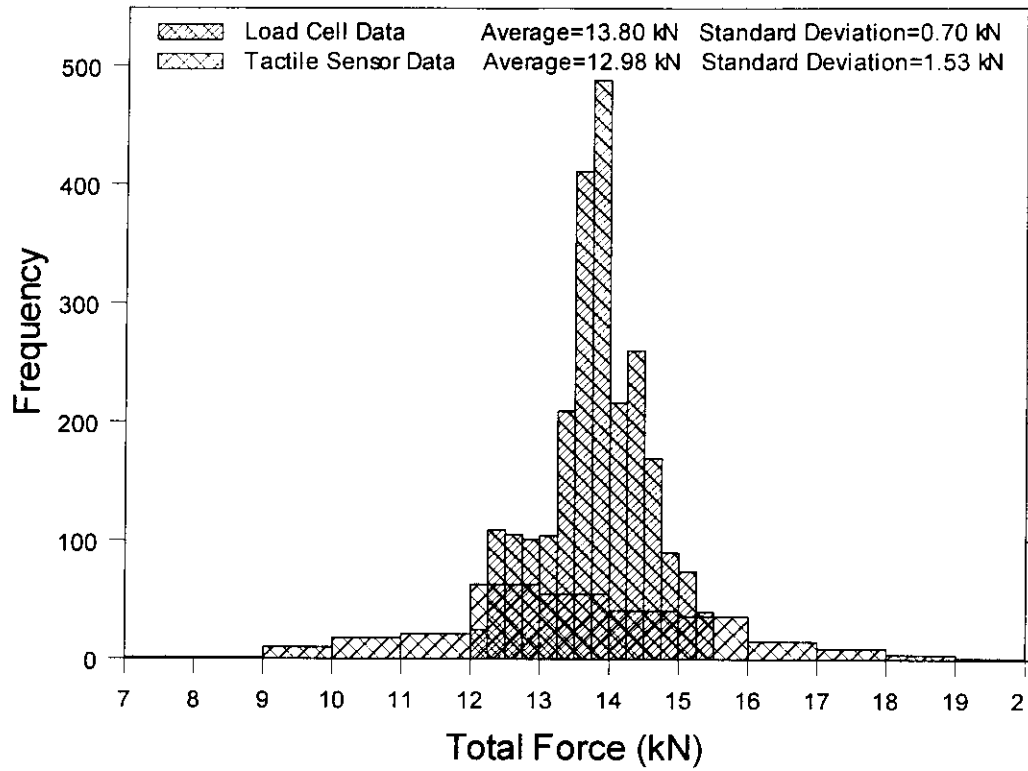
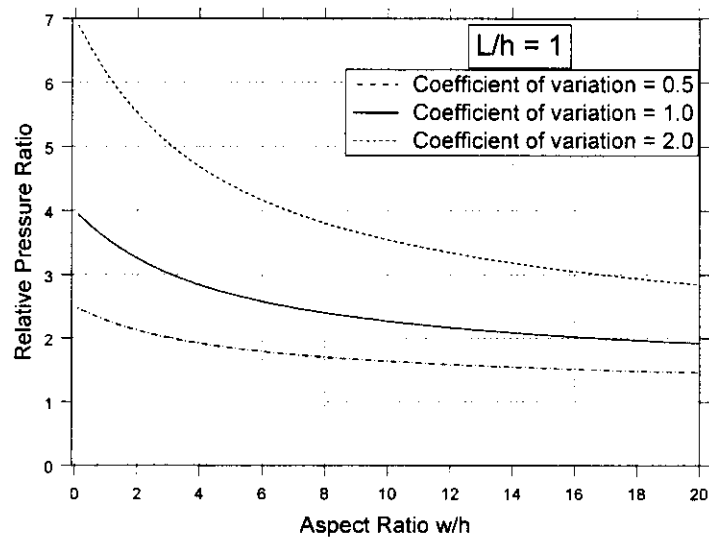


Figure 13. Distribution of total force measured during Test 93 by load cells and tactile sensors. The indenter width and the ice thickness were 146 and 42 mm, respectively.

(a)



(b)

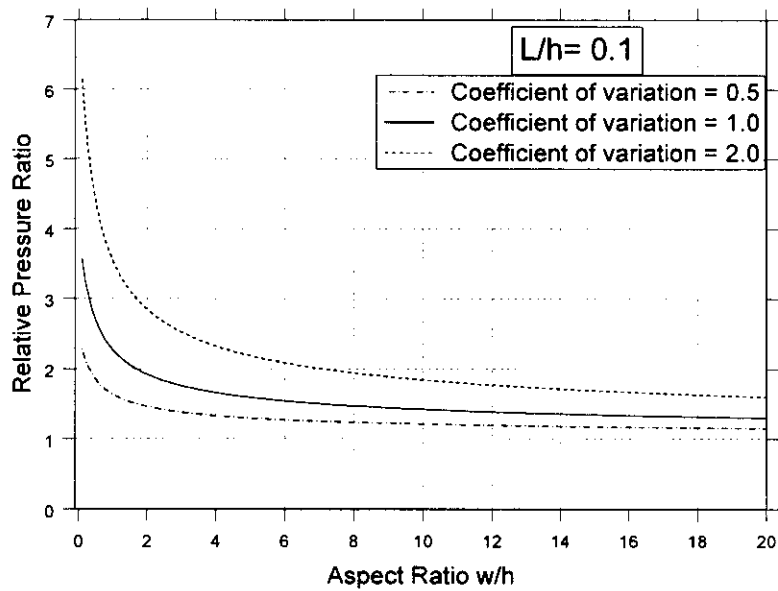


Figure 14. Plots of relative pressure ratio ($p_{\max}h/\mu_{(t)}$) versus aspect ratio (w/h) for three values of coefficients of variation and for: (a) $L/h = 1$ and (b) $L/h = 0.1$.

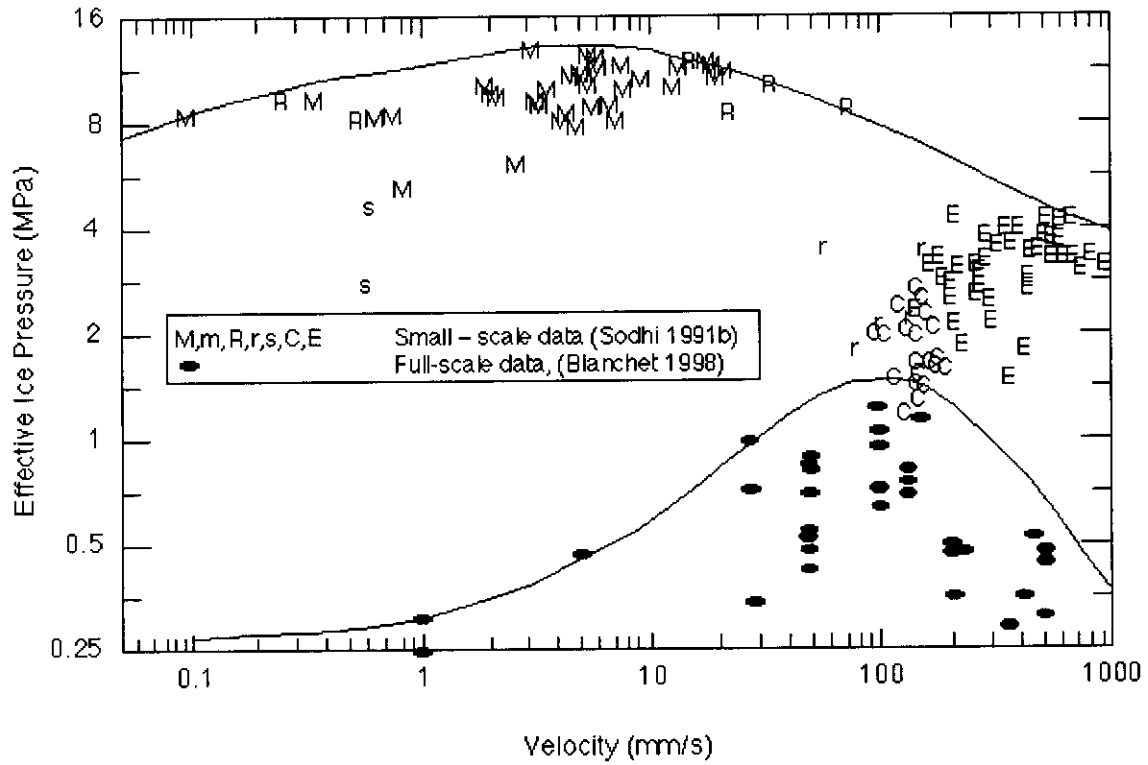
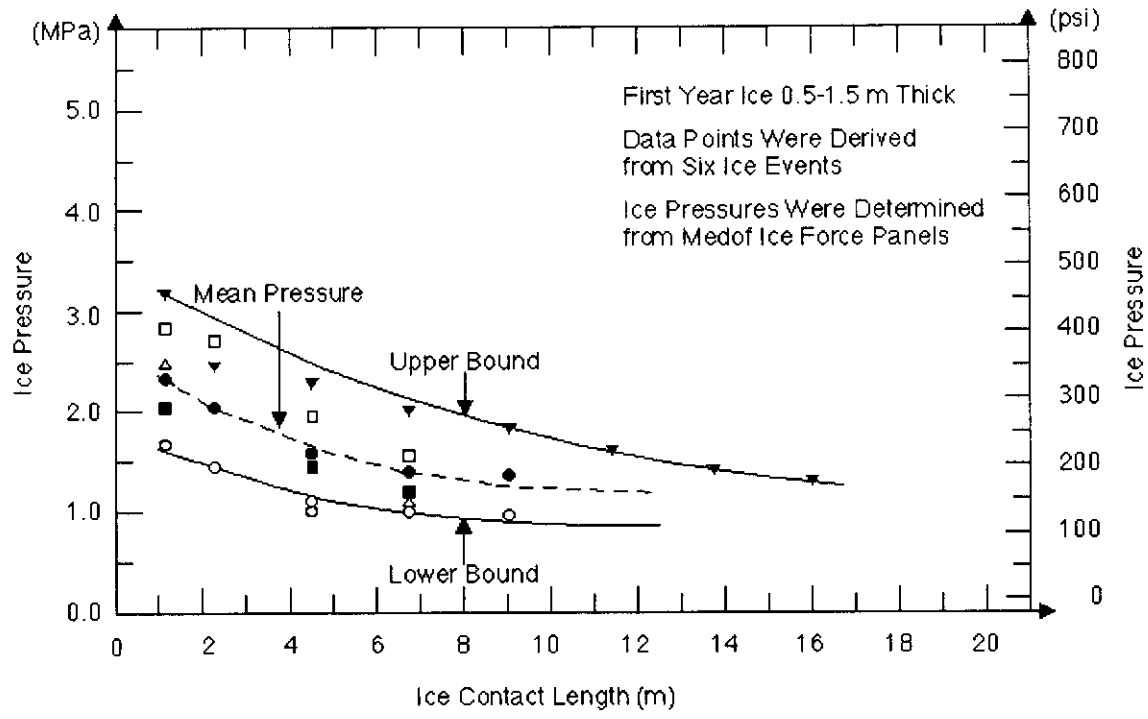
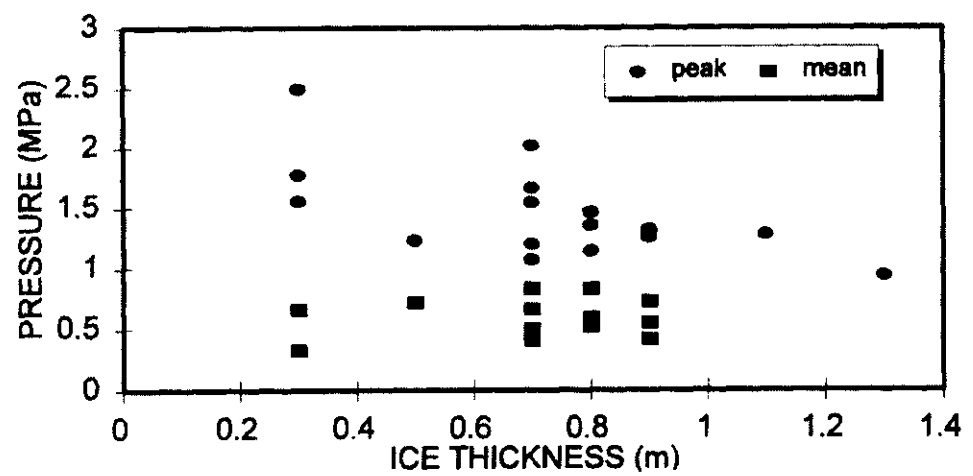


Figure 15. Plots of effective pressure measured on full-scale structures and during small-scale indentation tests with respect to ice drift velocity (from Blanchet 1998 and Sodhi 1991b).



Sodhi-001

(a)



(b)

Figure 16. Plots of effective pressure measured at (a) Tarsuit P-45 (from Wirght et al. 1986), and (b) Tarsuit P-45 and Amauligak I-65 (from Wright and Timco 1994) locations.

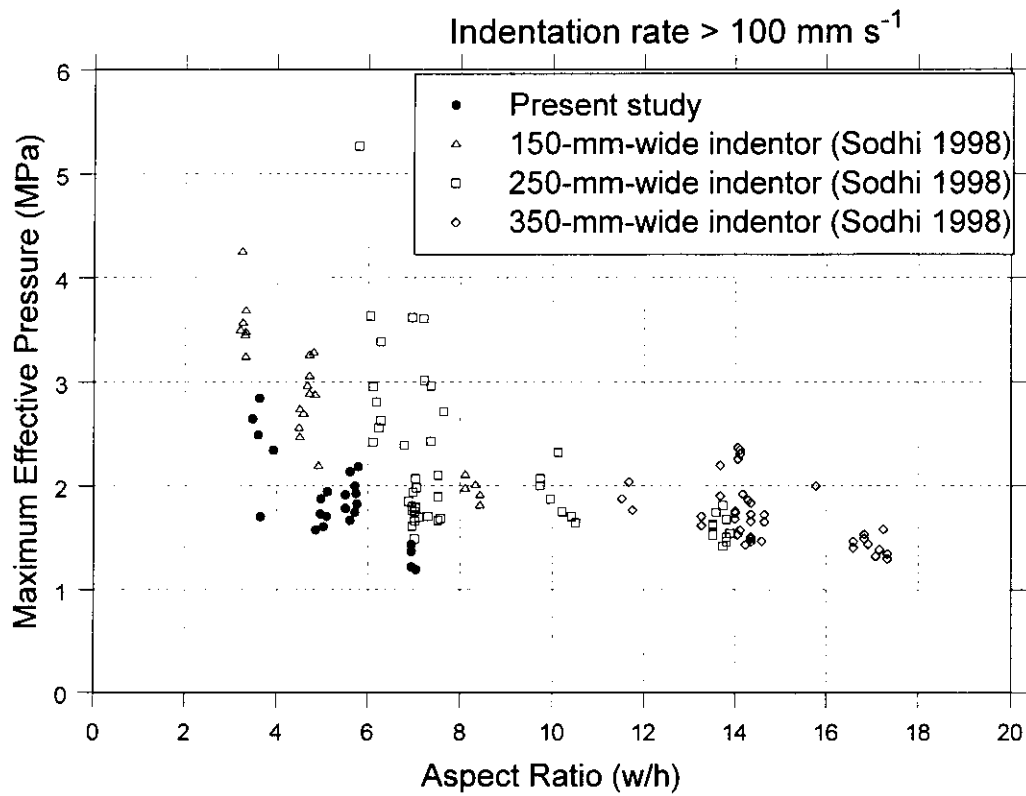


Figure 17. Plots of maximum effective pressure measured during indentation tests at indentation rates greater than 100 mm s⁻¹ with respect to aspect ratio (w/h).

The Ice Aspects of Ice Scour

Mombetsu - February 2000

Presented by: Ken Croasdale
Collaborators: Richard McKenna Ryan Phillips

Ice Aspects of Ice Scour - Rationale

- The conventional approach to ice scour is to place pipeline below "deepest scour"
- This requires good knowledge of ice scour statistics for the region - these can be in error due to:
 - infilling
 - relic scours & water level changes
 - lack of repetitive scour surveys over many years

Ice Aspects of Ice Scour Rationale - 2

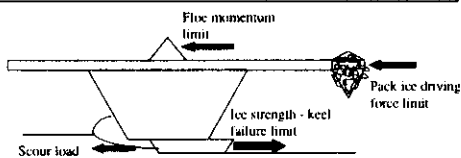
- Even if deepest scour is known: sub-scour disturbance may require deep burial
- Pipelines may lose their cover
- Ice based methods have been developed for scour statistics but suffer from validated knowledge of ice processes
- Better knowledge of ice processes during ice scour can lead to alternative approaches for ice scour design and risk assessment

Ice Aspects of Ice Scour Outline & Objectives of Review

- To review how ice processes limit ice scours
- To quantify ice limits to ice scour in first year ice regions such as Sakhalin
- To speculate on direct ice action on pipelines
- To consider need for future work & its directions

(Note: emphasis of review is sea ice - not icebergs)

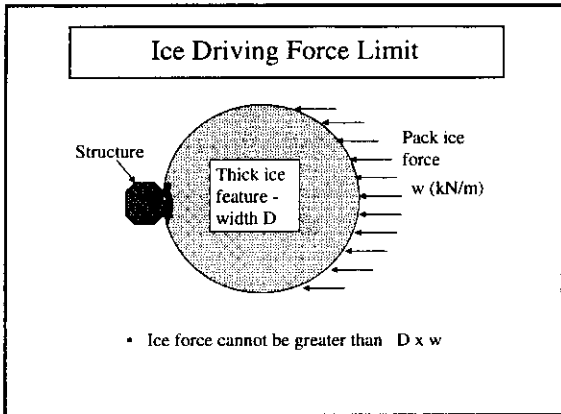
Limits to Ice scour from Ice Processes



- Load available for scouring is the lowest of either
 - The keel failure load (floe keeps moving)
 - Or the pack ice driving force combined with load from dissipation of momentum (floe stops)

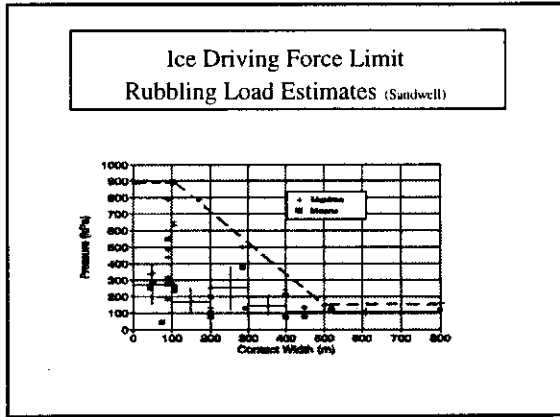
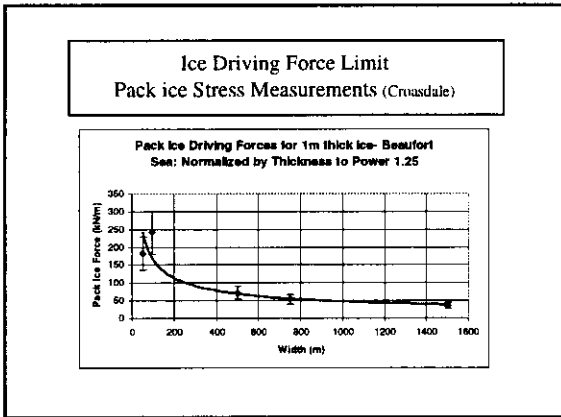
Ice Driving Force Limit - Background

- The limiting driving force concept has been examined in detail for loads on structures
- Simple concept is a thick ice feature in front of structure acted on by surrounding pack ice



Ice Driving Force Limit - Background contd.

- Pack ice forces are considered to be limited by ridge building (w)
- Field work has addressed the estimation of ridge building forces
- Experience with structures has also given insights into ice rubbing forces (w for narrower features)



Ice Driving Force Limit

- Based on these data, pack ice driving forces are assumed to be a function of ice thickness and width of ice feature
- Thickness relationship:
 $w_t = w_l(t)^{1.25}$
- Width relationship:
 - Width: 0 to 100m: $w_l = 500(t)^{1.25}$
 - Width: > 500m: $w_l = 150(t)^{1.25}$
 - Width: 100 to 500m: linear interpolation

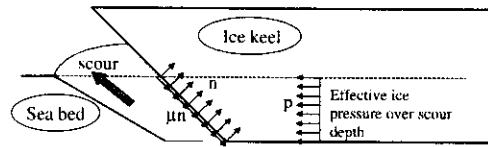
Ice Driving Forces Compared to Typical Scour Loads

Ice feature width (m)	Driving force 0.5m ice (MN)	Driving force 1.0m ice (MN)	1.0m deep scour load (MN) (15m wide in sand)		2m deep scour load (MN) (15m wide in sand)		4m deep scour load (MN) (15m wide in sand)	
			S.F.=1	S.F.=2	S.F.=1	S.F.=2	S.F.=1	S.F.=2
50	10.5	25	1.24	2.0	5.70	9.64	28.6	51.63
100	21	50	1.24	2.0	5.70	9.64	28.6	51.63
300	29.4	70	1.24	2.0	5.70	9.64	28.6	51.63
500	37.8	90	1.24	2.0	5.70	9.64	28.6	51.63
700	44.1	105	1.24	2.0	5.70	9.64	28.6	51.63

Ice Driving Force Limit - Findings

- Pack ice driving forces will not limit extreme scour depths
- Pack ice driving forces may limit number of scours in probabilistic calculations - due to the sometime presence of thin ice and open water

Ice Strength Limit to Ice Scour - Scheme



- Effective ice pressure required to scour is function of: Scour depth; Scour surcharge; soil type; angle of keel; ice soil friction.
- Limit to ice scour depth is when effective ice pressure equals ice crushing strength or pressure to cause keel shear failure

Ice Strength Limit to Ice Scour - Solid Ice e.g. Multi-year ice

- Cold multi-year tested in lab can have strengths as high as 10 MPa
- Maximum crushing pressures measured against structures in range 1 to 1.5MPa (cold ice)
- Interaction of warm ice at Hans Island gave maximum crushing pressures of about 0.5 MPa (mean 0.2 MPa)
- Size effects are apparent (area, thickness, aspect ratio)
- Temperature effects present in lab results and Hans Island data

Ice Strength Limit to Ice Scour - Solid Ice

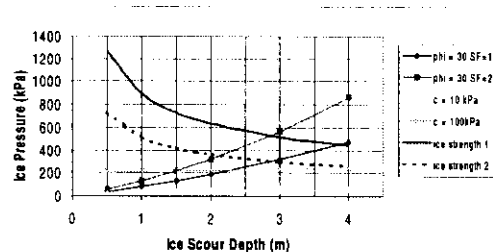
- Various pressure area/thickness curves can be tried to compare scour depths and ice strength.
- e.g.

$$p = 4A^{-0.5}$$

$$p = 2A^{-0.5}$$

(Note these compare with Sanderson (1986) of $p = 8A^{-0.5}$ for cold surface ice)

Comparison of Typical Ice Pressures Required to Scour with Possible Keel Strengths (Solid Ice)



Ice Strength Limit to Ice Scour - Solid Ice Findings

- Deep scours ($>> 4$ m) are possible in cohesive soils
- Scours in sand from M-Y ice appear to be limited to about 3m
- But depending on strength relationship used, may be limited to 2m
- Results sensitive to surcharge and assumed temperature effects on ice strength

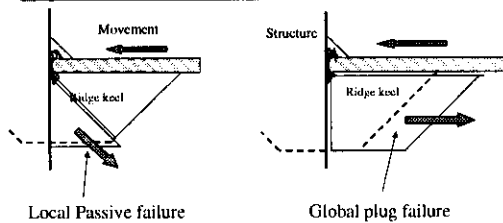
First Year Ridges

- F-Y ridges do not have keels of solid ice
- It is known that F-Y ridge keels consist of ice rubble held together by buoyancy, friction and cohesion
- Recent research has focussed on ice loads on platforms due to F-Y ridges (e.g. Canadian JIP)

First Year Ridges and Ice Loads

- Model tests confirm that keels fail by a combination of local passive failure and global plug failure
- Loads dependent on keel depth, ridge breadth, ice density, friction angle & cohesion

Ridge Keel Failures on Structures



Typical Ice Loads due to F-Y Ridges

Structure width	Consolidated layer load	Cons. layer ice pressure	Keel load	Keel average ice pressure
(m)	(MN)	(kPa)	(MN)	(kPa)
100	250	1000	136	62
20	30	1500	48	109

Note: relatively low ice pressures due to keel

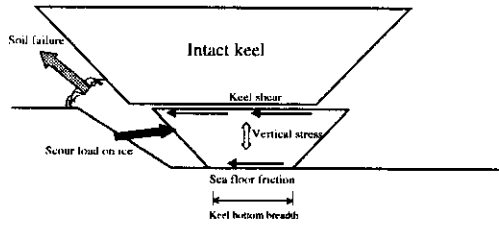
First Year Ridges - Keel Strength

- Properties of ice rubble have been subject to much uncertainty. Earlier reviews showed ranges of ϕ from 10 to 70, and cohesion (c) from 0 to 30 kPa
- New bi-axial lab tests on saline ice show friction angles up to 45° (in NRC's 1m cube "squish box") (but generally less for realistic conditions)
- However, temperature at ridge formation and effects of internal stress over time are considered important. As is possibility of progressive failure of ice rubble
- Recognition led to large-scale, in-situ tests in Canada and Russia, commencing in 1996

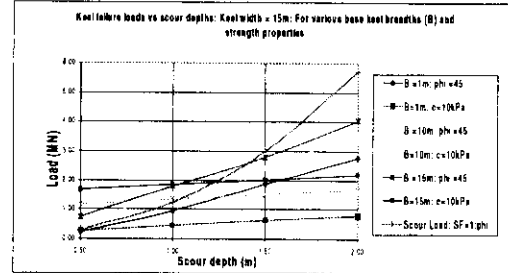
Application of F-Y Keel Load Models and Ice Strength Knowledge to Ice Scour

- Keel failure models for ice scour should recognize:
 - local passive failure will be prevented by the sea floor
 - keel plug failure will control (grounding pressures may increase the plug load)
 - little is known about ice rubble strengths at base of the keel
- Based on above considerations, a preliminary model has been derived for bottom plug failure

Keel Failure Model for Limit to Ice Scour



Typical Results: F-Y Keel Failure Loads



F-Y Keel Failure Limit on Ice Scour Preliminary Results

- Keel scouring capacity dependent on:
 - ridge bottom breadth
 - whether rubble cohesion or friction governs
 - values for keel cohesion at keel bottom
- In sand, scour depths appear limited to 0.5 to 1.5m range
- Range of keel failure loads: 0.5 to 3 MN (15m wide keel)
- Range of equivalent ice pressures: 70 to 120 kPa

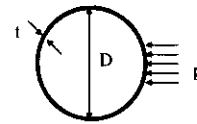
Consequences of Direct Ice Action on Sea Floor Facilities

- Ice pressures from sea ice keels are lower than used in platform design (5 to 10 times lower)
- So designing for direct ice action is certainly feasible
- However, actual ice pressures to be used are still subject to lack of knowledge because of historical focus on avoiding direct ice contact

Direct Ice Action From F-Y Ridges

- Ice pressures from direct contact of F-Y ridges are likely in range: 70 to 200 kPa
- Pipelines can be designed to resist local effects of such pressures
- Assessment of global stability of pipelines to resist keel loads requires more work to assess practicality

Example - Ability of Pipeline to take F-Y Ice Local Pressures



P (MPa)	D (m)	t (m)	Denting Stress (MPa)
0.2	1.0	0.03	53
0.2	1.2	0.03	77
0.5	1.0	0.03	133
0.5	1.2	0.03	192

The Ice Aspects of Ice Scour Conclusions - 1

- Ice scours are mostly limited by ice keel strengths not by driving forces
- Bottom breadth of F-Y ridges may be increased during initial contact with sea floor - increasing their capability to scour in shallower water
- Scour depth capability depends on whether friction or cohesion governs the behaviour of keel rubble

Ice Aspects of Ice Scour Conclusions - 2

- This review suggests scours in sand from F-Y ridges are limited to less than about 1.5m
- Corresponding ice pressures are in the range of 70 to 200 kPa
- Direct ice action at these pressures need not be catastrophic
- Designing for direct ice action may be desirable (e.g. in regions of high sediment transport)
- Proper risk assessment should account for accidental direct ice contact

Ice Aspects of Ice Scour - Future Work

- Preliminary models for ice scour/ice keel interaction should be refined:
 - by analysis
 - by model tests (and/or centrifuge)
- We need better full-scale in-situ strengths of ice at the bottom of keels
- Full scale tests with instrumented device on sea floor should be investigated

COMPARISON OF ICE STRENGTH AND SCOUR RESISTANCE

Jack I. Clark and Fanyu Zhu
C-CORE
Memorial University of Newfoundland
St. John's, NF, A1B 3X5
Canada

ABSTRACT

This paper considers the interaction between ice and soil during scour events. The failure pressure of ice decreases with contact area while the bearing capacity of soil increases with footing size. In the analysis of ice/soil interaction, the ice surface in contact with the soil is treated as an inclined footing. The strengths of ice and soil versus contact area are compared when the friction angle of soil ranges from 20 to 50 degrees. It is concluded that for ice/soil interaction the failure mode is dependent on contact area. Depending on the amount of contact area, either ice or soil may fail. The larger the contact area, the more likely it is for the ice to fail rather than the soil.

1. INTRODUCTION

In cold ocean areas, including the continental shelf regions of the Arctic Ocean and the Canadian east coast, ice-induced hazards are an important consideration in the design, construction and operation of offshore facilities. Ice scour occurs when drifting icebergs or sea ice pressure ridge keels contact and move through seafloor sediments. Ice scour is well known in Canadian and other offshore regions where oil and gas exploration has been underway in ice invaded regions for several decades. Ice scour is a potential hazard to seabed structures and to oil and gas pipelines buried on the sea floor. Considerable research on ice scour has been carried out, including field, experimental and theoretical studies (Lach, 1996; and Clark et al., 1998). The average ice scour in the Canadian Beaufort Sea is 0.5 m deep and 26 m wide in water depths ranging from 10 to 40 m, while the estimated scour length is 5 to 10 km. The maximum recorded depth, width and water depth for Beaufort Sea scours are 7.1, 1375 and 72 m respectively (Lewis et al., 1990). In the area of the Grand Banks of Newfoundland, iceberg scours and iceberg-created seabed pits were observed in water depths up to 230 m, with mean scour depth of 1.3 m and mean scour width of 25 m. The most recent scours on the northeast Grand Banks are in a water depth of approximately 180 m.

A buried pipeline may be damaged if it is located above the base of the scouring ice keel and is in direct contact with ice during scouring. A pipeline may also be endangered when it is buried at a greater depth and does not contact the ice directly (Palmer et al., 1990). In this case, the large forces imposed on the seabed during scouring will be transmitted to the soil under the scour and cause high stresses and large deformations in the soil. The response of a buried pipeline under scour will depend on the deformation of soil in the vicinity of the pipeline (Kenny et al., 2000).

Laboratory tests (Prasad et al., 1986; and Paulin, 1992) and centrifuge modelling (Lach, 1996) of ice scouring have been carried out to investigate scour forces and soil deformations and to verify

theoretical models. Clark et al. (1989) described two modes of soil failure during a scour event. The first mode involves ploughing of near-surface soil and subsequent lateral movement to berms on both sides along the path of the ice, while the second mode is a bearing capacity failure in which both downward and lateral movement of the soil below the ice keel occurs. In the experimental and theoretical modelling of the interaction between ice and soil during scour events, it is implicitly assumed that scour-induced stresses exceed the strength of soil, therefore failure is assumed to occur within the soil. However, scour forces increase with the size of the scour and the strength of soil. In a large-scale scour event, the interaction pressure between the ice and soil may exceed the strength of ice, leading to the failure of the ice rather than the soil.

This paper presents a comparison of ice strength and soil resistance in scour events. The strength of ice presented comes from experimental data collected by Sanderson (1988) while the resistance of soil is estimated from the bearing capacity theory for inclined footings.

2. ICE STRENGTH

Ice is generally considered to be an inhomogeneous, anisotropic and nonlinear viscoelastic material. As discussed by Cammaert et al. (1988), the strength of sea ice is related to a number of factors including grain size, crystallographic orientation, porosity and brine content, stress or strain rate, temperature, confinement, and scale. The strength of ice is influenced by strain rate. Ranges of the strain rate can be classified primarily as ductile and brittle. In the brittle range of strain rate, the influence of strain rate on the strength of ice is limited (Cammaert et al, 1988). In the ductile range, the strength increases with increasing strain rate. Uniaxial compression test data of ice as compiled by Cammaert et al. (1988) indicate that when the strain rate is up to 10^{-3} s^{-1} , the behaviour of ice is ductile, conversely at a higher strain rates the behaviour of ice is brittle. In the strain rate range from 10^{-6} s^{-1} to about 10^{-3} s^{-1} , a ten-fold increase of strain rate will lead to an increase in strength of as high as 70%.

According to experimental results, Sanderson (1988) indicates that there is no simple failure pressure for ice. The strength of ice in laboratory tests ranges from 10 to 20 MPa while large-scale field tests fail at pressures as low as 1 MPa. It is important to note that the failure pressure of ice is dependant on contact area.

A wide range of data from tests of full-thickness edge indentations were plotted by Sanderson (1988) showing peak pressure as a function of gross contact area where $A = WH$. As shown in Figure 1, W is the width of the structure in contact with the ice while H is the ice thickness. The test data are raw and the influences of temperature and salinity have not been corrected. The test data that falls naturally into four principal clusters was obtained from four groups of test conditions, as shown in Figure 2.

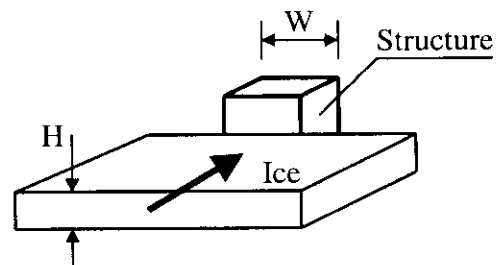


Figure 1: Ice indentation geometry

The data in Group A was obtained from small-scale laboratory tests with aspect ratios (W/H) from 0.21 to 83 and contact areas from about 5×10^{-5} to 3×10^{-2} m²; the failure pressure varies approximately from 0.8 to 24 MPa. In Group B, the data came from medium-scale tests including various in situ jacking tests, floating freshwater lake ice tests, measurements on river bridge-piers, and sea-ice data from lighthouses. In this group, the contact area ranges from about 0.07 to 7 m² and the failure pressure ranges from 0.3 to 12 MPa. In Group C, the data came from measurement of full-scale islands, including Beaufort Sea artificial islands and the Hans Island tests, with contact areas from about 54 to 1400 m² and peak pressures from 0.03 to 2 MPa (except for one point at which the aspect ratio is about 800, as discussed below). The data in Group D was obtained from theoretical models for simulating the large-scale overall dynamics of the Arctic Ocean and its ice cover, in which the gross compressive strength of polar ice is used as a parameter that has to be inserted into the governing equations and adjusted to match observed behaviour. The strength of ice obtained from the theoretical models ranges approximately from 2 to 35 kPa while the contact area is of the order of 10^5 m². The data in Group D from theoretical models with aspect ratios of the order of 10^4 are less reliable and beyond the interest of the present study and are not used in this ice-soil interaction analysis.

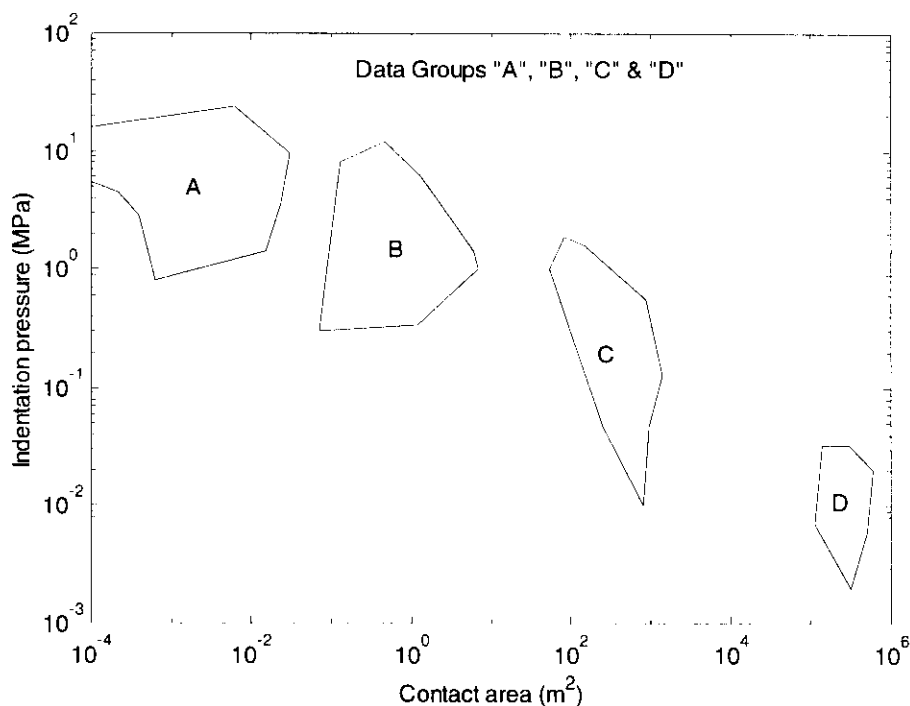


Figure 2: Data groups of ice strength versus contact area (after Sanderson, 1988)

The test data in Groups A, B and C indicate that the strength of ice decreases with increasing contact area. Figure 3 displays the lower and upper bound relationship of ice strength versus contact area. For contact areas from 10^{-4} to 10^3 m², the lower bound strength decreases approximately from 0.7 to 0.01 MPa, while the upper bound strength changes from about 50 to 0.5 MPa.

It can be argued that the reduction of ice strength as presented by Sanderson (1988) may be due to the mixed effects of contact area, aspect ratio and loading rate, rather than solely due to the effect of contact area. The data in Groups A, B and C, except for one point in Group C of which the aspect ratio is about 800, show a trend of reduction of ice strength with aspect ratio (W/H). The approximate ranges of ice strength and aspect ratio of Groups A, B and C are listed below.

	Group A	Group B	Group C
Ice strength (MPa):	0.08 to 24	0.3 to 12	0.03 to 2
Aspect ratio (W/H):	0.2 to 80	0.4 to 20	5 to 200

The influence of aspect ratio on ice strength is not significant; it is especially insignificant for data in Groups A and B. In addition, test data of Kry (1979), in which ice was adfrozen to the indenter, does not seem to show any effect of aspect ratio on ice strength. Therefore, the effect of aspect ratio on the relationship between ice strength and contact area, shown in Figure 3, should be limited.

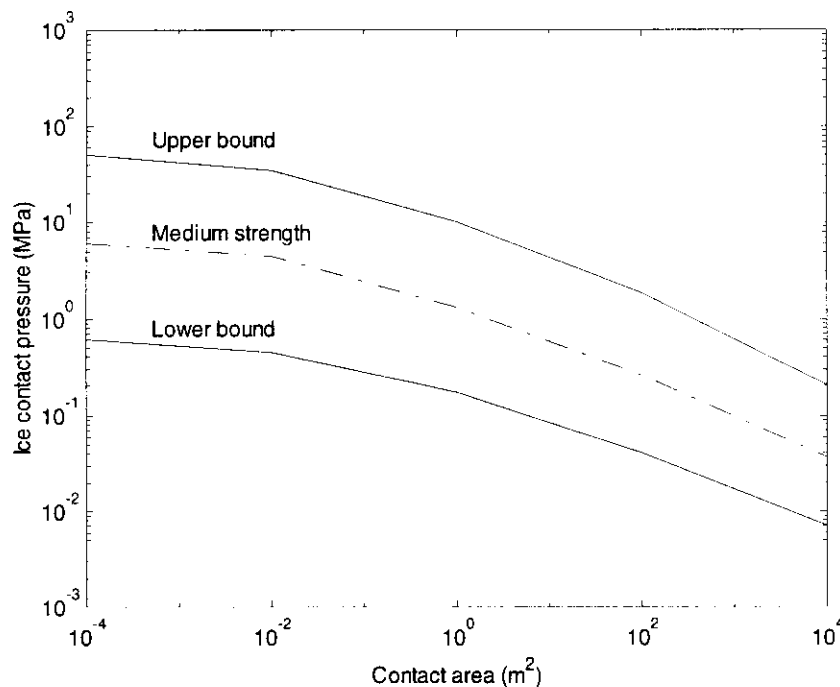


Figure 3: Ice strength versus contact area (after Sanderson, 1988)

3. SCOUR RESISTANCE OF SOIL

A number of theoretical models have been proposed for the prediction of ice scour forces, such as the Chari model (Chari, 1975), the Been model (Been et al., 1990) and the C-CORE models (Walter et al., 1998). The ice scour model presented by Chari for cohesive soils is an energy model that balances the energy available to drive an iceberg with the soil resistance to scour of a sloping seabed. The Been model is also an energy model. It calculates the energy of the advancing ice and the energy dissipated due to scouring of the sea floor over prescribed

displacement intervals. Determination of soil resistance is based on a passive pressure rupture zone at the front of the scouring ice. In the Been ice scour model, effective strength parameters of soil are used and fully drained conditions are assumed.

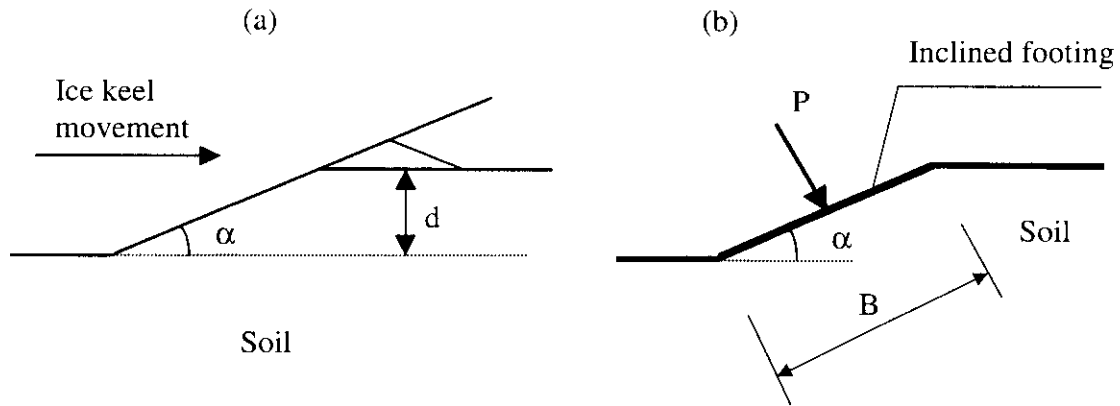


Figure 4: (a) Ice/soil interaction in scouring; (b) Simplified model

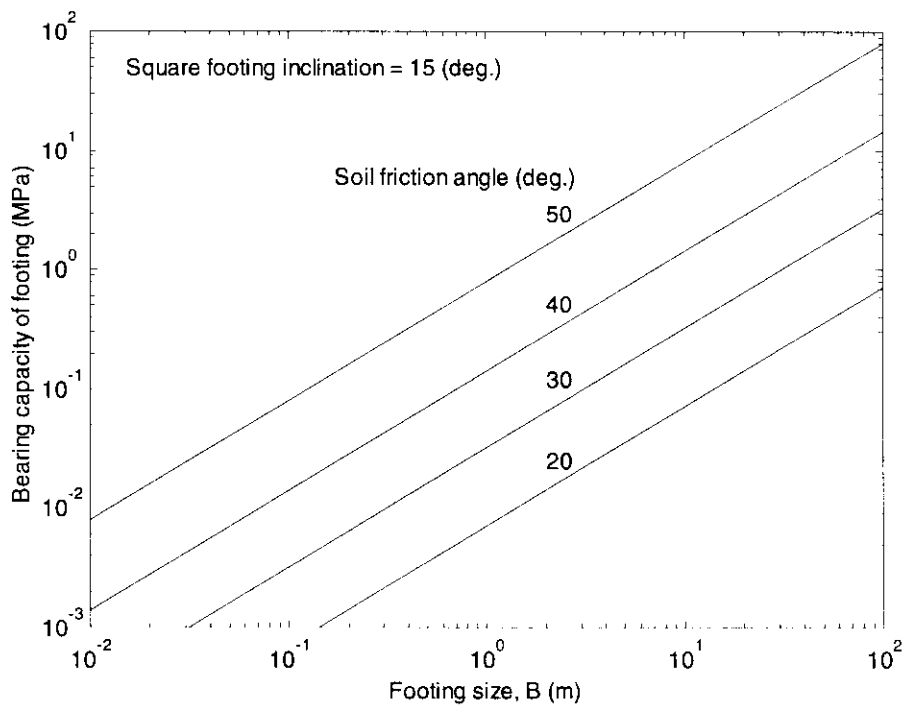


Figure 5: Bearing capacity versus footing size

In order to estimate the pressure between the soil and scouring ice, the soil resistance to a scouring ice keel in this study is evaluated using the bearing capacity theory for inclined footings. Figure 4(a) shows the interaction of ice and soil during scouring and Figure 4(b) shows

a simplified model of an inclined footing for the evaluation of scour forces. The soil resistance pressure can be estimated using the bearing capacity theory for an inclined square footing on cohesionless soil (Chen and McCarron, 1991), expressed as

$$[1] \quad q_u = 0.3\gamma BN_\gamma b_\gamma$$

where q_u is the bearing capacity, γ is the effective unit weight of soil (10 kN/m^3), and B is footing width. The footing inclination factor b_γ is expressed as

$$[2] \quad b_\gamma = (1 - \alpha \tan \phi)^2$$

where α is the inclination angle of the footing and ϕ is the friction angle of soil. The bearing capacity factor N_γ can be derived using Brinch Hansen's expression written as

$$[3] \quad N_\gamma = 1.5[e^{\pi \tan \phi} \tan^2(\pi/4 + \phi/2) - 1] \tan \phi$$

The bearing capacity obtained from Equation [3] increases with footing size and soil friction angle. An increase of footing inclination will result in a reduction of the bearing capacity. For a footing inclination angle $\alpha = 15^\circ$, the effect of footing size and soil friction angle on the bearing capacity is shown in Figure 5. For a footing size of 10 m, the calculated bearing capacities are approximately 0.07, 0.33, 1.5 and 8.1 MPa when the soil friction angles are 20° , 30° , 40° and 50° respectively. For a constant ϕ , the calculated bearing capacity increases linearly with footing size.

The scour depth is defined by $B \sin \alpha$. For a square contact area of 100 m^2 , the scour depth is approximately 2.6 m if the ice has the strength indicated for the given soil type. For a very strong soil with $\phi = 50^\circ$, ice with a strength of 2 MPa would penetrate a maximum of 0.6 m before failing.

4. COMPARISON OF ICE AND SOIL STRENGTH

The analysis and discussion presented above demonstrates that the strength of ice decreases with contact area while the bearing capacity of soil increases with footing size. For a given type of soil under scouring, there is a critical contact area (A_c). When the actual contact area between the ice and the soil is less than A_c , the failure occurs in the soil, conversely if the contact area is greater than A_c the failure occurs within the ice.

Figure 6 shows the comparison of ice strength and soil resistance or contact pressure when the scour angle (footing inclination angle) is 15 degrees. The critical contact areas (A_c) are approximately 460, 100, 20 and 3 m^2 for the medium strength of ice when soil friction angles are 20° , 30° , 40° and 50° respectively. A relation of smaller critical contact area equating to stronger soil is revealed. When the friction angle of soil increases from 20° to 50° degrees, the critical contact area is reduced from about 67 to 0.25 m^2 for the lower-bound strength of ice, while it is reduced from approximately 2900 to 25 m^2 for the upper-bound strength of ice. Selecting the proper strength of ice is important in estimating the critical contact area. For soil

friction angle $\phi = 40^\circ$, the critical contact area is about 2.1 m^2 when the lower-bound strength is selected, while the critical contact area becomes 140 m^2 if the upper-bound strength of ice is used.

Figure 7 presents a strength comparison of ice and soil when the ice scour angle (footing inclination angle, α) is assumed to be 30 degrees. The soil resistance shown in Figure 7 is less than the soil resistance in Figure 6 due to an increased footing inclination angle. When the friction angle of soil increases from 20 to 50 degrees, the critical contact area is reduced from 87 to 1.1 m^2 for the lower-bound strength of ice, while it is reduced from 3500 to 97 m^2 for the upper-bound strength of ice. The values of critical contact area from Figure 7 have increased slightly compared with those obtained from Figure 6.

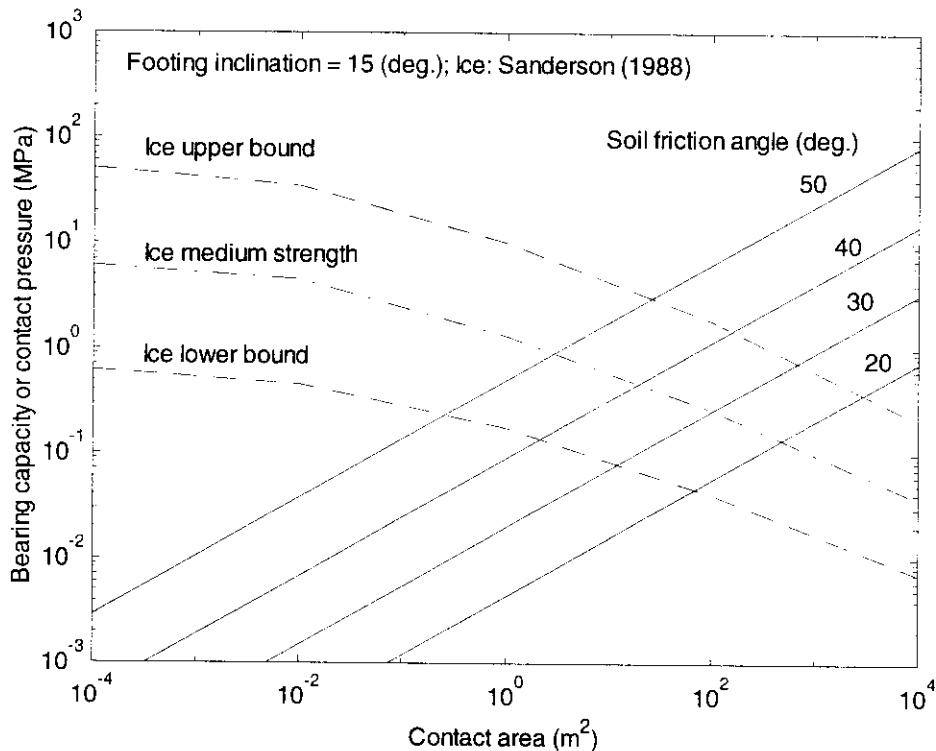


Figure 6: Comparison of ice strength and soil scour resistance ($\alpha = 15^\circ$)

5. SUMMARY

A comparison of ice strength and scour resistance of soil has been presented in terms of contact area. The failure pressure of ice decreases with decreasing contact area while the soil resistance increases. When the contact area between ice and soil is less than the critical contact area the failure occurs in the soil, otherwise if the contact area is greater than the critical area, the failure will be within the ice. In ice scour events, an increase of soil strength will result in a reduction of the critical contact area. It is concluded that for ice/soil interaction, the failure mode is dependent on contact area.

The depth to which an ice keel will penetrate the soil before it fails is very much dependent on ice strength. When the ice is weak due to high temperature, salinity, or size of contact area, it may not penetrate even moderately strong soil more than a fraction of a metre. This could account for the fact that in environments such as the Grand Banks, most scours from major icebergs that impact the seabed are less than 1 m deep. Although reasonably good large scale strength data for icebergs exist, there is a lack of data on strength of ice keels. Investigating the strength of ice keels could lead to be a very fruitful line of research.

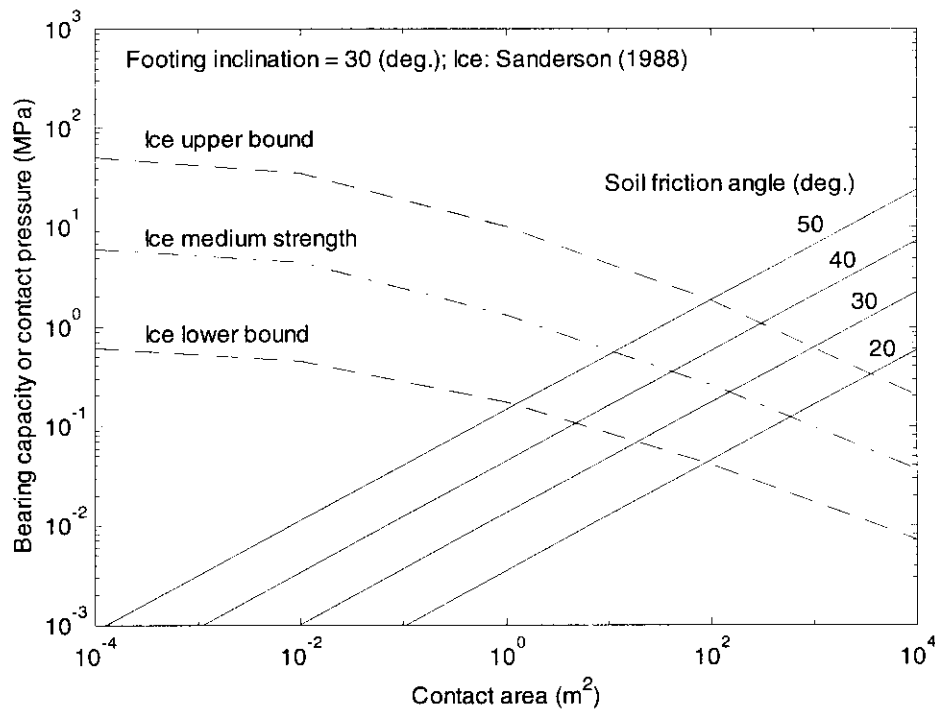


Figure 7: Comparison of ice strength and soil scour resistance ($\alpha = 30^\circ$)

REFERENCES

- Been, K., Kosar, K., Kachey, J., Rogers, B.T., and Palmer, A.C. (1990). "Ice Scour Models." Proc. The 9th International Conference on Offshore Mechanics and Arctic Engineering, Vol. 5, pp. 179-188.
- Cammaert, A.B., and Muggeridge, D.B. (1988). *Ice Interaction with Offshore Structures*. Van Nostrand Reinhold, New York.
- Chari, T.R. (1975). "Some Geotechnical Aspects of Iceberg Grounding." *Ph.D. Thesis*, Memorial University of Newfoundland, St. John's, Canada.
- Chen, W.F., and McCarron, W.O. (1991). "Bearing Capacity of Shallow Foundations." In *Foundation Engineering Handbook*, edited by H.Y. Fang, Van Nostrand Reinhold, New York, pp. 144-165.
- Clark, J.I., Phillips, R., and Paulin, M.J. (1998). "Ice Scour Research for Safe Design of Pipelines: 1978-1998." *Proc. Ice Scour and Arctic Marine Pipelines Workshop*, Momobetsu, Hokkaido, Japan, February 1998, pp. 1-7. (Published by C-CORE, St. John's, Canada, November 1998)

- Clark, J.I., and Poorooshab, F. (1989). "Protection of Sea Bottom Facilities in an Ice Scoured Environment." *Proc. 1989 Annual Conference of the Canadian Society for Civil Engineering*, pp. 617-632.
- Kenny, S., McKenna, R.F., Phillips, R., and Clark, J.I. (2000). "Response of Buried Arctic Marine Pipelines to Ice Scour Events." *Proc. ETCE/OMAE 2000 Joint Conference*, ASME, OMAE 00-5001, New Orleans, LA.
- Kry, P.R. (1979). "High Aspect Ratio Crushing Tests of Ice." *APOA Project*, No. 93.
- Lach, P.R. (1996). "Centrifuge Modelling of Large Soil Deformation Due to Ice Scour." *Ph.D. Thesis*, Memorial University of Newfoundland, St. John's, Canada, 685 p.
- Lewis, C.F.M., and Blasco, S.M. (1990). "Character and Distribution of Sea-Ice and Iceberg Scours." *Proc. The Workshop on Ice Scouring and the Design of Offshore Pipelines*, Calgary, Canada, pp. 57-101.
- Palmer, A.C., Konuk, I., Been, K., and Comfort, G. (1990). "Ice Gouging and the Safety of Marine Pipelines." *Proc. The 22nd Offshore Technology Conference*, Houston, pp. 235-244.
- Paulin, M.J. (1992). "Physical Model Analysis of Iceberg Scour in Dry and Submerged Sand." *M.Eng. Thesis*, Memorial University of Newfoundland, St. John's, Canada, 183 p.
- Prasad, K.S.R., and Chari, T.R. (1986). "Some Factors Influencing Iceberg Scour Estimates." *Proc. The 14th International Conference on Offshore Mechanics and Arctic Engineering*, Calgary, Canada.
- Sanderson, T.J.O. (1988). *Ice Mechanics: Risks to Offshore Structures*. Graham & Trotman Ltd., London, UK, 253 p.
- Walter, D.J., and Phillips, R. (1998). "PRISE – Force Models for Drained and Undrained Steady State Ice Scouring." Contract Report for PRISE Participants, C-CORE Publication 98-C33, C-CORE, St. John's, Canada.
- Weeks, W., and Assur, A. (1967). "Mechanical Properties of Sea Ice." *CRREL Monograph IIC3*, Hanover, NH.

Discrete Element Simulation of Ridge Keel Resistance During Scouring: A Preliminary Study

¹M. Lau, ¹R. Phillips, ¹R. McKenna and ²S. J. Jones

¹*C-CORE, Memorial University, St. John's, Newfoundland, Canada*

²*Institute for Marine Dynamics, National Research Council of Canada,
St. John's, Newfoundland, Canada*

INTRODUCTION

Ice scouring is a complex process that involves the interaction of a floating ice feature with the seabed. The load that can be transferred to the seabed depends on the environmental driving forces that are acting, the characteristics of the ice feature, and the seabed conditions. Conventional approaches have been focused on deformation behavior of seabed soil while assuming sufficient driving forces transfer through the ice feature to scour the seabed. While this assumption may be valid for solid ice features such as icebergs, validity of its application to ice features like loosely consolidated first-year ridge keels is uncertain. For ice ridges, the keel may deform and fail, therefore limiting the scour depth. In areas like the Beaufort Sea, where design ice features include first-year ridge keels, present methods may be too conservative as the ice scouring forces and the scouring depths imposed on sub-sea and seabed installations may be limited by the strength of the ridge keels (Croasdale, 1998).

Palmer et al (1990) estimated that the ice force required to form one of the large gouges frequently seen in the Beaufort Sea might result in an average contact ice pressure of 200 kPa. This estimate agrees with data obtained from centrifuge tests of ice scour (Yang et al, 1996). While soil-bearing pressure is estimated around 200 kPa, the strength of a loosely consolidated first-year ridge keel measured in the field is significant lower. For example, Leppäranta and Hakala (1989) measured the strength of several first-year ridges in the Baltic Sea and reported shear strengths from 1.7 kPa to 2.4 kPa. C-CORE has also conducted a number of field experiments (Bruneau et al, 1998) on the keel shear strength with similar results. These measurements compared reasonably well with small-scale laboratory results (McKenna et al, 1986; and Leppäranta and Hakala, 1989). Therefore, the *relevant question* is: How does a first-year ice keel develop its strength to cause significant ice scour?

This paper reports the preliminary results of a series of discrete element simulations. These simulations looked at the behavior of the ridge keel during idealized ice scouring events, and provided insights on how a scouring ice keel transmits the forces required for seabed scouring.

PROCESSES OF SEABED SCOURING AND POSSIBLE STRENGTH DEVELOPMENT

Shearer et al (1986) identified three principal stages of seabed scour process as shown in Figure 1:

- During the *Stage I*, of ice scouring, the scour depth increases but no rise-up is evident. At this point, the resistance of the soil to the scouring ice mass is apparently insufficient to prevent increasing penetration of the ice keel into the seabed.
- Further scouring may cause the *Stage II*, to develop, during which rise-up of the base of the scour occurs, but at a lesser rate than the change in water depth. This permits scour depths to continue to increase.
- The *Stage III*, occurs when the rise-up of the base of the scour and the decrease in water depth are equal, resulting in a constant scour depth.

During the vertical uplifting process of the second and the third stages of scour depth development, it is possible that increased frictional keel strength may be developed through keel compression.

PROBLEM SET-UP

In the present study, the problem of keel resistance during seabed scouring is treated as a two-dimensional problem using the DECICE2D, a two-dimensional version of the discrete element code DECICE (Intera Technology, Inc, 1986). The computer program was developed for solving complex solid mechanics problems involving multiple interacting bodies undergoing fracturing. It is particularly appropriate for cases in which contact behaviour between adjacent ice blocks governs the mechanical properties of the loosely consolidated ridge keel. The versatility of DECICE in modelling ice-related problems has been demonstrated in a number of recent works by the authors, which included ice interactions with a bridge pier (Lau, 1994a), jamming of floes at bridge piers (Lau, 1994b), modelling of rubble shear properties (Lau, 1999), and rubble loads exerted on multifaceted cones (Lau, 1999). A number of examples are shown in Figure 2.

Figure 3 shows the results of a series of ice force simulations with a 60° conical bridge pier in level ice (Lau, 1994a). The results were compared with model tests carried out in the tank of the Institute for Marine Dynamics (Spencer et al, 1993). A close agreement between the calculated peak force values and the experimental measurements suggests that DECICE is a promising simulation tool for complementing analytical and experimental work. The algorithmic details of DECICE are described in the DECICE theoretical manual (Intera Technology, Inc, 1986).

In the present study, a first-year ridge keel was prepared via a numerical free-floating process. First, a total of 950 pieces of randomly oriented ice blocks with a uniform piece size of 0.5 m thickness and 1 m width were generated within a rectangular area directly underneath a rigid plate. The density of ice was 900 kg/m³ and the density of water was 1024 kg/m³. After the random generation, the blocks were allowed to float and compact underneath the rigid plate by applying natural buoyancy to the elements. At the same time, a rigid moving plate element (simulating the inclined seabed) was allowed to move into location, contacting the bottom of the keel. Figure 4 shows the configuration of the ridge keel/seabed system after the initial compaction.

The keel was typically 81-m wide, 13-m deep and had a repose angle of 24 degrees. The upper plate provided a fixed boundary to constraint the vertical and horizontal motions of ice blocks at the waterline. The packing condition of the assembly was considered to be loose, and the cohesion was set to zero. Ice friction between the ice block surfaces in the keel specified as 0.4, 0.6 and 0.8 in different runs. The moving plate element was 37.5 m long with a standard inclination of 15°. The initial nominal contact length between seabed and the keel was about 27 m. The plate was moved relative to the keel with combinations of horizontal and vertical velocities to simulate a range of trajectory angles, β , from 0° to 29° from the horizontal. The relevant parameters analyzed in the present study included seabed inclination, α , trajectory angle, β , and ice-ice friction coefficient, μ .

Figure 5 shows the relationship between the internal friction angle and the contact ice friction of a similar ice rubble simulated in a previous series of bi-axial compression tests (Lau, 1999). (See top left figure in Figure 2.) The internal friction angle corresponding to ice friction coefficient higher than 0.4 were not obtained; however, we estimated this angle to be between 35° to 45° for the present ridge keels by extrapolating from the data.

SUMMARY OF RESULTS

Table 1 summarizes the results of the 10 simulations performed. Each simulation was run until the load plate penetrated the keel with a vertical distance of 3.5 m. The maximum nominal contact pressure, P_n , for each simulation is given in the table.

Load Cycles and Distributions

Figure 6 is the pressure-time history of a simulation with the 15° seabed, 0.8 ice friction and a trajectory angle of 7° (Case 6). The figure shows typical cyclical build-ups and releases of nominal contact pressure. Without exception, the magnitude of the pressure peaks increased with vertical plate (seabed) penetration for all simulations. Figure 7 shows a snapshot of the same simulation associated with one of the load peaks showing the principal stress on each ice block. The majority of the stress was distributed on the leading portion of the keel. The increase in keel confinement contributed to an increase in the shear strength of the keel with time. At the trailing end, the rubble ice was relatively free to deform, resulting in a lower resistance in this region.

Effect of Load Trajectory

Figure 8 shows the dependency of the nominal peak contact pressure on load trajectory for the simulations with the 15° seabed and an ice friction coefficient of 0.8. The vertical velocities ranged from 0 to 0.12 m/s, and the horizontal velocities from 0.22 to 0.88 m/s. The vertical motion tends to confine and compress the ridge keel, while the horizontal motion tends to favor stress release. Hence, the trajectory angle, which is defined as $\tan^{-1}(V_v/V_h)$, is a measurement of these two opposing tendencies. The data point corresponding to the trajectory angle of 0° is associated with the undeveloped keel

condition. With an increase in the trajectory angle, the degree of confinement increases, which leads to an increase in the maximum nominal contact pressure.

A typical limit for the compressive failure of the ice was estimated from $(1-n)\sigma_c$, where σ_c is the compressive strength and n is the porosity of a typical soil. A typical soil bearing pressure (but not actual) limit is given in Figure 8 showing that the resistance of a developed keel can exceed the resistance offered by the soil.

In the present analysis, failure of the individual ice blocks was not allowed, leading to excessive confinement near top of the keel. The maximum nominal pressure was computed to be 2.3 MPa. This was significantly higher than the crushing resistance estimated from the compressive strength of ice as shown in the figure, which suggested that keel failure might be partly controlled by failure of ice blocks.

Effect of Ice Friction

The ice friction coefficient also had a large influence on the load transferred through the ridge keel. Figure 9 shows the effect of ice friction for the simulations with the 15° seabed and a horizontal velocity of 0.44 m/s. Data associated with the trajectory angles of 7° and 15° are given on the plot. There was a linear increase in the maximum nominal pressure with ice friction due to the increase in internal friction.

PRELIMINARY CONCLUSIONS AND RECOMMENDATIONS

The preliminary results of a series of discrete element simulations have been presented. These simulations looked at the behavior of the ridge keel during idealized ice scouring events, and provided insights on how a scouring ice keel transmits the forces required for seabed scouring. The results suggest that the development of keel resistance may involve keel compression through reduction of keel draft. A large confining pressure may develop at the frontal contact area between the keel and the seabed during keel/seabed interaction. This confinement is highly dependent of the direction of keel movement, and may result in keel resistance significantly higher than that predicted from existing keel strength measurements. Furthermore, keel shear resistance can be more than soil resistance (Zone III) as anticipated by ice scouring observations. Keel failure may be partly controlled by the compressive failure of ice blocks.

To give a more realistic analysis, additional simulations including the following improvements are recommended:

- better simulation of keel strength by allowing compressive and flexural failures of ice fragments and using higher initial porosity;
- more realistic simulation of keel/seabed contact conditions by using smaller contact area, smaller seabed inclination, and lower trajectory angle, i.e., 0° – 10°;
- larger ice block sizes relative to keel geometry; and
- better simulation of the refrozen layer of the ice keel near the waterline.

ACKNOWLEDGEMENTS

The investigations presented in this paper were funded by a NRC/NSERC Research Partnership grant with the following partners:

University Partner: R. Phillips, C-CORE, Memorial University of Newfoundland
NRC Partner: S. Jones, Institute for Marine Dynamics
Industry Partner: K.R. Croasdale, K.R. Croasdale and Associates Ltd.

IMD provided DECICE for the present study. We gratefully acknowledge their support.

REFERENCES

- Bruneau, S.E., Crocker, G.B., McKenna, R.F., Croasdale, K.R., Metge, M., Ritch, R., and J.S. Weaver, 1998. *Development of Techniques for Measuring In Situ Ice Rubble Shear Strength*, Proceedings of IAHR, Potsdam, NY.
- Croasdale, K.R., 1998. *Review of Strength of First Year Ice Feature and Driving Forces Relating to Ice Scour*, Proceedings of Ice Scour & Arctic Marine Pipelines Workshop, Mombetsu, Hokkaido, Japan, pp. 31.
- Intera Technology, Inc., 1986. *DECICE Theoretical Manual*, Lakewood, Colorado.
- Lau, M., 1999. *Ice Forces on A Faceted Cone due to the Passage of a Level Ice Field*, PhD Thesis, Memorial University of Newfoundland, St. John's, NF.
- Lau, M., 1994a. *A Three Dimensional 'DECICE' Simulation of Ice Sheet Impacting a 60-Degree Conical Structure*, NRC/IMD Report CR-1994-16, National Research Council of Canada, Institute for Marine Dynamics, St. John's, Newfoundland.
- Lau, M., 1994b. *Pack Ice Jamming Simulation: DECICE2D*, Contract Report to NRC/IMD, National Research Council of Canada, Institute for Marine Dynamics, St. John's, Newfoundland.
- Leppäranta, M., and R. Hakala, 1989. *Field Measurements of the Structure and Strength of First-Year Ice Ridges in the Baltic Sea*, Proceedings of the 8th International Conference on Offshore Mechanics and Arctic Engineering, The Hague, Vol. 4, pp. 169-174.
- McKenna, R.F., Bruneau, S.E., and F.M. Williams, 1996. *In Situ Shear Strength Measurements of Model Ice Rubble Using a Punch Technique*, 49th Canadian Geotechnical Conference of the Canadian Geotechnical Society, St. John's, Newfoundland, pp. 297-286.
- Palmer, A.C., Konuk, I., Comfort, G. and K. Been, 1990. *Ice Gouging and the Safety of Marine Pipelines*, Proceedings of the 22nd Annual Offshore Technology Conference, Houston, Paper OTC6371, pp. 235-244.
- Shearer, J., Laroche, B., and G. Fortin, 1986. *Canadian Beaufort Sea 1984 Repetitive Mapping of Ice Scour*, Environmental Studies Research Funds, ESRF Report No. 32, by Geoterrex Ltd., Ottawa, Ontario.
- Spencer, D., McKenna, R., and M. Lau, 1993. *Ice Model Tests of a 60° Upward Breaking Bridge Pier for the Northumberland Strait Crossing*, NRC/IMD Report

TR-1993-05, National Research Council of Canada, Institute for Marine Dynamics, St. John's, Newfoundland.

Yang, Q.S., Poorooshasb, H.B., and P.R. Lach, 1996. *Centrifuge Modeling and Numerical Simulation of Ice Sour*, Soil and Foundations, Japanese Geotechnical Society, Vol. 36, No. 1, pp. 85-96.

Table 1. Maximum nominal contact pressure computed for each simulation

Case	Seabed Angle	Ice Friction	Horizontal Velocity	Vertical Velocity	Trajectory Angle	Maximum Nominal Pressure
	α ($^{\circ}$)	μ	V_h (m/s)	V_v (m/s)	β ($^{\circ}$)	P_n (MPa)
1	15	0.4	0.44	0.12	15.3	0.79
2	15	0.6	0.44	0.12	15.3	1.20
3	15	0.8	0.44	0.12	15.3	1.58
4	15	0.4	0.44	0.05	6.5	0.15
5	15	0.6	0.44	0.05	6.5	0.40
6	15	0.8	0.44	0.05	6.5	0.54
7	15	0.8	0.44	0.00	0.0	0.10
8	15	0.8	0.44	0.03	3.9	0.21
9	15	0.8	0.22	0.12	28.6	2.22
10	15	0.8	0.88	0.12	7.8	0.41

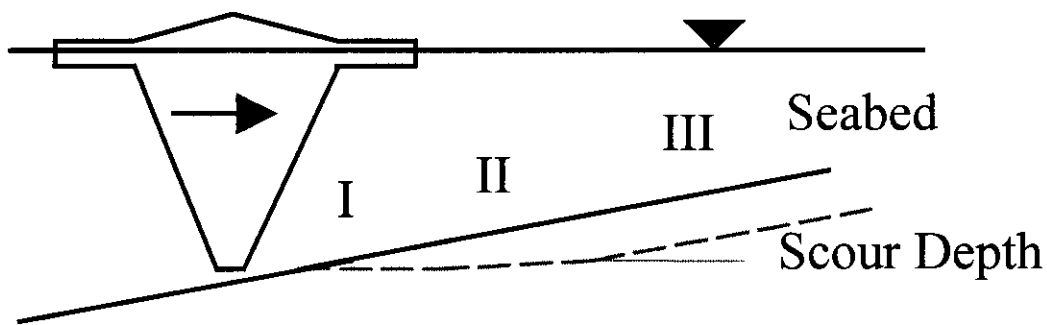
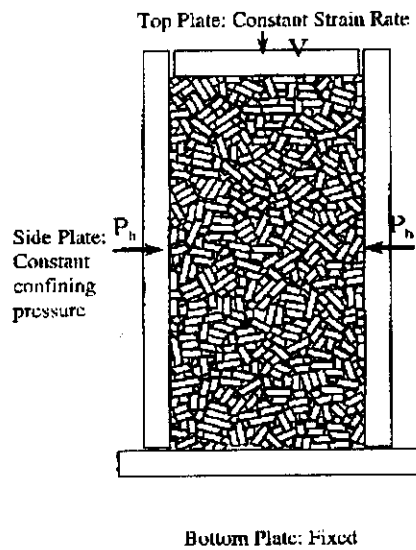
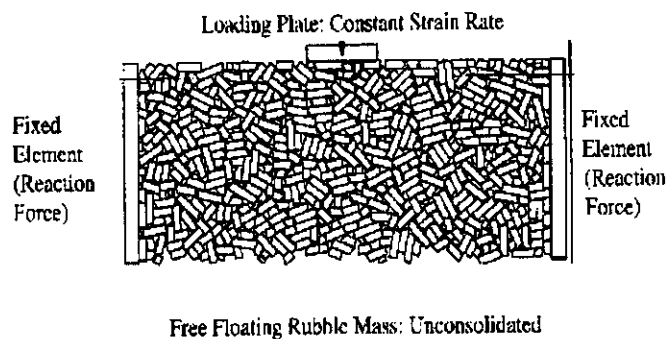


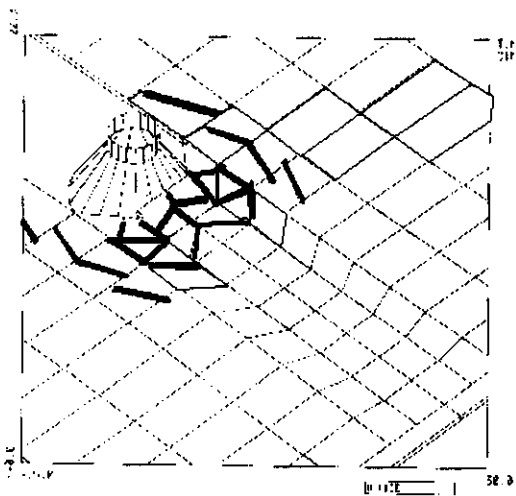
Figure 1. Three principal stages of seabed scour process showing three typical zones (after Shearer et al, 1986)



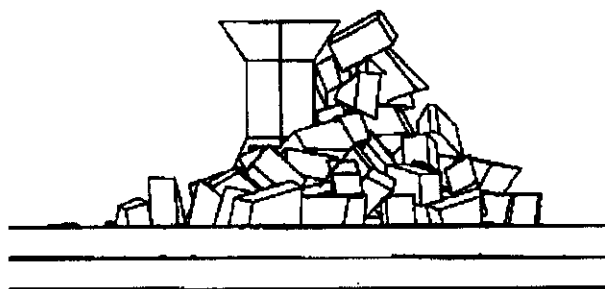
**Modeling of rubble shear properties
(Lau, 1999)**



Punching shear



**Ice Interaction with bridge pier
(Lau, 1994a)**



**Rubble loads exerted on multifaceted cones
(Lau, 1999)**

Figure 2. Examples of DECICE simulations of ice related problems.

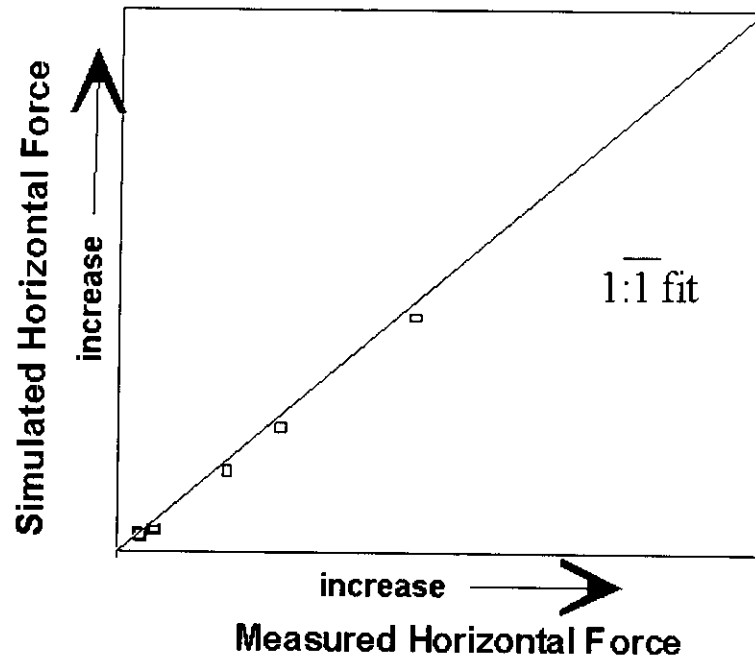


Figure 3. Level ice forces on a 60° cone: a comparison of DECICE simulations and ice tank measurements (Lau, 1994a)

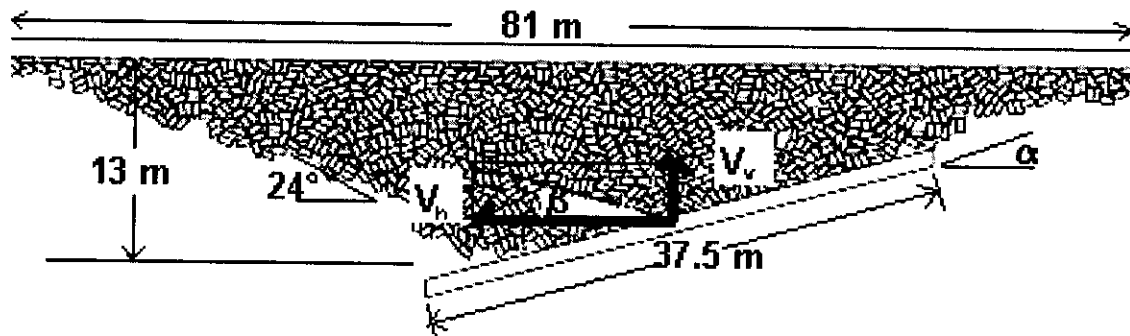


Figure 4. The initial configuration of the ridge keel/seabed system (10 simulations)

Typical Keel Dimensions:	Loading Plate (Seabed):		
81-m wide	nominal (initial) contact length = 27 m		
13-m depth	$\alpha = 15^\circ$		
24° repose angle	<u>Standard</u>	<u>Variations</u>	<u>Trajectory ($\tan^{-1}(V_v/V_h)$)</u>
Fixed boundary at the top	$V_h = 0.44$ m/s	0.22 & 0.88 m/s	$\beta = 0$ to 30°
$\mu = 0.4, 0.6 \text{ \& } 0.8$	$V_v = 0.12$ m/s	0, 0.03 & 0.05 m/s	

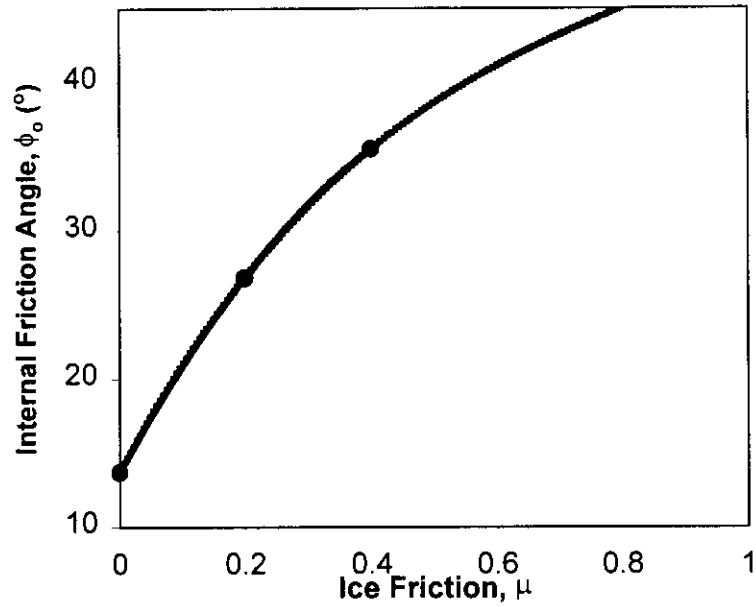


Figure 5. The relationship between the internal friction angle, ϕ_0 , and the contact friction of ice rubble, μ , simulated in a previous series of bi-axial compression tests (Lau, 1999). (See Figure 2, Top left). (The data were extrapolated to the range of ice friction used in the present study.)

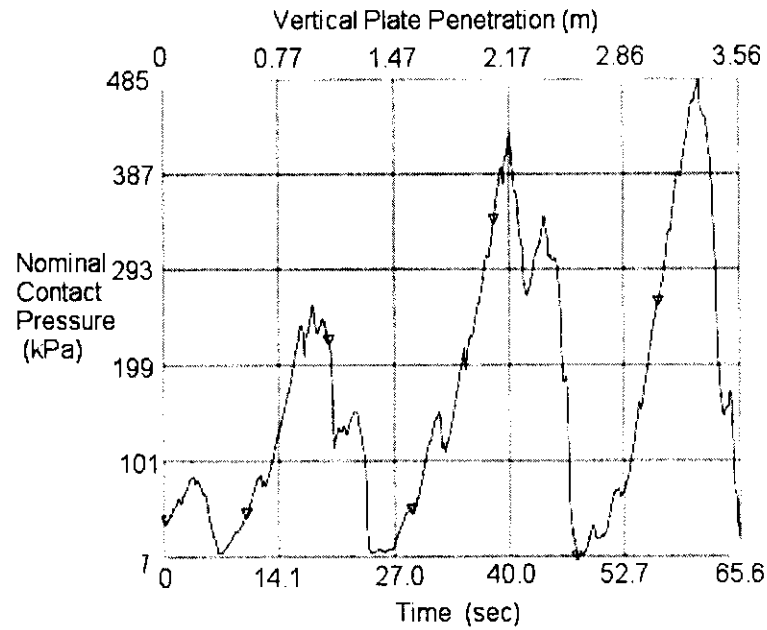


Figure 6. Typical pressure-time history showing increase of nominal peak pressure with vertical plate penetration (Case 6: 15° seabed, 0.8 friction coefficient & 7° trajectory)

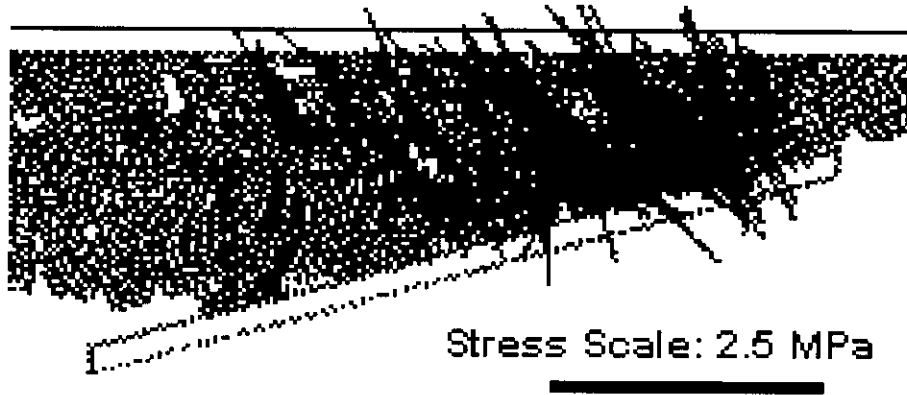


Figure 7. A snapshot of a DECICE simulation taken at the moment of peak stress showing a typical stress build-up at the leading region of the keel (Case 6: 15° seabed, 0.8 friction coefficient & 7° trajectory)

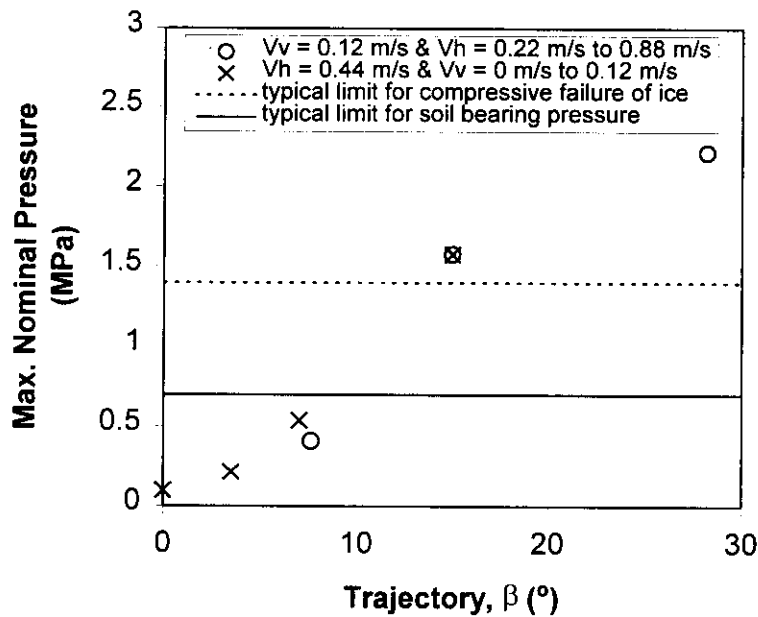


Figure 8. Maximum nominal contact pressure versus trajectory angle for a range of horizontal and vertical velocities for simulations with 15° seabed and $\mu = 0.8$. The horizontal lines show typical limits (but not actual) for compressive ice failure and soil bearing pressure calculated from compressive strength times porosity of the ice.

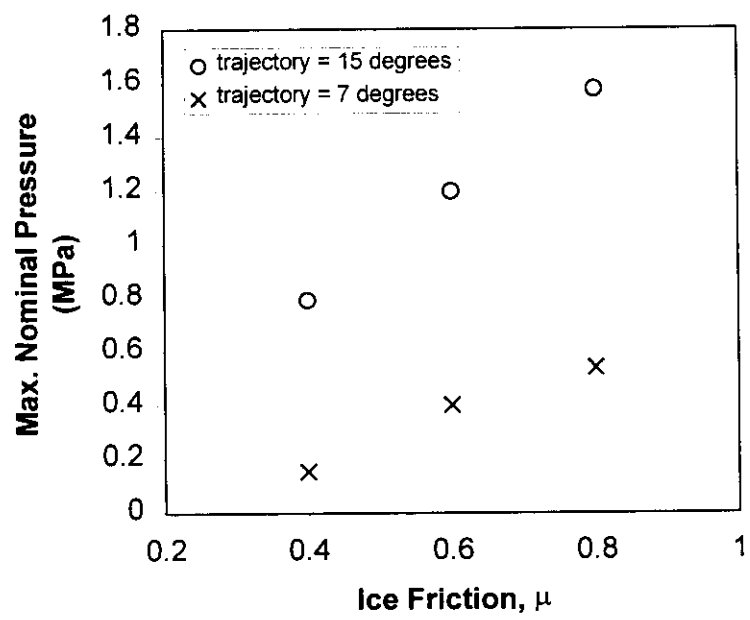


Figure 9. Maximum nominal contact pressure versus ice friction for simulations with 15° seabed and $V_h=0.44$ m/s

Behavior of Ridge Ice at a Time of Ice Scouring

Shinji Kioka¹, Yoshikathu Yasunaga¹, Hideyuki Nishimaki² and Hiroshi Saeki¹

1. Hokkaido University, Japan, Tel +81-11-706-6186, Fax +81-11-726-2296
 2. Shimada Kensetu Co, Ltd, Japan

1. INTRODUCTION

Ice scouring is a phenomenon which occurs when ice (pressure ridge, hummock or iceberg) moves in contact with seabed. It has been reported to have caused damage to communication cables and water intake pipelines. Therefore, it will be very important to estimate rational maximum scour depth due to complicate behavior of ice, and will also be very important to evaluate forces acting on sea bed and stress that is transmitted via the seabed and deformation of soil.

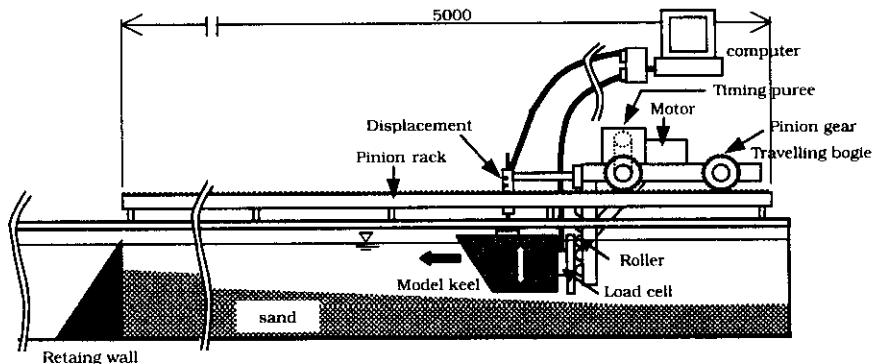
In our previous researches, we concluded that local fluctuations in ice forces (bulldozing forces) in the horizontal direction depended on the slope at the corresponding point on the scour curve (the path of motion of the model ice in plane), and in many cases, ice was tend to move upward. If we understand its mechanisms, we could estimate more rational maximum scour depth. So, it is important to acknowledge the behavior of ice at a time of ice scouring.

Now, we have developed the rational experimental device system as compared to previous device system (Kioka and Saeki, 1999). Under the renewal conditions, we conducted a lot of test series, and we revealed relationships between ice forces and behavior of ice, variations of its behavior due to varies condition (attack angle, travelling velocity). And we also revealed the probability distribution of some random variable under the same experimental condition.

2. EXPERIMENTS

2.1 Experimental equipment and method

Fig-1 shows the equipment used in the experiment, which was developed not merely to improve the experiments of Kioka and Saeki (1999), but also to make up for their shortcomings. First, sand was placed on a 60 cm-wide water channel for a slope of a constant gradient of 1/50. A steel model keel with three attack angles was pushed horizontally at constant velocities by a carriage travelling on a pinion rack of maximum length of 5 m. In addition, the results of the experiments by Kioka and Saeki (1999) proved that local changes of ice forces (bulldozing forces) occur in response to the changes in shapes of excavated ice surfaces. Thus, the model keel was not allowed to rotate, but rollers were placed between the model and the traveling carriage for free vertical movements to measure the relative vertical displacement at the center of gravity of the model using a displacement gauge. A load cell was placed between the model keel and the plate in contact with the rollers to measure the horizontal ice force. This horizontal ice force is the pushing force of the carriage, which is the horizontal drag force applied to the model keel.



The horizontal displacement of the model keel was calculated from the relationship between the four travelling velocities of the carriage and the elapsed times measured by software to process measured data, or by making some corrections through monitoring.

Figure 1. General view of the experimental equipment

2.2 Experimental conditions.

The model keel used in the experiment was made of steel and was

30 cm wide and had three attack angles of 30, 45, and 90 degrees (see Fig-2). The weights of the three model types (300N, the main part, the load cell, and the roller plate) and their initial draft depths (20 cm \pm 1 cm) were all designed to be identical as much as possible and to be adjusted by the weight and float. Next the travelling velocity of model keel was maintained at a constant range of 1-20 cm/s for each ice model. The travelling carriage (motor 200 W / AC 200V) was driven horizontally on the rack by the pinion gear.

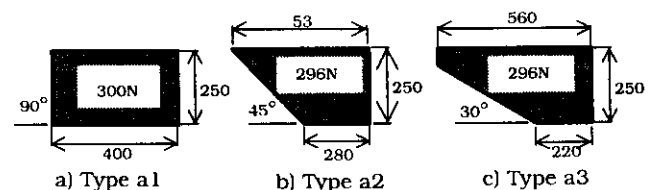


Figure 2. Type of model keel

The sand used was sandy soil available on the market (siliceous sand). For the soil conditions to be as uniform as possible, after completing of every experimental situation, sand maintenance was carefully performed, and sufficient time was taken to prepare for the next set of the experiment.

Table 1 shows the characteristics of the sand used.

Table 1 Characteristic values of the sand used

Mean grain diameter	0.147 mm
Angle of internal friction ϕ	37°
Submerged angle of repose θ	32°
Saturated unit weight	15.68 kN/m ³

The maximum scour length of the model keel was 5 m (the maximum length of the rack). However, the actual range of measurement was set at 3 m to include the possibility that excavated sand appears on the water surface and that the stability of behavior of the model keel deteriorates.

Table 2 shows the major and shows that the conditions of this experiment were nearer to reality than those of previous experiments.

Table 2 Comparison with past experimental conditions

	The previous study	This study
Travelling velocity	0.4-1.4 cm/s	1-20 cm/s
Attack angle	60, 75, and 90 (degree)	30, 45, and 90 (degree)
Scour length	50 cm	300 cm
Seabed slope	1/10 and 1/5	1/50
Driving device system	Oil jack system	Pinion rack system

3 MECHANICAL MODEL OF ICE SCOUR

The fundamental concept of mechanical model follows our previous method (kioka et al.1999). Considering that the range of attack angle is small compared to our previous experiments, in the case that we calculate the resistance force of sand acting on the front of the keel, we reformed its method slightly as follows.

Scouring by ice is thought to cause continuous shear failure of the sand on the sea floor. Here, as shown Fig-3, considering complete plastic deformation of the sand and assuming a uniform slip surface, firstly, we calculated

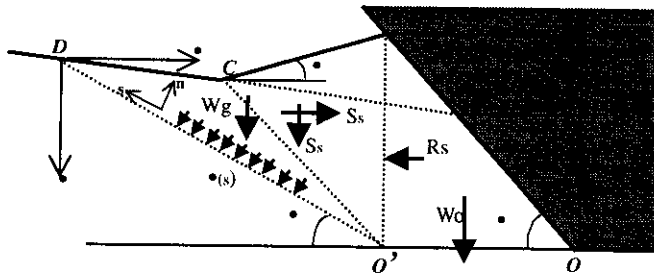


Figure 3. Mechanical model of Ice Scour

From eq(1)(2), we obtain R_s as follows.

$$R_s = \frac{Wg(\sin\psi + \tan\phi \cos\psi)}{\cos\psi - \tan\phi \sin\psi} \quad (3)$$

R_s and Rankine's passive earth pressure are consistent when attack angle θ is 90 degree, seabed slope i is 0 degree.

Considering the weight of sand in the area BO'O (W_g), we obtain the total horizontal resistance of the sand acting on the keel (Rsh).

$$Rsh = R_s + W_o \tan\phi + 2S_s \quad (4)$$

Where,

$$S_s = \gamma' K_p \int_A \eta \tan\phi d\eta d\xi \quad (5)$$

Similarly, the vertical resistance force of the sand acting on the keel (Rsv) is

$$Rsv = \frac{Wg \tan\psi \tan\phi}{1 - \tan\psi \tan\phi} + 2S_s \quad (6)$$

The accumulation height of sand in front of the keel (Z') is given by eq.(7)

$$Z'(X) = \left[\frac{B}{N} \exp\left\{-\frac{\cot\beta}{N} X\right\} \int_0^X \exp\left\{\frac{\cot\beta}{N} \xi\right\} (\xi \tan i - \zeta(\xi)) d\xi \right]^{1/2} \quad (7)$$

Where,

$$N = 0.5 \{ \cos(\theta + \psi) \cos(i + \psi) / \sin(\theta + \psi) \cos^2(\psi) - \tan\theta (1 - \tan\theta \tan i) \}$$

Equation of motion in the horizontal direction and in the vertical direction is given by the following equation respectively.

horizontal resistance of the sand acting on the part B-O' (R_s).

s-direction

$$R_s \cos\psi - Wg \sin\psi - B \int_s \sigma(s) \tan\phi ds = 0 \quad (1)$$

n-direction

$$Wg \cos\psi - R_s \sin\psi - B \int_s \sigma(s) ds = 0 \quad (2)$$

- R_s : horizontal resistance of the sand acting on the part B-O'
- W_g : weight of sand in the area BO'D, B : width of the keel
- σ : normal stress acting on the slip surface
- W_o : weight of sand in the area BO'O
- S_s : frictional force acting on the side part of the area OO'DB
- θ : angle between the slip surface and horizontal plane (here, assumed to be $\theta/4 \rightarrow \theta/2$)
- ψ : attack angle
- Z : scour depth, Z' : accumulation height of sand
- K_p : coefficient of Rankine's passive earth pressure
- γ' : submerge unit weight of the sand
- A : area OO'DB FR : fluid resistance force
- M : mass of the ice \bullet : Scour curve
- \bullet_s : coefficient of dynamic friction between ice and seabed
- K_v : subgrade reaction in the vertical direction (vertical force acting on the seabed)
- h_0' : initial draft depth h' : draft depth

$$-M \frac{d^2 X}{dt^2} - Kv \left(\mu_s + \frac{d\zeta}{dX} \right) - Rsh - FR + F = 0 \quad (8)$$

$$-M \frac{d^2 \zeta}{dt^2} + Kv \left(1 - \mu_s \frac{d\zeta}{dX} \right) - W + \left(h' Le + \frac{1}{2} h'^2 \tan \theta \right) B\gamma_w - \text{sign} \left[\frac{d\zeta}{dX} \right] \mu k F - Rsv = 0 \quad (9)$$

$$h' = h_0 - \zeta(X)$$

By comparing calculated values F with measurement value, we will verify the mechanical model indirectly and will grasp the mechanisms of Ice scour.

4 EXPERIMENTAL AND ANALYSIS RESULTS

As measured values are expected to show some deviations, each set of the experiment was performed many times. Table 3 summarizes the experimental sets and the number of measurements (n).

Table 3 Experimental sets and the number of measurements

Experimental set	Item		Number of measurements	
	Attack angle	Velocity	•(Z)	F
a1v1	90 (degree)	1 (cm/s)	5	5
a1v2	90 (degree)	5 (cm/s)	29	22
a1v3	90 (degree)	10 (cm/s)	6	6
a1v4	90 (degree)	20 (cm/s)	7	6
a2v2	45 (degree)	5 (cm/s)	5	4
a3v2	30 (degree)	5 (cm/s)	5	4

The differences between • and F were arose by omitting unusable results due to some kind of trouble, etc., in advance. One experimental set, (a1v2), was repeated much more than the others to analyze the degree of deviations, which is to be discussed later.

4.1 Probability distribution characteristics of the measurements

Many measurements were performed for one of the experimental sets (a1v2) to study the probability distribution characteristics of the measured values: F_{max} , F_{mean} , Z_{max}/h_0 , and • (the range of measurement: $0 < X < L$, $L = 300$ cm), where:

F_{max} : the maximum value of F ($L = 300$ cm)

F_{mean} : the time average value of F

Z_{max}/h_0 : the maximum scour depth made dimensionless by the initial draft depth

•: the amount of sand excavated by the model keel divided by the amount of sand excavated when the model keel is assumed to travel horizontally in the range of $0 < X < L$ is made dimensionless (conceptually, the time average value of F), which is denoted by the following equation:

$$\Omega = \frac{2 \int_0^L [\xi \tan i - \zeta(\xi)] d\xi}{L^2 \tan i} \quad (10)$$

First, Fig-4 (a) shows the histogram of F_{mean} . Here, provided a random variable, F_{mean} , conforms to the behavior of either normal distribution or log-normal distribution. Next, the measured values of this random variable were plotted on the probability papers. Fig-4 (b) and (c) show normal and log-normal papers, respectively, each with an R-square value. Thus, F_{mean} can be said to behave as a log-normal distribution rather than as a normal distribution.

Similarly random variable (F_{mean} , Z_{max}/h_0 , and •) were examined by plotting on the probability papers. These four random variable can be said to behave as log-normal distribution than as normal distribution.

In view these results, measured values of the other experimental sets are assumed to behave as log-normal distribution. Adopted as representative values are the mean value ••• and the median (X_m), which are denoted by the following equations:

$$\lambda = \ln \mu - \frac{1}{2} \zeta^2 \quad \zeta^2 = \ln \left(1 + \frac{\sigma^2}{\mu^2} \right) \quad (11)$$

$$X_m = \exp(\lambda)$$

4.2 Dependence of the ice force (bulldozing force) and the scour depth on the velocity

First, the dependence of F_{max}/W and F_{mean}/W , which represent values of F_{max} and F_{mean} made dimensionless by the dead weight of the ice, respectively, on the velocity of the model keel was studied. However, the attack angle was constant at 90 degrees. Fig-5 shows the ice force increase with increase in the velocity. When V_0 was below 5 cm/s, the ice force was almost constant irrespective of the value of V_0 . This propensity was similar to the results of the traditional experiments of Kioka and Saeki (1999), which were conducted in the range of 0.4 cm/s <

$V_0 < 1.4$ cm/s. Also, F_{max}/W and F_{mean}/W started to increase after V_0 exceeded 5 cm/s and markedly increased between 5 cm/s and 10 cm/s. When V_0 was larger than 10 cm/s, the rate of increase was negative. Possibly an inflection point existed in the range of 5-10 cm/s, where the rate of increase shifts from positive to negative, but this it cannot be confirmed because of the large value of the coefficient of variation of F_{max}/W (0.4), especially when V_0 was 10 cm/s and 20 cm/s. Therefore, the following factors are considered to be responsible for increasing the ice force with an increase in the velocity:

- 1) Increase in the vertical force of inertia of the ice
- 2) Increase in fluid resistance
- 3) When the travelling velocity of the model keel is larger than the rate of the sand excavated by the model flowing out to the sides of the model or the rate of forming the angle at rest in the sand, the apparent angle at rest of the sand accumulated in front of the model increases, and the amount of the sand flowing out to the sides of the model decreases. As a result, the drag force of the sand increases (the amount of the sand in front of the model increases).
- 4) Exposure of sand on the water surface, which made measurement difficult (increase in consistency and the unit weight of the sand exposed, as well as generating a meniscus and an apparent cohesiveness (because of 3) above)).
- 5) Generation of pore water pressure.

Unfortunately, dominant factors among these factor could not be confirmed, but the effects of Factors 1) and 2) are presumed to be numerically small.

Fig-6 shows the relations of Z_{max}/h_0 and \bullet both of which are defined above, to the travelling velocity. According to this figure, Z_{max}/h_0 and \bullet depend very little on the velocity, which agrees with the results of the experiments of Kioka and Saeki (1999). However, Z_{max}/h_0 and \bullet behave inversely to each other, although this may sound strange. And this value, $((Z_{max} \times Z_{mean})^{1/2}/h_0)$, was almost constant without respect to the travelling velocity.

Fig-7 show the transitions of the COV(coefficients of variation) of the measured values (F_{max}/W , F_{mean}/W , Z_{max}/h_0 , and \bullet) with respect to the travelling velocity. As the relationship described above, COV (coefficients of variation) of F_{max}/W and F_{mean}/W show an inverse relationship and do not depend on the velocity.

4.3 Dependence of the ice force (bulldozing force) and scour depth on the attack angle

Fig-8 shows the relations of F_{max}/W and F_{mean}/W to the attack angle when V_0 was constant at 5 cm/s. When the attack angle increased, F_{max}/W increased slightly, but F_{mean}/W decreased slightly. F_{max}/W and F_{mean}/W behaved inversely with each other. As the attack angle increased, the scour depth increased, and the drag force of the sand in turn increased. This tendency was caused by radical changes in forces loaded and unloaded due to the complicated process of formation of the sand slip surface (complicated mechanism of sand failure). In other words, an increase in the drag force of the sand, the mechanism of whose failure is complicated and uncertain, is caused by an increase in the attack angle, and the measured values deviate accordingly. In effect, the COV increase with an increase in the attack angle. However, changes in the values of F_{max}/W and F_{mean}/W with respect to the attack angle were minimal. It is possible that their dependence on the attack angle is not great.

Fig-9 shows the relationship between $Z_{max}/h_0 \bullet$ and its attack angle. The relationship is a systematic relationship, that is, a smaller attack angle causes less sand digging, verifying previous research (Kioka and Saeki 1999). When the sand shear resistance increases because of keel movement, slickness tends to occur on the boundaries of the surface of the keel front and the sand, increasing the upward movement.

Fig-10 shows the change in the COV of each measurement (F_{max}/W , F_{mean}/W , Z_{max}/h_0 , \bullet). This relationship is also systematic, indicating that the larger the attack angle, the larger the coefficient of variation. This means that a complicated and uncertain sand resistance caused by an increase in the attack angle increases accordingly. In other words, when the attack angle decreases, it can be freed from these complicated factors (fracture mechanism). That is, rough ice scouring shows indirectly that the friction movement between ice and sand is in an excellent and stable condition.

Although the above mentioned leads to an apparently odd conclusion that the difference in the sand digging quantity does not have much affect on the bulldozing force (F), but is attributed to the scour curve. That is, this is because the horizontal factor of the constraining forces increases by a first-derivative of the scour curve when considering ice scouring as a constraining motion along the scouring curve, for example, the rate of upward movement (that is, when the attack angle is small). Seemingly this seems to lead to the result that in spite of the difference in sand excavation quantity, the bulldozing force(F) does not change much (Refer to Section 4.5).

4.4 Behavioral characteristics of a model keel in ice scouring

4.4.1 Scour curve and scour depth

As the quantity of scraped sand does not depend on the speed of movement of the keel at the same attack angle as shown in 4.2, the behavioral characteristics of the keel in conjunction with the attack angle change at the same speed of movement. Fig-11 (a) to Fig-11 (c) show the relationship between the scour curve and scour length (dimensionless at h_0). The thick lines in the figures indicate the sub-sea bed. Fig-12 (a) to Fig-12 (c) show the relationship between scour depth and scour length. For the scour curve, ice basically displacing upward in all cases. This vertical displacement mechanism seems to be caused by 1) occurrence of sand sliding at the surface at the front of the keel (Soil clumps are instantaneously pulverized and ice also is displaced in the same direction), 2) sliding between the front of the keel and sand becomes marked when the shear resistance of sand increases. After all, measurements vary even in identical situations. The smaller the attack angle, the smaller the variation index, decreasing the degree of difference. Also, when the attack angle becomes smaller, the rate of upward displacement of ice increases.

Next when taking behavioral Fig-12(a) to 12(c) into consideration, the value of the scour depth generally

reaches a ceiling instead of increasing continuously if the scour length increases. In other words, an extreme value or a maximum and the scour-curve cannot be linear (straight line). When closely observing a group of figures and carrying logic to extremes, ice can be said to basically have a periodic motion based on the subseabed, and that the cycle becomes small when the attack angle decreases. As a dynamic mechanism, when the keel penetrates the ground and the sand resistance increases, the ice is displaced vertically (See the previous section) and will be restored to the initial state when freed from the large sand resistance, repeating this movement. The amplitude is also expected to decrease accordingly, indicating that observing the amplitude at the initial cycle is sufficient. However, this experiment was conducted under simple and ideal conditions. In reality, because of such factors as 1) the complicated shapes of keel parts, 2) the keel part contacting with an unconsolidated (floating) part of the sub-sea bed separation occurs (especially a first-year pressure ridge) and 3) the rotation of ice (iceberg), 4) ice stays at the limit of environmental forces, the above mentioned items are impossible to be concluded. In fact in 2), separation occurs at the unconsolidated (floating) part and the ice block that is formed is stuck in the sub-sea bed (Woodworth-Lynas, 1998). In addition, some researchers analyze ice scouring as horizontal or linear (Chari 1978,1979, Yoon 1997). However, in many cases the attack angle is within 20-45 degrees, and by its behavior all the ice is presumed to displace upward non-linearly when considering the separation of unconsolidated parts at the bottom. The result of this research is believed to be reasonable as it shows practical safety.

4.4.2. Relationship between the maximum and the average of scour depth

First, if considering Z_{max}/Z_{mean} as a random variable and analyzing it by the same method of section 4.1, this amount follows the log-normal distribution under the same conditions. Similarly, the mean value and median were adopted as the representative figures of each case, and the Z_{max}/Z_{mean} values of each case were plotted in Fig-13 which shows that Z_{max}/Z_{mean} does not depend on the speed of movement of the keel or the attack angle and generally show the fixed value. In addition, as shown in Table 4, the C.O.V of the Z_{max}/Z_{mean} is generally smaller than the C.O.V of each Z_{max} and Z_{mean} .

Table 4 Comparison of C.O.V. between Z_{max}/Z_{mean} and Z_{max} , Z_{mean}

Case No.	C.O.V (Z_{max}/h_0)	C.O.V (Z_{mean}/h_0)	larger or smaller	C.O.V (Z_{max}/Z_{mean})	Z_{max}/Z_{mean} (average)
a1v1	0.089	0.113	>	0.056	1.723
a1v2	0.239	0.219	>	0.074	1.461
a1v3	0.241	0.246	>	0.081	1.940
a1v4	0.123	0.069	-	0.090	1.671
a2v2	0.121	0.114	>	0.020	1.876
a3v2	0.105	0.085	-	0.089	1.711

The estimation of Z_{max} is practically important, but generally is difficult. Accordingly, these results show we can estimate the Z_{max} to be an average when investigating the partly lost scour site by the site survey or when measurements are relatively scarce. Or, by using some kind of methodology, Z_{max} can be estimated with relatively good accuracy by the average value of its entire range of intervals when simulating the scour curve (Assuming Z_{max} from its simulation probably requires an enormous number of simulation repetitions.)

4.4.3 Local variation response characteristics of the scour curves and the ice force (bulldozing force)

Fig-14 provides an example of local variations (first-derivative values) in the scour curves and F/W associated with the scour length. Although slight variations in the phase angles still remain, both curves are quite similar and are consistent in their peaking patterns, which is primarily due to variations in the horizontal constraining force proportional to the derivative of the scour curves in so far as the constrained movement of the ice along the scour curves is considered. Local variations in the ice force (bulldozing force) might therefore be understood as responses to local variations in the scour curves (see Section 4.5).

4.5 Assessment of the dynamic model

In this section, an assessment is made of whether the dynamic model assumed in Chapter 3 replicates actual events. The assessment is made indirectly by comparing the F obtained from simulating the dynamic model and the time series variability and their absolute values of the F actually observed.

4.5.1 Comparison of the observed values and the calculated values

Given the scope of our discussion, a typical case from each experiment is shown as an example, while the results from the simulation experiments are omitted. Two examples are given from Experiment a1v2 ($n=29$, $V_0=5\text{cm/s}$, attack angle=90 deg), which was repeated more than other experiments. Fig-15(a) to 15(c) represent the attack angle at 90, 45 and 30 degrees, with V_0 held constant at 5cm/s. Fig-16(a) to 16(d) represent V_0 at 1, 5, 10, 20cm, with the attack angle held constant at 90 degrees. The horizontal axis represents the quotient of the scour length divided by the initial water level (the actual time line). The thick line indicates observed values and the thin line indicates values from the simulation.

Fig-15(a) to 15(c) suggest a tendency in the variability of F to decrease as the attack angle diminishes, as discussed above. Moreover, the absolute value of F does not vary markedly with the attack angle, as discussed above. While the observed values are slightly greater, in absolute terms, than the values from the simulation, the phase angles

of the curves and the peaks match once again, indicating that the simulation usually replicated the behavior of the actual experiment, which indirectly indicates a constrained motion along the curvature with the ice. These findings show that our model is appropriate under the experimental conditions.

Fig-16(a) to 16(d) show an increase in F as the speed of the keel increases. Comparing the observed values and the values from the simulation, the absolute value of the movement speed below 5cm/s corresponds to the curves, but above 10cm/s, the observed values are greater, indicating that the behavior is not replicated accurately, which is attributable to the following possible reasons that were excluded from our calculations:

- 1) As the speed of movement of the keel surpasses that of the sand displaced by the keel towards the keel, or surpasses the speed at which the resting angle of the sand is formed, the apparent resting angle of the sand depositing on the frontal side of the keel increases, the amount of erosion to the side decreases, and the resistance of the sand increases (i.e. the amount of sand on the frontal side of the keel increases).
- 2) Because of 1), the sand at the surface of the water caused calculation errors (viscosity, meniscus, an increase in consistency, unit volume weight of the exposed sand).
- 3) Increases in the unit weight attributable to 1), the angle of the internal friction, and the shear strength, due to dilatancy effect.
- 4) Pore water pressure.

the scour curve must be considered, for even at the same scour depth the ice load on the ground at a point varies depending on the course of flow. When protecting a buried structure from ice, installing the structure below the maximum scour depth does not necessarily ensure safety. Estimating K acting upon the ground is important, because of stress transmission and deformation in the sand below the keel

4.5.2 Relationship between ice force (bulldozing force) and subgrade reaction

Fig-17 shows an example of the relationship between F and the load K_v that acts upon the ground surface. The results of simulation show a fairly strong consistency with the observed value F . Accordingly, K_v is greater than F , which indicates a constant of approximately 1.6 regardless of the attack angle or the scour length. In view of other studies, the results from our simulation are, despite slight differences in the definition of force, similar to the test results showing that the vertical ice load is 1 to 1.5 times the horizontal ice load (Poulin, 1992) and to the results from simulations based on the finite element method (approximately three times) (Yang, 1991). Therefore, once F is estimated, the load of the ice on the ground can also be obtained.

5 CONCLUSIONS

1. Under the same conditions, the observed variables (F_{max} , F_{mean} , Z_{max} , Z_{mean}) follow a log-normal distribution.
2. Generally, the ice force F (bulldozing force) increases as the speed V_0 of the keel increases and its growth rate stays constant at $V_0 < 5\text{cm/s}$, increases rapidly at $5 < V_0 < 10$ and decreases at $10\text{cm/s} < V_0$. The geometric mean of the scour depth Z and the maximum scour depth Z_{max} remain constant, regardless of the speed of movement of the keel. No systematic relationship is found between the COV in each experimental case and the moving speed of movement of the keel.
3. No apparent change in F due to the ice force (bulldozing force) at the attack angle is found. However, a systematic relationship exists with the scour depth: the smaller the attack angle, the less erosion tends to occur. Also, as the attack angle diminishes, the COV of the measured variables decreases.
4. Z_{mean}/Z_{max} , the ratio of the maximum scour depth and the mean scour depth, is constant at 1.73 and is independent of the speed of movement of the keel and the attack angle. Therefore, deducing Z_{max} from Z_{mean} in simulations and experiments seems logical.
5. In all experimental cases the model keel is generally displaced upward and as the attack angle diminishes the rate of climb increases. Scour depth does not increase with the scour length at a constant rate, but extreme and maximum values exist and the scour curve is not necessarily linear. The ice shows a periodic motion in reference to the sub-sea bed, and as the attack angle diminishes the cycle is expected to shorten and the amplitude decrease.
6. Local variations in the ice force (bulldozing force) or subgrade reaction K are responses to local variations in the scour-curve. Hence, even at the same point (scour depth), the load of the ice varies depending on its course (scour-curve).
7. Comparing observed values and calculated values, the absolute values and the variability (curve and peak phases) of the changes over a particular time frame seem fairly consistent. However, at $10\text{cm/s} < V_0$, the observed values were clearly greater, indicating the need to include the speed-dependent changes in the dynamics of the sand.
8. The ratio of F and the vertical subgrade reaction K_v , K_v/F from the simulation remained constant at approximately 1.6 independent of the attack angle and the scour length.

ACKNOWLEDGEMENT

We wish to thank Technology Research Center, Japan National Oil Corporation (JNOC) who has supported this work.

REFERENCES

- Chari,T.R.,and Muthukrishnaiah,K.: Iceberg threat to ocean structures, Proceedings, Symposium on Ice Problems, International Association for Hydraulic Reserch, Lulea, Sweden, pp.421-432,1978.
- Chari,T.R.: Geotechnical aspects of iceberg scours on oceanfloors, Canadian Geotechnical Journal Vol.16, no.2, pp379-390,1979.
- Kioka,S., et al : Mechanical model of Ice Scour, Proc.of 15th International Conference on Port and Ocean Eng. Under Arctic Conditions, Helsinki, Vol.●, pp.537-544, 1999.
- Paulin,M.J.: Physical model analysis of iceberg scour in dry and submerged sand. M.Eng.Thesis, Memorial University of Newfoundland, St.John's Newfoundland, 1992.
- Woodworth-Lynas,C.M.T.: Sub-Scour Deformation and the Development of Ideas from Field Work in the Last Decade, Proceeding of Ice Scour and Arctic Marine Piplines Workshop, Hokkaido, Japan. Published by C-CORE, pp.33-38, 1998.
- Yang,Q.S.et al.: Analysis of Subscour Deformation by Finite Element Method, Proceedings 4th Canadian Conference on Marine Geotechnical Engineering, St. John's, Newfoundland, Canada, pp.739-754.
- Yoon,.Y.et al.:A numerical Simulation to Determine Ice Scour and Pipeline Burial Depth, Proceedings of the 7th International Offshore and Polar Engineering Conference Honolulu, USA, pp.212-219, 1997.

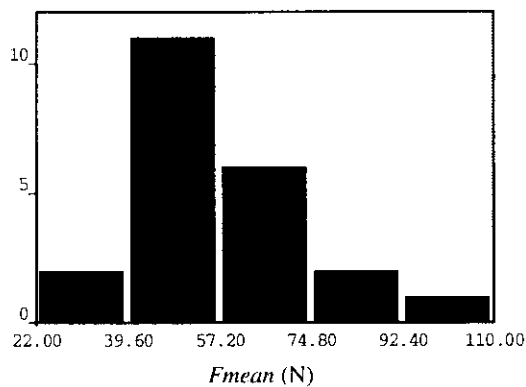


Figure.4(a) Histogram (Fmean)

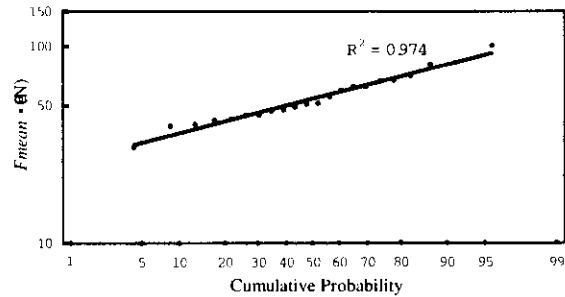


Figure 4(b) Probability paper (log-normal)

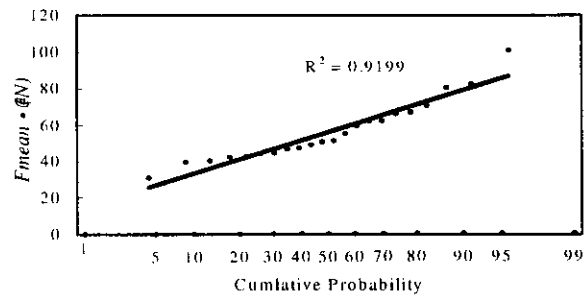


Figure 4(c) Probability paper (normal)

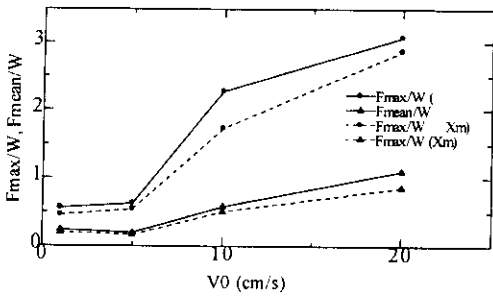


Figure 5. Dependence of the ice force on the velocity

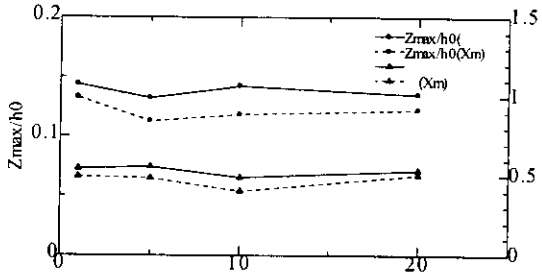


Figure 6. Dependence of the scour depth on the velocity

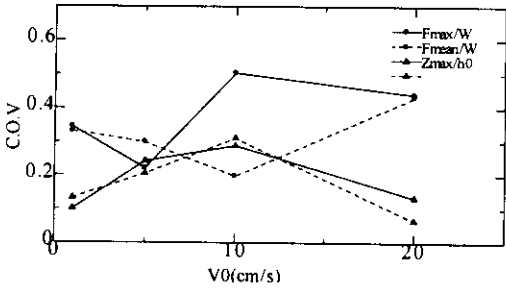


Figure 7. Transitions of the COV with respect to the velocity

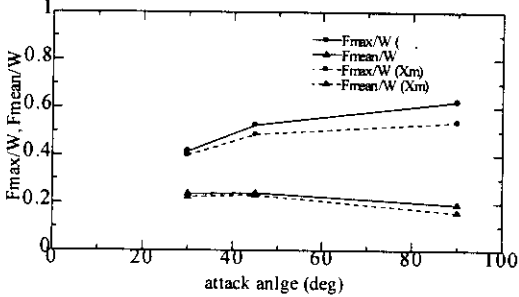


Figure 8. Dependence of the ice force on the attack angle

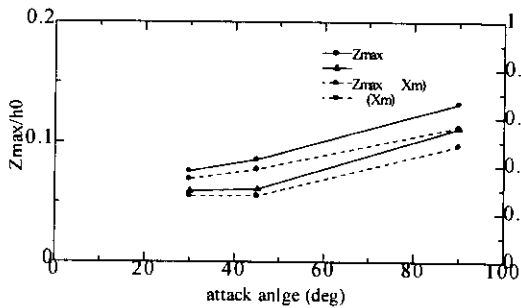


Figure 9. Dependence of the scour depth on the attack angle

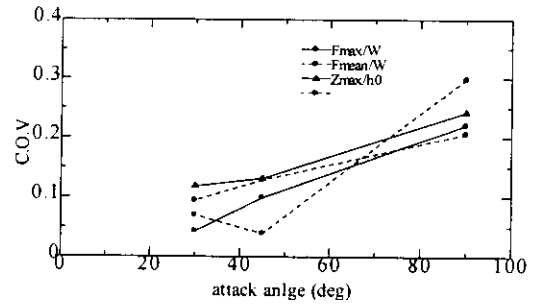


Figure 10. Transitions of the COV with respect to the velocity

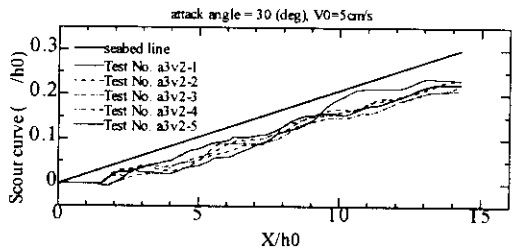
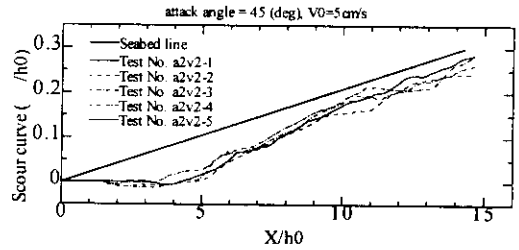
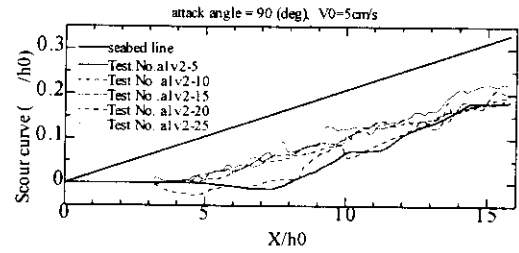
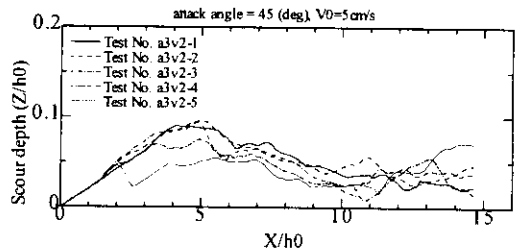
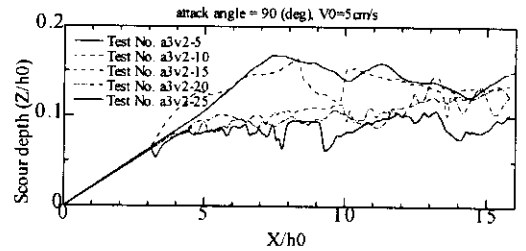


Figure 11 (a)-(c). Behavioral characteristics of a model keel in ice scouring



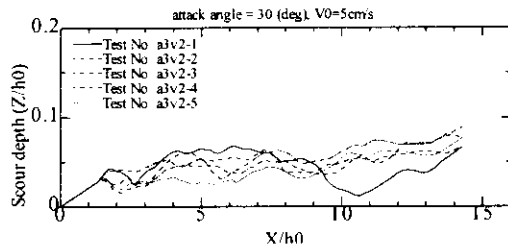


Figure 12 (a)-(c). Variation of scour depth in conjunction with the attack angle

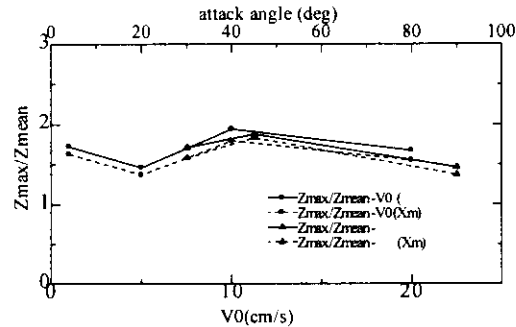


Figure 13. Dependency of Z_{max}/Z_{mean} on the velocity and the attack angle

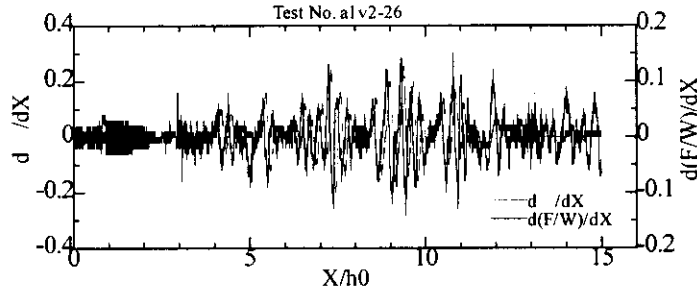


Figure 14. Local variation response characteristics of the scour curve and the ice force (bulldozing force)

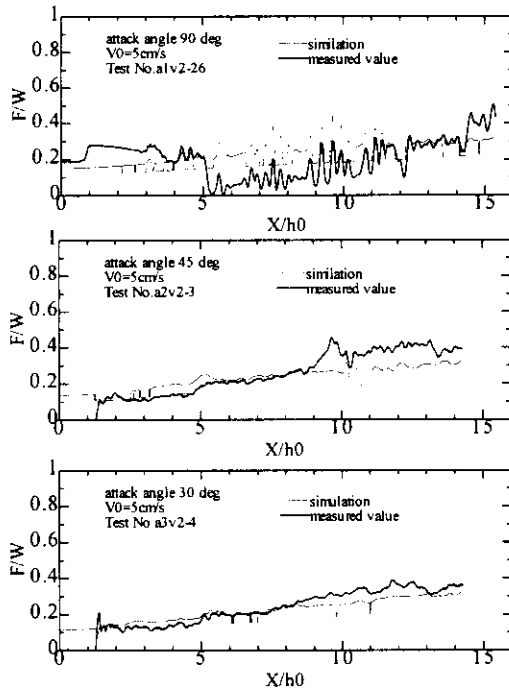


Figure 15 (a)-(c). Experimental and analytical result ($V_0=5\text{cm/s}$)

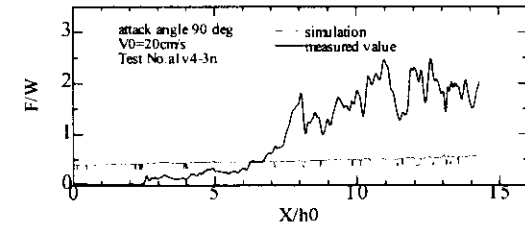
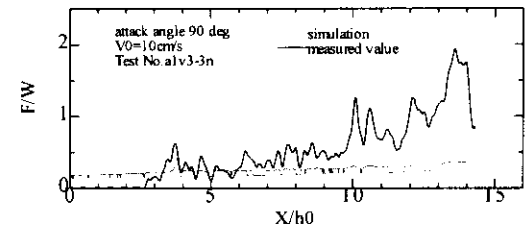
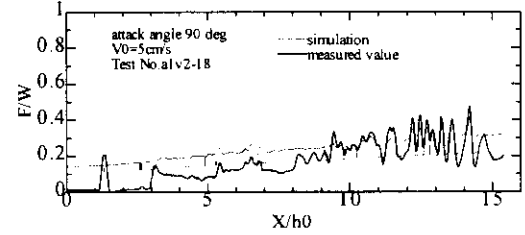
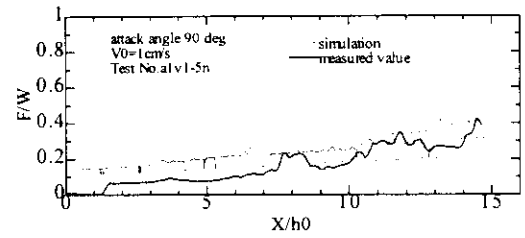


Figure 16 (a)-(d). Experimental and analytical result (attack angle = 90 deg)

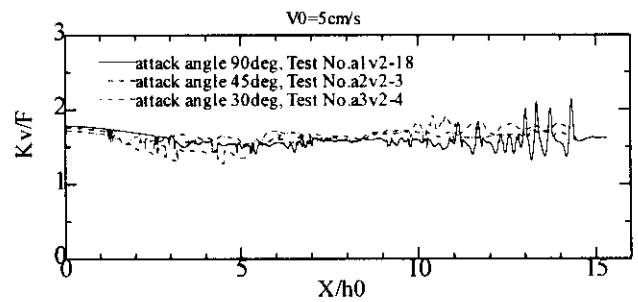


Figure 17. Relationship between ice force F (bulldozing force) and subgrade reaction K_v (the load that acts upon the ground surface)

**2nd ICE SCOUR & ARCTIC MARINE PIPELINES
WORKSHOP
Mombetsu, Hokkaido, Japan, 6-9 February 2000**

**NUMERICAL SIMULATION OF ICE SCOUR USING A STATIC ELASTO-
PLASTIC FEM ANALYSIS AND A STEADY STATE SEMI-ANALYTIC POWER
LAW SOLUTION**

A. FORIERO¹ and A. von KEVICZKY²

¹Département de génie civil, Université Laval, St.Foy (Québec), Canada

²Department of Mathematics, Concordia University, Montreal (Québec), Canada

1.0 Introduction

In recent years the subject of ice scouring has received considerable attention. In particular its effect on the serviceability of marine pipelines and other related sea bed structures is of major concern to decision makers. This even more so since the shift in the average temperature, as a result of global warming, undoubtedly increases the melt of glaciers and consequently of iceberg activity.

The main focus of studies in the past was the optimum depth of trenching necessary to place pipelines below the largest gouges (Clark et al., 1998). The reason being that pipelines must be trenched deeply enough to be completely safe, whilst sea depth is a significant cost factor.

Numerous experimental and theoretical studies have been undertaken to investigate large scour soil movements produced by ice features [Palmer, 1998; Kioka et al., 1998; Stepanov, 1998; Yang et al., 1996, 1994; Lach et al., 1993; Woodworth-Lynas, 1992; Been et al., 1990; Poorooshasb et al., 1990; Palmer et al., 1989]. Recently the authors (Foriero, 1998; Foriero and von Keviczky, 1999) considered strain-rate effects produced by ice features. The reason being that soils in general undergo time-dependent deformations under sustained shearing stresses. The advantage of this approach was to incorporate the steady state aspect of ice scouring by deriving a semi-analytical expression for the stress and strain field explicitly in terms of the iceberg velocity.

In the present paper the authors will compare their rate dependent model (Foriero and von Keviczky, 1999) with FEM simulations using a small strain plastic formulation. Specifically the finite element simulations are carried out by considering the ice feature in a pre-formed cavity, where the surrounding soil is assumed to be in its in-situ stress state. Subsequently, an elasto-plastic incremental analysis is carried out.

2.0 Modeling of Ice Scouring

Despite the many possible environmental conditions, field evidence indicates that by and large scour features are uniform in cross-section, while maintaining a relatively horizontal sea bed over long distances. A recent study by Blasco et al. [1998] confirms that the longest and deepest ice scour observed to date on the Canadian Beaufort Shelf occurs in marine clay, which has length of 50.5 km and maximum scour depth of 8.5m. The scour width recorded in that investigation varied from 80 to 20m. The water depths in the central shelf, where measurements were taken, ranged from 41 to 53m. Measurements were repeatedly mapped using sidescan sonar and echo sounders. A velocity of approximately 0.1m/s is generally observed as far as horizontal movements are concerned.

Hence for the present FEM simulations the following assumptions are formulated. As previously mentioned one of the dimensions (the width direction) is considered very large when compared to the depth of scour. It shall henceforth be assumed that soil movements are independent of the width direction (z-direction) and that the state of strain (plane strain), existing in the x-y plane, holds for all planes parallel to it. Moreover it is assumed that the ice feature produces an undrained loading of the surrounding sea bed soil. Consequently the FEM analyses, as related to drainage conditions, are of total undrained type where pore-water pressure changes could be computed on the basis of total stress changes by using the Skempton pore-pressure parameters.

Three interacting components of the ice scouring process are modeled in the present investigation. These are the ice feature, the ice-soil interface and the soil type.

The characteristic of the ice feature will be modeled using a linear elastic constitutive model to simulate a perfectly rigid body. We must point out this is only realistic in cases where the ice keel has sufficient strength to withstand the forces developed during scouring.

Slip elements were used to simulate the interface lying between the ice feature and the marine soil. This is necessary if one wishes to model slippage of the ice feature along the marine bottom. The constitutive model used for the slip surface element in the present simulations is a linear elastic one.

To model the marine soil a classic elastic perfectly plastic model is used in the FEM simulations. This constitutive behavior was chosen since it can readily be shown that the steady-state solution of viscoplastic problems is identical to the corresponding conventional static elasto-plastic solution.

3.0 Finite Element Simulations

The finite element meshes for the insitu and ice scouring analysis are shown in Figures 1 and 2 respectively. The finite element analysis in this study was carried out with the SIGMA/W software from Geo-Slope International. As observed in these figures the ice feature is modeled as a rigid body with an ice keel having an angle of attack of 15° , its flat base lying at a depth of scour 2m below the level of the marine bed. The implication, here, that a representative stationary shape of the ice feature is achieved during the ice scouring process.

The extent of the problem geometry (which entails the ice feature, interface and soil) in the x and y directions is respectively 100m and 60m. A total of 6500 elements were used to model the region of interest. Quadrilateral elements were assigned different material properties or soil models. Thus for the ice a very high Young modulus was assumed in order to model the ice feature as a rigid body. The interface properties were such that a high value of normal rigidity was imposed to indicate the slip surface has little or no compressibility, and a very low value of shear rigidity to allow for slippage along the surface. As far as the soil type is concerned the only available parameters were those of Speswhite kaolin clay, also used by Yang et al. (1996) in their simulations.

In the first phase of the present simulations the ice feature was modeled using quadrilateral elements with linear elastic properties, a soil interface with quadrilateral slip elements having linear elastic properties with no maximum shear strength, and a soil with quadrilateral elements having elastic plastic properties. The parameters used in the simulations are as follows:

Ice feature

Material Model: Linear Elastic
Parameter Type: Total
E modulus: $5.73E+009$ kPa
Poisson's ratio: 0.49

Interface condition

Material Model: Linear Elastic
Parameter Type: Effective
Normal Stiffness: $K_n = 1.0E+007$ kN/m
Tangential Stiffness: $K_s = 1.0E-03$ kN/m

Soil type

Material Model: Elastic Plastic
Parameter Type: Total
E modulus: 5730 kPa
Poisson's ratio: 0.49
Cohesion: 20 kPa
Unit weight: 16.68 kN/m³

As mentioned all simulations of ice scouring were preceded by an insitu analysis. In general soil behavior is a function of the stress state. The total vertical insitu stress is computed on the basis of the unit weight of the soil, the redistributed net unit weight of

the ice feature $((\text{total weight of ice feature} - \text{buoyant force})/(\text{total ice feature volume}))$ and the hydrostatic water pressure acting on the seabed (water level assumed at 16 m above the seabed). The lateral boundaries of the mesh are fixed against horizontal movements while the bottom boundary is fixed against vertical ones. The horizontal stress is computed as the vertical stress multiplied by a K_0 -value set at 0.95 in the present simulations. The stress field resulting from the insitu analysis then provides the initial condition for the subsequent ice scouring event.

The ice scouring event was simulated by imposing a horizontal displacement at all nodes residing on the boundary of the ice feature. A total horizontal displacement of 0.1m was applied over 50 time increments during the ensuing incremental plasticity analysis (Fig. 3). A maximum of 20 iterations was allowed per time step, with a convergence criterion of 1% pertaining to the desired percentage difference in the norm of the nodal displacement vector between two successive iterations.

4.0 Results of FEM Simulation

Figure 4 depicts the deformed FEM mesh resulting from the imposed rigid movement of the ice keel (corresponding to the last time increment). One observes from this figure that the ice feature is shifted to the right and downwards. A closer look at this figure also indicates a severe distortion of the interface slip elements. However the finite elements representing the soil mass did not present significant distortions which confirms the utility of slip elements in modeling interface conditions.

The no volume change condition imposed in the simulations was also clearly distinguishable in this figure (Fig.4). This is noticeable from the heaving produced in front of the ice feature.

Figure 5 illustrates the horizontal displacements in the soil mass, as a function of depth, at a horizontal distance of 43.74 m from the origin. Specifically these displacements originate in the soil mass at points below the midpoint of the ice keel. Clearly the relative displacement between the ice feature and the soil mass is quite evident if one keeps in mind that the imposed rigid displacement of the ice feature over 50 time increments equaled 0.1m. This results from the assumption that the interface was simulated as completely smooth.

Results (Fig. 5) also indicate a decrease in the horizontal displacement with depth. Interestingly enough the vertical displacements as a function of depth (Fig. 6), for the same points, indicate vertical displacements approximately 30% lower than the previous horizontal ones. This is attributed to the inclined face of the ice keel and consequently vertical displacements should not be overlooked. Vertical displacements are important even though the ice movement in the present simulations is imposed as horizontal (no vertical constraint along the boundaries of the ice feature).

Figure 7 depicts the deviatoric strain as a function of depth over the different time increments considered. In general the deviatoric strain increases, as expected, with the ice feature movement. However with respect to a time increment, the deviatoric strain increases beyond the depth of scour, to then decrease continuously. We also show in this figure the semi-analytic solution (hereafter described) which yields in general larger value of deviatoric strain.

Another interesting observation is that of the state of stress produced in the soil at the midpoint immediately below the ice keel. Figures 8 and 9 for the respective time increments of 1 and 50 demonstrate a rotation of the major and minor principle stresses as the ice keel is displaced horizontally.

5.0 Semi-analytic Solution

This section describes a semi-analytic approach to determine the stress and strain rate field, in a strain rate mode of deformation (Foriero and Kevicsky, 1999; Foriero 1998). The model described herein is valid for a stationary state of stress, attained after a continuous redistribution beginning with the initial elastic state. However one must keep in mind the model does not take account of the initial resistance of the soil. The model reacts only to imposed horizontal velocities of the ice feature which is the problem of real interest here. Consequently one must not neglect to add the initial stress field to the one obtained with the herein semi-analytic model.

A conformal mapping scheme is utilized to transform the physical domain of interest to the canonical complex plane, in order to determine the velocity field. A bounding technique, based on the principle of virtual work, is then employed to determine a global force at the ice-soil interface. The strain field is determined by integrating the strain rate field along different strain paths.

Figure 10 describes the region considered for simulating ice scouring, wherein the previously mentioned two-dimensional plane strain analysis is applied. The angle θ of attack of the ice keel has as its initial side the positive real axis and is measured counterclockwise.

The idealized ice keel geometry is polygonal in nature and is composed of sharp corners, which renders the determination of the velocity field in the physical z -plane quite difficult. For this reason a suitable co-ordinate transformation is required to conformally map the z -plane onto the canonical ζ -plane and vice-versa. The conformal mapping $z = f(\zeta) = (\xi + i\eta)$ is obtained via the Schwarz-Christoffel transformation for polygons, whose most general form is

$$z = M \int_0^{\zeta} \prod_{i=1}^n (s - \xi_i)^{\frac{\alpha_i}{\pi} - 1} ds + N \quad (1)$$

[Behnke and Sommer, 1962]. Herein ξ_i are fixed complex numbers denoting the n corners of the polygon in the canonical ζ -plane, α_i are the respective internal positive corner angles measured in radians, and M and N are constants to be determined. Based on Fig. 10, the application of the Schwarz-Christoffel transform reduces [1] to

$$z = M \int_0^{\zeta} s^m (s-1)^{-m} ds + N, \quad (2)$$

where for reasons of simplification $m = \theta / \pi$ (θ is the angle of attack of the ice keel). The constants M and N are calculated from the boundary conditions

$$z = 0 \quad \text{if} \quad \zeta = 0, \quad z = a + id \quad \text{if} \quad \zeta = 1, \quad (3)$$

where d represents the scour depth and $a = d/\tan(\theta)$ as depicted in Fig. 10. After substituting conditions [3] into equation [2], one obtains

$$N = 0, \quad M = \frac{\sqrt{a^2 + d^2} \sin(m\pi)}{m\pi}. \quad (4)$$

Equation [2] is therefore rewritten as

$$z(\zeta) = z(\xi + i\eta) = x + iy = \frac{\sqrt{a^2 + d^2} \sin(m\pi)}{m\pi} \int_0^{\xi + i\eta} s^m (s-1)^{-m} ds \quad (5)$$

and further transformed, in order to reduce the numerical difficulties one encounters while computing integrals (a closed form solution of integral [5] is not possible except for few specific values of m).

The integration of equation [5] is achieved via the substitutions

$$s = (\xi + i\eta)t, \quad ds = (\xi + i\eta)dt, \quad (6)$$

which lead to

$$x + iy = \frac{\sqrt{a^2 + d^2} \sin(m\pi) (\xi + i\eta)^{1+m}}{m\pi} \cdot \int_0^1 t^m [(\xi + i\eta)t - 1]^{-m} dt \quad (0 \leq t \leq 1) \quad (7)$$

as a consequence of [5]. Expressions for $x(\xi, \eta)$ and $y(\xi, \eta)$ are readily obtained as

$$\begin{aligned}
x(\xi, \eta) = & \frac{\sqrt{a^2 + d^2} \sin(m\pi) (\xi^2 + \eta^2)^{\frac{(1+m)}{2}}}{m\pi} \cdot \cos \left\{ 2(m+1) \cdot \arctan \left(\frac{\eta}{\sqrt{\xi^2 + \eta^2 + \xi}} \right) \right\} \cdot D(\xi, \eta) + \\
& \frac{\sqrt{a^2 + d^2} \sin(m\pi) (\xi^2 + \eta^2)^{\frac{(1+m)}{2}}}{m\pi} \cdot \sin \left\{ 2(m+1) \cdot \arctan \left(\frac{\eta}{\sqrt{\xi^2 + \eta^2 + \xi}} \right) \right\} \cdot E(\xi, \eta)
\end{aligned} \tag{8}$$

and

$$\begin{aligned}
y(\xi, \eta) = & \frac{\sqrt{a^2 + d^2} \sin(m\pi) (\xi^2 + \eta^2)^{\frac{(1+m)}{2}}}{m\pi} \cdot \sin \left\{ 2(m+1) \cdot \arctan \left(\frac{\eta}{\sqrt{\xi^2 + \eta^2 + \xi}} \right) \right\} \cdot D(\xi, \eta) - \\
& \frac{\sqrt{a^2 + d^2} \sin(m\pi) (\xi^2 + \eta^2)^{\frac{(1+m)}{2}}}{m\pi} \cdot \cos \left\{ 2(m+1) \cdot \arctan \left(\frac{\eta}{\sqrt{\xi^2 + \eta^2 + \xi}} \right) \right\} \cdot E(\xi, \eta),
\end{aligned} \tag{9}$$

where

$$D(\xi, \eta) = \int_0^1 t^m \left[(\xi t - 1)^2 + \eta^2 t^2 \right]^{-\frac{m}{2}} \cdot \cos \left\{ 2m \cdot \arctan \left(\frac{\eta t}{\sqrt{(\xi t - 1)^2 + \eta^2 t^2 + \xi t - 1}} \right) \right\} dt \tag{10}$$

and

$$E(\xi, \eta) = \int_0^1 t^m \left[(\xi t - 1)^2 + \eta^2 t^2 \right]^{-\frac{m}{2}} \cdot \sin \left\{ 2m \cdot \arctan \left(\frac{\eta t}{\sqrt{(\xi t - 1)^2 + \eta^2 t^2 + \xi t - 1}} \right) \right\} dt. \tag{11}$$

Typical meshes for angles of attack of 15°, 30°, 60° and 90° degrees (of the ice keel) are shown respectively in figures 11, 12, 13 and 14. These were obtained by means of equations [8] to [11] using a uniform mesh representing the transformed domain. This demonstrates the versatility of the conformal mapping generation scheme by observing, that straight lines in the canonical plane ζ transform into different curves emerging from the ice keel shape in the physical plane (Fig. 11, 12, 13 and 14) for all positive angles of attack of the ice keel. One immediately notices from the previous figures, that an increase in the angle of attack produces a conformal decrease in the elementary area of the

physical domain. Moreover, the previous conformal mapping scheme (Equations [8] to [11]) is a valid tool for generating FEM meshes in the case of piles as well as embankments.

The two-dimensional incompressible complex potential flow solution is obtained as follows. In the physical plane

$$V_x - iV_y = -\frac{d\Omega}{dz} = -\frac{d\Omega}{d\zeta} \frac{d\zeta}{dz} = -\frac{d\Omega/d\zeta}{dz/d\zeta}, \quad (12)$$

while in the transformed (canonical) plane the complex potential takes the form

$$\Omega = U\zeta. \quad (13)$$

The velocity field in the physical plane, calculated from [12], becomes

$$V_x = -V \cdot \left[\frac{(\xi-1)^2 + \eta^2}{\xi^2 + \eta^2} \right]^{\frac{m}{2}} \cos \left\{ 2 \cdot m \cdot \arctan \left(\frac{\eta}{\sqrt{(\xi-1)^2 + \eta^2 + \xi - 1}} \right) - 2 \cdot m \cdot \arctan \left(\frac{\eta}{\sqrt{\xi^2 + \eta^2 + \xi}} \right) \right\} \quad (14)$$

and

$$V_y = V \cdot \left[\frac{(\xi-1)^2 + \eta^2}{\xi^2 + \eta^2} \right]^{\frac{m}{2}} \sin \left\{ 2 \cdot m \cdot \arctan \left(\frac{\eta}{\sqrt{(\xi-1)^2 + \eta^2 + \xi - 1}} \right) - 2 \cdot m \cdot \arctan \left(\frac{\eta}{\sqrt{\xi^2 + \eta^2 + \xi}} \right) \right\}. \quad (15)$$

The strain rates in the physical plane are expressed in terms of

$$\dot{\varepsilon}_{xx} = \frac{\partial V_x}{\partial x}, \quad \dot{\varepsilon}_{yy} = \frac{\partial V_y}{\partial y}, \quad \dot{\varepsilon}_{xy} = \frac{1}{2} \left(\frac{\partial V_x}{\partial y} + \frac{\partial V_y}{\partial x} \right), \quad (16)$$

in which the terms $\dot{\varepsilon}_{xx}$, $\dot{\varepsilon}_{yy}$ and $\dot{\varepsilon}_{xy}$ are respectively the normal strain rate in the x-direction, the normal strain rate in the y-direction and the tensorial shear strain rate. These are given as

$$\dot{\varepsilon}_{xx} = -\frac{m^2\pi}{\sqrt{a^2+d^2}\sin(m\pi)} \cdot V \cdot (\xi^2 + \eta^2)^{\frac{-2m-1}{2}} \cdot \left((\xi-1)^2 + \eta^2 \right)^{\frac{2m-1}{2}} \cdot \cos \left((-4m-2) \cdot \arctan \left\{ \frac{\eta}{\sqrt{\xi^2 + \eta^2 + \xi}} \right\} + (4m-2) \cdot \arctan \left\{ \frac{\eta}{\sqrt{(\xi-1)^2 + \eta^2 + (\xi-1)}} \right\} \right) \quad (17)$$

$$\dot{\varepsilon}_{yy} = \frac{m^2\pi}{\sqrt{a^2+d^2}\sin(m\pi)} \cdot V \cdot (\xi^2 + \eta^2)^{\frac{-2m-1}{2}} \cdot \left((\xi-1)^2 + \eta^2 \right)^{\frac{2m-1}{2}} \cdot \cos \left((-4m-2) \cdot \arctan \left\{ \frac{\eta}{\sqrt{\xi^2 + \eta^2 + \xi}} \right\} + (4m-2) \cdot \arctan \left\{ \frac{\eta}{\sqrt{(\xi-1)^2 + \eta^2 + (\xi-1)}} \right\} \right) \quad (18)$$

and

$$\dot{\varepsilon}_{xy} = \frac{m^2\pi}{\sqrt{a^2+d^2}\sin(m\pi)} \cdot V \cdot (\xi^2 + \eta^2)^{\frac{-2m-1}{2}} \cdot \left((\xi-1)^2 + \eta^2 \right)^{\frac{2m-1}{2}} \cdot \sin \left((-4m-2) \cdot \arctan \left\{ \frac{\eta}{\sqrt{\xi^2 + \eta^2 + \xi}} \right\} + (4m-2) \cdot \arctan \left\{ \frac{\eta}{\sqrt{(\xi-1)^2 + \eta^2 + (\xi-1)}} \right\} \right) \quad (19)$$

Constitutive power law creep model

The rationale for adopting herein the constitutive equation are as follows: extensive practical applicability, clear comprehensibility, computer program adaptability and a single step creep test at various stresses and temperatures is adequate for solvability.

In general, the total strain ε comprises of an instantaneous strain ε_0 and a delayed or creep strain $\varepsilon^{(c)}$ as given by

$$\varepsilon = \varepsilon_0 + \varepsilon^{(c)} \quad (20)$$

The instantaneous strain may contain an elastic and a plastic component, while the creep strain is generally composed of both primary and secondary (steady-state) strains. For the considerations discussed in this article, stationary or secondary creep is considered according to

$$\varepsilon = \varepsilon^{(i)} + \varepsilon_{\min}^{(c)} t \quad (21)$$

Herein $\varepsilon^{(i)}$ and $\varepsilon_{\min}^{(c)} \left(= \frac{d\varepsilon^{(c)}}{dt} \right)$ stand for the fictitious instantaneous strain response and the minimum strain rate respectively, where $\varepsilon^{(i)}$ is obtained by extrapolating the constant rate portion of the creep curve back at $t = 0$. In terms of the available literature on creep [Hult, 1966, Ladanyi, 1972], it is has been established that both $\varepsilon^{(i)}$ and $\varepsilon_{\min}^{(c)}$ are expressible as

$$\varepsilon^{(i)} = \varepsilon_k \left(\frac{\sigma}{\sigma_{k\theta}} \right)^k, \quad \dot{\varepsilon}_{\min}^c = \dot{\varepsilon}_c \left(\frac{\sigma}{\sigma_{c\theta}} \right)^n \quad (22)$$

where $\sigma_{k\theta}$ is a temperature-dependent modulus corresponding to a reference strain rate ε_k ($k \leq 1$ an empirical exponent), and $\sigma_{c\theta}$ is the temperature-dependent creep modulus corresponding to the reference strain rate $\dot{\varepsilon}_c$, while $n \geq 1$ is an experimental creep exponent. As previously mentioned the semi-analytic solution presented herein does not incorporate the initial strain.

For the strain rate portion of the power law, the experimental strain rate parameters were unavailable for the Speswhite kaolin clay. However based on the undrained shear strength value of $c_u = 20\text{kPa}$ a realistic estimate was made possible.

For saturated clays in undrained shear Prapaharan et al. (1989) propose the following expression Ladanyi (1999)

$$q_u = q_\alpha \left[1 + \beta \ln \left(\frac{\dot{\varepsilon}}{\dot{\varepsilon}_\alpha} \right) \right] \quad (23)$$

where q_u is the undrained compression strength at a strain rate $\dot{\varepsilon}$, q_α is the undrained compression strength at a reference strain rate $\dot{\varepsilon}_\alpha$, and β is the slope of normalized strength against logarithm of strain rate line. Different investigators show that β in the previous equation varies approximately between 7% and 10%.

If this data is replotted in a log (normalized stress) against log(strain rate), a set of approximate straight lines fitting the strain rate equation 22 results. This yields a value of $n = 25$ (Ladanyi, 1999) which is much lower then the value $n = 3.29$ obtained for the

Saint Jean-Vianney clay (Vaid et al., 1996) and used in past simulations by the authors (Foriero and Ladanyi, 1999). This is quite normal since Saint Jean-Vianney clay is extremely stiff clay. This ain't the case for Speswhite kaolin clay, which as previously mentioned, is quite soft ($c_u = 20$ kPa). For simulation purposes the following parameters were utilized in equation (22): $n = 25$, $\sigma_{cb} = 40$ kPa and $\dot{\epsilon}_c = 0.01\%$ / min. This is reasonable because if $n \rightarrow \infty$ (perfect plasticity), $\sigma = \sigma_{cb} = 40$ kPa which yields the undrained shear strength of Speswhite kaolin clay.

In the present semi-analytic model the multiaxial creep law of the form

$$\dot{\epsilon}_e = \frac{\dot{\epsilon}_o}{\sigma_o^n} \sigma_e^n = A \sigma_e^n, \quad (24)$$

is utilized where the effective strain rate and stress are given as

$$\dot{\epsilon}_e = \left(\frac{2}{3} \dot{\epsilon}_{ij}^c \dot{\epsilon}_{ij}^c \right)^{\frac{1}{2}}, \quad \sigma_e = \left(\frac{3}{2} S_{ij} S_{ij} \right)^{\frac{1}{2}} \quad (25)$$

in terms of Einstein summation convention for the indices ij ($1 \leq i, j \leq 3$).

Deviatoric stress field

For creep of a solid under the condition of multiaxial stress, the creep process is path dependent. One generally writes the theory in rate form, which provides a means of incorporating the path into the formulation. The creep strain rates are written in terms of the stress deviator tensor as follows

$$\dot{\epsilon}_{ij}^c = \lambda S_{ij} = \frac{3\dot{\epsilon}_e}{2\sigma_e} S_{ij} \quad (1 \leq i, j \leq 3), \quad (26)$$

where $\dot{\epsilon}_{ij}^c$, S_{ij} and λ are the respective creep strain rates, deviatoric stresses and a proportionality factor to be determined hereafter. The deviatoric tensor S_{ij} is derived from the total stress tensor σ_{ij} via

$$S_{ij} = \sigma_{ij} - \sigma_{oct} \delta_{ij} \quad (1 \leq i, j \leq 3), \quad (27)$$

where δ_{ij} is the Kronecker delta ($\delta_{ij} = 0, 1$ according as $i \neq j$ or $i = j$) and $\sigma_{oct} = \frac{1}{3} \sigma_{kk}$ is the octahedral shear stress ($1 \leq k \leq 3$).

The effective strain rate for the two dimensional idealization of ice scouring is obtained as:

$$\dot{\epsilon}_e = \frac{2}{\sqrt{3}} \left\{ \frac{m^2 \pi}{\sqrt{a^2 + d^2} \sin(m\pi)} V (\xi^2 + \eta^2)^{-\frac{2m-1}{2}} \left((\xi-1)^2 + \eta^2 \right)^{\frac{2m-1}{2}} \right\}. \quad (28)$$

Figure 15 represents the contours of the effective strain rates $\dot{\epsilon}_e$ during undrained scouring by an ice feature with angle of attack of 15° in Speswhite kaolin clay. Simulations were done with a horizontal velocity of $V = 6.0$ m/min. and at a vertical depth of $d = 2$ m. Computations (not shown here) also indicated that as the angle of attack increases, the range of influence exerted by the ice feature extends to greater distances. In particular, the effective strain rates of the same order of magnitude occupy a smaller region as the angle of attack increases.

Expressions [26] and [24] allows us to solve for the deviatoric stress field S_{ij} in terms of the strain rate fields $\dot{\epsilon}_{ij}$, specifically

$$S_{ij} = \frac{2}{3} \left(\frac{\sigma_o^n}{\dot{\epsilon}_o} \right) \sigma_e^{1-n} \dot{\epsilon}_{ij} \quad (1 \leq i, j \leq 3), \quad (29)$$

which further reduces to

$$S_{ij} = \frac{2}{3} \left(\frac{\sigma_o^n}{\dot{\epsilon}_o} \right)^{\frac{1}{n}} (\dot{\epsilon}_e)^{\frac{(1-n)}{n}} \dot{\epsilon}_{ij} \quad (1 \leq i, j \leq 3). \quad (30)$$

The deviatoric stress field is thus given as

$$S_{xx} = -\frac{1}{\sqrt{3}} \left[\left(\frac{\sigma_o^n}{\dot{\epsilon}_o} \right) \left(\frac{2}{\sqrt{3}} \right) \left[\frac{m^2 \pi V}{\sqrt{a^2 + d^2} \sin(m\pi)} \right] (\xi^2 + \eta^2)^{-\frac{2m-1}{2}} \left((\xi-1)^2 + \eta^2 \right)^{\frac{2m-1}{2}} \right]^{\frac{1}{n}}. \quad (31)$$

$$\cos \left\{ (-4m-2) \arctan \left(\frac{\eta}{\sqrt{\xi^2 + \eta^2 + \xi}} \right) + (4m-2) \arctan \left(\frac{\eta}{\sqrt{(\xi-1)^2 + \eta^2 + (\xi-1)}} \right) \right\},$$

$$S_{yy} = \frac{1}{\sqrt{3}} \left[\left(\frac{\sigma_o^n}{\dot{\epsilon}_o} \right) \left(\frac{2}{\sqrt{3}} \right) \left[\frac{m^2 \pi V}{\sqrt{a^2 + d^2} \sin(m\pi)} \right] (\xi^2 + \eta^2)^{-\frac{2m-1}{2}} \left((\xi-1)^2 + \eta^2 \right)^{\frac{2m-1}{2}} \right]^{\frac{1}{n}}. \quad (32)$$

$$\cos \left\{ (-4m-2) \arctan \left(\frac{\eta}{\sqrt{\xi^2 + \eta^2 + \xi}} \right) + (4m-2) \arctan \left(\frac{\eta}{\sqrt{(\xi-1)^2 + \eta^2 + (\xi-1)}} \right) \right\}$$

and

$$S_{xy} = \frac{1}{\sqrt{3}} \left[\left(\frac{\sigma_o^n}{\dot{\epsilon}_o} \right) \left(\frac{2}{\sqrt{3}} \right) \left[\frac{m^2 \pi V}{\sqrt{a^2 + d^2} \sin(m\pi)} \right] (\xi^2 + \eta^2)^{-\frac{2m-1}{2}} \left((\xi-1)^2 + \eta^2 \right)^{\frac{2m-1}{2}} \right]^{\frac{1}{n}} \cdot \sin \left\{ (-4m-2) \arctan \left(\frac{\eta}{\sqrt{\xi^2 + \eta^2 + \xi}} \right) + (4m-2) \arctan \left(\frac{\eta}{\sqrt{(\xi-1)^2 + \eta^2 + (\xi-1)}} \right) \right\}. \quad (33)$$

By substituting equations [31] to [33] into [25], the expression for the effective stress σ_e becomes

$$\sigma_e = \left[\left(\frac{\sigma_o^n}{\dot{\epsilon}_o} \right) \left(\frac{2}{\sqrt{3}} \right) \left[\frac{m^2 \pi V}{\sqrt{a^2 + d^2} \sin(m\pi)} \right] (\xi^2 + \eta^2)^{-\frac{2m-1}{2}} \left((\xi-1)^2 + \eta^2 \right)^{\frac{2m-1}{2}} \right]^{\frac{1}{n}}. \quad (34)$$

Figure 16 depicts the effective stress contours σ_e during undrained scouring by an ice feature with an angle of attack of 15° in Speswhite kaolinite clay. Just as for the effective strain rates, simulations were carried out for a horizontal velocity of $V = 6.0$ m/min. and a vertical depth of $d = 2$ m. As expected, results of other simulations indicate, that effective stresses increase with an increase in the angle of attack. Similarly, as in the case of the effective strain rates, specific values of effective stress occur at bulb shaped contours.

Global reaction based on the principle of virtual work

Based on the principles of virtual work one obtains

$$\frac{1}{V} \left(\frac{n}{n+1} \right) \left(\frac{\sigma_o^n}{\dot{\epsilon}_o} \right)^{\frac{1}{n}} \int_{Vol} (\dot{\epsilon}_e)^{\frac{(n+1)}{n}} dV \geq P, \quad (35)$$

(Calladine and Drucker, 1962; Drucker and Prager, 1952) which after substitution of the expression [28] for $\dot{\epsilon}_e$ yields

$$V^{\frac{1}{n}} \left(\frac{n}{n+1} \right) \left(\frac{\sigma_o^n}{\dot{\epsilon}_o} \right)^{\frac{1}{n}} \left(\frac{2}{\sqrt{3}} \right)^{\frac{n+1}{n}} \left(\frac{m^2 \pi}{\sqrt{a^2 + d^2} \sin(m\pi)} \right)^{\frac{n+1}{n}} \Pi \geq P. \quad (36)$$

Further, the quantity Π appearing in inequality [36] is the improper integral

$$\Pi = \int_{\xi=-\infty}^{\xi=\infty} \int_{\eta=0}^{\eta=-\infty} \left[(\xi^2 + \eta^2)^{\frac{-2m-1}{2}} \left((\xi-1)^2 + \eta^2 \right)^{\frac{2m-1}{2}} \right]^{\frac{n+1}{n}} \det \begin{pmatrix} \frac{dx}{d\xi} & \frac{dx}{d\eta} \\ \frac{dy}{d\xi} & \frac{dy}{d\eta} \end{pmatrix} d\eta d\xi \quad (37)$$

and it is rewritten in the following form

$$\Pi = \frac{(a^2 + d^2) \sin^2(m\pi)}{(m\pi)^2} \int_{\xi=-\infty}^{\xi=\infty} \int_{\eta=-\infty}^{\eta=0} (\xi^2 + \eta^2)^{\frac{-(2m+1)(n+1)}{2n} + m} \left((\xi-1)^2 + \eta^2 \right)^{\frac{(2m-1)(n+1)}{2n} - m} d\eta d\xi. \quad (38)$$

This global force per linear width P is evaluated numerically for different geometric and creep-parameter values. Alternatively, one can also calculate this value by integrating the deviatoric stress field at the ice-soil interface. The two approaches lead to different values of overall resistance [Foriero and Ladanyi, 1989].

Evaluations of the expression [36] for attack angles 15° is depicted in Fig. 17. Simulations were executed using the aforementioned Speswhite kaolin clay creep stress parameters, at a scouring depth $d = 2m$. One can clearly see that for a constant angle of attack, the overall reaction increases with the velocity of the ice feature. Moreover results of computations also indicate that for a constant velocity of ice scouring, the overall reaction is an increasing function of the angle of attack. This is explained by the change in projected area of the ice feature, as the angle of attack is increased.

In this case the FEM solution yields a higher value of global resistance then that obtained by the semi-analytic solution.

Conclusion

From the previous study one can conclude that both FEM and semi-analytic solutions are very parameter-sensitive. Overall behavior of the semi-analytic solution is encouraging particularly since it links the stress, strain rate and strain field directly to the ice feature velocity. It is truly a steady state solution. Specifically, in order to obtain the total solution, one must establish and account for the initial solution.

It is evident that undrained shear parameters, obtained at different strain rates, are required to fully assess the proposed semi-analytic solution. There is lack of such values for saturated clays in undrained shear at the moment. Nevertheless even with approximate values the semi-analytic solution does seem to capture the steady state aspect of the problem. Finally full scale tests are also needed and would be more appropriate for verification purposes.

Acknowledgement

The first author acknowledges the financial support by the organizing committee of the 2nd ISAMP Workshop, the Natural Sciences and Engineering Research Council of Canada (NSERC) and the Fonds pour la Formation de Chercheur et l'aide a la Recherche (FCAR).

References

Been K., Kosar K., Hachey J. and Rogers B.T. (1990) - *Ice scour models*. Proceedings, Ninth International Conference on Offshore Mechanics and Arctic Engineering, Houston, 5, pp. 179-188.

Behnke, H. und Sommer, F. (1962) - *Theorie der analytischen Funktionen einer komplexen Veränderlichen*. Springer-Verlag, Berlin, Gottingen, Heidelberg, pp 1-603.

Blasco S. M., Shearer J. M. and Myers R. (1998) - *Seabed Scouring by Sea-Ice: Canadian Beaufort Shelf*. Proceedings of Ice Scour and Arctic Marine Pipelines Workshop, Thirteenth International Symposium on Okhotsk Sea & Sea Ice and The Ice Scour and Arctic Marine Pipelines Workshop, Mombetsu, Hokkaido, Japan , pp. 53-58.

Calladine C. R. and Drucker D. C. (1962) - *Nesting surfaces of constant rate of energy dissipation in creep*. Quarterly of Applied Mathematics, 20(1), pp. 79-84.

Clark J. I., Phillips R. and Paulin M. (1998) - *Ice Scour Research for the Safe Design of Pipelines: 1978-1998*. Proceedings of Ice Scour and Arctic Marine Pipelines Workshop, Thirteenth International Symposium on Okhotsk Sea & Sea Ice and The Ice Scour and Arctic Marine Pipelines Workshop, Mombetsu, Hokkaido, Japan, pp. 1-7.

Drucker D. C. and Prager W. (1952).- *Soil mechanics and plastic analysis or limit design*. Quarterly of Applied Mathematics, Vol. 10(2), pp. 157-165.

Foriero, A. and Keviczky, A. (1999) - Schwarz-Chritoffel transform in steady state analysis of ice scouring of marine clay, Proceedings of the 52nd Canadian Geotechnical Conference, Regina, Saskatchewan, Canada, pp.7-13.

Foriero A. (1998) - *Steady state ice scouring of the sea bed*. Proceedings of Ice Scour and Arctic Marine Pipelines Workshop, Thirteenth International Symposium on Okhotsk Sea & Sea Ice and The Ice Scour and Arctic Marine Pipelines Workshop, Mombetsu, Hokkaido, Japan, pp. 83-99.

Hult J.A.H. (1966) - *Creep in engineering structures*. Blaisdell Publishing Co., Waltham, Mass.

Kioka S., Terai Y., Otsuka N., Honda H. and Saehi H. (1998) - *Mechanical model of ice gouging on sloping sandy beach*. Proceedings of Ice Scour and Arctic Marine Pipelines Workshop, Thirteenth International Symposium on Okhotsk Sea & Sea Ice and The Ice Scour and Arctic Marine Pipelines Workshop, Mombetsu, Hokkaido, Japan pp. 71-76.

Lach P. R., Clark J.I. and Poorooshab F. (1993) - *Centrifuge modelling of ice scour*. 4th Canadian Conference on Marine Geotechnical Engineering, St. John's, Newfoundland, pp. 356-374.

Ladanyi, B. (1999) - *Creep Behaviour of Frozen and Unfrozen Soils - A Comparison*. Proceedings of Cold Regions Conference, New Hampshire, pp.173-186.

Ladanyi B. (1972) - *An engineering theory of creep of frozen soil*. Canadian Geotechnical Journal, 9, pp. 63-80.

Martin J. B. (1964) - *A displacement bound technique for elastic continua subjected to a certain class of dynamic loading*. Journal of the Mechanics and Physics of Solids, 12, pp. 165-175.

Palmer A. (1998) - *Geotechnical evidence of ice scour as a guide to pipeline burial depth*. *Canadian Geotechnical Journal*, 34, pp. 1002-1003.

Palmer A., Konuk I., Love J., Been K. and Comfort G. (1989) - *Ice scour mechanisms*. Proceedings, Tenth International Conference on Port and Ocean Engineering under Arctic Conditions, Lulea, 1, pp. 123-132.

Poorooshab F., Clark J.I. and Woodworth-Lynas C.M.T. (1990) - *Small scale modelling of iceberg scouring of the seabed*. Proc. 10th International Conference on Port and Ocean Engineering under Arctic Conditions, Lulea, Sweden, Vol. 1, pp. 133-145.

Prapaharan, S., Chameau, J-L, & Holtz, R.D. (1989)- *Effect of strain rate on undrained strength derived from pressuremeter test*. *Geotechnique*, 39, 4, pp. 615-624.

Stepanov I. V. (1998) - *Statistical analysis of the shape characteristics of hummocks in Baydaratskaya Bay*. Proceedings of Ice Scour and Arctic Marine Pipelines Workshop, Thirteenth International Symposium on Okhotsk Sea & Sea Ice and The Ice Scour and Arctic Marine Pipelines Workshop, Mombetsu, Hokkaido, Japan, pp. 71-76.

Vaid P. Y., Robertson P.K. and Campanella R.G. (1979) - *Strain rate behaviour of Saint-Jean-Vianney clay*. *Journal of Geotechnical Engineering*, 16, pp. 34-42.

Woodworth-Lynas C.M.T. (1992) - *Observed deformations beneath relict iceberg scours*. Proc. Workshop on Ice Scouring and the Design of Offshore Pipelines, Calgary, Alberta, pp. 103-125.

Yang Q. S., Poorooshab H.B. and Lach P.R. (1996) - *Centrifuge modelling and numerical simulation of ice scour*. Soils and Foundations, Vol. 36, No. 1, pp. 85-96.

Yang Q. S., Poorooshab H. B, Lack P.R. and Clark I.J. (1994)- *Comparison of physical and numerical models of ice scour*. Computer Methods and Advances in Geomechanics, Siriwardane & Zaman (eds.), pp. 1795-1801.

Finite Element Mesh
Initial Conditions

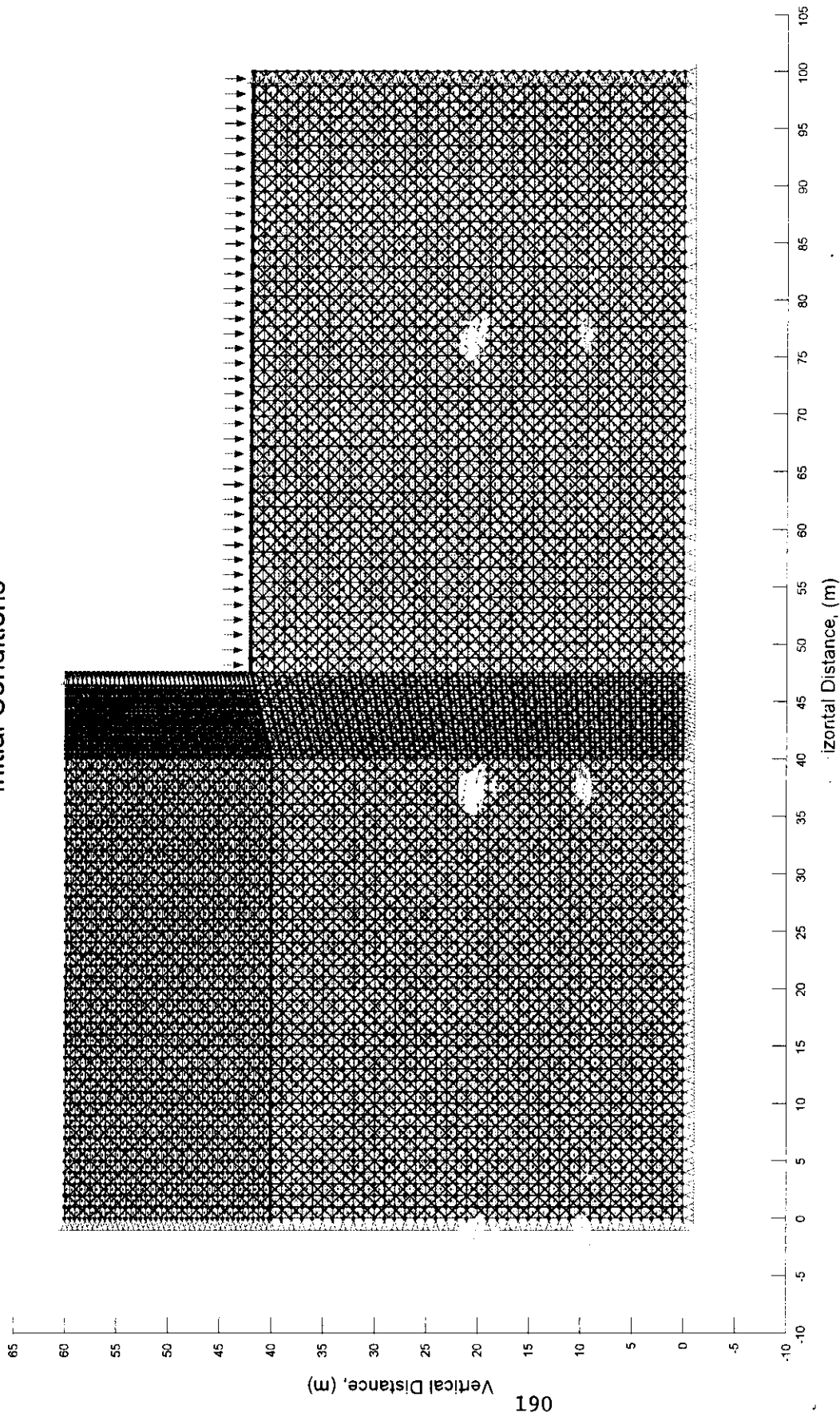


Figure 1. Finite element mesh used for initial condition simulations.

Finite Element Mesh

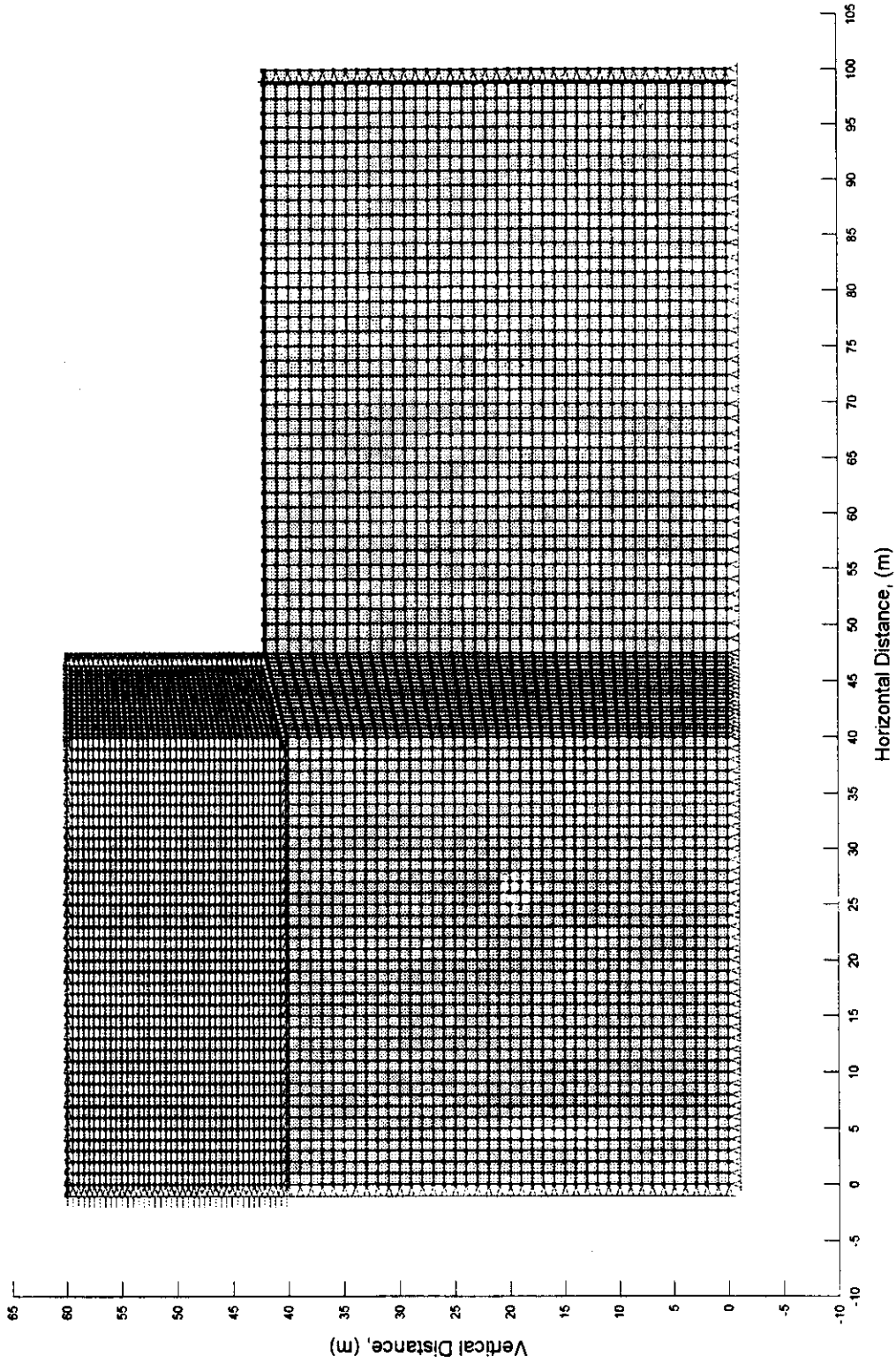


Figure 2. Finite element mesh used in ice scour simulations.

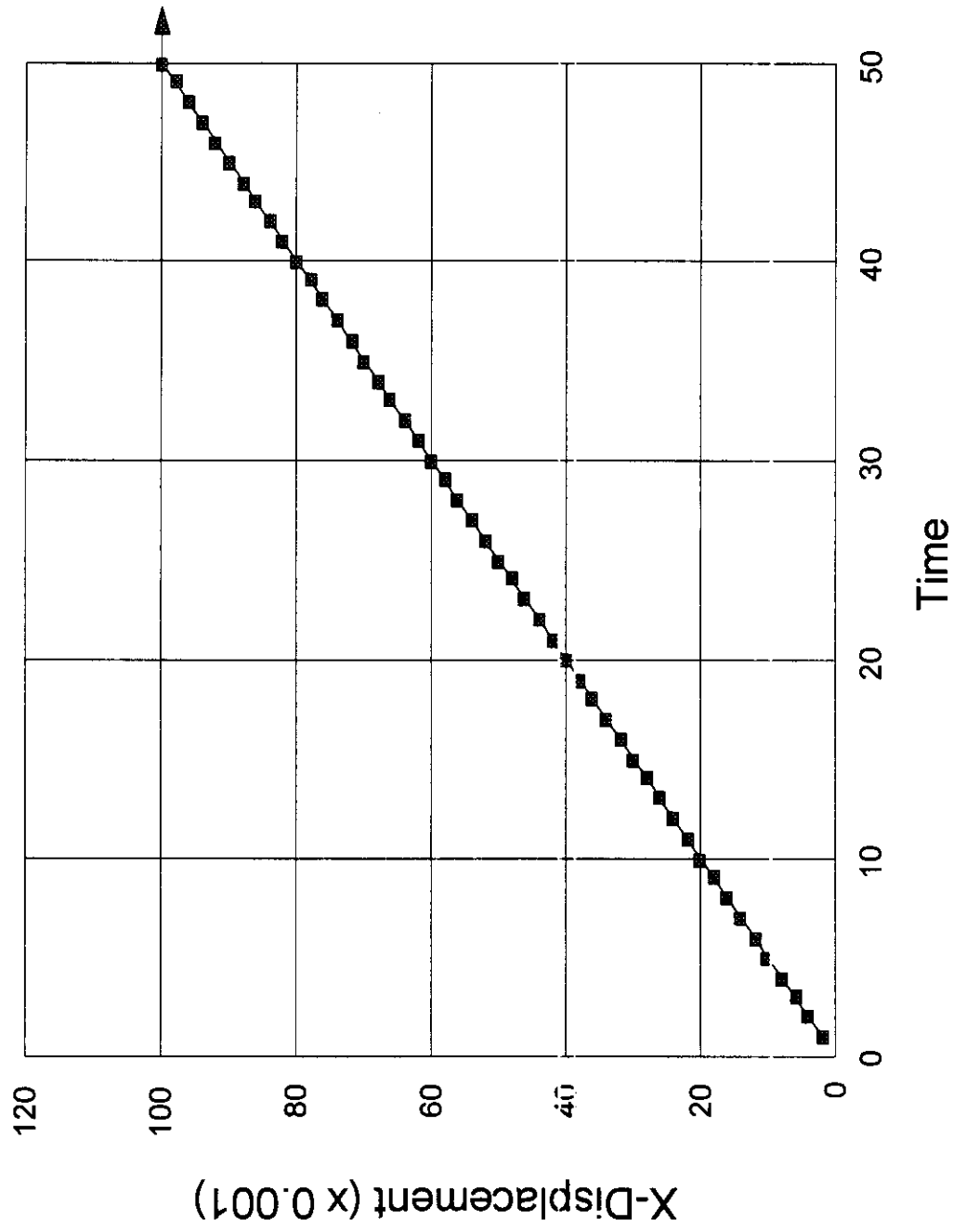


Figure 3. Imposed horizontal movement of ice feature.

Deformed Mesh
Horizontal Displacement of Ice Feature = 0.1 m

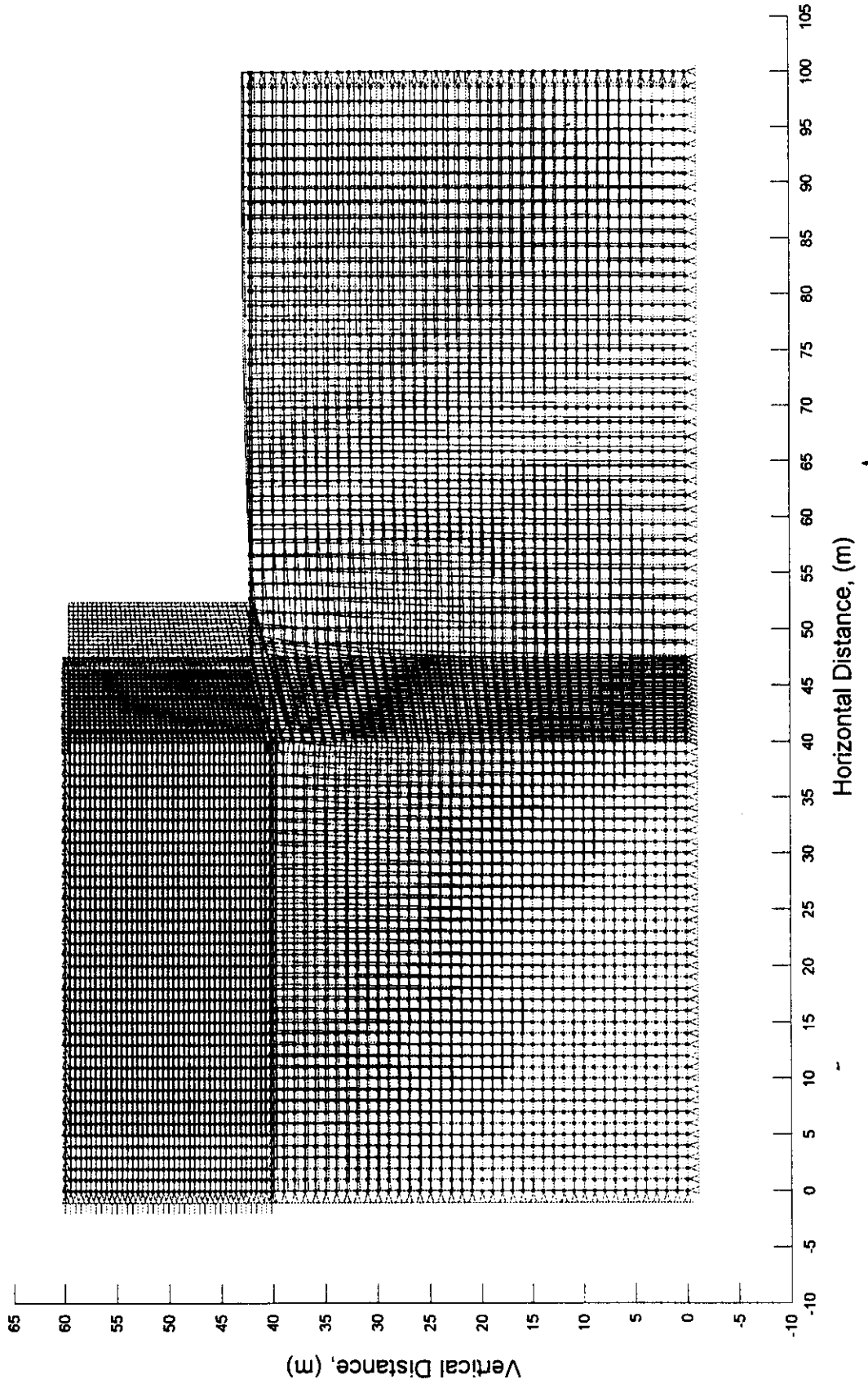


Figure 4. Deformed FEM mesh resulting from the ice feature movement.

Horizontal Displacement vs. Y-coordinate at
 $X = 43.740 \text{ m}$

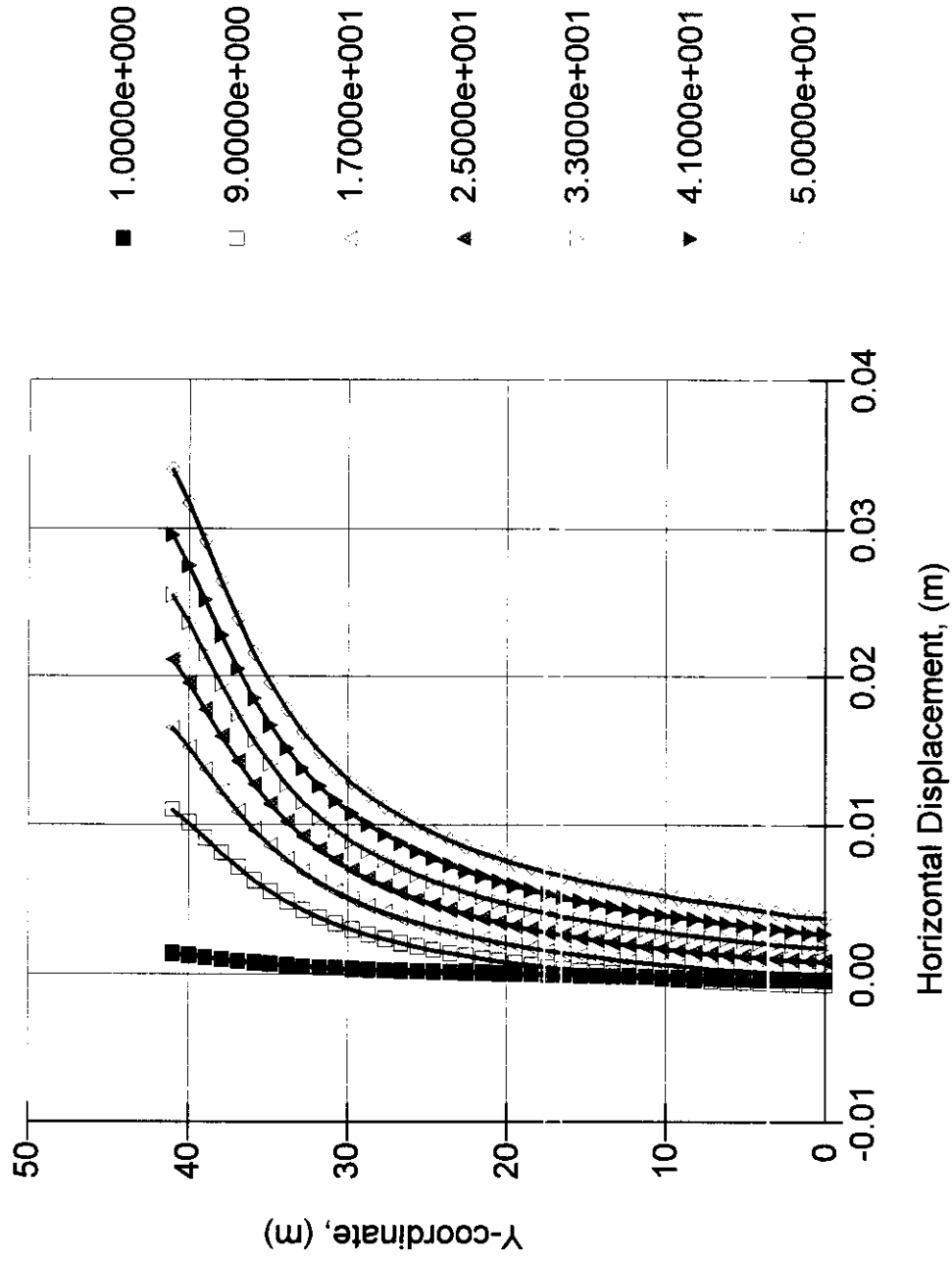


Figure 5. Horizontal displacements below inclined face of ice keel.

Vertical Displacement vs. Y-coordinate at
 $X = 43.740 \text{ m}$

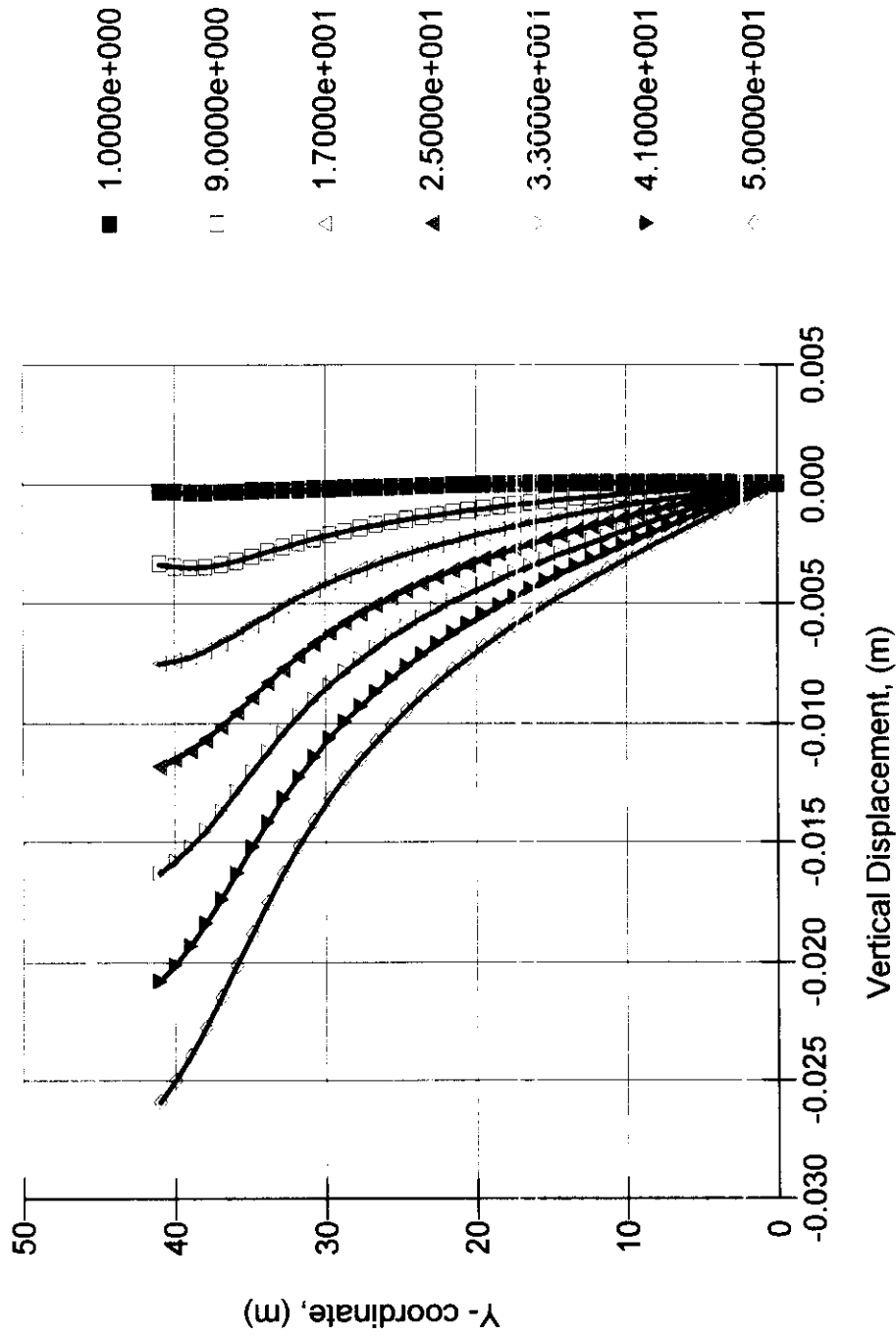


Figure 6. Vertical displacements below inclined face of ice-keel.

Deviatoric Strain vs. Y-coordinate at X = 43.74 m

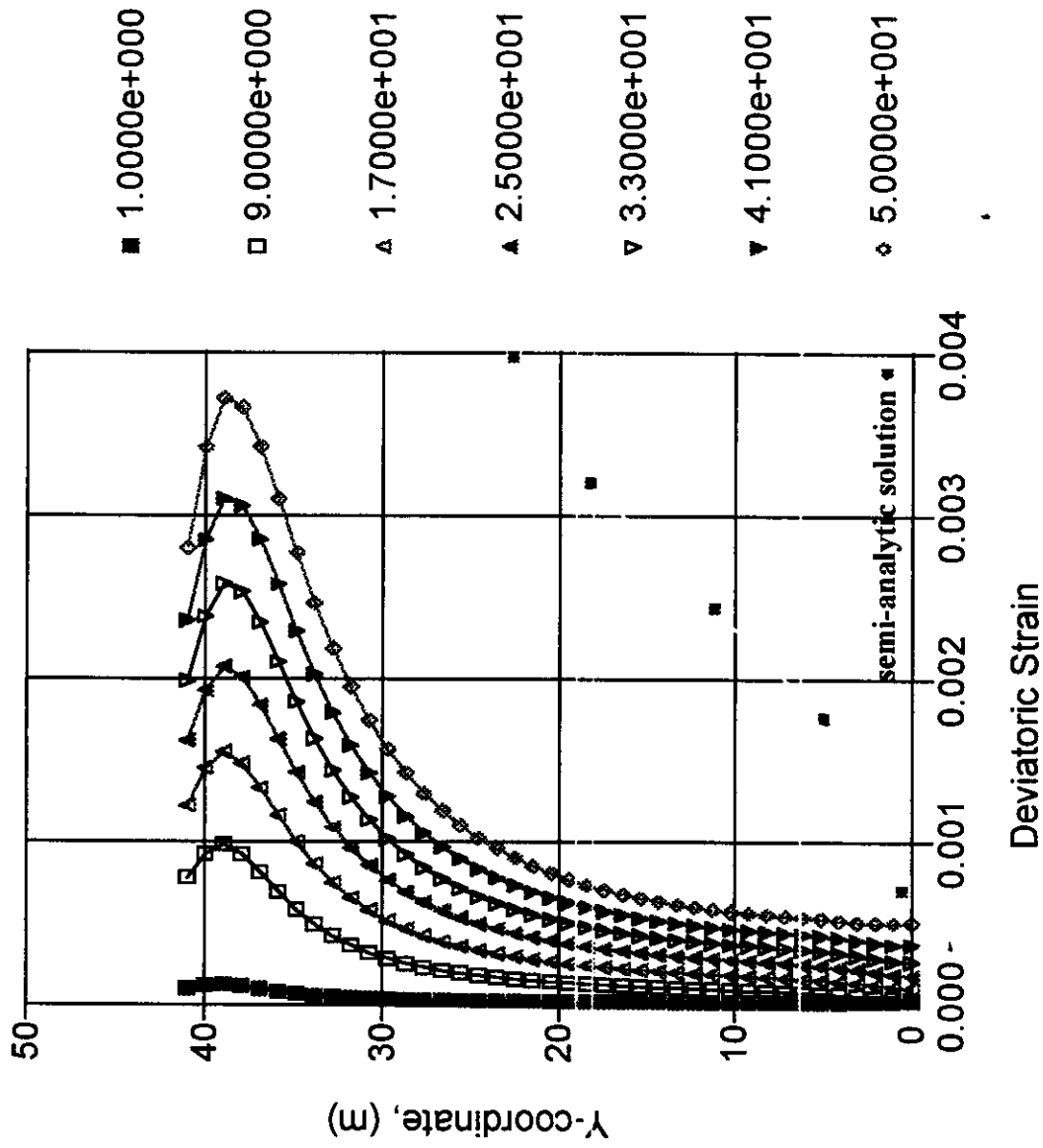


Figure 7. Deviatoric strain as a function of depth below inclined face of ice-keel.

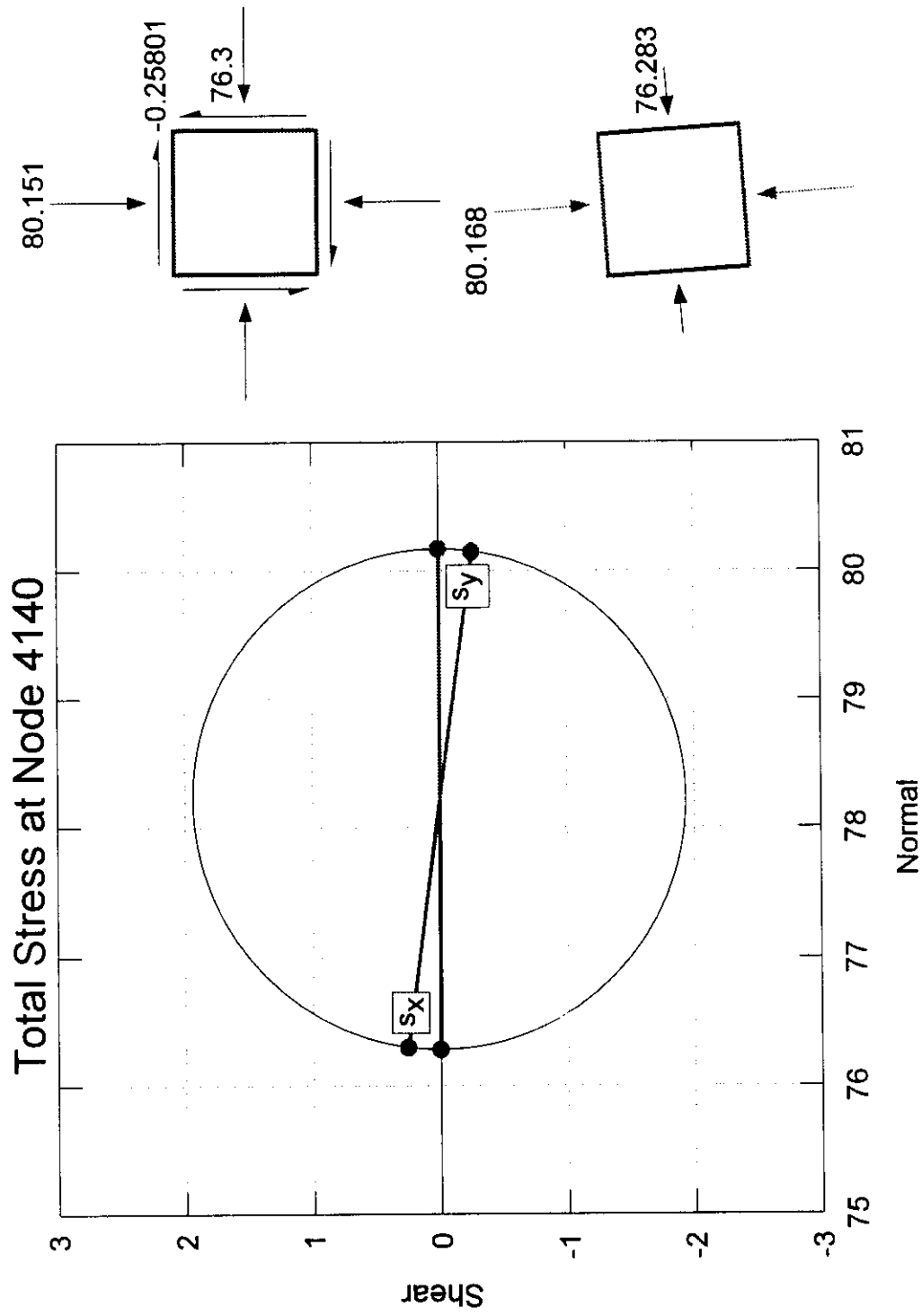


Figure 8. State of stress for first time increment at a point below inclined face of ice-keel.

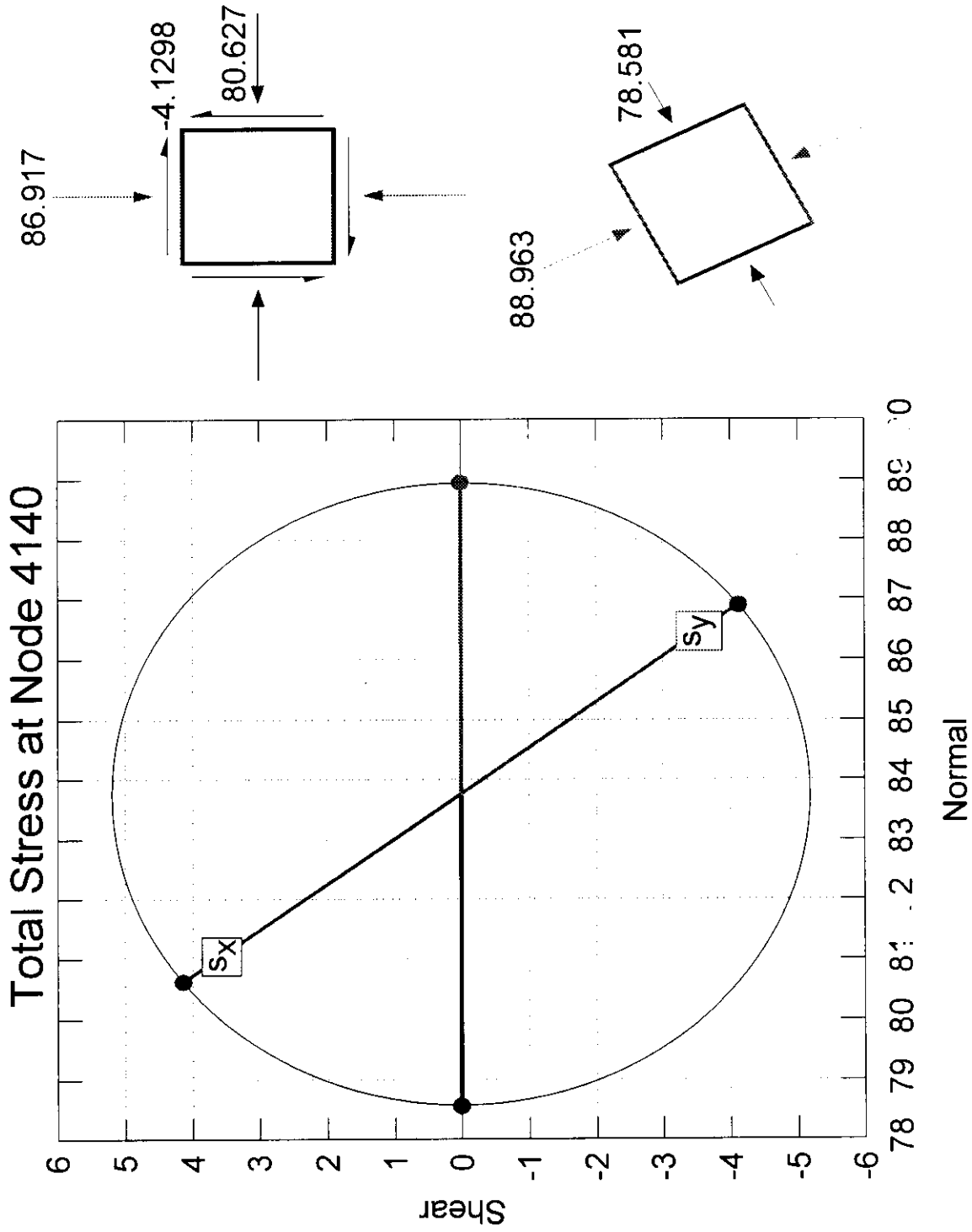
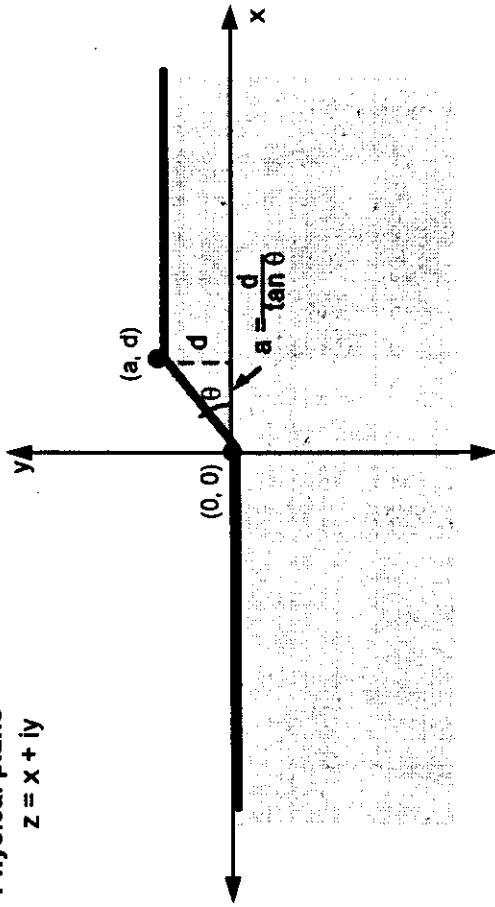


Figure 9. State of stress for last time increment at a point below inclined face of ice-keel.

Physical plane
 $z = x + iy$



Plane used in mapping

$$\zeta = \xi + i\eta$$

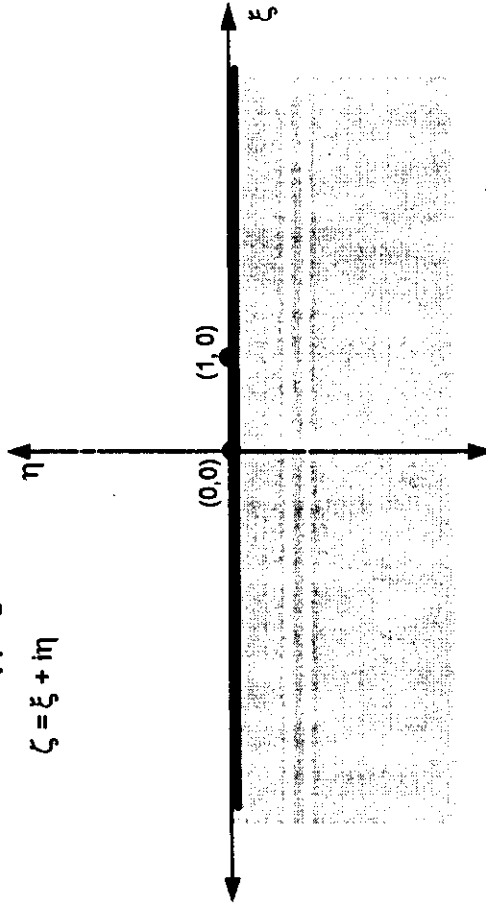


Fig. 3. Conformal mapping scheme

Figure 10. Conformal Mapping Scheme.

**MESH OF CONFORMALLY MAPPED DOMAIN
PHYSICAL PLANE $Z = X + iY$**

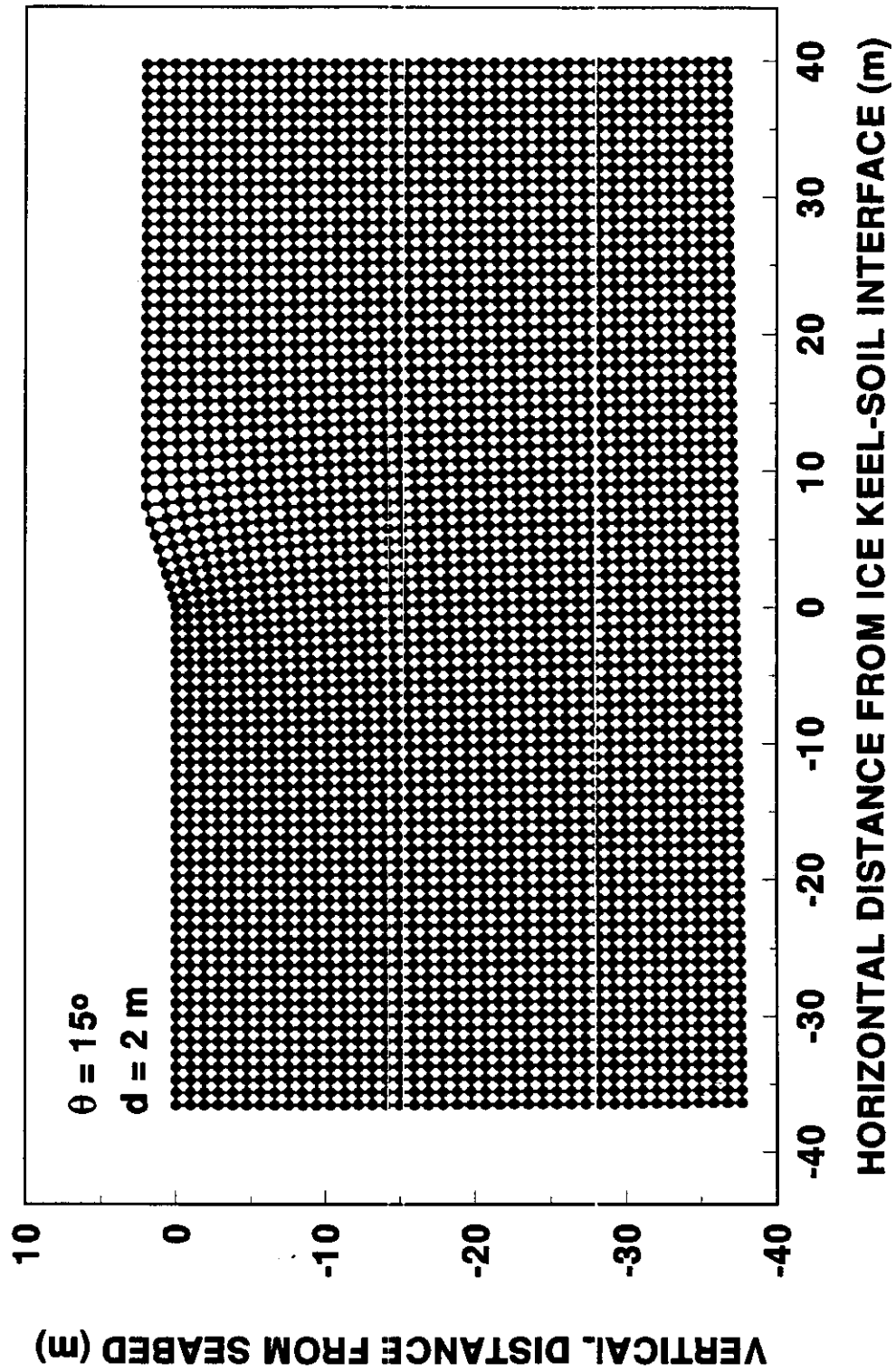


Fig. 11. Mesh generated by conformal mapping.

**MESH OF CONFORMALLY MAPPED DOMAIN
PHYSICAL PLANE $Z = X + iY$**

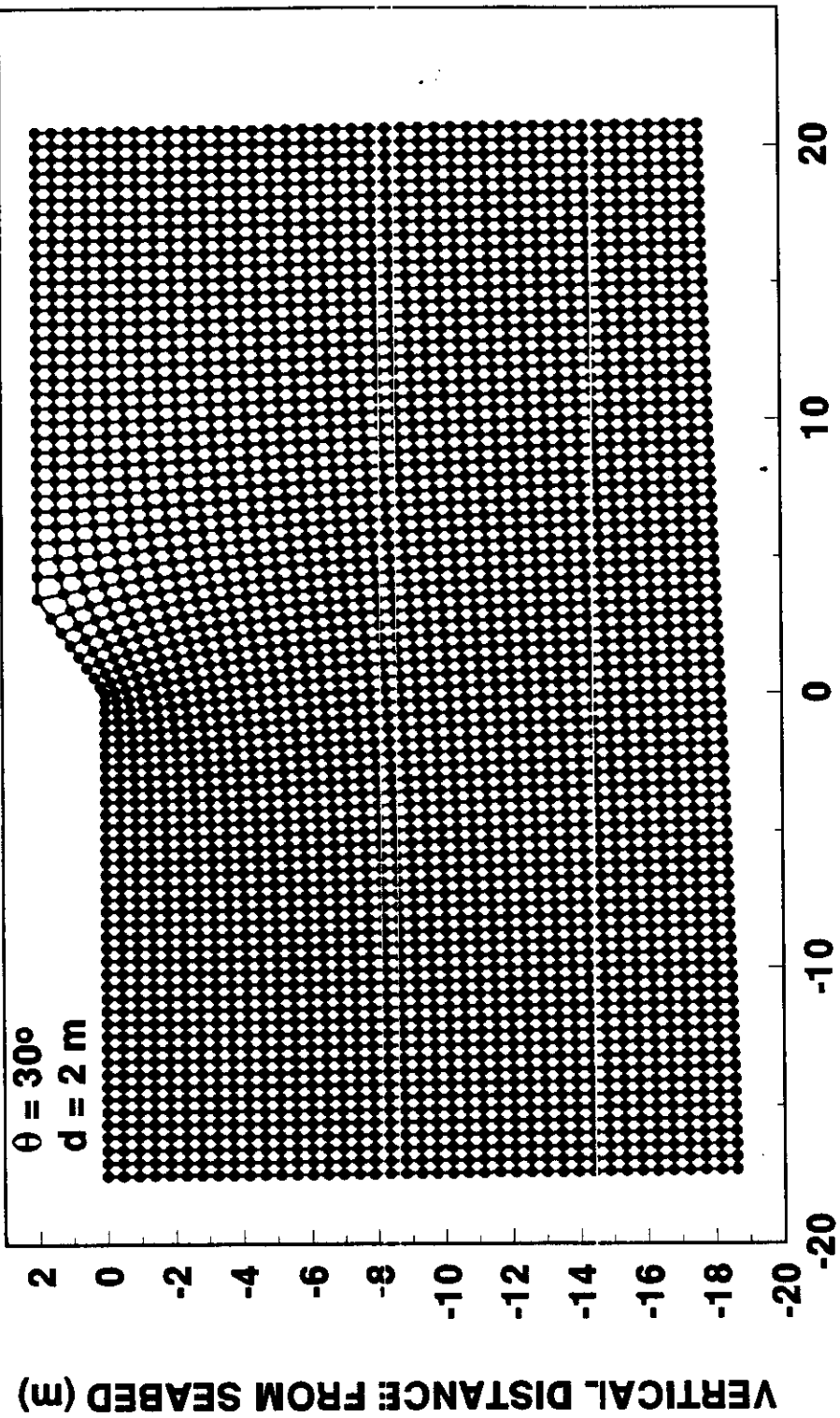


Fig. 12. Mesh generated by conformal mapping.

**MESH OF CONFORMALLY MAPPED DOMAIN
PHYSICAL PLANE $Z = X + iy$**

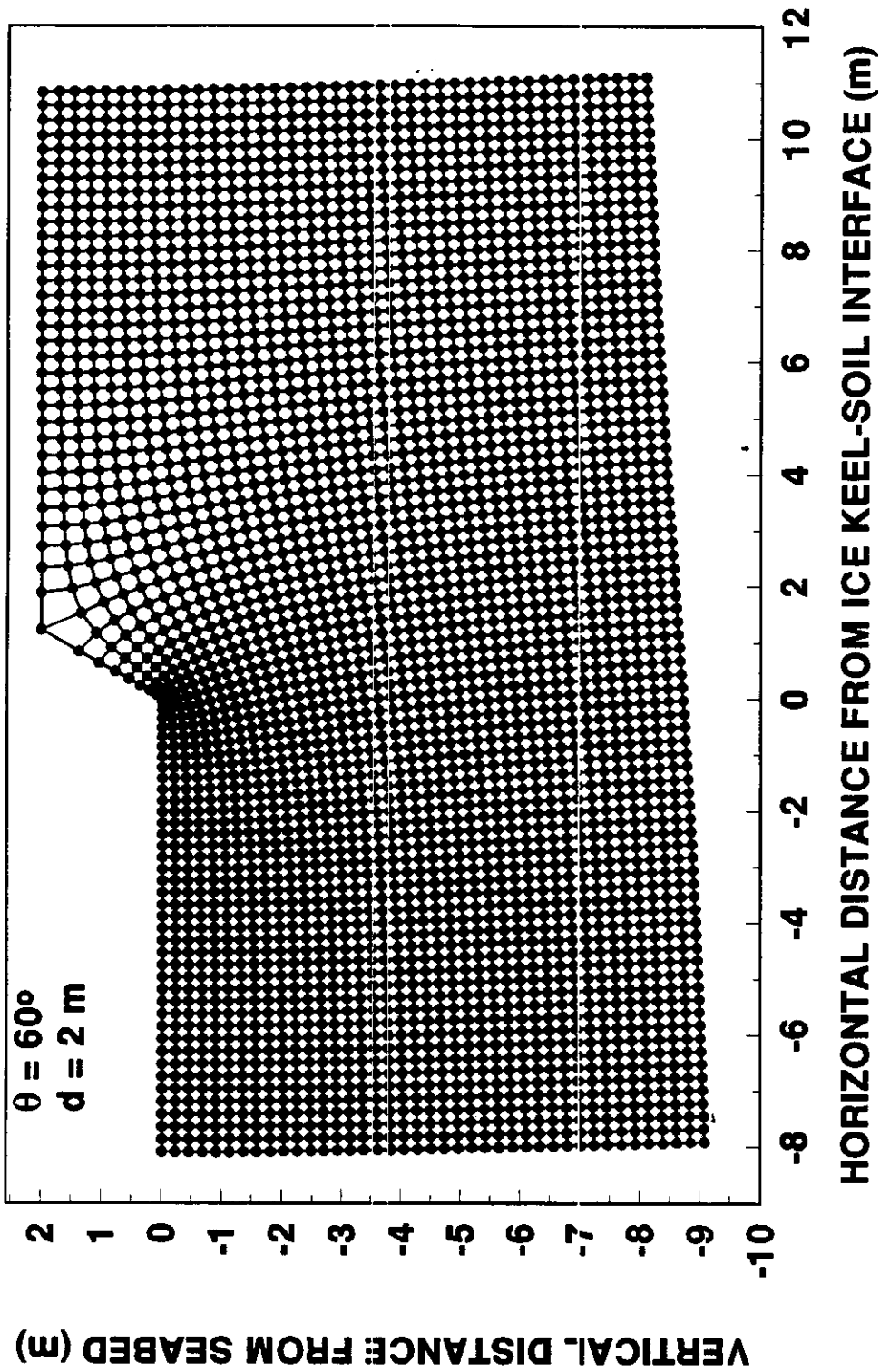


Fig. 13. Mesh generated by conformal mapping.

**MESH OF CONFORMALLY MAPPED DOMAIN
PHYSICAL PLANE $Z = X + iy$**

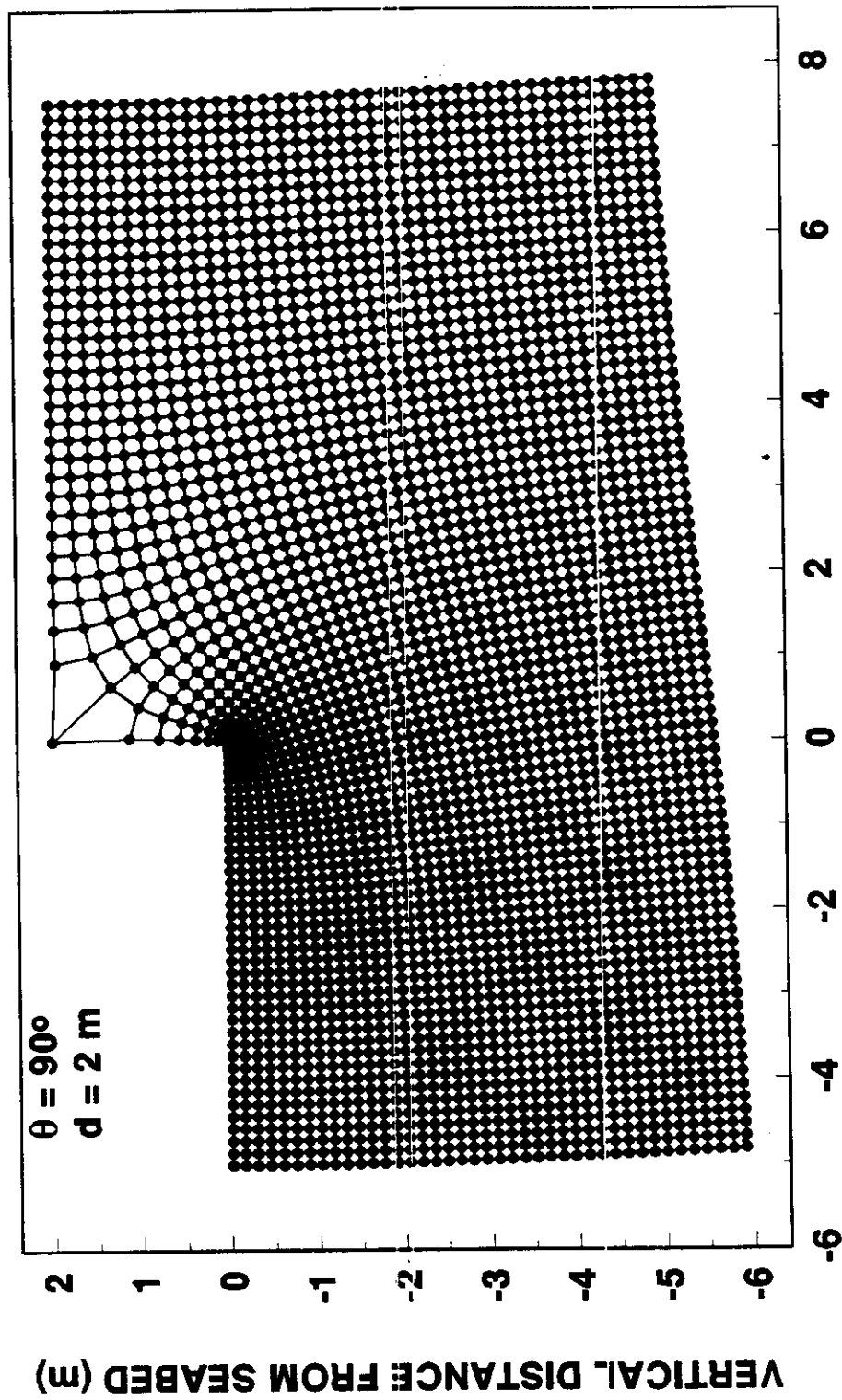


Fig. 14. Mesh generated by conformal mapping.

Effective Strain-rate Contours Speswhite kaolin clay

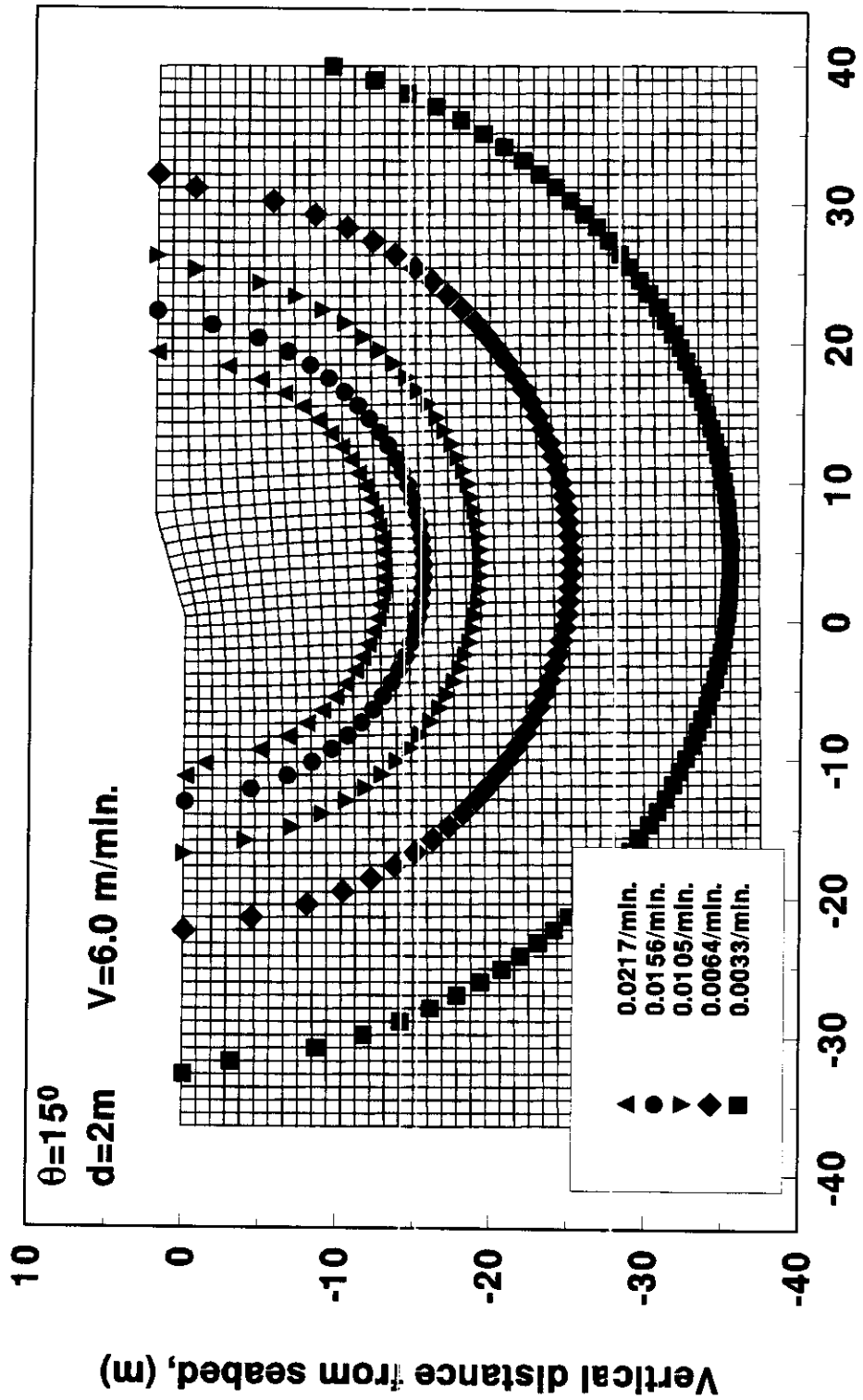


Figure 15. Contours of effective strain rates.

Effective Stress Contours
 Speswhite kaolin clay

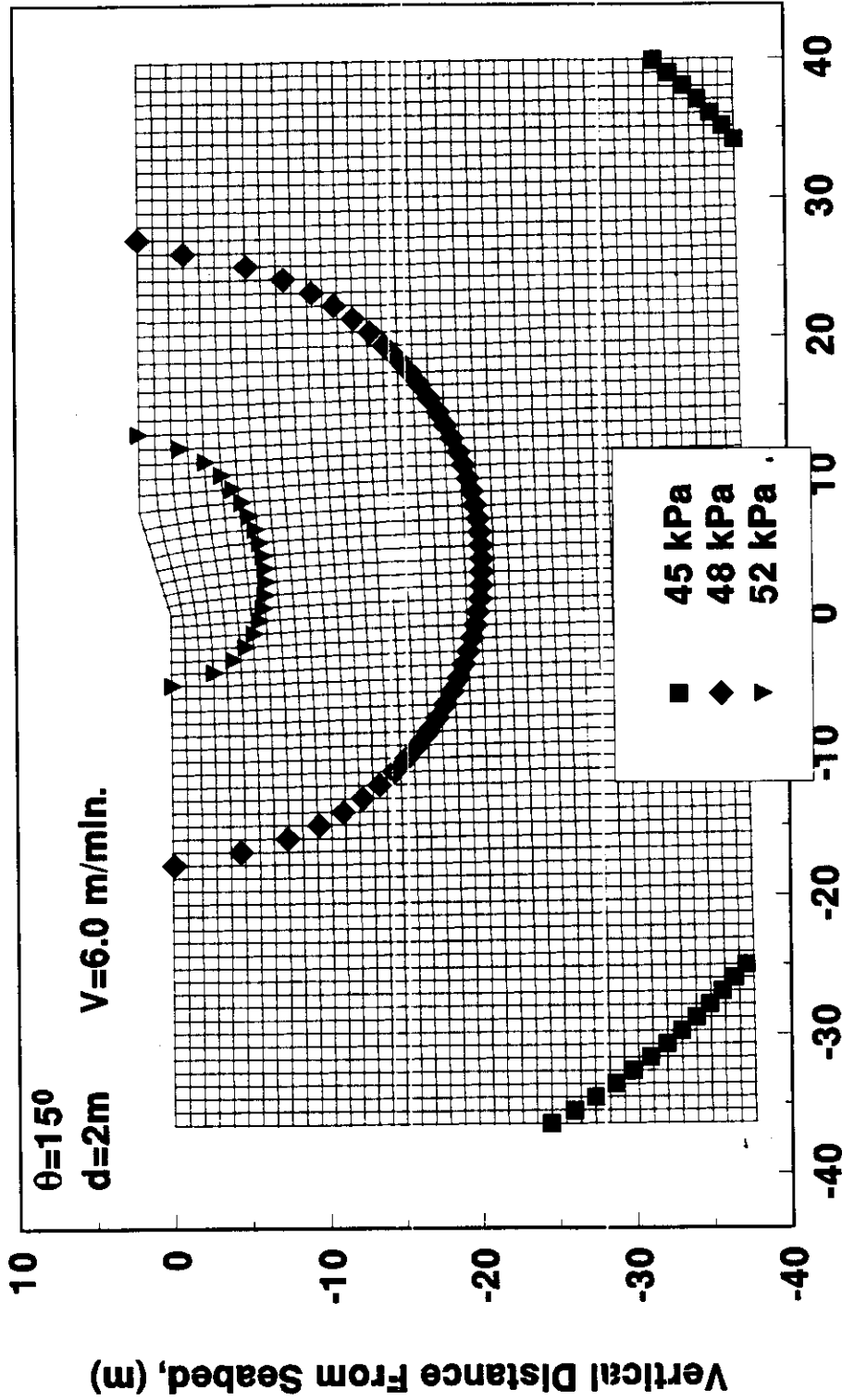


Figure 16. Contours of effective stress.

Global Force Per Linear Width
Speswhite kaolin clay

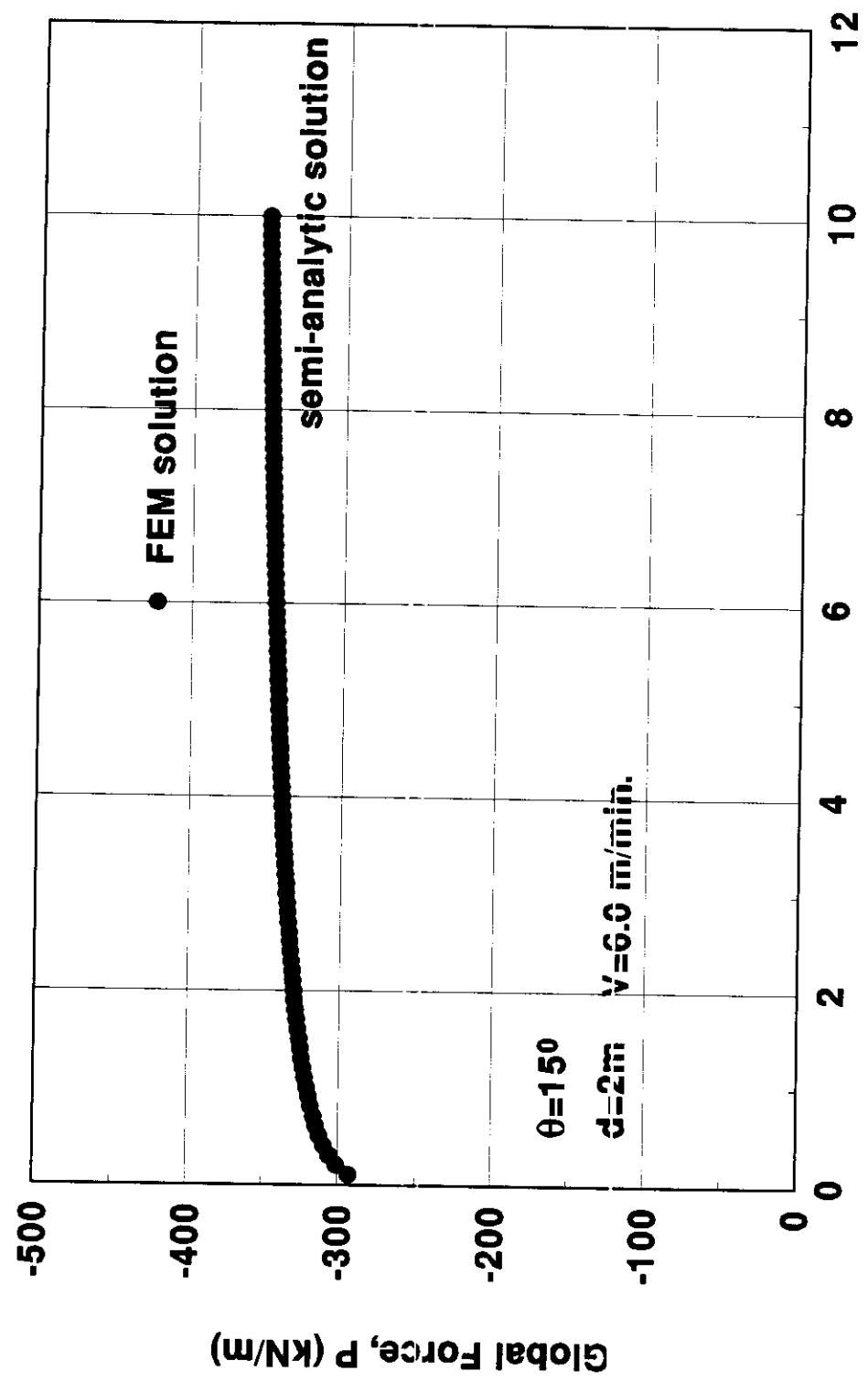


Figure 17. Global force per linear width.

CHOOSING OPTIMUM UNDERWATER PIPELINE BURIAL PROFILE ON NORTHEAST SAKHALIN SHELF

Surkov¹ G.A., Truskov³ P.A., Zemluk² S.V., Polomoshnov¹ A.M. and Astafyev¹ S.V.

(1) Sakhalin Oil and Gas Institute, Okha, Sakhalin, (2) Rosneft – Sakhalinmorneftegaz Company, Yuzhno-Sakhalinsk, and
(3) Sakhalin Energy Investment Co., Moscow

INTRODUCTION

In order to determine the optimum burial depth of an underwater pipeline in Arctic seas, one needs to specify the desired probability of no hummock-pipeline contact over a period of time, e.g., a year. The minimum burial depth h_b that is consistent with this probability will be deemed optimum.

The probability of no hummock-pipeline contact over a period of time is hinged on two parameters: (1) the probability density of drifting hummock-dug bottom gouge depths $p(h)$, where h is the hummock penetration depth into bottom soil, and (2) the expected number m of grounded-hummock gouges crossing the pipeline over a period of time (usually a year).

The probability of no contact with the pipeline in an environment with pipeline crossing expectation m is given by:

$$P_n = \left[\int_0^{h_b} p(h) dh \right]^m \quad (1)$$

Here, the bracket defines the probability of no hummock-pipeline contact for a burial depth h_b in case of a single hummock crossing the pipeline route.

1. MATHEMATICAL MODEL OF HUMMOCK-BOTTOM INTERACTION

For the purpose of this analysis, we assume that the mechanism of hummock interaction with the surrounding ice field is as follows. A separate hummock freely moving in an ice field contacts the bottom and expends its kinetic energy to gouge a trench in the bottom soil until a halt. After this halt, it can be subjected to impacts of surrounding drifting ice floes, smaller hummocks, currents, waves, and wind.

This cause of events from a drifting to stationary hummock is typical of the northeastern Sakhalin shelf, especially in the spring period when the hummock mass is a maximum, and ice fields are 100% broken floes. An analysis of ice reconnaissance data indicates that, in this period, the ice cover is split into such floes that an ice formation exceeding the stationary hummock in size is virtually improbable. In other words, the energy that the stationary hummock has had considerably exceeds that of a drifting floe or another hummock, therefore the interaction of the latter with a stationary hummock cannot produce its further penetration into the bottom.

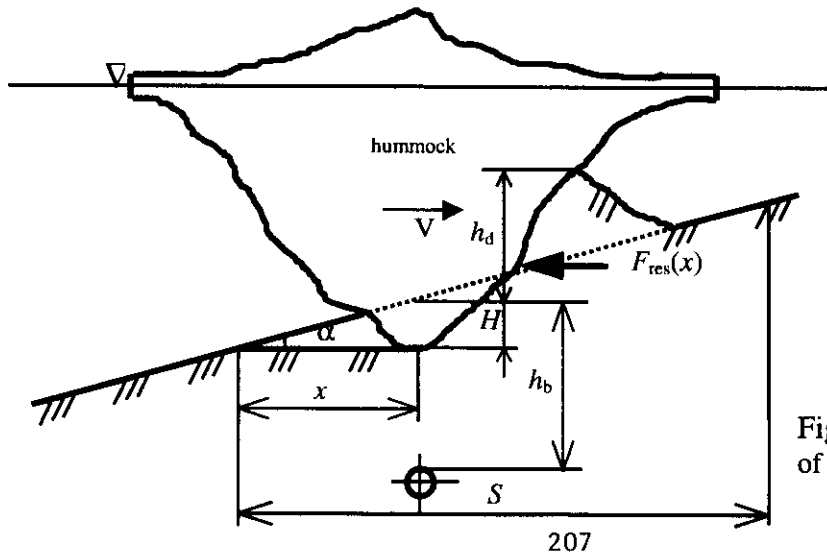


Fig. 1. Illustrating the penetration of a hummock into the bottom soil.

Figure 1 illustrates the geometry of hummock-bottom slope interaction. In order to estimate the energy expended in hummock penetration in the bottom soil, we assume that the hummock moves with a constant speed, and, while in contact with the bottom, its center of mass moves along the velocity vector, i.e., without rotation or uphill sliding over a constant slope.

The soil resistance increases as the hummock penetrates into the bottom, that is, this force is a variable quantity. We assume that the x axis is aligned with the hummock's velocity vector. The soil resistance is the function $F_{\text{res}}(x)$ of the path length x traveled by the hummock from the incipience of penetration. The work of the soil resistance force along the travel path S from the gouging incipience to the final stop is:

$$E_{\text{kin}} = E_{\text{res}} = \int_0^S F_{\text{res}}(x) dx \quad (2)$$

From this expression one may determine the path length S and the maximum penetration depth H (see Fig. 1).

Thus, the key parameter of the hummock – bottom soil interaction model is the soil resistance force $F_{\text{res}}(x)$. Today one may determine $F_{\text{res}}(x)$ with a sufficient reliability only using a soil mechanics formalism. However, this theory requires that the hummock surface geometry in contact with the soil should be known. Investigations of the subsurface part of hummocks (keels) appearing on the Sakhalin northeastern shelf indicated that the ice surface in contact with the bottom can have an intricate geometry with multiple recessions and protrusions.

It would be natural then to approximate the hummock shape by elementary geometrical figures. However, this approximation would be aggravated by the need to adequately reflect the hummock-soil interaction. The geometry chosen for approximation would sensibly affect the final result, that is to say, the penetration depth. Such depths may differ by a factor of ten and more for different geometries. This circumstance renders doubtful the use of such models for estimating the maximum hummock penetration depth, leave alone the wisdom of this quantity. However, many authors (Green et al, 1983; Astafyev, 1985; Lee and Eranti, 1986; Bekker, 1989) used the geometrical approach for this purpose. Almost all of them approximated the hummock by a rectangular prism.

We introduce certain idealizations into this approximation of the hummock. The assumption of a flat vertical front face implies that, from the standpoint of soil resistance, the real front face of the hummock with local irregularities is equivalent to an even vertical wall of a given width, that is, the resistance of soil is identical for the vertical and real surfaces. However, this assumption may not hold. The soil resistance for the model and a real-geometry may differ significantly. Soil mechanics suggests that this difference can be eliminated by introducing a slope of the wall from the vertical. Below we demonstrate that the resistance of soil is directly proportional to the horizontal component of passive soil pressure that takes into account the slope of the front wall. This linear dependence allows one to use the hummock approximation by a rectangular parallelepiped for a qualitative analysis of hummock-bottom soil interaction.

Astafyev et al. (1997), Gnezdov and Surkov (1998) have approximated the resistance offered by the soil by the expression:

$$F_{\text{res}}(x) = \psi \cdot x^2, \quad (3)$$

where

$$\psi = \frac{1}{2} \gamma \left(\tan \alpha + 0.85 \cdot \sqrt{\tan \alpha \cdot \tan \varphi + \tan^2 \alpha} \right)^2 \lambda_h B, \quad (4)$$

γ is the specific weight of soil in water, λ_h reflects the horizontal component of passive soil pressure, φ is the angle of internal friction, and B is the hummock width.

In deriving equation (3) we have not allowed for soil cohesion because bottom soils of the northeastern Sakhalin shelf are mainly coarse and fine sands with insignificant cohesion. In addition, equation (4) takes into account the effect of bulldozed soil.

2. NUMERICAL MODELING

The deterministic model describing the interaction of hummocks with bottom soil enables one to determine the hummock gouge depth. It requires, however, the knowledge of the width of hummock soil interface, hummock's kinetic energy and drift direction, seafloor slope α , and mechanical properties of soil. In addition, the hammock mass M , and drift velocity are required to determine its kinetic energy. Below we present the relationships that were used in numerical modeling. As a rule, they are derived in the form of integral curves. In numerical modeling, guided by a random number generated in the interval $[0, 1]$, the algorithm picks up a parameter value from an integral curve. In this model, the algorithm used the following variable parameters: the width of hummock-soil interface (gouge width), mass of hummock contacting with ground, hammock velocity, and the direction of gouging.

The gouge width was derived from field studies performed offshore northeast Sakhalin. In the simulation model of Astafyev et al. (1997), the gouge width was assumed to be proportionally distributed in the interval 10 to 30 m. The gouge direction was derived from the integral curve of ice drift direction shown in Fig. 2 (Astafyev et al., 1997). The drift direction was recorded by a radar stationed in the Odoptu Bay region. Figure 3 represents the drift velocities of ice formations, as heavy as 100 kton, offshore northeastern Sakhalin (Truskov, 1989).

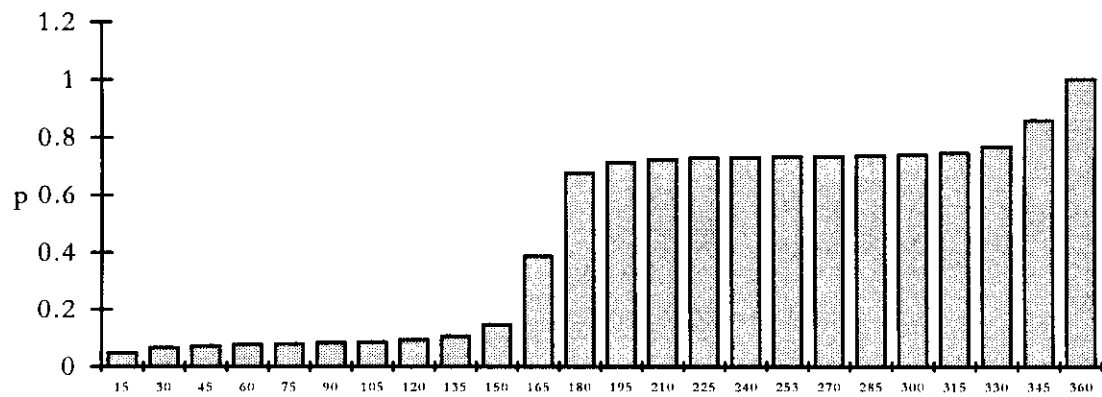


Fig. 2. Ice drift direction histogram obtained in 1992.

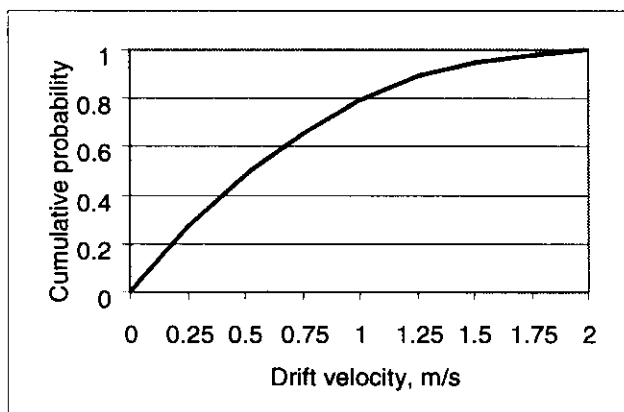


Fig. 3. Drift velocity distribution of ice formations weighing up to 10 kt as observed offshore northeastern Sakhalin.

The mass of hummocks used in this model was based on field studies performed offshore northeast Sakhalin. Common hummocks met in 10-m deep waters weigh 10 to 30 kt. In deeper waters, hummocks as large as 70 to 80 kt or even heavier can be observed. Figure 4 shows the hummock mass distribution over water columns from 5 to 25 m (Truskov, 1987, 1989). Field investigations revealed that hammocks vary considerably in size even in waters of the same depth. On the basis of available information, we assumed that hammocks obey a proportional law between 10 and 30 kt, and gouges range in width from 10 to 15 m, in 10-m deep water columns. If we denote this mass and

depth as M_{10} and H_{10} , then on the assumption that the hummock keel is a frustum of a cone, its mass at depth H can be determined as

$$M = (H/H_{10})^3 M_{10}.$$

This approach obviously needs the mass ratio of hummocks at H_{10} and H to be known. If hummock-soil interface is wider than 15 m, then the mass can be determined by the formula:

$$M'_{10} = M_{10} \left[1 + \frac{1}{2} \left(\frac{B}{15} - 1 \right)^2 \right].$$

In this hummock gouging model, we also assumed that soil particle cohesion $c \approx 0$, and the angle of internal friction $\phi = 32^\circ$. In computer simulation, we varied the seafloor slope from 0.2° to 1.0° and the water depth, between 10 and 25 m.

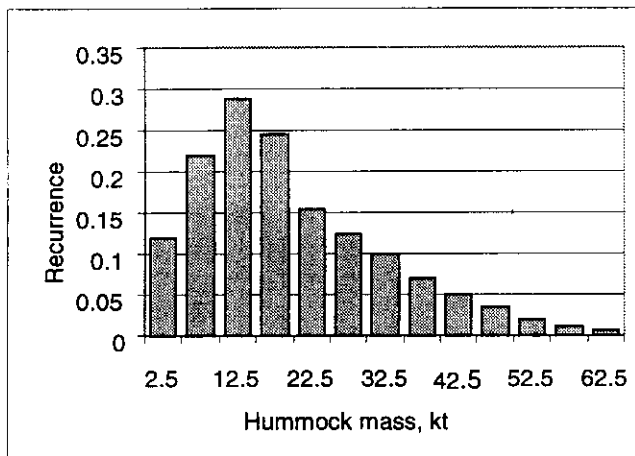


Fig. 4. Hummock mass histogram for water depths from 5 to 25 m offshore northeastern Sakhalin.

For each set of α and H , we made up to 10,000 computer runs, thus simulating 10,000 gouging cases. In each run, a random number generator picked up a hummock mass, velocity, hummock-soil interface width, and drift direction from the respective integral curves.

We run a number of numerical experiments with ground resistance factor λ allowed to vary in different ranges. These were actually qualitative experiments run with the purpose to determine the distribution of gouge depths. An analysis of gouge depth histograms obtained for a number of bottom slope – water depth combinations indicated that they may be described by an exponential law

$$p(h) = k \exp(-k h) \quad (5)$$

A chi-square goodness of fit test proved that this hypothesis was true with confidence probability above 0.95.

3. REAL VALUES OF HUMMOCK GOUGE DEPTH

Any experiment modeling (physically or numerically) hummock gouging into bottom soil should recognize how realistic the model used is. No unambiguous answer can be derived from solely theoretical prerequisites, because the true value of λ , the horizontal component of passive soil resistance, remains unknown. For a particular value of λ , values of $p(h)$ and m can differ as far as ten times.

In order to determine the more realistic value of λ , we used the fact that gouge depths are distributed exponentially, and made use of field gouge depth data (Truskov and Surkov, 1991; Surkov, 1995; Astafyev et al., 1997).

Experimental hummock gauge depths, found by thermal drilling to lie in the range from 0.3 to 2.13 m, are plotted in Fig. 5. Since no gouge depths shallower than 0.3 m was found, gouge depths

below 0.3 m are believed to suggest that an ice ridge has not enough size to be treated as a grounded hummock.

The probability to found a gouge depth within some interval, e.g. from h_1 to ∞ , can be determined by the classic frequency formula:

$$P_{1,\infty} = \frac{m}{n}, \quad (6)$$

where m is the number of hummocks in the interval from h_1 to ∞ , and n is the total number of hummocks studied in the interval from h_0 to ∞ ; or else it can be derived as the geometric (area) probability

$$P_{1,\infty} = \frac{S_2}{S_1} = \frac{\exp(-kh_1)}{\exp(-kh_0)}. \quad (7)$$

Equating (6) and (7) after some algebra yields:

$$k = \frac{\ln(n/m)}{h_1 - h_0}. \quad (8)$$

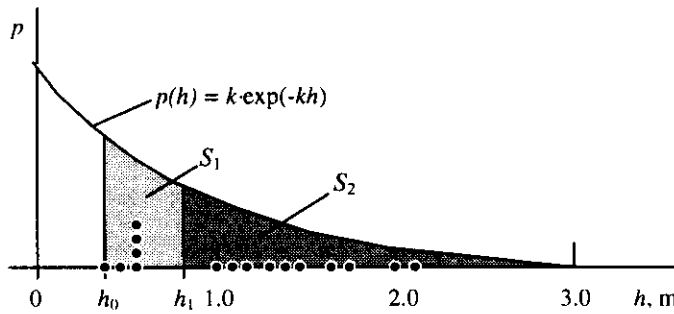


Fig. 5. Hummock gouging depth distribution density.

- field gouge depth data;
- S_1 area for $[h_0, \infty]$;
- S_2 area for $[h_1, \infty]$;

Thus, equation (8) yields a realistic gouge depth distribution parameter. Before this expression is used, one needs to know the water depth H and bottom slope angle α to which it refers. In studied hummocks, these parameters varied in some range; however, on average, we assume $\bullet = 10$ m and $\alpha = 1.0^\circ$ (Astafyev et al., 1997).

Using this equation we calculated the gouge depth distribution parameter for three hummock gouging cases: (1) $h_0 = 0.3$ m, (2) $h_0 = 1.0$ m, (3) $h_0 = 1.5$ m and different h_1 .

1) for $h_0 = 0.3$ m and (\bullet) $h_1 = 1.0$ m, $n/m = 1.6$ and $k = 0.671$; (b) $h_1 = 1.5$ m, $n/m = 4.0$ and $k = 1.155$; (c) $h_1 = 2.0$ m, $n/m = 8.0$ and $k = 1.223$;

2) for $h_0 = 1.0$ m and (\bullet) $h_1 = 1.5$ m; $n/m = 2.5$ and $k = 1.83$; (b) $h_1 = 2.0$ m; $n/m = 5.0$ and $k = 1.61$;

3) for $h_0 = 1.5$ m and $h_1 = 2.0$ m, $n/m = 2.0$ and $k = 1.39$.

These findings led us to draw the following conclusions. For $h_0 = 0.3$ m, the k values vary widely and are underestimated as compared to other cases. This occurs mainly owing to scarce data for $h < 1.0$ m. For the same reason, the third case ($h_0 = 1.5$ m) is hardly acceptable. The second case ($h_0 = 1.0$ m) looks more stable: the k values vary insignificantly for two h_1 (1.5 and 2.0 m). It is expedient, therefore, to assume the average value of k for the second case, i.e. $k_{av} = 1.71$, for further calculations. On the whole, the data are extremely scarce, and thus impair the reliability of results.

It should be noted that this k is the maximum gouge depth distribution parameter, i.e., holds when hummocks are brought to halt. This value should be doubled when used to analyze the probability of hummock's impact on the pipeline. The coefficient 2 owes its existence to the exponential law and to the fact that the point where the gouge crosses the pipeline is proportionally

distributed over the gouge length. This reasoning yields $k = 3.42$ for the pipeline. This k value is characteristic of the Canadian sector of the Beaufort Sea.

With selected $H = 10$ m and $\alpha = 1.0^\circ$ we performed a number of numerical experiments for some λ to find by matching that to $k = 1.71$ there corresponds $\lambda = 3.25$. With this real value of λ we performed numerical experiments for a number of water depths and bottom slopes. The k values were determined for the distribution of gouge depths where hummock stops, i.e., the one for maximum gouge depths. Figure 6 shows the values of k inferred statistically from relative frequency histograms for maximum gouge depths. Figure 7 shows gouge lengths obtained in a similar way.

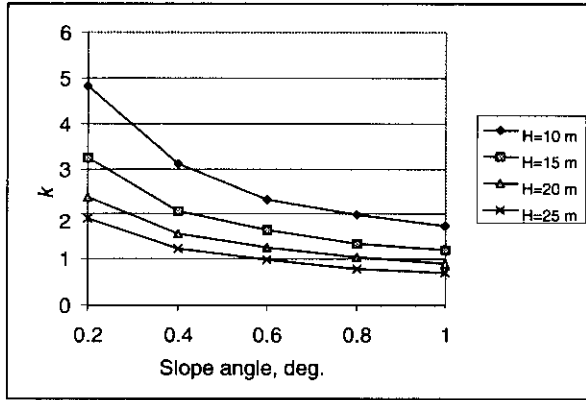


Fig. 6. Parameter k of maximum gouge depth distribution density versus slope angle.

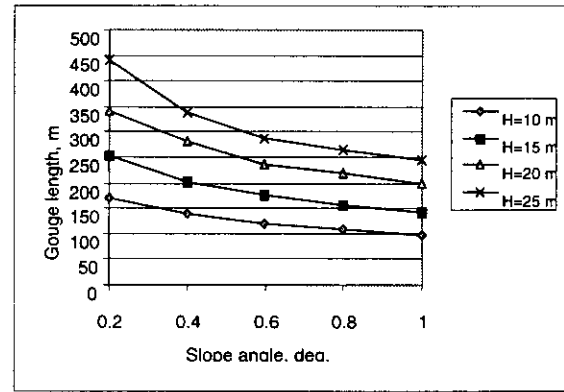


Fig. 7. Gouge length as a function of bottom slope.

4. ESTIMATING THE NUMBER OF GOUGE-PIPELINE CROSSINGS

Surkov (1998) suggested a method for estimating parameter m . This method is a modified Buffon problem of probability theory. For a gouge arbitrarily oriented relative to the pipeline, it was demonstrated that

$$m = 2\pi^{-1} L \cdot n \cdot l_m \quad (9)$$

where L is the pipeline length, n is the gouge number density per square kilometer, and l_m is the mean gouge length.

For a pipeline laid on the northeastern Sakhalin shelf at right angles with the shoreline (Surkov, 1998):

$$m = 0.177 \cdot L \cdot n \cdot l_m \quad (10)$$

In order to determine n we assumed that the number of hummock intrusions into bottom soil per unit area corresponds to the density of hummock occurrence. For the northeastern Sakhalin shelf, the average hummock occurrence density is 2-3 (for water depths of 11-13 m), but can be as high 8 (Astafyev et al., 1997; Gnezdov and Surkov, 1998). For sections at large depths, n will decline exponentially with parameter $k = 0.6$ (Gnezdov and Surkov, 1998).

5. FORMALISM TO DETERMINE OPTIMAL UNDERWATER PIPELINE BURIAL PROFILE

We developed an optimization computer code to seek for an optimal pipeline burial profile. For each segment of pipeline, it yields its slope α , length L , and length-average sea depth H . Parameters α and H are necessary to determine the gouge depth distribution parameter k and the mean number m of pipeline crossings produced by hummock-dug gouges. A knowledge of segment length is necessary to determine the capital expenses for pipeline construction (including the cost of burial).

The algorithm seeks for an optimal burial profile by exhaustive search of burial combinations for all pipeline sections. For a burial profile, one determines the number of contacts with hummocks

at each section and the cost of pipeline. These quantities are summed up over all sections and compared in one of these parameters.

The cost of a pipeline section with allowance for its burial into the Sakhalin shelf may be represented in the form:

$$C_i = a \cdot \exp(b \cdot h_b), \quad (11)$$

where a and b are parameters depending on the pipeline diameter and sea depth. For a diameter of 500 mm, these parameters can be approximated as follows:

$$a = 176.65 \cdot H^{0.0306} \cdot \exp(0.001576 \cdot H),$$

$$b = 0.14467 \cdot H^{-0.050018},$$

(12)

where H is the sea depth in meters.

The optimality criterion is given by the expression:

$$\sum_{k=1}^N C_i = \min, \quad P_n \geq P_{st}, \quad (13)$$

where N is the number of pipeline sections and P_{st} is the stipulated level of reliability.

Before commencing the optimization calculations, we assumed for each section of the pipeline the maximum burial depth and the minimum burial depth. In accordance with the international practice of underwater pipeline construction, we assumed the maximum burial depths of 4 m, and the minimum burial depth of 0 m. This range was uniformly broken down and was swept with a predetermined step. The optimization problem was to determine the cost of pipeline as a whole for all combinations of burial depths for all pipeline sections and the probability of pipeline contact with a hummock subject to the condition (13).

The optimization program was tested for sensitivity (robustness) with respect to pipeline cost. For this purpose, we experimented with this code letting parameter a (a is the cost of 1 km of pipeline less the cost of burial) to gradually increase. The optimal pipeline burial profile did not respond to these variations. It proved to be robust with respect to a rather wide variation of cost parameter b .

6. EVALUATING A PIPELINE BURIAL PROFILE FOR THE PILTUN-ASTOKHSKOYE FIELD

The above numerical optimization technique was implemented to determine the optimal burial profile of an underwater pipeline on the Piltun-Astokhskoye field (platform A) (Gnezdov and Surkov, 1998). The resulted optimal burial profile may be found in Polomoshnov et al. (1999). Table 1 presents the input data for optimization analysis. Table 2 summarizes the resultant optimal pipeline burial profile calculated for various no-contact probabilities.

Table 1. Input optimization data for pipeline burial on the Piltun-Astokhskoye field, platform

Section	Section length, km	Average sea depth, m	Average bottom slope, deg.	Distribution parameter k	Average gouge length, km	Average number of hummocks per km ²	Number of crossings, m	Pipeline cost parameters (500 mm dia)	
								a	b
I	1.23	12	0.19	8.3	0.209	9	1.97	194.25	0.128
II	1.15	15	0.1	10.2	0.328	0.82	0.26	196.5	0.126
III	1.7	18	0.13	7.42	0.354	0.13	0.07	198.5	0.125
IV	2.0	22	0.11	6.8	0.450	0.012	0.009	201.0	0.124
V	0.78	21.5	0.52	2.56	0.259	0.017	0.003	200.7	0.124

Table 2. Optimal pipeline burial on the Piltun-Astokhskoye field, platform •

Section	Probability of no contact with a hummock during a year				
	0.999	0.9995	0.9999	0.99995	0.99999
I	0.88	1.00	1.13	1.25	1.38
II	0.56	0.63	0.81	0.81	1.00
III	0.50	0.56	0.81	0.88	1.13
IV	0.19	0.31	0.50	0.63	0.88
V	0.25	0.44	1.28	1.56	2.19

7. LITODYNAMIC PROCESSES

A final pipeline burial profile should take into account litodynamic considerations. Numerous measurements beyond sea depths of 10 m on the northeastern Sakhalin shelf revealed the largest scour of 1.5 m (Gnezdov and Surkov, 1999). Scour seems to be local in nature: soil scoured in one area is deposited and accumulated in another. Thus the bottom surface is in a dynamic equilibrium. If such a dynamic equilibrium takes place, the litodynamic variations over such areas may not be taken into account or included as a minor factor. Much depends on the specific bottom profile before hummocks arrive.

A long and failsafe operation of the pipeline across the Nevelskoi Strait (western Sakhalin) suggests that litodynamics alone is of no much hazard. The bottom profile across the Nevelskoi Strait was measured periodically from 1958 to 1983. Some measurements were made from shore ice (if ice thickness allowed), others were produced by bottom profiling with an echo sounder. The bottom profiles recorded from 1958 to 1983 are compared in Fig. 8. The bottom envelope curve may be treated as a profile of ultimate scour.

Over the years of pipeline operation the bottom profile has undergone considerable changes with the moving layer being as thick as 5 m on some sections. However, such profound soil movements has not produced any harm to the pipeline. Thus, litodynamics alone or in combination with local hydrodynamic factors does not present a special hazard for pipelines (provided that measures were taken against pipeline surfacing).

Moreover, active litodynamic processes in this area produced a considerable (2–5 m thick) protective layer of soil overlaying the pipeline. Thus, the initial probability of pipeline damage by grounded hummocks has fallen sharply with years.

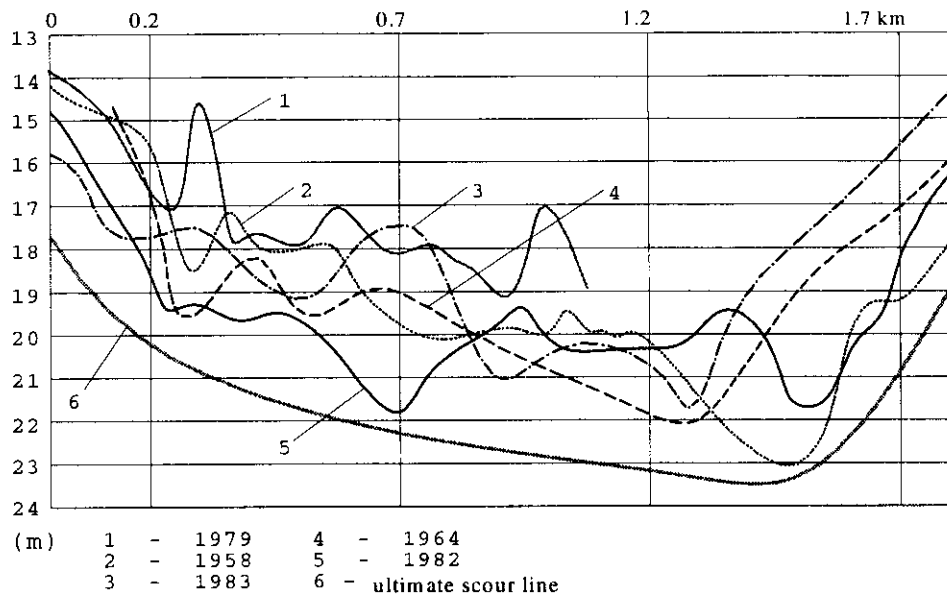


Fig. 8. Profile of the 1958-1983 underwater crossing over the Nevelskoi Strait. (Deep section). Scales: horizontal 1:10000 / vertical 1:100.

REFERENCES

- Astafyev V.N., 1985, Operational reliability of underwater pipelines (practice of the shelf of the Sea of Okhotsk), Cand. Sci. (Eng.) Dissertation, Ufa Oil Institute: Ufa. (in Russian)
- Astafyev V.N., Surkov G.A., Truskov P.A. Hummocks and stamukhas of the Okhotsk Sea (monograph). "Progress-Pogoda", St-Petersburg, 1997. - 197 p. (in Russian).
- Bekker A.T. and Truskov, P.A., Impact of drifting hummock formations on seabed, in Materials of Conferences and Meetings on Offshore Technology, Leningrad: Energoatomizdat, 1989, pp. 98-103. (in Russian)
- Gnezdov V.P., Surkov, G.A. "Development of Design Criteria for the Optimal Burial Profile of Underwater Pipelines for the Sakhalin 2 Project". Research and Engineering Center, Closed-End Joint Stock Company, Okha, 1998. -150 P.
- Green, H.P., Reddy, A.S., and Chari, T.R., 1983, Proc. of the 7th Int. Conf., on Port and Ocean Eng. under Arctic Conditions (Poac). - Espoo, vol. 1, pp. 280-288.
- Lee G.C. and Eranti E. Cold region structural engineering. - McGraw - Hill Book Company, 1986. - 530 p.
- Polomoshnov A.M., Astafyev V.N., Surkov G.A. Method for Selecting Subsea Pipeline Route under Ice Conditions (for the Sakhalin Offshore Case) //Proc. of the 14-th Int. Symp on "Okhotsk Sea & Sea Ice" and "International Workshop on Rational Evaluation of Ice Forces on Structures", Mombetsu, 1999, pp.130 - 136.
- Surkov, G.A., 1995, Method of evaluation of an optimal burial profile for underwater pipelines in freezing seas, Cand. Sci. (Eng.) Dissertation, Vladivostok: DVG TU. (in Russian)
- Surkov G.A. Evaluation of number of contacts of drifting ridges with pipelines // Proc. of the 13-th Int.Symp on "Okhotsk Sea & Sea Ice" and the "Ice scour and Arctic marine pipelines Workshop", Mombetsu, 1998. - pp.233 - 238.
- Truskov, P.A., 1987, Ice effects in development of offshore oil and gas fields, in: Offshore Engineering Facilities. Vladivostok: DVGU, pp. 89-94. (in Russian)
- Truskov, P.A., 1989, Ice conditions for design of oil and gas production facilities, Cand. Sci. (Geogr.) Dissertation, Leningrad: AANII. (in Russian)

Truskov, P.A. and Surkov, G.N., 1991, Scour depth distribution on the Northern Sakhalin offshore, Proc. of the First ISOPE Conf., Edinburgh, United Kingdom, 11-16 August, vol. 2, pp. 467-470.

RESPONSE OF BURIED ARCTIC MARINE PIPELINES TO ICE GOUGE EVENTS

Kenny, S., Phillips, R., McKenna, R.F. and Clark, J.I.
C-CORE, St. John's, NF Canada

ABSTRACT

For Arctic marine pipelines, the risk of potential damage due to ice gouges caused by pressure ridges and icebergs is a significant concern. Some fundamental parameters for both ice/soil and soil/pipe interaction are addressed. Pipeline response to subgouge soil deformations is modelled by fully nonlinear finite element analysis using two-dimensional pipe elements coupled to discrete soil springs. The effects of internal pressure, ice bearing pressure, ice gouge width and depth on the longitudinal strain response of a buried pipeline are investigated. Characteristics of the soil response functions are reviewed and implications on pipeline design are addressed.

Reference:


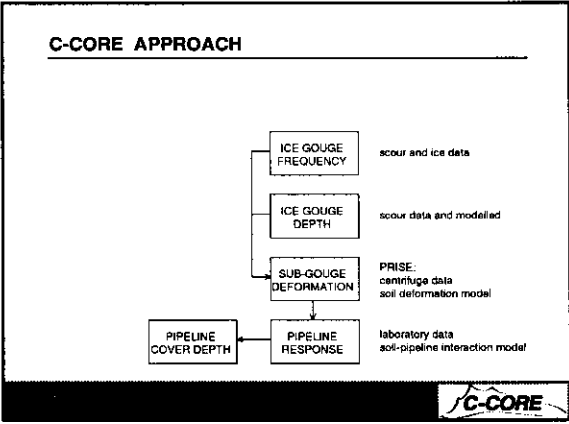
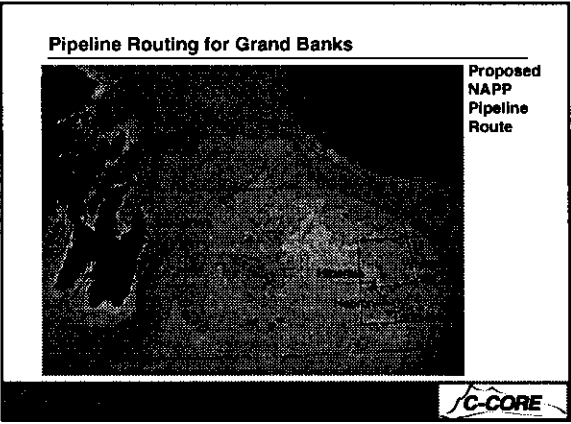
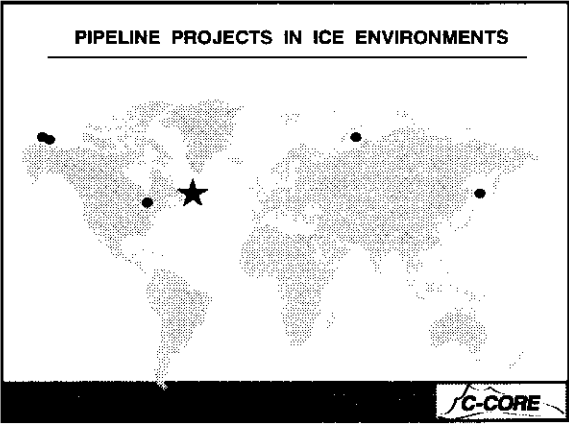
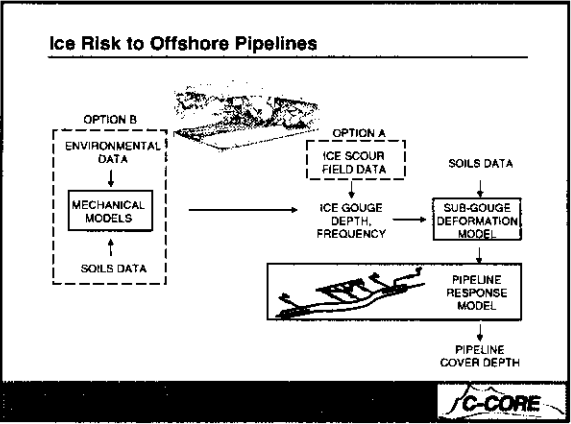
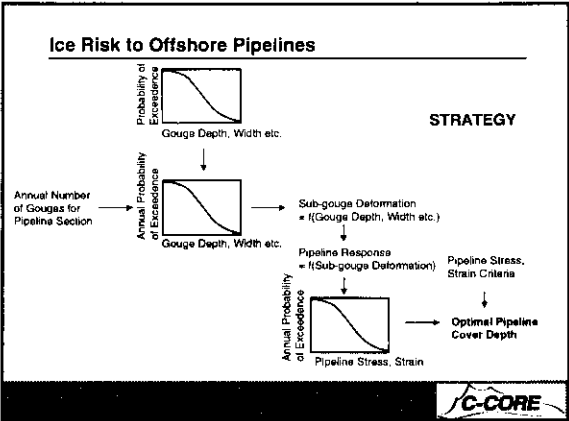
Kenny, S., Phillips, R., McKenna, R.F. and Clark, J.I. (2000). "Response of Buried Arctic Marine Pipelines to Ice Gouge Events." Proceedings, ETCE/OMAE2000 Joint Conference, Energy for the New Millenium, New Orleans, LA, USA, Paper Number OMAE00-5001.

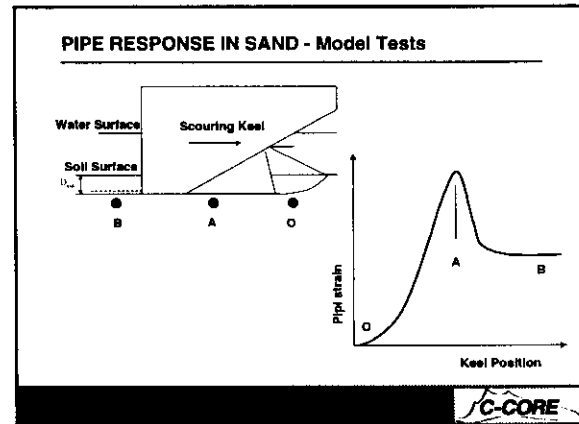
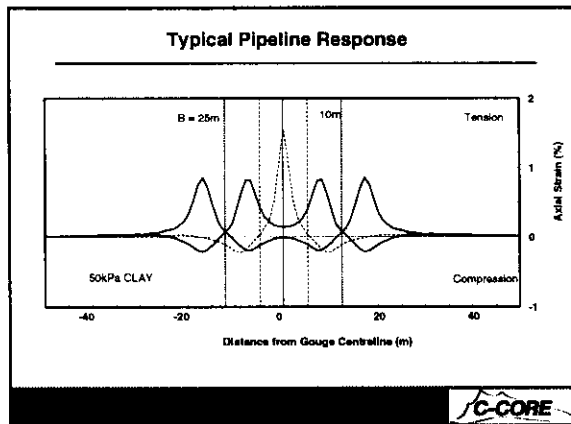
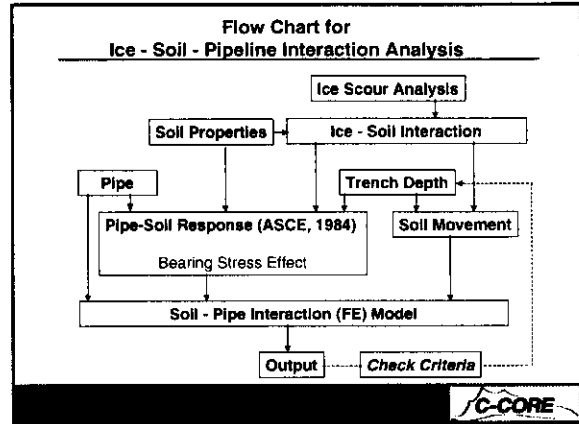
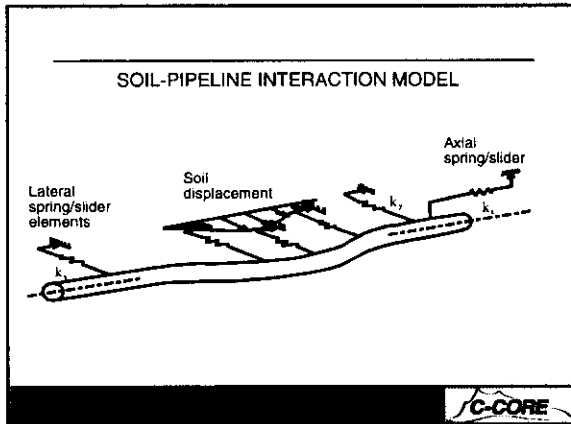
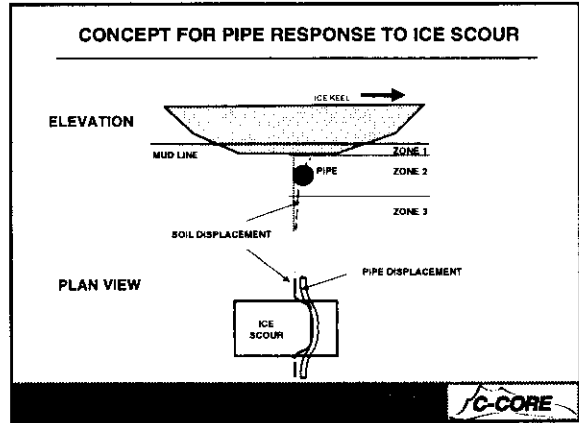
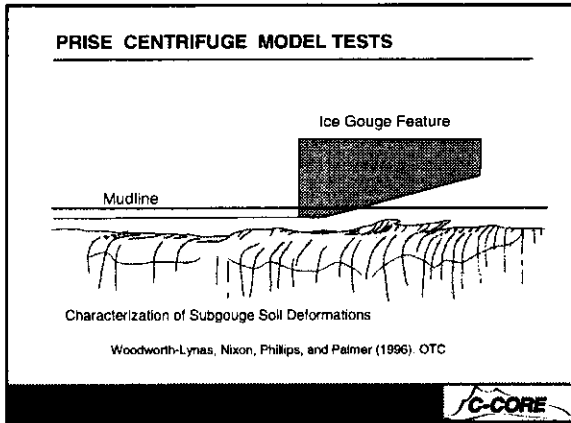
Response of Buried Arctic Marine Pipelines to Ice Gouge Events

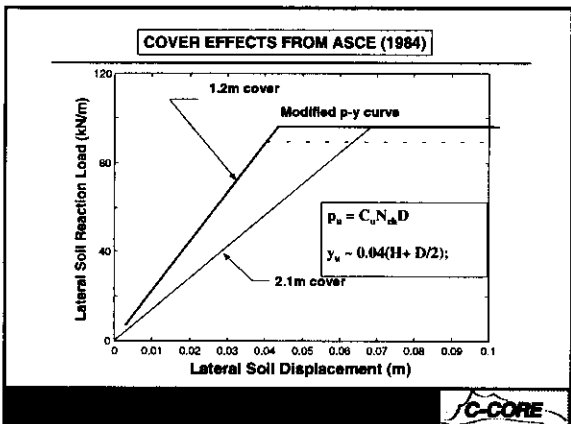
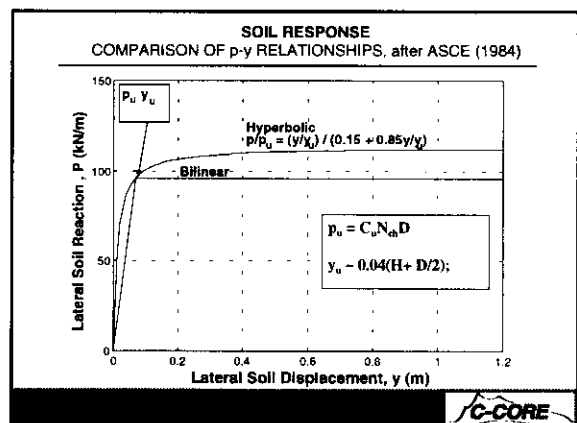
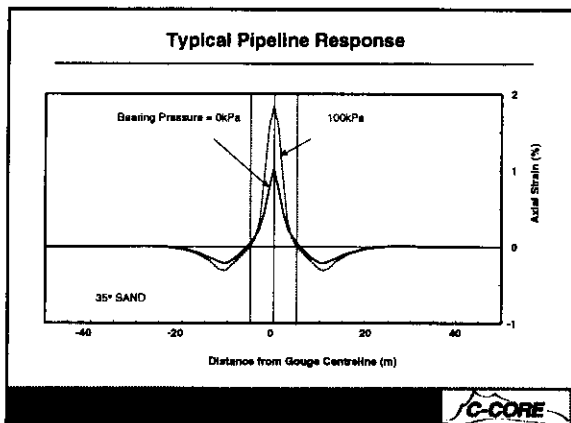
Shawn Kenny, Ryan Phillips, Richard McKenna and Jack Clark

C-CORE, Canada

See paper in OMAE 2000





- ### SUMMARY
- RISK ANALYSIS TO ASSESS NEED FOR BURIAL
 - COMPLEMENTARY USE OF SCOUR DATA AND MODELS
 - PIPE RESPONSE TO SUB GOUGE DEFORMATIONS
 - NEED FOR STRAIN BASED DESIGN
 - IMPORTANCE OF KEEL BEARING STRESS
 - APPROPRIATE SELECTION OF P-Y CURVES
- IC-CORE**

WELDING CHALLENGES FOR STRAIN-BASED DESIGN

Robin Gordon¹, John Hammond², Greg Swank³

1. INTRODUCTION

Pipeline engineering has seen an increasing trend toward strain-based design. This trend is particular to offshore pipelines where designs are evaluated with exacting site specific data, loading conditions, and material mechanical properties. Existing pipeline design codes are predominantly stress based whereby less rigorous detailed engineering analysis is required to produce acceptable pipeline safety. Strain-based designs place a greater onus on pipeline designers to ensure that integrity, safety, and environmental protection is not compromised. The rigors of strain-based analyses pose a number of challenges particularly related to pipeline girth welds and general material behavior. Consideration of greatest importance includes evaluation of tensile requirements, strain localization, brittle/ductile fracture toughness, weld procedure qualification tests, full-scale demonstration tests, fitness-for-service analysis, nondestructive evaluation, and future operational life cycle engineering critical assessment.

Proper analysis of all design loading conditions, including environmental factors affecting girth welds, is critical for the strain-based design to function in a determinant state.

2. REVIEW OF EXISTING PIPELINE CODES

2.0 General

The design, specification and construction of a strain-based design pipeline demands particular care to ensure appropriate code compliance and fitness-for-service. In the simpler mechanistic approaches that are appropriate for conventional stress based designs, it is possible to be guided almost entirely through the process by the code documents. This is not the case for strain-based design where, at each stage of the process, it may be necessary to demonstrate that a sound engineering approach has been adopted and implemented. In essence, few, if any codes offer the designer full assistance in this process and each step requires careful consideration of all engineering aspects. Essentially there are three separate issues of standards and code that must be taken into account at the outset, namely:

- Pipeline design codes (e.g., ANSI B31.4 and B31.8, BS 8010, ISO 13623, CSA Z662-M1996 and DNV 96)

¹ J. R. Gordon, Edison Welding Institute

² J. Hammond, BP Amoco plc.

³ G. Swank, Alaska Dept. of Natural Resources, Joint Pipeline Office

- Linepipe Standards (e.g., API 5L, ISO 3183, EN 10208 and DNV 96)
- Pipeline Construction Standards (e.g., API 1104, BS 4515 and DNV 96)

2.1 Design Codes

From review of the pipeline design codes, it is apparent that the older ones offer little guidance to assist strain-based design although BS 8010 Part 3, starts to address the issues.

Much interest is focused on DNV Rules for Submarine Pipelines (DNV 96) which is written as supplement to ISO DIS 13623 (Petroleum and Natural Gas Industries - Pipeline Transportation Systems) and purports to give detailed guidance on how to fulfil the ISO requirements. DNV 96 does consider limit states: namely, serviceability limit state (SLS), ultimate limit state (ULS), fatigue limit state (FLS) and accidental limit state (ALS) which are of relevance to pipeline systems. Furthermore, it specifies that for pipeline designs using displacement controlled capacities, only material of certain specified quality levels may be used. This document is perhaps unusual in that it specifies, in some detail, the qualities and grades of linepipe (although unfortunately it does not utilize the recently published ISO 3183 (Petroleum and natural gas industries - Steel pipe for pipelines - Technical delivery conditions Part 3: Pipes of requirement class C). A proposed draft revision of DNV 96 draws partially on the ISO standard, but still maintains a separate DNV grade. The extent of material and weld testing, even production weld testing, is greater than conventionally required. Specific guidance is given for the required limit state checks for pressure containment, buckling, fatigue, ovalization, accumulated plastic strain (APS), and fracture. Analysis of susceptibility to plastic collapse (buckling), accumulated plastic strain (from stress concentration factors (SCF) and possible local yielding) and fracture use engineering critical assessment (ECA) methods such as level 2 or 3 methods of PD 6493:1991 is suggested. (Note PD 6493 has recently been published as a full British Standard BS 7910). Specifically considering APS, DNV 96 considers that where the APS is less than 0.5% then simple non-destructive testing (NDT) requirements are adequate, where the APS is greater than 0.5%, but less than 2.0% an ECA is required to determine the crack tip opening displacement (CTOD) value in addition to NDT requirements (for use in conjunction with NDT) and where the APS is greater than 2.0%, additional requirements must be specified for the linepipe.

The recently published third edition of API RP1111 (July 1999) includes offshore hydrocarbon pipeline and limit state design methodology. This code includes criteria for several different limit states, but deals in particular detail with burst as the limit state and the appendices include detail of the methods and criteria for burst testing. It is clear that for limit state design, materials of high toughness and ductility are a pre-requisite to maintain ductile ultimate failure modes in burst, tension, bending, collapse, and combined loading. In qualifying a material and welding procedure for determining burst design criteria the practice recommends a minimum of six burst tests. Although this is only one of several limit states that have to be considered, the message is that for any limit state

pipeline design considerable additional testing is required to prove material performance and validate the design.

2.2 Linepipe Standards

Turning to the linepipe standards in common use, it is apparent that few begin to adequately address the specification and control of the most important mechanical properties such as yield and tensile strength and toughness in the context of strain-based pipeline design. Many pipelines operating in the world today are constructed in linepipe grades procured to the standard API 5L. The 41st edition of this standard specifies minimum values for yield and tensile strength, no limit on yield to tensile ratio (except for cold expanded pipe) and, with the exception of mandatory minimum toughness requirements for grade X80 (SMYS 80 ksi or 551 MPa), any toughness testing is an optional supplementary requirement (SR5 or SR6). However, it is common practice for client companies or contractors to procure such pipe to individual specifications that supplement API 5L.

Supplements that are frequently applied include an upper limitation on the yield strength (typically 15 ksi or 100 MPa above the SMYS) although in some cases the pipe supplier may seek to negotiate a higher upper limit to yield strength as, it is claimed, the specified upper and lower limits of yield strength are demanding targets for the steel makers and create production difficulties in the pipemill. Where this occurs, it is imperative that the designer's approval is obtained for any concession sought. Acceptance of a high upper limit of yield strength can result in weld metal under-matching difficulties even for conventionally designed pipelines, but the effects of over-strength parent pipe are more profound in strain-based pipelines as discussed later in this paper. Some newer standards such as ISO 3183 Parts 2 and 3 and EN 10208-2 do specify minimum and maximum yield strengths in which the yield strength range for higher strength grades; e.g., grade 415 and above is limited to 120 MPa (approximately 17.5 ksi), but stipulates only a minimum value for ultimate tensile strength. Larger yield strength ranges are permitted for lower grades. However, limiting yield to tensile strength ratio values are specified for each grade.

DNV 96 adopts a similar approach by imposing a limit on actual yield strength for all grades which must not exceed SMYS by more than 120 MPa (17.5 ksi). The ISO and EN standards specify precise Charpy toughness criteria, which in the case of ISO 3183-3 are for the avoidance of both brittle fracture and running ductile fracture in high-pressure lean gas pipelines. Considerable care must be taken with the specification of the parent pipe. For example, to achieve the necessary high toughness and ductility, specific composition ranges and manufacturing process measures (e.g., quench and temper treatments) may need to be agreed with the supplier.

2.3 Pipeline Construction Codes

Finally, the pipeline construction codes need to be considered. Two widely used codes (API 1104 and BS 4515) have been developed over the years as the construction codes for conventional pipelines but may be used with supplements and in combination with other codes and standards for the detailed testing and construction welding for strain-based pipelines. In general, these codes can be used to set a high standard for qualifying the welding and construction procedures for pipeline together with the qualification of welding personnel and mechanical and non-destructive test procedures.

Particular requirements for strain-based pipelines may need to be developed as addenda. Careful application of these standards and, in particular, compliance with the “essential variables” in welding procedure qualification testing and close control of the same parameters in pipeline welding should ensure that weld metal and weld joint mechanical performance is consistent and uniform. In many cases, additional separate measures such as the batch testing of welding consumables may be needed to supplement the code requirements.

Strain-based design is likely to require validation by ECA. Appendix A of API 1104 provides for alternative acceptance standards for girth welds, together with requirements of greater stringency for welding procedures and fracture toughness testing. The 1984 edition of BS 4515 (and the 1987 amendment to BS 4515) specified precise detail of CTOD specimen selection from qualification weldments together with reference to the now superseded BS 5762 for the detailed CTOD testing procedure. This combination of standards has been used to obtain CTOD values for girth welds and heat-affected zones (HAZ) for one strain-based pipeline design, the ECA then being carried out to BS PD 6493:1991. In the recent (1996) revision of BS 4515, the prescriptive directions for sampling and CTOD testing have been discontinued, but the user is directed to BS 7448 which supersedes BS 5762. Although DNV 96 calls up CTOD testing when an ECA is required, for detail and methodology it references BS 7448, API RP 2Z and PD 6493 for failure assessment.

2.4 Recommendations for Strain-based Design

- Given that there appear to be no, or few, comprehensive standards for strain-based design, pipeline designers should select from the various appropriate codes for their intended application. This approach may necessarily mean that sections of several different codes are used in the pipeline design and construction and for any ECA.
- Where sections from different codes and standards are used for limit state design of pipelines the designer must check to ensure compatibility between the design codes and standards used for the specification of pipeline and for construction.

- Particular care must be exercised to specify lower and upper limits of yield strength and of yield/tensile strength ratio for linepipe for limit state design.

3. GIRTH WELD STRENGTH REQUIREMENTS FOR STRAIN BASED DESIGN

3.0 General

It is generally accepted that pipeline girth welds should overmatch the tensile properties of the pipe material to avoid excessive strain accumulation in the girth weld during pipeline laying or normal operation. This is generally achieved by selecting welding consumables that produce higher tensile properties than the pipe material.

In selecting welding consumables for pipeline applications, there are two important issues that must be considered:

- Parent Pipe Tensile Properties
- Variability in Weld Metal Properties.

3.1 Parent Pipe Tensile Properties

With regard to parent pipe tensile properties all pipe material standards specify minimum yield and tensile strength requirements for each pipe grade. For example, the minimum yield and tensile requirements for API X52 pipe are as follows:

- Minimum Yield Strength: 52 ksi
- Minimum Tensile Strength: 66 ksi

However, while all pipe material standards specify minimum properties, many standards do not place limits on maximum properties. As a result, pipe ordered to a specific pipe standard may exhibit tensile properties well above minimum requirements. With regard to welding consumables, it is critical that consumables are selected based on actual pipe properties rather than minimum specified properties to avoid the possibility of unintentional undermatching. This can be demonstrated using the following example:

Material/Consumable	Yield Strength (ksi)	Tensile Strength (ksi)
API X52 Specification	52 (min)	66 (min)
Measured Pipe Properties	60-70	70-80
E7010G	57-65	70-78
E8010G	67-83	80-94

In this example, the measured pipe properties are typical of X52 pipe, i.e., the measured yield and tensile strength exceed minimum requirements by 10-15 ksi. Based on the X52 specification it would appear that the E7010G consumable is well suited for welding X52 pipe as it provides a small level of overmatch. However, based on the measured pipe properties, E7010G could result in undermatched girth welds. Based on measured properties, the E8010G consumable is a better selection since it will ensure that the weld metal overmatches the pipe material in both yield and tensile strength. In comparison, an E7010G consumable could give rise to a girth weld that undermatches the pipe material in both yield and tensile strength, which could be very serious in a strain-based design since the weld would become a source of strain localization.

In the above example, the measured yield and tensile properties exceeded the minimum required properties by 10-15ksi, which is not excessive. Nevertheless, the authors have experience of pipeline projects in which the measured pipe tensile properties exceeded minimum requirements by more than 30 ksi. This can give rise to major problems in not only selecting weld consumables, but in developing weld procedures that provide acceptable levels of strength and toughness. For this reason, the authors recommend that all pipe specifications for strain-based design include both minimum and maximum properties for yield and tensile strength.

3.2 Variability in Weld Metal Properties

In general, weld metal tensile properties show a much larger variability than parent material tensile properties. For this reason it is important that weld metal properties be established for each welding consumable / procedure combination being considered rather than relying on manufacturers' quoted values. Although cross weld tensile tests are useful for demonstrating overall joint strength, they do not provide reliable measures of weld metal yield and tensile strength. For this reason weld metal tensile properties should ideally be established by conducting all weld metal tensile tests on specimens extracted from girth welds produced using representative weld procedures.

In addition to within-batch and batch-to-batch variability, there can also be significant variability in weld metal tensile properties around the circumference of a girth weld. Indeed, investigations of weld metal strength variability in pipeline girth welds have shown variability of 10 ksi around the circumference with the lowest values typically at the 6 o'clock position as shown in Figure 1.

As a result, weld consumable selection should account for the variability in weld metal tensile properties between batch to batch and around the circumference of a pipeline girth weld.

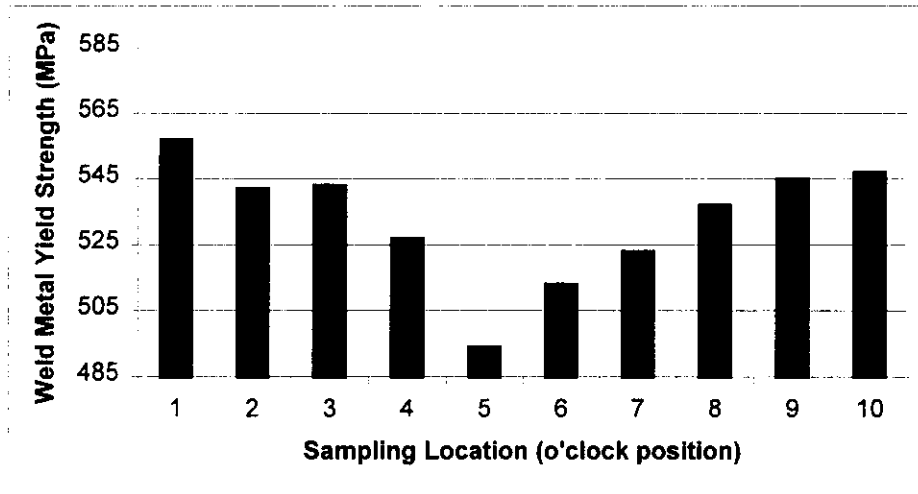


Figure 1. Average Weld Metal Yield Strength Values as a Function of Sampling Location for E9010 Electrode Deposits[1]

While most welding codes require overmatched welded joints, there are, however, a number of reasons why excessive overmatching should be avoided, particularly for high strength linepipe. The potential drawbacks of excessive overmatching include:

- Weld metal toughness decreases as weld metal strength increases.
- The likelihood of hydrogen cracking increases as weld metal strength increases.
- The likelihood of weld flaws increases as weld metal strength increases (i.e., reduced weldability).
- The possibility of localized hard zones increases as weld metal strength increases.

For the reasons listed above, pipeline designers should select welding consumables that provide a small but safe margin of overmatch for strain-based design rather than selecting consumables that will result in excessive overmatching.

3.3 Strain Accumulation

In any strain based design application there is a need to ensure that localized strain accumulation is limited. In pipeline girth welds strain accumulation can occur in either the parent pipe, weld metal or heat affected zone (HAZ) region.

Localized strain accumulation can occur in the parent pipe in situations where the pipe material has a high yield to tensile strength (Y/T) ratio. In such cases local strain concentrations (e.g., local thin areas resulting from corrosion in service) can lead to high localized strain accumulation due to the low work hardening capacity of the pipe material. Over the last 10 - 20 years the maximum acceptable Y/T ratios for linepipe

materials has increased from approximately 0.85 to 0.9 - 0.92. Although high Y/T ratios (i.e., > 0.9) are becoming increasingly accepted for stress based design pipelines they can give rise to problems in strain based design. For this reason linepipe specifications for strain based design should place specific limits on Y/T ratio. In the absence of definitive guidance the authors would recommend an upper Y/T limit of 0.92 for strain based design pipelines.

Weld metal strain accumulation occurs when the girth weld undermatches the parent pipe. In cases of girth weld undermatching, strain accumulation tends to focus in the weld root region that is frequently welded with lower strength consumables to reduce the risk of cracking. Strain localization can also occur in the weld root region in cases where the girth weld nominally matches the parent pipe due to the “V” shaped weld geometry. In cases where the weld root is produced using consumables which undermatch the parent pipe it is important that the fill passes are welded using overmatching consumables as this will shield the weld root region.

While proper weld consumable selection and procedure development can minimize the possibility of strain accumulation in the girth weld, there is still the possibility of heat-affected zone (HAZ) strain accumulation. HAZ softening in pipe girth welds is not a new issue and has been responsible for a number of service failures, particularly on applications which see high levels of cyclic plastic strain (e.g., reeling). HAZ softening is more prominent in high strength steels and in cases where welds are fabricated at high heat inputs. Soft HAZs can be minimized by modifying pipe chemistry (e.g., addition of niobium) and controlling weld heat input.

Over the last 20 years there has been extensive research into the structural significance of weld metal mismatch (undermatch and overmatch). This research has demonstrated that the tensile behavior of undermatched welded joints is dominated by the surrounding material if the weld is sufficiently narrow. This is due to the restraint provided by the surrounding material that resists plastic deformation of the weld (contact strengthening). Although there has been less research into the structural significance of soft HAZs, the available research supports the same findings obtained from the mismatch studies. That is, provided the soft region is small in comparison to the material thickness (e.g., less than $\frac{1}{4}$ to $\frac{1}{2}$ of plate thickness) the tensile behavior is dominated by the surrounding material. In addition, the circumferential restraint provided by a girth weld will also limit the development of plasticity in soft HAZs of pipeline girth welds. A recent study[2] funded by the Pipeline Research Committee International (PRCI) found that the strain concentration in soft HAZs is not affected by weld metal strength. Moreover, the strength and ductility of pipes is not affected by the worst-case HAZ softening provided the loading is not cyclic and there are no significant defects in the weldment.

3.4 Recommendations

- Pipe specifications should include both minimum and maximum tensile properties and place a maximum limit on Y/T ratio (e.g., 0.92).
- Weld consumable selection should be based on measured pipe properties rather than minimum specified properties
- Weld metal tensile properties should be confirmed (by testing) for each welding consumable / procedure combination being considered.
- Weld consumable selection should account for both batch-to-batch variability and variability in weld metal tensile properties around the circumference of a girth weld. Procedure qualification tests should be conducted to demonstrate acceptable weld metal tensile properties.
- HAZ softening should be minimized through parent pipe chemistry and pipe making practices and weld procedure development.

4. GIRTH WELD TOUGHNESS REQUIREMENTS FOR STRAIN-BASED DESIGN

4.0 General

It is critical that all pipeline girth welds possess adequate toughness to prevent brittle or ductile fracture during pipeline laying and operation. With advances in steel, pipe making, and welding technology, brittle fracture is nowadays only a concern for low temperature applications (e.g., Arctic service). Ductile fracture, however, remains a concern for all pipelines; particularly those designed to accommodate high strains.

It is now common practice to specify minimum toughness requirements for pipeline girth welds to ensure adequate resistance to brittle and ductile fracture. Minimum toughness requirements are generally determined by conducting fitness-for-service assessments assuming the worst case loading condition and the maximum permissible flaw size. Over the last 20 years standard fitness-for-service assessment methods have been developed for stress-based loading. The Failure Assessment Diagram (FAD) approach is now the most widely accepted method of performing fitness-for-service assessments. Using this approach, it is possible to assess the likelihood of fracture and plastic overload simultaneously. While the same concepts can be extended to strain-based loading, the assessments can become increasingly complicated particularly for high strain loadings (>1.5 yield strain).

4.1 Brittle Fracture

The CTOD Design Curve approach was one of the earliest methods proposed for conducting fitness-for-service assessments of welded structures. This approach was developed by correlating the results of full size fracture tests with small-scale fracture toughness tests. Although the original work focused predominantly on brittle fracture, the CTOD Design Curve approach can also be used to assess ductile fracture.

The CTOD Design Curve method has been adopted by a number of pipeline codes including API 1104 and BS 4515. Although the original CTOD Design Curve equations were developed as a function of applied strain, they are now more commonly stated in terms of applied stress. As a result, unlike the FAD based assessment methods (which are essentially stress-based) the CTOD Design Curve method provides a convenient approach to assess fracture under strain controlled loading. While the CTOD Design Curve has been superseded by more advanced assessment methods, this approach, nevertheless, still provides a simple and validated approach for assessing resistance to brittle fracture under strain-based loading.

Using the CTOD Design Curve approach it is possible to develop minimum toughness (CTOD) requirements for pipeline girth welds for different levels of applied strain and flaw size. Nevertheless, in developing minimum toughness requirements for a specific application, the designer must take into account the expected loading and temperature histories that the pipeline girth weld will see during construction, pipe laying, and operation. For example, in the case of an Arctic sub-sea application, a pipeline girth weld may experience its lowest temperature during pipe laying but may see the highest applied strain under operating conditions which could be at a much higher temperature. In such cases it is important that toughness requirements are developed for all limiting combinations of load (strain) and temperature and the most demanding requirement adopted. This is illustrated in Figure 2 which shows a schematic CTOD transition curve with minimum toughness requirements superimposed for both pipe laying and operation. In this case, the maximum applied strain during pipe laying was assumed to be approximately 50% of the maximum applied strain in operation. In this example it can be seen that if toughness tests were conducted at the normal pipeline operating temperature they would exceed the minimum toughness requirements determined assuming maximum operating loading conditions. However, toughness tests conducted at the pipe laying temperature would not satisfy the minimum toughness requirements determined for the loading conditions during pipe laying. In this example, the pipeline laying operation is more demanding than normal operation conditions even under maximum loading. In cases like the above example the designer should either determine the limiting (most demanding) event or alternatively specify minimum toughness requirements for multiple temperatures.

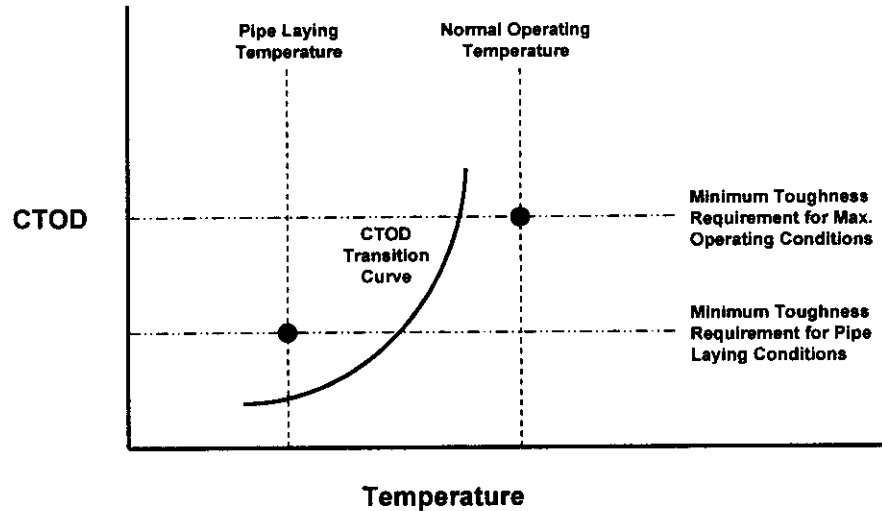


Figure 2. Minimum Toughness Requirements

4.2 Ductile Fracture

Unlike brittle fracture, a materials resistance to ductile fracture is not strongly dependent on temperature. For ductile fracture it is normal practice to characterize a materials resistance to ductile fracture in the form of a crack growth Resistance Curve (R-Curve). The material R-Curve information can then be incorporated into a fitness-for-service assessment to establish the limiting flaw size.

In the case of strain-based design, it is critical to minimize localized strain development to limit the possibility of ductile fracture. This is best achieved by developing weld procedures that produce girth welds that overmatch the parent pipe. In cases where it is necessary to adopt welding consumables for the root pass that undermatch the parent pipe, it is particularly critical that the fill passes overmatch the pipe material to avoid local strain development in the weld root region.

4.3 Recommendations

- The CTOD Design Curve method provides a simple and validated approach for assessing the resistance to brittle fracture under strain-based loading.
- Minimum toughness requirements should be based on the limiting combination of temperature and loading experienced during construction, pipe laying and operation. If the limiting combination is not apparent, toughness requirements should be specified at multiple temperatures (e.g., transition curve).
- Girth welds should overmatch the actual pipe material properties to increase the resistance to ductile crack growth, particularly in the weld root region.

5. WELDING PROCEDURE QUALIFICATION FOR STRAIN-BASED DESIGN

5.0 General

The selection of the welding process and consumable welding filler materials, together with the specification and qualification of the welding procedure for construction of a strain-based design pipeline is inevitably more stringent than for a conventional design of pipeline. Selection of the actual welding process should be made at the design stage taking full account of the anticipated performance requirements of the welds at each stage of the construction and operation of the pipeline. At this stage it should be possible to optimize the choice of welding process and short list suitable consumables. This does not imply that the welding process and procedure needs to be technically complex or expensive, although in some cases this will be the case. In many instances the competent application of conventional welding technology and materials with attention to specific detail and augmented with specific testing designed to demonstrate the fitness of the welded joint for the intended application will be appropriate. The individual nature of each limit state design pipeline means that no list of recommendations in a paper such as this can be wholly comprehensive and each design must be subject to individual detailed analysis.

5.1 Special Weld Procedure Qualification Considerations

The following example summarizes the measures adopted for one offshore strain-based design pipeline for an arctic environment. This pipeline will be welded and laid in the arctic winter months, during which period it will be subject to extreme cold temperatures (typically minus 50°F) soon after welding (although welding will be carried out in heated, mobile shacks which enclose the pipeline) and during the laying operation. For the construction and pipelay stage, it is important that the linepipe and girth welds have the requisite toughness and ductility to ensure freedom from hydrogen induced cracking during and after welding and that weldment toughness is sufficient to permit the limiting pipelay strains to be safely accommodated when this operation also occurs at low temperature. Once laid, the pipeline is at a higher temperature (arctic seawater at 29°F) and then when in full operation, its inventory raises its temperature further to around 50° F. However, it is the operational stage that presents a high strain situation in which ground or ice movement may impose higher strains on the pipeline. The test program to validate the design which included an ECA to qualify the welding procedure and to test the materials was extensive and included the following tasks which may be applicable to other strain-based designs.

- Supplementation of the API 5L X52 seamless linepipe procurement specification to ensure high toughness and ductility via restricted chemical composition utilizing quench and temper manufacturing treatment and more stringent dimensional

tolerances to enhance resistance to plastic collapse by minimising internal misalignment.

- Careful specification of the welding procedure for the girth weld. Several techniques and materials were considered, but it was found that SMAW using conventional pipe welding techniques with E8010-G cellulosic coated welding electrodes met the specified mechanical requirements. The procedure was qualified at high and low levels of heat input under conditions simulating site pipe welding to demonstrate that the mechanical properties could be maintained at the limits of the welding parameter envelope.
- Full mechanical and physical testing of coupons from the welding procedures qualification tests (to API 1104), supplemented by CTOD tests on test coupons sampled from around the clock positions of the weld circumference. The mechanical and physical testing on test pieces from pipe nipples qualifies the welding procedure in conventional terms. The CTOD data is used to validate the design parameters and, in particular, to confirm the maximum size of flaw that would be acceptable in the weld under the specified pipelay and operating conditions.
- The complete weld zone, comprising weld metal, HAZ and parent pipe is of importance for strain-based design. CTOD testing with notch positions in weld metal, and fusion line/HAZ at $\frac{1}{4}t$, $\frac{1}{2}t$ and $\frac{3}{4}t$ positions through thickness to confirm representative toughness measurement within the welded joint.
- Where girth welding is to be performed by the SMAW cellulosic technique, knowledge of the hydrogen content of the girth welds on completion is of value as hydrogen reduces weld metal toughness. As hydrogen diffuses from the weld (time and temperature dependent) toughness recovers. In the example given, samples taken from similar welds were shipped under refrigeration to Edison Welding Institute (EWI) for determination of weld metal diffusible hydrogen content and a hydrogen evolution curve plotted.
- Supplemental tests on full length joints, which were welded under simulated production pipelay (site) conditions and subjected to repeated simulated pipelay strain at temperature of minus 50°F. The purpose of these tests was to investigate any effect of diffusible hydrogen on weld metal toughness, to validate the ECA flaw size and to evaluate any adverse performance for arctic pipelay. The size and form of the defects was later verified by fractographic examination in the laboratory. These tests indicated a high degree of tolerance to acceptable size anomalies at the expected temperature and strains of the pipelay. This type of simulation test is perhaps analogous to the multiple reverse bending tests often carried out on welding pipe strings for reeled offshore pipelines.

- It may be prudent to conduct tests to determine the effects of variables without the specified welding parameters. In the example quoted, the full length joint girth welds were made and allowed to cool rapidly in the arctic environment (more rapidly than would be allowed by the qualified welding procedure) and similarly subjected to simulated pipelay strain, followed by CTOD testing and hydrogen determination. The purpose of these tests was to investigate if residual diffusible hydrogen in the weld resulted in low toughness and caused any adverse performance for arctic pipelay. The results of these tests were satisfactory.
- Finally, in order to determine the recovery of CTOD value with hydrogen evolution, two further test welds were made using the qualified procedures and shipped under refrigeration to the test laboratories. CTOD test pieces were machined and tested in a specified sequence over three weeks during which the untested samples were held in ice/water at approx 32°F while the second control set were held at room temperature. This allowed the holding time-CTOD value relationship to be plotted and such data could be used to optimize the timing of the pipelay operation.

5.2 Small-Scale Testing Considerations

In testing any limit state design pipeline the value of small versus full-scale tests needs to be carefully evaluated and this may be a variable from design to design. In the example given above, the validity of the welding procedure qualification tests being performed initially on short pipe nipples was questioned on the basis that welding full length joints in the WPQT better simulates actual field welding conditions as a result of axial constraint. It was also considered that such a condition results in maximum residual stresses in the weld which will be reflected in the CTOD values obtained. However, it is generally accepted that pipe joints that exceed $5\sqrt{Rt}$ in length will guarantee full field axial and circumferential residual stress distributions in girth welds, as illustrated in Figure 3. Later, this was confirmed by CTOD tests on samples from welds of full pipe joints which gave virtually identical results to those carried out on the original WPQT welds.

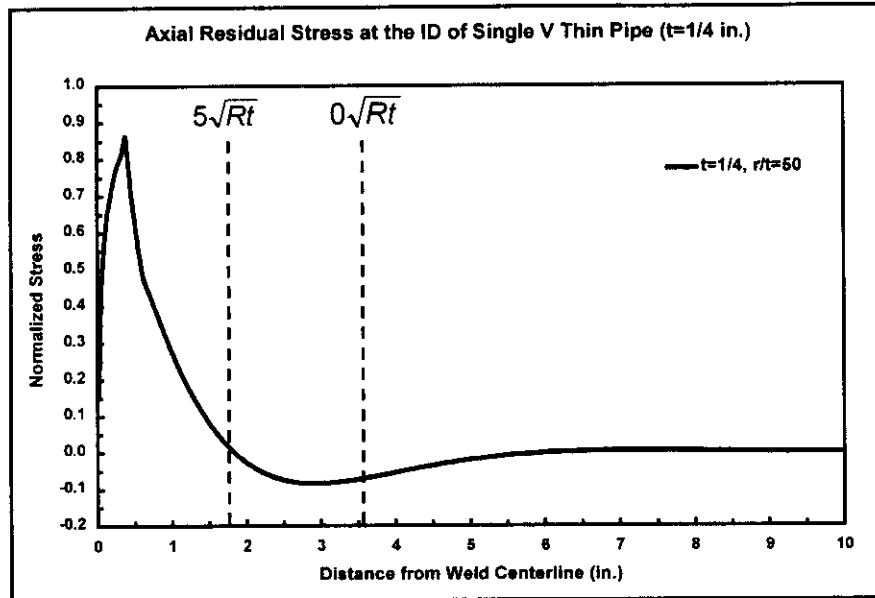


Figure 3. Typical Residual Stress Distribution in Pipeline Girth Welds

5.3 CTOD Temperature Validation

Another consideration of testing was the validity of CTOD test results relative to the installation and operating temperatures of the pipeline. Although the qualification tests welds were made under conditions that simulated production pipelay welding, a time lapse occurred between manufacture of the welds and machining and testing of the CTOD specimens, during which time the material temperature was higher than would be expected during pipelay. The later tests took this into account and shipped test pipe rings under refrigeration by solid carbon dioxide and machining was done cold to retain diffusible hydrogen in the test piece. The results of this series of tests enabled the dynamics of hydrogen diffusion and toughness recovery to be understood and will assist in the planning and execution of pipe welding and pipelay.

5.4 Need / Benefit of Full Scale Testing

The series of small scale mechanical and metallurgical tests provide necessary base data in much the same way as for conventional pipelines but some full scale tests may be required to validate the extreme limit state condition, in this case that of high strain bending. A series of four full size internally pressurized and instrumented bending tests were carried out, one on parent pipe and three on the girth welded pipe. The girth welds in two of the test pipes contained artificially implanted root and buried defects. The bending tests were carried out to a tightly specified procedure at low temperatures, under internal pressure and in each case were successful, the pipe string being bent to a strain level of more than three times the extreme strain considered in the design basis. The fourth test involved bending to a strain far in excess of the design basis with the intention of investigating the form in which any fracture in the weldment would occur. However,

the final form of failure was plastic collapse (buckling) of the pipe at a high level of strain. Detail of this test will be the subject of another paper at this conference

5.5 Recommendations for Selection and Qualification of Welding Procedures for Strain-Based Design Pipelines

- Each strain-based design (limit state design) pipeline should be considered as unique and welding and construction methods and materials should be an integral part of the design process. This necessarily involves the pipeline contractor at the design stage.
- The design process defines the applicable limit state or states and the mechanical properties required for each state. Selection of the welding process and materials together with specification of the welding procedure (with any necessary refinements) must ensure that the welds produce the mechanical properties required for joint integrity for each limit state.
- Qualification of the welding procedure will ensure compliance to a recognized pipeline welding code, but for strain-based design pipelines this is only the starting point and additional small and/or large-scale tests will generally be required. The exact type of test and amount of testing will depend of the particular pipeline design and operating criteria but will generally include fracture toughness testing on small-scale specimens.
- In some cases it will be necessary to carry out purpose designed, larger scale tests on weldments for strain-based design pipelines to demonstrate the design calculations and prove the materials and methods of construction. Examples of such type-tests include pressurized bending tests at or below operating temperature, or for reeled pipe a sequence of reverse bending tests at strain levels and rates to simulate the reeling operation or where burst is the limit state criteria, several burst test may be required.
- Limit state pipelines require close attention to detail at the design stage and detailed review of apparently minor factors must be taken into account and may warrant specific testing. The effect of hydrogen content on weld metal toughness is just one typical example.

6. SUMMARY

Rigorous engineering analysis utilizing detailed site-specific data can result in acceptable strain-based designs that operate within acceptable integrity, safety, and environmental protection limits. Progress is being made relative to pipeline welding evaluation, however, no prescriptive guidance for strain-based design procedure qualification testing is currently available. A need to develop general pipeline welding procedure guidance when imposing a strain base design exists. The authors suggest that in the interim,

designers should use best engineering practices to evaluate the adequacy of the girth welded joint to perform to the intended limit states plus perform full scale demonstration bend tests as required. Further recommendations on weld metal strength, toughness and supplemental weld procedure qualification tests are provided for designer's consideration and evaluation.

7. REFERENCES

1. Denys, R. M., Lefevre, T., Glover, A. G., "Weld Metal Yield Strength Variability in Pipeline Girth Welds", Pipeline Technology, Vol. II, pp. 591-598.
2. Dexter, R. J. and Lundin, C. D., Plastic behavior of pipeline girth welds with softened heat-affected zones and undermatched weld metal. Mis-Matching of Welds. ESIS 17 (edited by K.-H. Schwalbe and M. Kocak) 1994. Mechanical Engineering Publications. London, pp. 741-755.

8. BIBLIOGRAPHY

ASME B31.4	ASME Code for Pressure Piping B.31. An American National Standard Liquid Transportation Systems for Hydrocarbons, Liquefied Petroleum Gas, Anhydrous Ammonia and Alcohols
ASME B31.8	ASME Code for Pressure Piping B.31. An American National Standard Gas Transmission and Distribution Piping Systems
API 5L	Specification for Line Pipe. 41 st Edition 1997
API 1104	Welding of Pipelines and Related Facilities
API RP 2Z	
API RP1111	Design , Construction, Operation and Maintenance of Offshore Hydrocarbon Pipelines (Limit State Design). 3 rd Edition 1999
BS 4515-1:1996	Welding of Steel Pipelines on Land and Offshore
BS 5762: 1979	Methods for crack opening displacement testing. (Withdrawn and superseded by BS 7448 Part 1: 1991)
BS 7448: 1991	Fracture Mechanics Toughness Tests. Part 1. Method for determination

	of K_{Ic} , critical CTOD and critical J values of metallic materials. (Superseded by BS EN ISO 12737:1999)
BS 7910:1999	Guidance on Methods for assessing acceptability of flaws in fusion welded structures. (Supersedes PD 6493)
BS 8010	Code of Practice for Pipelines. Part 3: Pipelines Sub-sea; Design Construction and Installation
BSI PD 6493: 1991	Guidance on methods for assessing acceptability of flaws in fusion welded structures
CSA Z662-M1996	Oil and Gas Pipeline Systems. 3 rd Edition
DNV 96	Rules for Submarine Pipeline systems
EN 10208 technical	Petroleum and Natural Gas Industries - Steel pipe for pipelines - delivery conditions. Part 1: Pipes of requirement class A: 1996 Part 2: Pipes of requirement class B: 1996
ISO 3183 technical	Petroleum and Natural Gas Industries - Steel pipe for pipelines - delivery conditions. Part 1: Pipes of requirement class A: 1996 Part 2: Pipes of requirement class B: 1996 Part 3: Pipes of requirement class C: 1999
ISO DIS 13623 Systems	Petroleum and Natural Gas Industries - Pipeline Transportation
ISO WD 16708 Systems	Petroleum and Natural Gas Industries - Pipeline Transportation Reliability Based Limit State Methods. (Document in early draft)

TO A PROBLEM OF CONSTRUCTION OF SEA PIPELINES IN THE FREEZING SEAS

Alexandre T. Bekker

INTRODUCING

The exploration of offshore deposits of oil and gas on continental shelf is one of priority directions of progressing of economics of Russia. One of actual problems of a construction of offshore deposits in the freezing seas of our country is oil and gas transportation on land. The most abundant transportation way in these conditions is applying of sea pipelines.

At designing and construction of sea pipelines and other communications in the freezing seas it is necessary to account for ice cover action. The drifting hummocks and icebergs are the most dangerous objects for pipelines.

One of main and most abundant methods of pipeline protection from possible external damages, is the ground bottom. At bottom penetration of the pipeline in a ground on sufficient depth affecting external environment are greatly dropped. However the construction cost is rapidly increased with pipeline depth in ground.

On the data of some authors concerning residual furrows at ploughing by hummocks of seabed in northern seas, the depth of furrows can change over a wide range, depending on water depth and hummock mass: from 0.5 m up to 5 m, and in rare cases up to 7 m. The present experience of pipeline construction is limited to bottom penetration on 1.5 m. Allowing all this it is expedient to consider a combined protection way, at which one the pipeline is deepened on smaller depth, and the affecting of an drifting hummock is perceived by a construction of complementary protection working together with the pipeline.

1. PARAMETERS OF RIDGES AND HUMMOCKS

The main area of location of oil and gas fields on Far East is in eastern part of northern Sakhalin shelf. The ice conditions in the given area are determined by the eastern Sakhalin ice massive. As a result of studies some relationships of forming of ice morphological features in offshore area were found. The greatest probability of presence of ridge deformations having full contact with ground, is in range of depth 7-15 m, on depths of 15-20 m - much less, and 30 m – only single formations.

Mass of hummocks changes in significant limits. There are more often ice formations is powerful 15-35 thousand tons, characteristic for depths 10-15 m, on larger depths the appearance of hummocks is probable up to 70-80 thousand tons, and the separate formations can reach 1 mln. t, and drifting velocity 1,5 m/s. The area of above water parts of hummocks is in limits from 1000 m up to 5000 m² [3].

The mechanism of hummock forming is till now not investigated. Knowledge of this phenomena are bounded only to ascertaining of formation season, ice age, water depths, where were recorded.

In a general view the hummock consists of three large parts:

- the top located above of a water boundary, is derived, in main more by new ices.

The magnitude of a fill factor of a hummock was 0,7-0,8;

– the mean part is folded predominantly from chunks coastal ice, fill factor 0,8-0,9;

– the hummock bottom is composed of loose ice, has more thin, than in top of a hummock, mean fill factor 0,6-0,7.

The power of hummocks (i.e. its vertical sizes) is inflected from 10 up to 20 m, mean power of 15,3 m. All these hummocks are laied out on depthes up to 15 m. However hummocks meet and on no-bottoms, in particular on depth of 30 m. Therefore, the power of hummocks can achieve 40 m and more [4].

The greatest concern at study of ridge formations, from the point of view of use reliability of sea pipelines, is introduced by the max depth of furrow from ploughing of ground by a underwater part of a hummock. By results of studies greatest of the measured depthes was 2.13 m, and least 0.4 m.

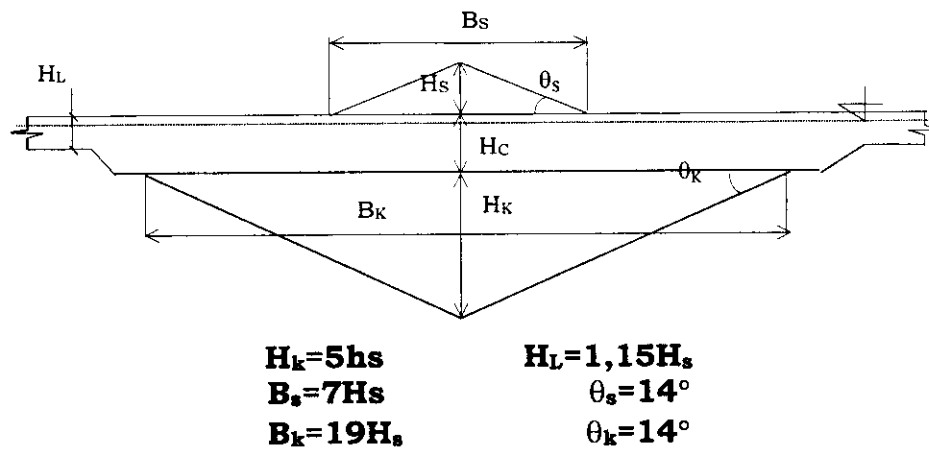


Fig 1. Scheme of an one-years drifting ridge.

The full-scale investigations of drifting hummocks and specially stamukh are small. In main observations their sizes were fixed the form of sail and keel parts of hummocks. The deirect data on depth of keel penetrance of hummock into bottom ground, parameters of movement of hummocks at landing on a ground, the geometry of stamukh keel has not enough, its are single.

The full-scale investigation procedure of study of one-year stamukh on coast of the Okhotsk sea made by Design and research institute «SakhalinNIPImorneft», envisioned topographic surveys of stamukh surfaces and bottom in direct proximity, thermal drilling, diving inspection, geophysical methods. It has allowed to determine not only exterior stamukh shapes, but also internal structure, keel shape, deepened into bottom and etc.

2. FEATURES OF HUMMOCK ACTIONS ON SEABED

Generally at interaction of drifting hummocks with bottom can originate: an penetration of keel of a hummock in seabed; partial breaking down, lining of hummock keel; sliding up of a hummock on a underwater shore slope; hummock plan turn around of instant center of rotation - interaction point with bottom; hummock stop at ending of drop energy; breaking down of ice field on contact with

hummock; repetitive hummock movements at ice field action.

The penetration process of hummock into seabed, therefore, and penetration depth are depended: geometrical parameters (bottom configuration, hummock keel shape, thickness and area of ice field); kinematic characteristics of drifting hummock and ice field (velocity, angle between a direction of movement and isobath); dynamic characteristics (mass of hummock and adjoining ice field, water added mass, position of mass center and velocity of current, wind velocity); physical-mechanical characteristics of bottom soil (density, angle of internal friction, cohesion); ice strength characteristics.

The max penetration depth of hummock keel into bottom is determined by drop energy of drifting ridge formation. At ploughing of bottom by moving hummock together with an ice field, adjoining to it the significant penetration depths are possible, while the hummock will not stop or there will be no breaking down of ice.

The moved hummock has significant drop energy Φ . At interaction with seabed this energy is lost on an penetration into bottom E_{Φ} , vertical displacement Φ_{Σ} , turn in the plan and in a vertical plane $\Phi_{||}$, breaking down of a part of a hummock Φ_{\perp} . The power losses on breaking down of hummock keel depend on its configuration, layout density and strength characteristics of ice pieces and bottom soils. The full scale observations have shown, that the hummock keel parts has sufficient structural integrity and density. If to consider the most unfavorable case from the point of view of depth of communication location in bottom seabed, it is necessary to neglect E_{Σ} , $E_{||}$ and Φ_{\perp} .

3. PENETRATION DEPTH OF HUMMOCK KEEL INTO BOTTOM

Fig. 2 shows the interaction scheme of hummock with a underwater coastal slope [1]. We accept following assumptions for an estimation of power losses during penetration:

- Up to grounding the hummock moves forward with constant velocity;

- At interaction with bottom the mass center of a hummock is displaced on a direction of velocity vector, i.e. sliding and turn are absent;
- Bottom slope is constant.

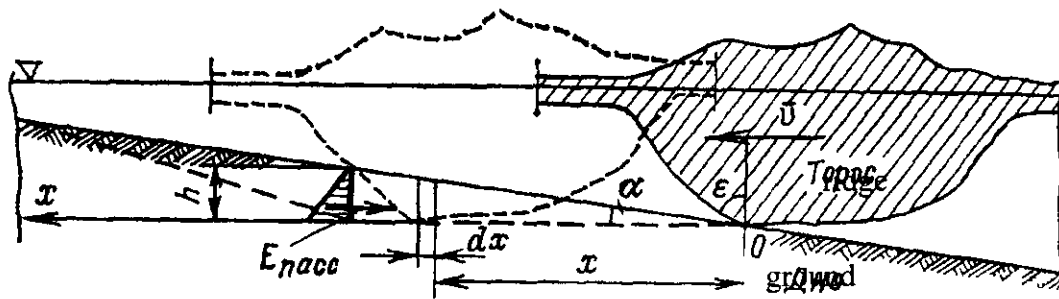


Fig. 2. Scheme of hummock interaction with shore

Accepting a coordinate axis x of the velocity, directional on a vector, v , we shall receive expression for power losses on an penetration on infinitesimal distance dx

$$dE = F_{nac} dx \quad (1)$$

where $F_{(0)}$ is soil passive resistance.

The soil passive resistance according to the theory of limiting equilibrium, is determined under the formula [2]

$$F_{nac} = \frac{1}{2} \rho g h^2 \lambda_p b \quad (2)$$

where ρ is soil density; h is soil layer height, m; λ_p - coefficient of lateral passive resistance; b - hummock width in cross section, m.

Taking into account apparent ratio $h=x \operatorname{tg} \alpha$, we shall receive a total energy expended on introduction

$$E = \int_0^x dE = \frac{1}{6} \rho \cdot g x^3 \cdot \operatorname{tg}^2 \alpha \cdot \lambda_p b \quad (3)$$

Taking, that all kinetic energy of ridge formation is spent for overcoming of penetration resistance up to stop stop, using the original positions of the theory of

limiting equilibrium [2], we shall receive maximal depth of keel penetration

$$h = \sqrt[3]{\frac{3mv^2 \operatorname{tg} \alpha}{\rho g b \lambda_p}} \quad (4)$$

where m is mass of ridge formation including hummock mass, mass of adjoining ice field and added mass, t ; v - velocity, m/s.

At designing of possible ridge penetration depth in a ground bottom it is necessary take account of drop energy losses. In some cases its can be considerable.

During penetration process the hummock rise on magnitude Δh relatively sea-level, and the necessary force will be determined as

$$F_s = S \rho_s g \Delta h \quad (5)$$

where ρ is ice density; S is hummock top area, m^2 .

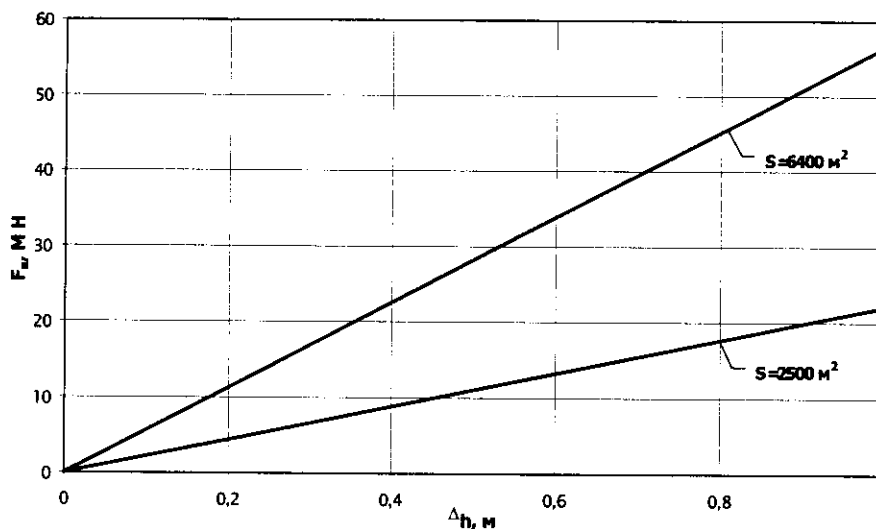


Fig. 3. Dependence of vertical force F from raising height Δh .

Fig. 3 shows that the force F can be considerable, therefore power losses on vertical displacement are rather significant.

In ridge expended process on size Δh take place energy expenditure of resistance overcoming of ridge ground friction forces.

The full kinetic energy expended by a hummock on penetration, accounting for rise and friction of keel is determined as

$$\frac{mv^2}{2} = \int_0^{x_{\max}} F_i dx + \int_0^{\Delta h_{\max}} F_s d\Delta h + \operatorname{tg} \varphi \int_0^{\Delta h_{\max}} F_s d\Delta h \quad (6)$$

where F_g is soil passive resistance, N; F_b is rising force, MN; φ is angle of soil-ice friction.

Fig. 4 shows the forces on ridge during penetration.

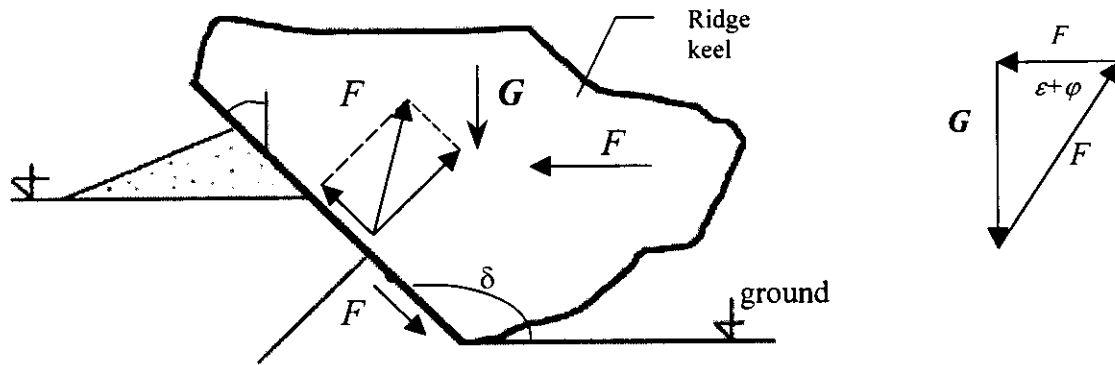


Fig. 4. Forces on ridge during penetration

$$F_s = F_i \cdot \operatorname{tg}(\varepsilon + \varphi) \quad (7)$$

where ε is angle to a vertical line.

In view of the formula (7) magnitudes of raising of a hummock Δh , will be determined as function from horizontal moving

$$\Delta h = \frac{F_i \cdot \operatorname{tg}(\varepsilon + \varphi)}{S\rho_s g} = f(x) \quad (8)$$

Energy expended on raising of a hummock

$$E_{\text{expm}} = F_s \Delta h = \frac{F_i^2 \operatorname{tg}^2(\varepsilon + \varphi)}{S\rho_s g} \quad (9)$$

Power losses on raising of a hummock at moving it on infinitesimal distance dx

$$dE_{\text{expm}} = \frac{1}{4} \rho^2 \cdot g^2 \cdot \operatorname{tg}^4 \alpha \cdot \lambda_p^2 \cdot b^2 \cdot \frac{\operatorname{tg}^2(\varepsilon + \varphi)}{S\rho_s g} \cdot dx^4 \quad (10)$$

Total energy of hummock rise

$$E_{\text{expm}} = \frac{1}{4} \rho^2 g \cdot \operatorname{tg}^4 \alpha \cdot \lambda_p^2 b^2 \frac{\operatorname{tg}^2(\varepsilon + \varphi)}{S\rho_s} \int_0^{x_{\max}} 4x^3 dx = \frac{1}{4} \rho^2 g \cdot \operatorname{tg}^4 \alpha \cdot \lambda_p^2 b^2 \frac{\operatorname{tg}^2(\varepsilon + \varphi)}{S\rho_s} x_{\max}^4 \quad (11)$$

The similarity with ground developing process by excavation machines equipped with simple knife of bulldozer or scraper type with process of keel

penetration allows to consider last from positions of the theory of soil resistance to cutting.

The soil resistance to cutting depends on its strength. But, besides it rather considerably depends on so-called geometric conditions of this process (width and thickness of cut, cutting angles) [6].

One of the most essential features of the process is the spatiality of interaction of the cutting instrument with soil. It is shown, in particular, in different nature of relations of cutting force from width and thickness of cut. While the relation of cutting force on cutting width has a linear view (in practical limits of cutting width), dependence of cutting force from thickness of cut (cutting depth), in practical limits by last, is a rapidly increasing function.

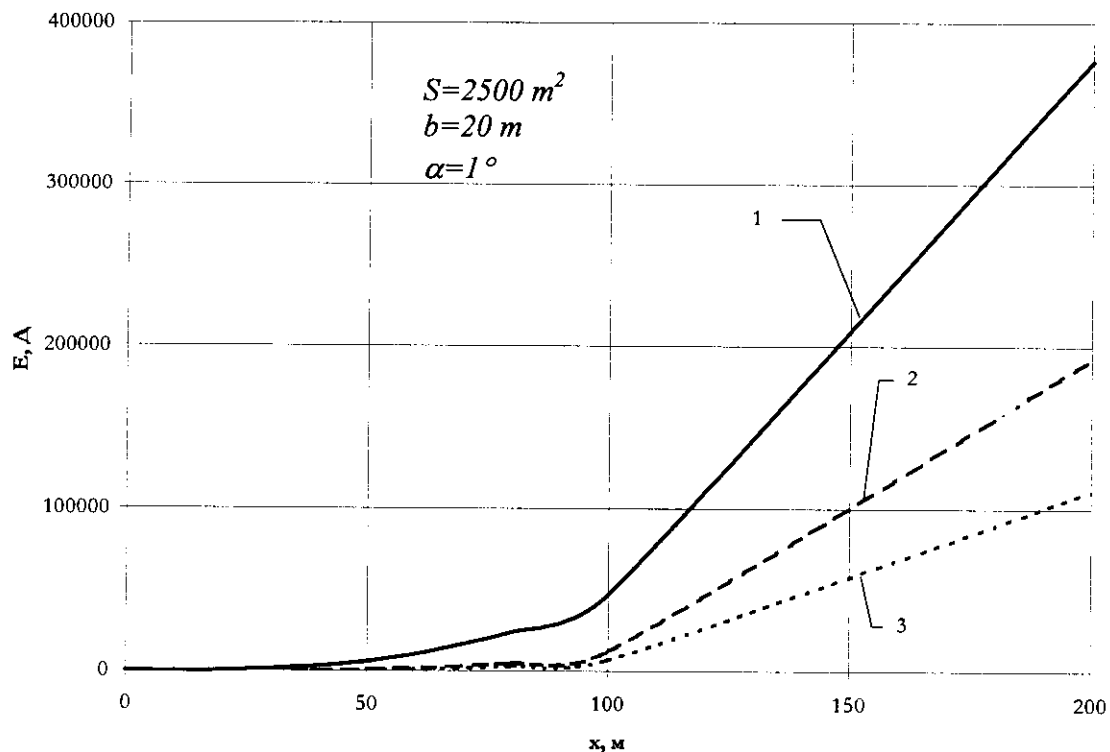


Fig. 5. Graph of power losses on hummock penetration, rise and friction of keel:

1- penetration; 2- rise; 3- friction

Soil failure during cutting process happens as a result of complex stress state: before a frontal knife side (mainly shear and splitting at compression, in lateral expansions of a gash – tension). Besides the considerable effect on force of cutting renders a cutting angle.

In the general view the force for overcoming head resistance to a knife F , proportional to square of a frontal part and cut width depending from a cutting angle and from soil strength is determined as

$$F_{pe3} = q_{cb} \phi \cdot S_{pe3} = q_{cb} \phi \cdot bh \quad (12)$$

where S is sectional cutting area, m^2 ; q_{cb} - specific force of cutting in any part of a gash; ϕ is coefficient taking into account effect of a cutting angle and describing the ration of force F at the given cutting angle to its magnitude at a cutting angle 45° [6].

It is necessary to note, that on magnitude of force of cutting the noticeable effect renders coefficient, which values can be received on the basis of deductions of the theory of a limiting equilibrium of non-cohesive medium. The values ϕ and q_{cb} on the data of experiences are reduced in [6]. For cutting angles of major 60° values of coefficient ϕ are received by approximation (fig. 6).

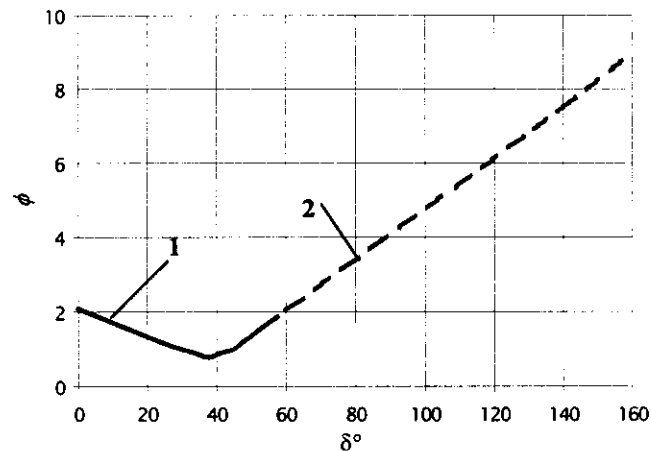


Fig. 6. Dependence of coefficient ϕ from magnitude of a cutting angle δ

1- field observation; 2- approximation.

Taking into account, that $h=x \operatorname{tg}\alpha$, the power losses on penetration in view of cutting are determined as

$$E_{pe3} = \int_0^x m_{cb} \phi \cdot bgx \cdot dx = \frac{1}{2} m_{cb} \phi \cdot bgx^2 \quad (13)$$

The penetration depth in this case is determined under the formula

$$b = \sqrt{\frac{mv^2 \operatorname{tg}^2 \alpha}{m_{\text{с}} \phi \cdot bg}} \quad (14)$$

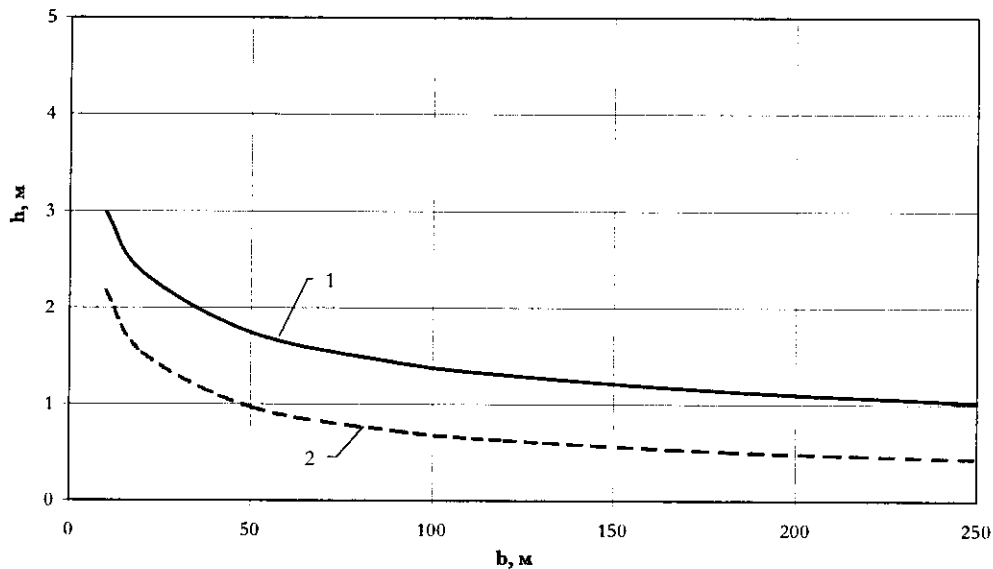


Fig. 7. Comparison of penetration depth of keel at calculations of earth passive pressure and theory of soil cutting

CONCLUSIONS

1. The necessary underlay depth of underwater pipelines can be determined accounting for action of ridge keel and its additional protection.
2. At an estimation of ridge penetration depth into seabed it is necessary to take into account power loss for score of an operation of a vertical component of resistance and friction forces.
3. For the substantiated analysis of keel penetration process of drifting ridge into seabed it is necessary to study resistance forces both from positions of passive resistance, and from positions of resistance forces to ground cutting (theory of cutting). For this purpose it is necessary to realize the substantiated physical modeling.

4. For the substantiated solution of a problem of reliable underwater pipeline protection from drifting ridges it is necessary to continue the studies of morphological and structural characteristics of its underwater part (keel).

REFERENCES

1. Bekker . . , Truskov P. . Action of drifting ice ridge formations on seabed// Proc. of conferences and meetings on hydraulic engineering, Leningrad, Energoatomizdat Publ., 1989. pp. 98-102.
2. Building_Regulation II-55-79. Retaining walls, nagivation locks, fish-passing and fisg-protective structures. Moscow, Stroyizdat Publ., 1980.
3. Beketsky S.P., Astafiev V.N., Truskov P.A. Structure of hummocks on offshore of Northern Sakhalin. Sakhalin Oil & Gas Institute, Okha, Russia.
4. Beketsky S.P., Astafiev V.N., Bogdanchikov S.M. Technique of determination of design parameters of hummocks. Proc. of 16th Int. Conf. on Offshore Mechanics and Arctic Engineering and 14th Int. Conf. on Port and Ocean Engineering under Arctic Conditions, 1997, vol. IV. pp. 230-244.
5. Astafiev V.N., Surkov G. . , Truskov P.A. Hummocks and stamukhs of the Okhotsk sea. Joint-stock company "Rosneft-Sakhalinmorneftegas", 1997.
6. Vetrov Yu. . Calculations of cutting forces at soil excavations. Kiev, 1965.

BP Amoco



Northstar Pipeline Project Beaufort Sea, Alaska Supplemental Leak Detection System

February, 2000

Les Owen

BP Pipelines (Alaska), Inc.

Background

The BP Amoco Northstar Project, a new oil field with enhanced recovery, is located approximately six miles offshore in the Alaskan Beaufort Sea and about 10 miles north of Prudhoe Bay. The Project includes full production facilities on Seal Island with a gas supply line and a crude oil sales pipeline. During Year 1 of the Northstar Project, gas will be sent to Seal Island for drilling support. Year 2 of the project begins the standard use of the pipelines after oil production has begun.

There are two main components of Northstar, the off-shore structure and facilities on Seal Island and the two pipelines.

Off-shore Structure and Facilities

The present body of Seal Island, which lies in 39 feet of water, will be built-up so as to be able to contain the on island required facilities. The island will be constructed using 585,000 cubic yards of pit run gravel with no mechanical alteration prior to placement. Transportation of material to the island will be by ice road during the winter and by combinations of boat, barge, and helicopter during breakup/freezup and summer seasons. The work surface (465' by 421') will be sized to accommodate drilling, processing, and infrastructure needs. The dock surface will allow for the movement of all equipment and materials onto the island; will provide access for supplies during the operational life of the project; will permit the removal of the drilling rig; and will permit the placing of a drilling rig to drill a relief well. The design life of the island will be 15 years.

The island infrastructure includes three modules: permanent living quarters, accommodating 74 people, utility support, and a warehouse.

Pipeline

Produced crude will be transported by pipeline from Seal Island to the receiving location at Pump Station 1. A 10 inch OD x 0.594 inch WT pipeline with cathodic protection and 40 mils of external fusion bonded epoxy (FBE) coating will be used for the offshore section. Onshore, the pipeline will be 10 inch OD x 0.307 inch WT and will have 2 inches of insulation. The off-shore portion of the pipeline will be buried under the sea.

Gas from CCP will be transported to Seal Island by means of a sister pipeline. Onshore the dimensions will be 10 inch OD x 0.307 inch WT, and the pipeline will have 2 inches of insulation. Offshore, the pipeline will be 10 inch OD x 0.594 inch WT and will have a 20 mils thick external FBE coating.

The pipelines will be bundled and will run the six mile offshore segment in a common trench excavated in the seabed. Onshore, they will continue South using common, newly built VSMs for approximately seven miles. The oil pipeline will then continue South to PS-1 on new VSMs for a distance of approximately four miles. The gas pipeline will turn East and run on new VSMs for a distance of approximately three miles until it reaches CCP.

All pipelines and components will be made of carbon steel. Pipeline construction will be "all welded" type. Non sour service conditions will be specified for all pipelines. All pipelines and components will be designed to operate for a service life of 20 years.

For protection of the pipelines against "ice gouging" in the marine segment, the pipelines will be installed in a prepared trench having a depth of eight to ten feet as measured from the bottom of the trench to the undisturbed natural seabed in the immediate area. This will achieve a "depth of cover" of seven to nine feet as measured from the top of pipe to the undisturbed seabed. The trench will be back-filled with native soils once the pipeline is in place. The operation of trenching, pipeline installation and back-fill is intended to be accomplished within a single winter construction season.

Leak Detection Requirements

In May of 1999, the U.S. Army Corps of Engineers issued the Department of Army Permit No. N-950372 for the Northstar Project. Attached to the permit was a Special Condition No. 18 requiring that:

"The permittee shall design, construct, install during pipeline trenching activities, operate, and maintain a prototype oil spill leak detection system, external to the carrier pipeline to detect an oil spill below current threshold detection limits (systems currently to be used are Pressure Point Analysis systems and traditional

mass balance systems). The intent of this condition is to provide for an early leak detection of an oil spill into to the environment. The permittee shall submit the design of the prototype oil spill leak detection system for review and approval by the Corps, in consultation with the federal resource agencies, no later than 90 days prior to initiating pipeline trenching activities. The system shall be designed with objective of detecting oil leaks at 50-foot intervals or less along the entire subsea pipeline length, and have a minimum capability of detecting a 32.5 barrel per day chronic leak. The permittee shall provide progress reports at three and six months from the date of this permit. The progress reports shall delineate the progress being made on the concepts and describe the prototype system(s), problems encountered and proposed solutions, and schedule for the remaining activities.”

In response to this stipulation, BP Amoco has contracted with Siemens of Germany to supply and install the Leak Detection and Location System (LEOS) leak detection system. LEOS is a passive leak detection system that is capable of detecting and locating a small hydrocarbon leak (approximately 0.3 bbls per day for Northstar) in the vicinity of a pipeline, underground piping, or oil storage facility. LEOS will compliment the proposed Northstar EFA Mass Balance Line Pack Compensation and Pressure Point Analysis systems (which are capable of detecting a leak greater than 100 bbls per day). LEOS will not affect or compromise the integrity of the Northstar subsea pipelines. The system is described in more detail in the following:

System Design

LEOS comprises a small diameter (3/8 ins) hollow plastic tube (Figure 1) perforated with closely spaced pattern of small holes. The tube has an outer acetate layer that is impermeable to liquid but allows gas or molecular hydrocarbons to diffuse through the layer to the inside of the tube. The tube is filled with air at atmospheric pressure. The air is used as a carrier medium, so that if a leak occurs near the tube, the hydrocarbon molecules diffuse and surround the tube and eventually , concentrate on the inside of the tube. The air is pumped out of the tube which is adjacent to the entire pipeline length. The air is passed over six highly sensitive sensors whose resistivity changes rapidly and dramatically in the presence of small amounts (> 6 - 10 PPM) of molecular hydrocarbons, such as methane, ethane and on through C5 and C6 components. The leak can be located by comparing the time it takes to evacuate the air from the tube and the time of arrival of the indicator trace gases. A crude oil leak would be indicated by a sensor response to several hydrocarbons at once.

The LEOS tube is made entirely from plastic and is inert in seawater. Therefore, it will not affect the pipeline or cathodic protection system. The LEOS tube will be installed inside a 2 ins diameter plastic protective conduit that will also be perforated with holes to allow the saturated soil to contact the tube and “communicate” with the LEOS tube on the

inside. The purpose of the conduit is to protect the LEOS tube from mechanical damage during transportation and installation, as well as during trench backfilling. The plastic tube containing the LEOS tube will be delivered to site in coiled spools that will be straightened into 1000-ft lengths. These will be transported along-side the pipeline where the oil and gas pipe strings are being bundled together. The LEOS sections will be spliced together using short lengths of stainless steel tubing as connectors. The stainless steel tubing will fit inside the LEOS tube which will be crimped to the tube. A heat shrink sleeve will enclose the entire splice assembly. The newly attached sections of LEOS tube will be pneumatically tested (at approximately 7-8 psig) to ensure water tightness. A robust mechanical connector made of the same material as the protective plastic conduit will connect the sections of protective conduit. These materials have been laboratory tested at low temperature.

LEOS Installation

Pipeline bundling will not be affected by the installation of the LEOS system. Pipeline bundling will entail attaching a pipeline spacer to the outboard pipe, after which the protective conduit will be manipulated into place in a preformed slot in the top of the spacer. The second pipe will be brought along-side the first and strapped to the spacer. Placing the LEOS tube as part of the bundle will add extra steps to the bundling process but should not impair the rate of pipeline installation. Extra crews will be required to straighten the LEOS tube coil and handle the protective conduit. Siemens will train the contractor's personnel to splice the LEOS tube and make the protective conduit connections. Siemens personnel will audit the contractor through these activities, including the pneumatic continuity testing. In this manner, the LEOS system will be installed along with the pipe bundle.

Description of Land-based Equipment

Equipment cabinets will be installed at either end of the LEOS system. These will comprise self-contained cabinets, housing air conditioning, sensing equipment, a computer and an air pump. The air conditioning equipment will be installed at the pipeline shore crossing in the RTU building next to the pipeline valve pad. This cabinet will house a container of silica gel desiccant and an activated carbon cartridge to remove particulate matter. It is referred to as the Test Peak Generating cabinet (TPG). The air intake will feed into the air conditioning cabinet inside the RTU building. The air intake tubing will be stainless steel tubing. After exiting the RTU building it will be routed to bottom of the pipeline riser shaft where it will be connected to the LEOS tube. A small electrolytic cell will also be part of the air conditioning cabinet whose purpose will be to generate a small amount of hydrogen gas (2-3 cc) that will be used to calibrate the LEOS system every time the air is pumped out of the tube.

The LEOS sensing equipment will be located within the warehouse on Seal Island. This cabinet will house; the sensing module with circuitry; a data logger; a computer with printer, and an air pump. The tubing from the pipeline transition onto the island will be stainless steel tubing, heat traced and insulated, so that any moist air in the tube will not condense inside the tube. The sensing module will operate once every 24 hours. Air will be pumped out of the LEOS tube over a 5 to 6 hour period. The fresh air in the tube will remain stationary for approximately 18 hours before pumping begins anew. The data logger will store data from the previous 125 sampling cycles. The system is completely self checking and will alarm if the preset checks are not within operating parameters. (See Figure 2)

System Operating Considerations

There is little maintenance required of the LEOS equipment. Power requirements at the shore crossing are minimal (< 50 W). The desiccant, activated carbon filter and electrolyte at the shore crossing must be refurbished once a year. The sensing equipment and computer in the warehouse, likewise, require little routine maintenance.

This will be the first time LEOS has been installed in an arctic environment. As such, there may be upset operating situations that affect the system performance. For instance, the equipment modules will not function well when the temperature falls below freezing. The RTU building, in particular, may be subject to outages, from time to time, and subsequent heat and power loss during the winter. Siemens has anticipated such an event and has included circuitry to shut down the TPG temporarily. This will not affect the operation of the leak detection system per se, since the air pump is located at the island in the warehouse which should never experience a shutdown. The pump will continue to operate and the leak sensor will detect hydrocarbons, if present. However, the hydrogen test peak would be missing from the time trace until the TPG cabinet is back within its normal operating temperature range.

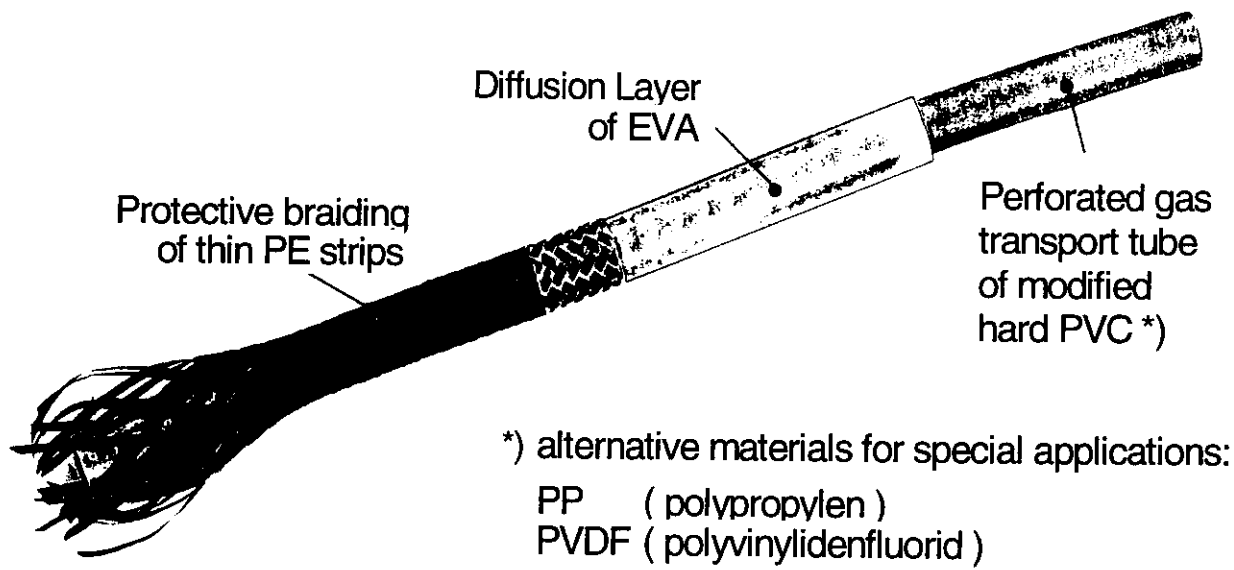
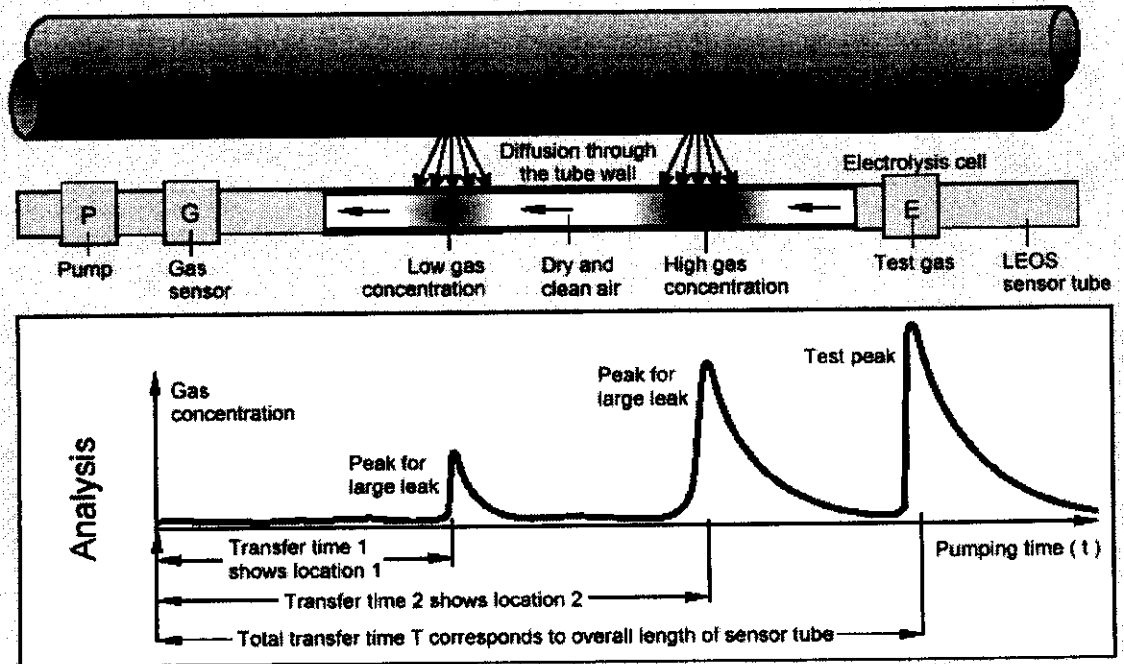


Figure 1 - Detector Tube Details

SIEMENS

Mode of Operation



LEOS (Leak Detection and Location System)

NP / L
F 07/86-07
LEOS_16E.DRW

Figure 2 - System Operation

Pictures Courtesy of Siemens -
<http://www.mms.gov/tarp/workshop25/Presentations/JaxLEOS.PDF>

DISCUSSION SESSION:
Definition of Future Directions & Research Needs
Notes by Ryan Phillips

Dr Andrew Palmer opened and led the discussion session by identifying issues raised during workshop presentations:

1. Subgouge Deformation - there are conflicting views. Some see this as a prime concern, others ignore it. Questions: how large are they? What have we learned?
Physical modelling, centrifuge testing, FE analyses, analytical methods, field observations from contemporary and relic scour all provide input into this consideration.
2. Ice Gouging - there is no consensus on ice forces on offshore structures. There may be a little consensus on ice gouging, but a multi year keel behaves differently to a first year keel to an iceberg. There are areas where one might expect deeper scours, but nothing significant is seen, eg offshore Sakhalin and Melville Island.
3. Increased confidence - needed in face of public challenge and current debates.

(There was discussion throughout this session of the Northstar pipeline project that was unrelated to the definition of future directions and research needs for ice scour. This discussion is not therefore reported here.)

Charles Smith: What do we consider are the top 2 or 3 ice scour issues, what are the next steps? Field verification test? More model tests? Ice strength determinations?

Andrew Palmer: The Northstar pipeline will be the 1st proper offshore pipe subject to ice scour. The opportunity should not be lost as information needed for future lines. Panarctic Drake F76 was not monitored and that experience is essentially lost.

Steve Blasco: I have spent 8yrs writing proposals to look at Drake F76. There is little interest on the Canadian side. This might change if international interest was expressed. I will push the proposal again this year, as built data are available.

Steve Blasco: Instrumentation may be required to measure the strength properties of ice keels. NSF has a new plan from May 1 for \$500k/yr for innovative instrumentation development for use in environmental regions. Need US lead to access these funds. Paperwork should be available in next 2 months.

Ken Croasdale: We need to rethink consequence of different ice keels. What is the attack angle of an ice keel with regard to subgouge deformation? Some areas only have first year ridge keels, others multi year keels, other icebergs.

Steve Blasco: I am not convinced that subgouge deformation exists in all cases. What are the vertical loads? For example, in Resolute only 36 gouges had evidence of subbottom deformation from subbottom profiles.

Denis Blanchet: The presence of the pipeline will change the interaction. What is the effect of consolidated versus unconsolidated keels, soil properties, presence of pipe, direct impact of ice and pipe.

Charles Smith: The issues the appear to be

- 1) Subgouge deformations under scours
- 2) Strength of keels (govern scour depth)
- 3) Need for field experimental database (measurement program)
- 4) Large scale (not full scale) tests, with inclinometers, cause gouge, (PRISE Phase 4)

In Beaufort Sea, there is a high probability of scour /yr from breakup of land-fast ice ridges. Should the indenter be mechanical or natural in nature?

Ken Croasdale: There is also need to refine analyses of ice keel strength, and do larger parametric study in DEICE for example.

Steve Blasco: Dome proposed to lay a 2km length of pipe in old scour trough and monitor it. Could now use Radarsat to monitor movement of large ice features.

Someone: There seems to be more conservatism now in ice scour pipe design than at Calgary workshop

Andrew Palmer: The majority of people at that workshop did not accept subgouge deformation. There is now apparently more conservatism because we understand more of the phenomena and have removed the gross oversimplification that was adopted previously. How do first year ridge keels develop?

Igor Stepanov: I support the ideas being developed. My first choice is a better understanding of strength of 1st year ridge keels. The most promising directions are:

- a) DEM simulations, and
- b) Full scale measurements similar to those done previously by Ken Croasdale.

The Finns are now able to evaluate internal keel geometry using topographic technique to obtain 3D map of porosity and block size (rather than using measurements from a single borehole). What is the keel contact area and internal structure? This understanding will be useful for pipelines and ice loads on offshore structures.

The consensus of the discussion was:

- a) It would be good to find out more about the 40-year-old pipeline off Sakhalin. Any gouges? Surveys?
- b) Bury a pipe in zone 1 & see what happens - possible location Canadian Beaufort Sea due to high impact rates
- c) Monitor ice ridges in the field, especially for resistance for scouring.

- d) Improve analytical model of ice keel resistance
- e) Do more laboratory tests
- f) Do field tests involving creation of real gouges.
- g) Investigate the geologic record for contemporary and relic scours data

